



HAL
open science

Towards an integrated assessment framework for existing structures: Study of riveted lattice girders in French train sheds of 1850-1930

Hannah Franz

► **To cite this version:**

Hannah Franz. Towards an integrated assessment framework for existing structures: Study of riveted lattice girders in French train sheds of 1850-1930. Civil Engineering. Ecole Centrale de Nantes (ECN), 2024. English. NNT: . tel-04679701

HAL Id: tel-04679701

<https://univ-eiffel.hal.science/tel-04679701>

Submitted on 28 Aug 2024

HAL is a multi-disciplinary open access archive for the deposit and dissemination of scientific research documents, whether they are published or not. The documents may come from teaching and research institutions in France or abroad, or from public or private research centers.

L'archive ouverte pluridisciplinaire **HAL**, est destinée au dépôt et à la diffusion de documents scientifiques de niveau recherche, publiés ou non, émanant des établissements d'enseignement et de recherche français ou étrangers, des laboratoires publics ou privés.



Distributed under a Creative Commons Attribution 4.0 International License

MÉMOIRE DE DOCTORAT DE

L'ÉCOLE CENTRALE DE NANTES

ÉCOLE DOCTORALE N° 602
Sciences de l'Ingénierie et des Systèmes
Spécialité : *Génie civil*

Par

Hannah FRANZ

**Towards an integrated assessment framework
for existing structures:**

Study of riveted lattice girders in French train sheds of 1850-1930

Projet de recherche doctoral présenté et soutenu à l'Université Gustave Eiffel - Campus de Nantes, le 27 mai 2024

Unité de recherche : Département MATériaux et STructures (MAST) - Université Gustave Eiffel

Rapporteurs avant soutenance :

Abdelhamid BOUCHAIR Professeur des universités, Université Clermont Auvergne

Ine WOUTERS Professor, Vrije Universiteit Brussel, Belgique

Composition du Jury :

Président :	Stéphane SIRE	Professeur des universités, Université de Bretagne occidentale
Examineurs :	Abdelhamid BOUCHAIR	Professeur des universités, Université Clermont Auvergne
	Ine WOUTERS	Professor, Vrije Universiteit Brussel, Belgique
	Patrice CARTRAUD	Professeur des universités, Ecole Centrale Nantes
	Alexis SAUVAGEON	Dr, Chargé de recherche, AREP, Paris
Dir. de recherches doctorales :	Lamine DIENG	Directeur de recherche, Université Gustave Eiffel
Co-enc. de recherches doctorales :	Emilie LEPRETRE	Dr, ITPE, Université Gustave Eiffel
Co-enc. de recherches doctorales :	Mario RINKE	Professor, Universiteit Antwerpen, Belgique

ACKNOWLEDGEMENTS

I would like to start by expressing my gratitude to my main supervisor, Lamine Dieng, and to Sylvain Chataigner. They were the first researchers to commit to supervising my doctoral project and helping me obtain funding despite my atypical profile. Their trust and guidance were instrumental in making this project happen. I am equally grateful to Jean-Luc Martin and Thotsakane Phoumsavanh, who sponsored my project at AREP. They helped me identify several practical issues related to structural assessment and believed in the value of research in addressing them.

I extend my gratitude to all my academic supervisors Lamine Dieng, Emilie Lepretre and Mario Rinke, who helped me grow as a researcher through their clear insights and kind and constructive criticism. I wish to express my deepest appreciation to Jean-Luc Martin for his continuous mentoring and support throughout the thesis. I also want to thank my monitoring committee members Karen Bowie and Stéphane Sire for their useful perspectives. Special thanks to Alexis Sauvageon with whom I had the pleasure of co-supervising an internship.

Particularly helpful to me during my time as a Ph.D. student were the technicians of the SMC laboratory, who greatly contributed to setting up and carrying out my experiments: Jean-François David, Richard Michel, Pauline Bochereau, Nicolas Séjourné, and Romain Vannier. I also appreciate the help of Xavier Chapeleau for my quasi-static experiments. I gratefully acknowledge Agnès Gaudicheau's assistance in all administrative tasks. Thanks should also go to all lab members for providing a friendly work environment.

I am extremely grateful to Véronique Veston and Aurélie Martin-Lebredonchel, whose extensive knowledge of train sheds and renovation practices was very helpful. Many thanks also to my former colleagues and project managers at Bollinger + Grohmann: Claudia Groth, Simone Murr, and Laure Vandeputte. By sharing their practical renovation know-how, they inspired and trained the young structural engineer that I was.

I very much appreciate all the people who gave me some of their time to share ideas and provide insights into history or heritage assessment: Marina Gasnier, Paul Smith, Karl-Eugen Kurrer, Bertrand Lemoine, Matteo Porrino, Jean-Louis Kerouanton, Anne-Laure Carré, Jean-François Belhoste, Benjamin Delaunay, Arthur Emile. Thanks also to Karen Bowie, Claude Lebreton and Alice Talpin, who helped me get into archival research. I am deeply indebted to the people who included me in research groups or programs, enabling me to take part in inspiring workshops: Marina Gasnier, Clara Jiva-Schulte, Roland May,

and Werner Lorenz. I also wish to thank the scientific committee of the association *Rails & histoire* for granting me their scholarship for three years.

I would like to thank all the people who contributed to keeping my spirits up during this time. I express my deep appreciation to all members of the structural engineering team of AREP in Paris, who always made me feel welcome and gave me a sense of belonging. I also acknowledge the support of my fellow Ph.D. students on campus, especially Elsa, Noémie and Raphaël, as well as the jolly team of My thesis in 180s. Many thanks to all my friends and family for their ever-lasting support.

Finally, I extend my deepest gratitude to my husband, Shehryar, who has constantly been by my side in times of joy and discouragement, and to my son, Isaac, who has given me another reason to be.

SUMMARY

Extending the service life of existing structures promotes economic, environmental, and cultural sustainability. However, due to insufficient knowledge or inadequate technical standards, current practices often needlessly demolish or intervene invasively in historic constructions. This thesis, therefore, proposes a novel integrated assessment framework aiming to take better advantage of an existing structure's load capacity and intervene as respectfully as possible when adapting the structure to new needs and requirements. The approach advocates a structural assessment that considers historic design intentions and heritage value, as well as renovation strategies that take better account of the impact of retrofitting operations on the structure. The application of those principles is explored through the study of riveted lattice girders in French metallic train sheds built between 1850 and 1930.

Iron and steel structures from the 19th and early 20th centuries are markedly present in France's built heritage. Riveted lattice girders are essential constituents of this heritage as they were widely used, especially in roof structures of buildings such as factories, market halls or train sheds. About 90 historic train sheds have been preserved. In recent train shed restorations conducted by the French national railway company SNCF, lattice girders have often been reinforced because of numerically identified stability problems. In reality, however, excessive deformations due to buckling are rarely witnessed in routine SNCF inspections. The implementation of preventive and sometimes invasive strengthening measures reflects shortcomings both in the current engineering practice and in the cultural perception of the heritage value of those structures.

The proposed integrated assessment framework is decomposed into three main steps: i) identifying restoration challenges, ii) refining modelling assumptions, iii) adapting verification methods.

- The first step enhances that prior to any calculations, it is important to analyse structural features conveying heritage or cultural value and needing to be preserved, and to pool knowledge from previous restorations on similar structures. Train sheds constitute a large family of structures whose study provides us with a valuable database. From the perspective of engineering history, we discuss the cultural significance of lattice girders and, using a survey of recent train shed restorations, we highlight the impact of strengthening measures on their authenticity.

- The second step consists in removing some uncertainties regarding modelling assumptions, firstly by comparing original design intentions with current practices, and secondly by conducting experimental and numerical investigations. Drawing on historical research, we evidence the lackings in the original design of riveted lattice girders, especially their web members. The review of recent literature characterises uncertainties regarding the rotational stiffness of riveted joints. To assess the out-of-plane rotational stiffness of single-riveted joints, we carry out modal and quasi-static tests on a reclaimed riveted lattice girder and show that its riveted joints exhibit a rigid behaviour. Furthermore, the experiments yield insight into the contribution of joint behaviour to global behaviour, especially the effect of joint stiffness variations and the role of joint stiffness in the effective restraint of web members.
- In the third step, the current verification procedures derived from the Eurocodes are critically discussed, as they were intended for the design of new structures and are in some aspects inadequate for the assessment of historic structures. As material properties are key parameters to determine the structural resistance, we examine which design values of the elastic limit should be considered for wrought iron and mild steel, by discussing the use of information provided by historical design reports or material sampling. Focusing on buckling resistance, we then show that the buckling of lattice girders was historically not verified by calculations but prevented by constructive measures. Relying on our experimental findings regarding joint behaviour and using a numerical case study, we assess the potential of advanced numerical calculations to decrease the predicted buckling risk and thus reduce the necessary strengthening measures.

The proposed methodology, combining structural engineering, technical history, and heritage studies, sets the basis of an assessment framework that could be extended to iron and steel structures of the 19th and early 20th centuries, to heritage structures made of other materials and virtually to most types of existing structures.

RÉSUMÉ

Allonger la durée de vie des structures existantes favorise résolument la durabilité économique, environnementale et culturelle. Cependant, en raison d'une connaissance insuffisante ou de normes techniques inadéquates, les pratiques actuelles engendrent des démolitions inutiles ou des interventions invasives dans les constructions historiques. Cette thèse propose donc une méthodologie novatrice d'évaluation intégrée visant à mieux tirer parti de la capacité portante d'une structure existante et à intervenir de manière aussi respectueuse que possible lors de l'adaptation de la structure à de nouveaux usages ou exigences. L'approche préconise une évaluation structurale qui prenne en compte les intentions de conception historiques et la valeur patrimoniale, ainsi que des stratégies de rénovation qui se soucient de l'impact des interventions sur la structure. L'application de ces principes est explorée à travers l'étude des poutres treillis rivetées des halles de gare françaises à charpente métallique construites entre 1850 et 1930.

Les structures métalliques du 19^{ème} et début du 20^{ème} siècle sont très présentes dans le patrimoine bâti français. Les poutres treillis rivetées sont des éléments essentiels de ce patrimoine car elles étaient largement utilisées, en particulier dans les charpentes de bâtiments tels que les halles industrielles, halles de marché ou de gare. Environ 90 halles de gare historiques ont été préservées. Lors des récentes restaurations de telles halles menées par la SNCF, les poutres treillis ont souvent été renforcées en raison de problèmes de stabilité identifiés numériquement. Or, en réalité, les déformations excessives dues au flambement sont rarement observées lors des inspections de maintenance de la SNCF. La mise en œuvre de mesures de renforcement préventives et parfois invasives reflète ainsi des lacunes à la fois dans la pratique actuelle de l'ingénierie et dans la perception culturelle de la valeur patrimoniale de ces structures.

La méthodologie d'évaluation intégrée proposée est décomposée en trois étapes principales : i) identification des défis de restauration, ii) affinement des hypothèses de modélisation, iii) adaptation des méthodes de vérification.

- La première étape défend qu'avant tout calcul, il est important d'analyser les caractéristiques structurelles véhiculant une valeur patrimoniale ou culturelle et devant être préservées, et de recenser les connaissances issues de restaurations antérieures sur des structures similaires. Les halles de gare constituent une grande famille de structures dont l'étude nous fournit une base de données précieuse. La valeur patrimoniale des poutres treillis est d'abord démontrée en s'appuyant

sur l'histoire de l'ingénierie. L'impact de décisions architecturales ainsi que des mesures de renfort liées aux rénovations sur leur authenticité est ensuite mise en évidence à l'aide d'une étude des rénovations récentes de halles de gare.

- La deuxième étape consiste à lever certaines incertitudes concernant les hypothèses de modélisation, tout d'abord en comparant les intentions de conception originales avec les pratiques actuelles, et ensuite en menant des investigations expérimentales et numériques. Grâce à des recherches historiques, les lacunes de la conception originale des poutres treillis rivetées, en particulier de leurs montants et diagonales, sont mises en évidence. Les incertitudes concernant la raideur rotationnelle des assemblages rivetés sont caractérisées à travers une revue de littérature. Afin d'évaluer la raideur rotationnelle hors-plan des assemblages mono-rivets, des essais vibratoires et quasi-statiques sont réalisés sur une poutre treillis rivetée récupérée d'une démolition. Il apparaît que les assemblages ont un comportement rigide. En outre, les essais permettent de mieux comprendre l'influence du comportement des assemblages sur le comportement global, en particulier l'effet des variations de raideur de certains assemblages et le rôle de la raideur des assemblages dans le maintien effectif des montants et diagonales.
- Dans la troisième étape, les procédures de vérification actuelles dérivées des Eurocodes sont analysées de manière critique, car elles ont été prévues pour la conception de nouvelles structures et sont, à certains égards, inadéquates pour l'évaluation des structures historiques. Les propriétés des matériaux sont des paramètres clés pour déterminer la résistance structurale. Les informations fournies par les rapports de conception historiques ou les diagnostics de matériaux sont examinées au regard de leur pertinence pour déterminer des valeurs nominales de limite élastique pour le fer puddlé et l'acier doux. Concernant la résistance au flambement, il est ensuite montré que le flambement des poutres treillis n'a originellement pas été vérifié par des calculs, mais qu'il a été évité par des mesures constructives. Enfin, les résultats expérimentaux concernant la raideur des assemblages rivetés sont utilisés pour développer une étude de cas numérique qui évalue le potentiel de calculs numériques avancés dans la réduction du risque de flambement et des mesures de renfort associées.

La méthodologie proposée, qui combine l'ingénierie des structures, l'histoire de l'ingénierie et des études patrimoniales, offre un cadre qui pourrait être étendu aux structures métalliques du 19^{ème} et début du 20^{ème} siècle, aux structures patrimoniales de tous matériaux et plus généralement à la plupart des structures existantes.

CONTENTS

Acknowledgements	III
Summary	V
Résumé	VII
Contents	IX
List of figures	XIII
List of tables	XIX
Abbreviations	XXI
Introduction	1
Context	2
The case of riveted lattice girders in French train sheds	5
Objectives and methodology	7
Thesis outline	10
I IDENTIFYING RESTORATION CHALLENGES	13
1 Identifying significant structural features	15
1.1 Train sheds and heritage recognition	16
1.2 Methodology	17
1.3 Significance of the main “architectural” features	21
1.3.1 Principles of a roof structure	21
1.3.2 Roof trusses	22
1.3.3 Skylights and glazed gables	26
1.4 Significance of riveted lattice girders	26
1.4.1 Beams or trusses?	26

1.4.2	Ornamental role	28
1.4.3	Construction details	30
1.5	Conclusion	32
2	Reviewing restoration practices	33
2.1	Purpose of train shed restorations	34
2.2	Methodology	35
2.3	Roofing materials	35
2.3.1	Historical evolution of roofing materials	36
2.3.2	Weight associated with roofing systems	40
2.3.3	A change in perspective?	44
2.4	Maintenance equipment	46
2.5	Structural interventions	47
2.5.1	Skylights and glazed gables	47
2.5.2	Repair or replacement of structural elements	49
2.5.3	Strengthening measures	49
2.6	Conclusion	54
 II REFINING STRUCTURAL ANALYSIS ASSUMPTIONS		
57		
3	Capitalising on previous assumptions	59
3.1	Historical structural analysis methods	60
3.1.1	Theory of trusses for triangular systems	60
3.1.2	Structural analysis methods for lattice girders	61
3.2	Joint modelling	64
3.2.1	Pinned, rigid or semi-rigid	64
3.2.2	Understanding of riveted connections	68
3.3	Discussion based on the case study	71
3.3.1	Geometry	71
3.3.2	Historical loads	71
3.3.3	Structural analysis	72
3.4	Conclusion	75

4	Assessing the rotational stiffness of riveted joints by modal testing	77
4.1	Applications and techniques of modal testing	78
4.1.1	Applications of modal testing for civil engineering structures	78
4.1.2	Principles and techniques of modal testing	79
4.2	Proposed methodology	88
4.2.1	Experiments	89
4.2.2	Finite element modelling	96
4.3	Results and discussion	100
4.3.1	Comparison of experimental results with the reference model	100
4.3.2	Preliminary sensitivity analyses	102
4.3.3	Assessment of the average rotational stiffness of the riveted joints	105
4.3.4	Effect of local variations of the joint stiffness	107
4.4	Conclusion	111
5	Assessing the rotational stiffness of riveted joints by load testing	113
5.1	Proposed methodology	114
5.1.1	Test specimen	114
5.1.2	Experimental setup	114
5.1.3	Preprocessing of the experimental data	117
5.1.4	Finite element modelling	119
5.2	Results and discussion	119
5.2.1	Validation of the rotational stiffness of the joints	119
5.2.2	Measurement and modelling of the apparent rotational stiffness	121
5.3	Conclusion	128
III	ADAPTING VERIFICATION METHODS	131
6	Determining design values of material properties	133
6.1	Historical perspective on iron and steel varieties	134
6.2	Historical “design resistance”	136
6.2.1	Recommendations from historical literature and regulations	137
6.2.2	Working stresses used in practice for train sheds	140
6.2.3	Discussion	141

6.3	Material sampling and characteristic values	143
6.3.1	Definition of characteristic values according to the Eurocodes	143
6.3.2	Test results from the literature	145
6.3.3	Test results from train shed samples	146
6.3.4	Discussion	151
6.4	Conclusion	153
7	Assessing the buckling risk	155
7.1	Historical design against buckling	156
7.1.1	Evolution of the state of knowledge on buckling	156
7.1.2	Design criteria against buckling in France	159
7.1.3	Buckling safety in practice	160
7.1.4	Efficiency of lattice vs. solid-web girders	161
7.2	Assessment of the buckling risk according to Eurocode 3	164
7.2.1	Buckling curve approach	164
7.2.2	Estimation of the critical load	166
7.2.3	Second-order analysis with imperfections	169
7.3	Discussion based on the case study	170
7.3.1	Summary of findings from previous chapters	170
7.3.2	Original design checks under historical loads	171
7.3.3	Assessment according to Eurocode 3	173
7.3.4	Conclusion of the case study	177
7.4	Conclusion	178
	Conclusion	179
	Bibliography	185
	Archival sources	185
	Historical sources (1800-1940)	186
	Literature (1940-2023)	187
	Publications by the author	197
	Appendix	199
	Extract of the original design report of Bédarieux’s train shed	199

LIST OF FIGURES

Introduction

1	Examples of buildings with a load-bearing metal structure comprising riveted lattice girders	3
2	Example of a strengthening measure carried out on a riveted lattice girder because of the predicted buckling risk	5
3	Typical constructive detailing for riveted lattice girders	6
4	Schematic view of possible out-of-plane buckling shapes for a lattice girder.	6
5	Integrated assessment framework applicable to riveted lattice girders. . . .	8
6	Train shed of Montauban, with a view of the lattice purlin assessed in detail for the case study	10
7	Outline of the thesis' main parts and chapters.	10
1	Identifying significant structural features	
1.1	Map of France showing extant and demolished metallic train sheds	17
1.2	Schematic view of a metallic roof structure with designation of relevant structural elements.	22
1.3	Examples of roof truss typologies favoured in different countries	23
1.4	Typologies of roof trusses used for French train sheds	23
1.5	Map of surviving railway stations with a metallic shed, according to their original railway company	24
1.6	Series of similar train sheds	25
1.7	Largest spans featured by sheds of railway stations	25
1.8	Skylights and glazed gables	26
1.9	Examples of the 4 types of lattice purlins and rafters	28
1.10	Lattice bridge across the Loire - Pont de Varennes-Montsaureau	29
1.11	Examples of ornamental additions on lattice lXl-type beams	29
1.12	Ornamental and structural web pattern for a lattice girder, as suggested by Vierendeel	30
1.13	Repeated construction details in train sheds built by same contractor Daydé et Pillé	31

1.14	Lattice purlin of the Gare d’Agen	31
1.15	Various configurations of single-riveted joints	32
2	Reviewing restoration practices	
2.1	Example of complete replacement of the roofing	36
2.2	Opaque materials used for roofing	37
2.3	Translucent/transparent materials used for roofing	37
2.4	Proportional amounts of roofing materials used in the restoration wave of the 1970s-1980s	39
2.5	Proportional amounts of roofing materials used in restoration projects since 2005	41
2.6	Overview of the evolution of the loads associated with opaque roofing materials.	42
2.7	Overview of the evolution of the loads associated with opaque roofing materials.	45
2.8	Dresden Hauptbahnhof, built in 1898, after renovation in 2006	45
2.9	Gare d’Orléans, built in 2009	46
2.10	Maintenance equipment added on the course of restoration projects in the train shed of Bordeaux Saint-Jean	46
2.11	Glazed gables restored or modified	48
2.12	Local repairs of roof truss chords with added riveted plates in the train shed of Troyes renovated in 2021	50
2.13	Replacement of purlins in the train shed of Montauban	50
2.14	Invasive strengthening measures of the end of the 20 th century	51
2.15	Interventions increasing the cross-section of existing elements or replacing them	53
2.16	Interventions adding structural elements to provide buckling restraints	53
2.17	Principle of the strengthening measures implemented on the lattice purlins of the train shed of Montauban	54
2.18	Gare de Perpignan, built in 1896, before and after renovation	55
3	Capitalising on previous assumptions	
3.1	Truss analysed by Whipple in 1847	60
3.2	Navier’s bending theory applied to lattice girders	62
3.3	Lattice girder with crossed diagonals used by Schwedler as a case study	62

3.4	Calculation of the stress distribution in the chords of a lattice girder according to Schwedler and Navier	64
3.5	Classification of joints according to their stiffness and corresponding modelling in the case of elastic analysis	66
3.6	Classification of joints according to their stiffness and corresponding modelling in the case of elastic analysis	67
3.7	Stiffness classification boundaries	67
3.8	Characteristic load-deformation behaviour of a riveted joint and stress states in the various stages	69
3.9	Distribution of bending stresses in a riveted angle from a stringer-to-floor-beam connection	70
3.10	Geometrical details for the case study	72
3.11	Distribution of internal loads following Résal's approach for a lattice purlin of the train shed of Montauban under uniform loading.	73
3.12	Bending moment distribution in the chords when the chords are modelled as continuous beam elements	74
4	Assessing the rotational stiffness of riveted joints by modal testing	
4.1	Complex-to-real conversion of the modal constants	85
4.2	Original setting of the research object: the platform sheds of the station Paris Gare de l'Est	90
4.3	Elevation drawing of the tested lattice girder specimen.	90
4.4	Experimental setup in the laboratory	91
4.5	Sensor setups: (a) TC setup; (b) BC setup; (c) WEB setup.	92
4.6	Output acceleration signals	93
4.7	Inertance magnitude at point 17 in the BC setup.	94
4.8	Measured modal displacements after 1-scaling for the first six modes.	95
4.9	View of the finite element model, with associated element types	97
4.10	Connections modelled with rotational springs - detail of local coordinate systems at the connections	99
4.11	Comparison of experimental mode shapes and corresponding numerical mode shapes obtained with the reference model.	101
4.12	3d-view and top view of the deformed and original states of the structure for the 5 th mode, obtained with the numerical reference model	102

4.13	Comparison of experimental mode shapes and corresponding numerical mode shapes obtained with the model where the chords are modelled with elements type 52 instead of 79.	103
4.14	3d-view and top view of the deformed and original states of the structure for the 5 th mode, obtained with the “hinged” numerical model	107
4.15	Location of the riveted joints that were loose numerically.	108
4.16	ECOMAC[num ^{SD} , num ND] ($n = 6$) between the single-damaged model (d2B - $k_r = 0$) and the reference model with all joints rigid.	109
4.17	ECOMAC[num ^{SD} , exp] ($n = 6$) between the single-damaged model (d2B - $k_r = 0$) and the experiments.	110
4.18	$\Delta\xi$ [num ^{SD} , num ND] ($n = 6$) for the single-damaged model (d2B - $k_r = 0$).	110
5	Assessing the rotational stiffness of riveted joints by load testing	
5.1	Naming system for the chord and web members of the tested lattice girder	115
5.2	Gauge positions for the load tests	115
5.3	Global setup G_hor - global view and instrumentation	116
5.4	Global setup G_hor - details	116
5.5	Local setup L_v3	117
5.6	Expected stress distribution over the thickness of web member v3	118
5.7	Comparison of the experimental displacements and bending moments from the tests in the G_hor setup with the results from several numerical models	120
5.8	Comparison of the experimental displacements and bending moments from the tests L_v3 with the results from the corresponding numerical models	121
5.9	Linear extrapolation based on measured moments to compute the moment at the extremities of the loaded web member	122
5.10	Curve fitting on the measured displacements for the tests L_v3 with a piecewise third-order polynomial	123
5.11	Correction of the first-order derivative of the displacement to obtain the rotation angle due only to the deformation of v3	123
5.12	Moment rotation curves at the ends of v3	124
5.13	Mechanical model for the riveted connection	125
5.14	Geometrical parameters used for the stiffness calculations proposed by Lee, 2013	126
5.15	Adapted geometrical parameters used for the stiffness calculations, taking into account the boundary conditions in setup L_v3	127

6 Determining design values of material properties

6.1	Characteristic microstructures of cast iron, wrought iron and mild steel . . .	136
6.2	Evolution of the working stresses recommended in the literature for iron and steel between 1820 and 1930, compared with working stresses used for train sheds.	142
6.3	Definition of the characteristic value after Eurocode 0 based on the probability distribution of the considered variable	144
6.4	Results of mechanical tests on train shed samples	150

7 Assessing the buckling risk

7.1	Influence of the end conditions of a compressed member on its buckling shape and effective length.	157
7.2	Working stresses σ_{lim} for a compressed member as a function of its slenderness λ in French literature.	160
7.3	Compressed web members exhibiting stiffer cross sections than tensioned web members	162
7.4	Buckling curves prescribed by EN 1993-1-1, 2005 depending on the cross-section geometry.	165
7.5	Influence of the end conditions of a column on its effective length and the critical load.	167
7.6	Buckling length of the diagonals in the lattice purlin of Montauban depending on the assumptions regarding the riveted joints.	172
7.7	Determination of snow loads on the roof of Montauban's train shed	174
7.8	Airflow on a canopy roof	174
7.9	Shape of the first buckling mode of the most compressed diagonal of the studied lattice purlin	176

Appendix

A.1	Front cover of the original design report of Bédarieux's train shed.	199
A.2	Design calculations for the ridge purlin of Bédarieux's train shed.	200

LIST OF TABLES

1	Identifying significant structural features	
1.1	List of surviving metallic train sheds from the period 1850-1930, with documents gathered as a database for the inventory of structural specificities .	19
2	Reviewing restoration practices	
2.1	List of railway stations whose train sheds were restored in the wave of the 1970s and 1980s	38
2.2	List of railway stations whose train sheds were restored since 2005	41
2.3	Glazing characteristics and associated weights for recent train shed restoration projects.	44
2.4	List of railway stations restored since 2005, with or without strengthening measures	52
3	Capitalising on previous assumptions	
3.1	Comparison of internal loads and stresses obtained from various analytical and FE models	74
4	Assessing the rotational stiffness of riveted joints by modal testing	
4.1	Average frequencies of the first six experimental modes	94
4.2	Estimate of the measurement uncertainty for the frequency f , from the measurements of all accelerometers	96
4.3	Estimate of the measurement uncertainty for the frequency f and the FRF-magnitude $ H(\omega) $ for each mode, estimated from the outputs of 7 repeated tests for 3 sample accelerometers.	96
4.4	Set of modelling assumptions used for the reference model.	100
4.5	Comparison of the experimental results with results from the numerical reference model	100
4.6	Comparison of the numerical frequencies and L_r values for the modes paired with the experimental ones, when the chords are modelled with elements type 79 or type 52	103
4.7	Comparison of the numerical frequencies obtained for different mesh sizes.	104

4.8	Comparison of the numerical frequencies obtained for different input material properties.	104
4.9	Comparison of the numerical frequencies and L_r values for the modes paired with the experimental ones, when the support conditions are modelled as fully rigid (REF) or with an elastic foundation (E. F.).	105
4.10	Frequencies of the numerical modes in the frequency range [0-106.15] Hz. .	105
4.11	Quality criteria L_r [%] comparing numerical and experimental mode shapes for different values of k_r	106
5	Assessing the rotational stiffness of riveted joints by load testing	
5.1	Parameters used for the analytical computation of k_c and comparison of the resulting analytical stiffness $k_{app,ana}$ with the experimental stiffness $k_{app,exp}$.	127
6	Determining design values of material properties	
6.1	List of sources used to establish the evolution of working stresses of iron and steel between 1820 and 1930.	140
6.2	List of train sheds for which working stresses were collected.	141
6.3	Calculation of the characteristic value of the yield strength for wrought iron and mild steel, based on material sampling from train sheds	147
6.4	Test results from <i>mild-steel</i> specimens taken from French train sheds . . .	148
6.5	Test results from <i>wrought-iron</i> specimens taken from French train sheds. .	149
7	Assessing the buckling risk	
7.1	Comparison of working ratios obtained from historical design checks	173
7.2	Comparison of working ratios obtained from Eurocode design checks	176

ABBREVIATIONS

APC	Annales des Ponts et Chaussées
AREP	Architecture Recherche Engagement Post-carbone
BC	Bottom Chord
BV	Bâtiment Voyageur (Station Building)
CIFRE	Convention Industrielle de Formation par la Recherche
DFT	Discrete Fourier Transform
DOF	Degree of Freedom
GNIA	Geometrically Non-linear elastic Analysis with Imperfections
ECOMAC	Enhanced Coordinate Modal Assurance Criterion
EMA	Experimental Modal Analysis
ICOMOS	International Council on Monuments and Sites
FEM	Finite Element Method
FFT	Fast Fourier Transform
FRF	Frequency Response Function
JRC	Joint Research Center
LBA	Linear Buckling Analysis
MAC	Modal Assurance Criterion
MAST	Matériaux et Structures
MIMO	Multiple-Input-Multiple-Output
MDOF	Multiple-Degree-of-Freedom
OMA	Operational Modal Analysis
OMAX	Operational Modal Analysis with exogenous input

PLM	Paris-Lyon-Méditerranée
PSD	Power Spectral Density
SDOF	Single-Degree-of-Freedom
SIMO	Single-Input-Multiple-Output
SISO	Single-Input-Single-Output
SLS	Serviceability Limit State
SMC	Structures Métalliques et à Câbles
SNCF	Société Nationale des Chemins de fer Français
STRRES	Syndicat national des entrepreneurs spécialistes de Travaux de Ré- paration et de Renforcement des Structures
TC	Top Chord
ULS	Ultimate Limit State

INTRODUCTION

The introduction sets out the background of the research, arguing the need to preserve old iron and steel structures and the challenges involved in doing so. It presents the concrete concern rooted in practice that motivated the thesis, states the objectives of the work and outlines the developed methodology.



Gare de Hendaye: train shed built in 1880 and restored in 2013, with a detail of a lattice rafter, Hendaye, France (Picture from SNCF-AREP).

Contents

Context	2
The case of riveted lattice girders in French train sheds	5
Objectives and methodology	7
Thesis outline	10

This doctoral thesis presents the research work carried out in a CIFRE collaboration (Convention Industrielle de Formation par la Recherche) between AREP, a subsidiary of the French national railway company SNCF (Société Nationale des Chemins de fer Français), and the laboratory MAST-SMC (Matériaux et Structures - Structures Métalliques et à Câbles) of Université Gustave Eiffel - Nantes campus.

Context

Catching a train at Hendaye's railway station. Consulting archives in a former Peugeot factory. Shopping food in Rennes' Sunday market. Working in the centre of Paris in a transformed rail freight terminal. Those activities are made possible thanks to the preservation or adaptation of iron and steel structures from the 19th and early 20th centuries (Fig. 1). Such structures are still markedly present in France's built heritage, as in Europe and other parts of the world. They are significant testimonies to a building culture that drew on theoretical developments in structural engineering and technological advances in the metallurgical industry. Wrought-iron and mild-steel riveted lattice girders, which were widely used in metal structures from about 1850 to 1950, are a good example, owing much to the design methods and production and construction techniques specific to that period. Today, with their crisscross patterns shown in Fig. 1 and their smooth round-head connectors, they contribute to the much-appreciated industrial aesthetics.

Renovations and transformations of buildings with a load-bearing metal structure from the 19th and early 20th centuries are an opportunity to enhance industrial heritage (Casanelles et al., 2003; Gasnier, 2011). Given the environmental challenges facing the construction sector today, those structures are also valuable building resources. Reusing existing buildings, rather than demolishing them and constructing new buildings, is one of the most impactful forms of sustainable design (Abdulameer et al., 2020). Buildings with an old metal structure can be renovated, to extend their service life while maintaining their original function. This is often the case with train sheds or market halls. Buildings can also be rehabilitated to adapt them to a new use. This typically concerns empty industrial buildings, which represent a huge potential for urban renewal (Gudina et al., 2021; Real, 2015). Research is also being carried out on the adaptive reuse of heritage buildings (Vafaie et al., 2023). Finally, metal structures can be reused for a new purpose in a new place, as a whole or in parts, although this practice is very limited today. For the sake of saving materials and preserving the remains of an inventive and influential building culture, it is essential to facilitate sustainable, heritage-friendly, and cost-effective renovation, rehabilitation or reuse projects.

In the framework of restorations or transformations, the assessment of existing struc-

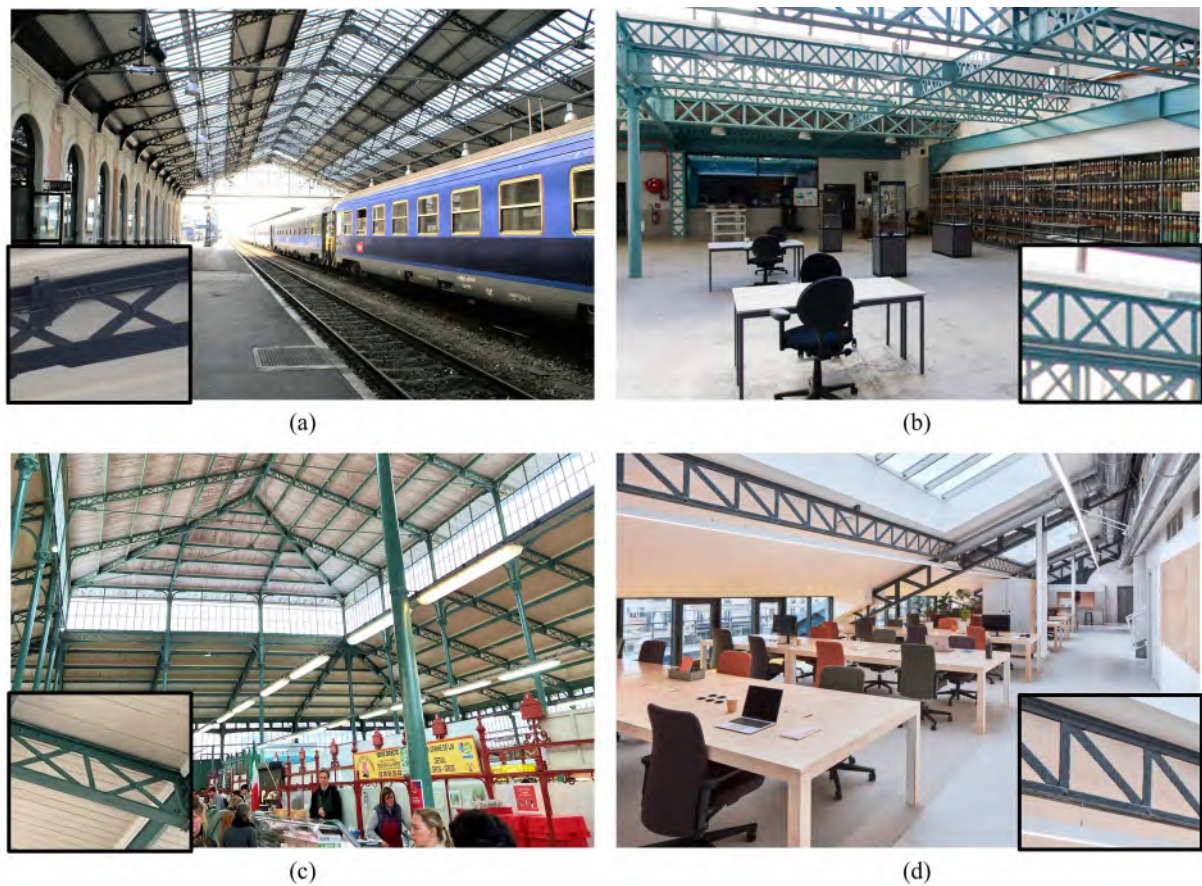


Figure 1 – Examples of buildings with a load-bearing metal structure comprising riveted lattice girders: (a) Gare de Hendaye: train shed built in 1880 and restored in 2013, Hendaye, France (Picture from SNCF-AREP); (b) Former Peugeot factory built around 1880 and converted in 2010 into an archive center, Hérimoncourt, France (Picture from Arbracam.org); (c) Market hall of the “Marché des Lices” built in 1864, Rennes, France (Picture by H. Franz); (d) Former rail freight terminal “Halle des Messageries” of Saint-Lazare railway station, built in 1886 and converted into an office space in 2020 (Picture by M. Giesbrecht).

tures is often necessary. It is required when the structure is deteriorated, or when the anticipated changes induce different or higher loads. Sometimes, even though the structure is in good condition and the loading conditions remain the same, the structure is re-assessed to ensure its actual reliability (Luechinger et al., 2015, p. 9). Accurately assessing the load capacity of existing structures is a challenge. The standard methods commonly used for the design of new structures are conservative and therefore not suitable for fully utilising an existing structure with minimal intervention. The current set of Eurocodes, the European standards for the design of civil engineering structures, provides very limited guidance tailored to the assessment of existing structures. From an engineering point of view, improving the structural assessment involves refining calculation methods or undertaking testing and monitoring. This strategy is integrated into the upcoming generation of Eurocodes to be published in 2027 (Formichi, 2019). However, structural assessment can also greatly benefit from considerations related to history and heritage. Extensive research was conducted in construction history regarding iron and steel structures from the

19th and early 20th centuries (Espion et al., 2018). Many investigations focused specifically on structural assessment issues, elaborating on material properties (O’Sullivan, 2013) or riveted connections (Collette, 2014). To effectively contribute to sensitive and targeted retrofitting operations, structural engineers may need to broaden the scope of their usual structural assessment procedures. Knowledge about the original design intentions, as well as previous interventions, can help identify weaknesses or extra capacities of the structure. Understanding the impact of repair or strengthening measures on the heritage value of the building can help select the most appropriate implementation variants. Practical guidelines exist that detail the various options (STRRES, 2014), but they do not provide critical insight into their consequences in terms of heritage value.

It can be argued that the assessment of an existing structure and the resulting elaboration of structural interventions is often case-specific. However, iron and steel structures from the 19th and early 20th centuries constitute a family of structures sharing specific design principles and manufacturing conditions. As a result, engineers frequently encounter similar issues when assessing these structures. To some extent, these issues can be addressed systematically, provided that underlying patterns are identified, properly investigated and translated into practice.

Iron is deeply intertwined with industrialisation and the infrastructure of our modern lives. The construction materials iron and later steel are inseparably linked with the establishment of a railway network in Europe throughout the 19th century. In several languages, the word for *railway* signifies this connection to this day: *chemin de fer*, *Eisenbahn*, *ferrovia*... France developed one of the first railway networks and was home to many progressive engineering and construction projects of the time. Numerous impressive original railway stations still dominate the centres of French cities. Since 2005, the French national railway company SNCF has carried out an ambitious restoration programme of their historic metallic train sheds, which were built between 1850 and 1930. As a component part of station buildings, train sheds have the function of covering railway tracks and platforms. Train shed restorations have already been completed in about twenty railway stations, while twice as many are still pending. As a subsidiary of SNCF and a multidisciplinary architecture practice, AREP participated in most of these operations. In 2019, SNCF identified the need to improve their asset management of train sheds, by prioritising and standardising restoration works. For this purpose, AREP’s heritage department carried out an extensive survey of surviving train sheds, to gather insight into their architectural features, their heritage value and their health condition. They also analysed past restorations to improve future specifications, in terms of scaffolding, roofing systems, corrosion protection or maintenance equipment. However, a contribution regarding structural interventions remained missing. In order to intervene as respectfully as possible on

the metal structure of train sheds or to make them more adaptable to new needs and requirements, it is crucial for SNCF to also refine and standardise their structural assessment procedures and their specifications on repair and strengthening measures. This industrial concern goes hand in hand with the need to address the challenges regarding the preservation and adaptation of old iron and steel structures, and existing structures in general. To identify recurring issues leading to structural interventions in train sheds, this thesis started out with conducting a survey of recent restorations building upon the study on train sheds carried out by AREP's heritage department. After careful analysis, it appeared that riveted lattice girders warranted further examination.

The case of riveted lattice girders in French train sheds

The survey of recent train shed restorations has shown that riveted lattice girders, which are typically used as purlins or rafters, are often subject to strengthening measures. Assessment reports have revealed that reinforcements are always decided upon due to stability problems identified through finite element modelling and standard design checks following the requirements of the Eurocodes. For example, the upper chords of the lattice rafters of the train shed of Gare d'Austerlitz in Paris were reinforced by welded plates in 2015 because of a predicted out-of-plane buckling risk (Fig. 2). In reality, however, excessive deformations due to buckling are rarely observed on riveted lattice girders during SNCF routine inspections. What's more, despite similar causes, strengthening measures vary greatly in their principle and their implementation from one train shed to the other. It is therefore of great interest to question the relevance of these structural interventions and the assessment procedures responsible for them.



Figure 2 – Example of strengthening measure carried out on a riveted lattice girder because of the predicted buckling risk: the rafters of the train shed of Gare d'Austerlitz, Paris, France. (a) Predicted buckling shape for the upper chord of the lattice rafter; (b) Reinforcement implemented in 2015 (Pictures from SNCF-AREP by M. L. Vigneau).

Riveted lattice purlins and rafters in train shed roof structures are made of wrought iron or mild steel and commonly consist of flats and angles assembled with single-riveted joints. Typically, the web members are flats, clamped at both ends between two angles forming the chord (Fig. 3). Rivets were the primary fasteners used to fabricate connections in metal structures between the 1840s and the 1940s (Collette, 2014). A manufactured rivet is a cylindrical bar of iron or steel with a head, generally in the form of a round cap. The joining technique “hot riveting” consisted of heating the rivet, inserting the rivet into the hole of the plates to be connected, and forming the second head of the rivet by crushing its protruding end. The longitudinal shrinking of the rivet due to cooling induces a clamping force applied by the rivet heads to the plates tightened together.

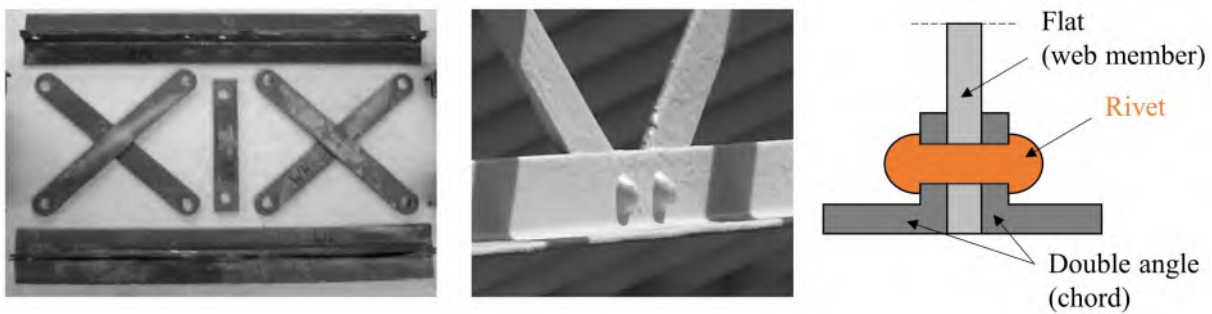


Figure 3 – Typical constructive detailing for riveted lattice girders: (a) flats for the web members and double angles for the chords (Picture from de Bouw, 2010, p. 94); (b) single-riveted joints (Picture from SNCF-AREP); (c) schematic cross-section of a single-riveted joint.

Stability issues concerning riveted lattice girders always correspond to out-of-plane buckling. The girders can be affected locally, through the buckling of web members, or globally, when the buckling of a chord drags along the whole girder (Fig. 4). The assessment of the buckling risk depends strongly on the modelling assumptions and the design criteria.

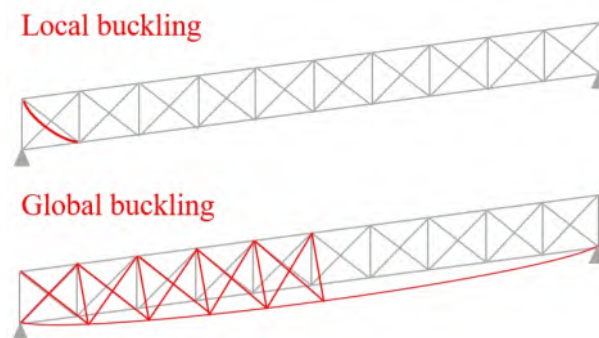


Figure 4 – Schematic view of possible out-of-plane buckling shapes for a lattice girder.

Classically, the buckling of a riveted lattice girder is verified in a way very similar to the design of a modern steel truss:

- A finite element (FE) model of the girder is built, using beam or truss elements for all the bars, to determine the internal loads using a first-order analysis.
- Each member is verified individually against buckling using the buckling curve approach prescribed by Eurocode 3 (EN 1993-1-1, 2005).

Many uncertainties are related to this assessment approach:

- Material properties: which design value for the limit of elasticity f_y should be used for verification?
- Boundary conditions: how do the riveted connections between the chords and the web members behave? In the out-of-plane direction, should they be considered pinned (free to rotate) or rigid (fully transmitting bending moments) for the connected members?
- Buckling verification: when the members are verified individually, what effective length should be used as input? Alternatively, how to take advantage of global analysis methods?

To address those uncertainties, some assumptions are commonly made, but the relevance and validity of these assumptions are questionable. Regarding material properties, mild steel and wrought iron are often likened to modern steel. Even when mechanical tests are carried out on samples of the existing structure of interest, the results are misused or even disregarded. Regarding boundary conditions, riveted joints are usually considered pinned out-of-plane despite the clamped geometry. This leads to conservative effective lengths for buckling verification. The effective length is a key parameter influencing the stability of a compressed bar member, depending on its end conditions. In practice, end connections are neither perfectly fixed nor perfectly hinged. Connections are semi-rigid and can be characterised by their rotational stiffness. Therefore, the out-of-plane rotational stiffness of single-riveted joints plays a decisive role in the assessment of the buckling risk for lattice girders.

To improve the structural assessment of riveted lattice girders and retrofitting operations in French train sheds, it is necessary to address the various uncertainties regarding the buckling risk and also to discuss restoration strategies. This endeavour constitutes an excellent case study for tackling the challenges regarding the structural assessment of existing structures.

Objectives and methodology

The aim of this PhD thesis is to propose a framework for an integrated assessment of riveted lattice girders in French train sheds of 1850-1930. Integrated assessment frameworks have been used in other contexts before, where interdisciplinary research was nec-

essary to address complex problems and provide guidance for decision and policy-making. Typically such frameworks were developed to draft environmental policies. Integrated assessment “is based on the notion that the quality of decisions is improved through broader representation of knowledge and values in the assessment process” (Salter et al., 2010). Thus, the proposed framework for the assessment of riveted lattice girders combines structural engineering, history of engineering and construction, and heritage studies, and shall provide a robust basis for elaborating structural interventions that are as non-invasive as possible (Fig. 5). Meeting economic, ecological and heritage challenges, this framework shall help develop a committed restoration strategy or even *policy* for restoring train sheds. Beyond this specific application, the ambition is to set the basis of an integrated assessment framework that can be extended to iron and steel structures of the 19th and early 20th centuries, and virtually to most types of existing structures.

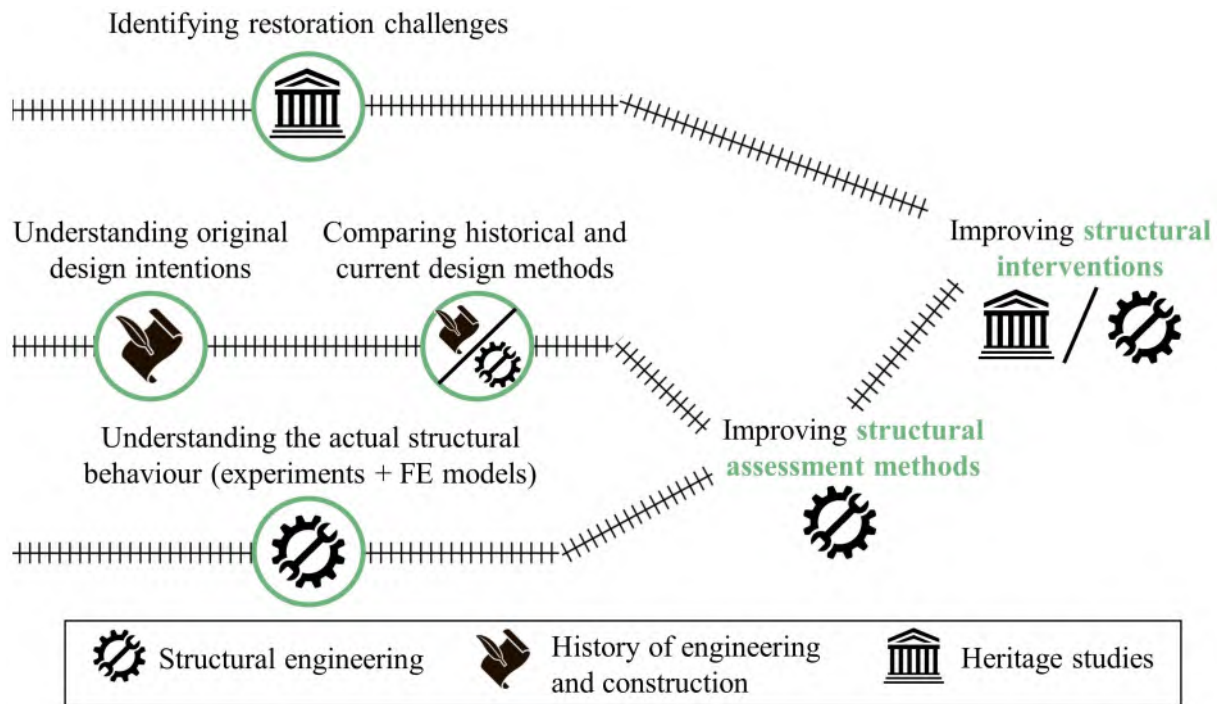


Figure 5 – Integrated assessment framework applicable to riveted lattice girders.

The main research question this thesis attempts to answer is: **“How can riveted lattice girders be assessed to use their full capacity while preserving their heritage value?”**

The proposed integrated assessment framework is structured around three parts. **Part I** answers the question “What shall be preserved, how and why?”, which is an essential preamble to structural assessment. We call this step “Identifying restoration challenges” because it consists of determining the criteria on which the restoration strategy should be based to best preserve the authenticity of the structure. For this purpose, significant structural features are identified and restoration practices are reviewed to assess the

impact of architectural choices or structural interventions. **Parts II and III** focus on improving structural assessment methods, answering the question: “How can the load-bearing capacity be assessed in a more meaningful and context-based manner?”. **Part II** deals with “Refining structural analysis assumptions”, which consists of determining which modelling assumptions are subject to uncertainty and trying to resolve some uncertainties. New insights are acquired by bringing together knowledge from original design intentions and a literature review on the one hand, and by extending knowledge based on experiments and numerical studies on the other hand. **Part III** is about “Adapting verification methods”. Verification methods used by default for structural assessment are discussed to make out how they can be adapted to become more tailored to historic structures. Historical knowledge is used to enhance the limitations of current design criteria. Together, the methodological steps carried out in **Parts I, II, and III** shall contribute to better adapted retrofitting operations. All three parts aim to reduce structural interventions, either by helping to integrate the preservation of the structure into the restoration strategy or by increasing the assessed capacity of the structure. If structural interventions are really necessary, **Part I** points out which interventions are acceptable from a heritage point of view, while **Parts II and III** can help elaborate interventions that are optimised from a structural point of view.

The scope of the study is limited by several boundaries. Firstly, the framework applies to healthy structures. The assessment of deterioration or damage (corrosion, deformations...) and its integration into the modelling is left out of the study. Indeed, in practice, when structural members are in bad condition, they are either repaired or replaced. They are then treated as healthy members in calculations. Secondly, the framework applies to structures that can only be assessed by calculation. Where an assessment based on past performance can be carried out, no interventions are necessary and one does not need to recur to the framework. Assessment based on past performance is, however, rarely carried out in practice, which may be due to doubts regarding the reliability of old structures designed with different requirements than the current ones. Thirdly, the framework applies to structures that are assessed following the Eurocodes. The proposed philosophy is valid also for assessment with other types of standards. However, the verification methods discussed in Part III are adapted from the Eurocodes.

Throughout the manuscript, a concrete case study is used to demonstrate the approach. The train shed of Montauban was built in 1903 by contractor Daydé et Pillé and retrofitted in 2012 by SNCF. In the framework of the restoration, the lattice purlins were reinforced. The assessment of those lattice purlins is used as a practical example. Calculations deal in more detail with the purlin experiencing the highest load (Fig. 6).

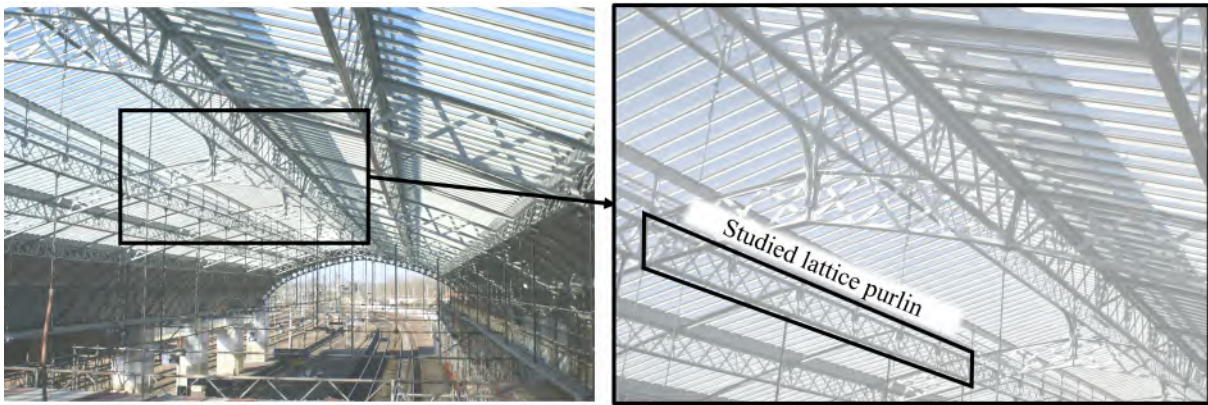


Figure 6 – Train shed of Montauban, with a view of the lattice purlin assessed in detail for the case study, Montauban, France (Pictures from SNCF-AREP).

Thesis outline

The outline of the thesis corresponds to the steps of the proposed assessment framework and is summarised in Fig. 7. Each of the three parts contains two or three chapters.

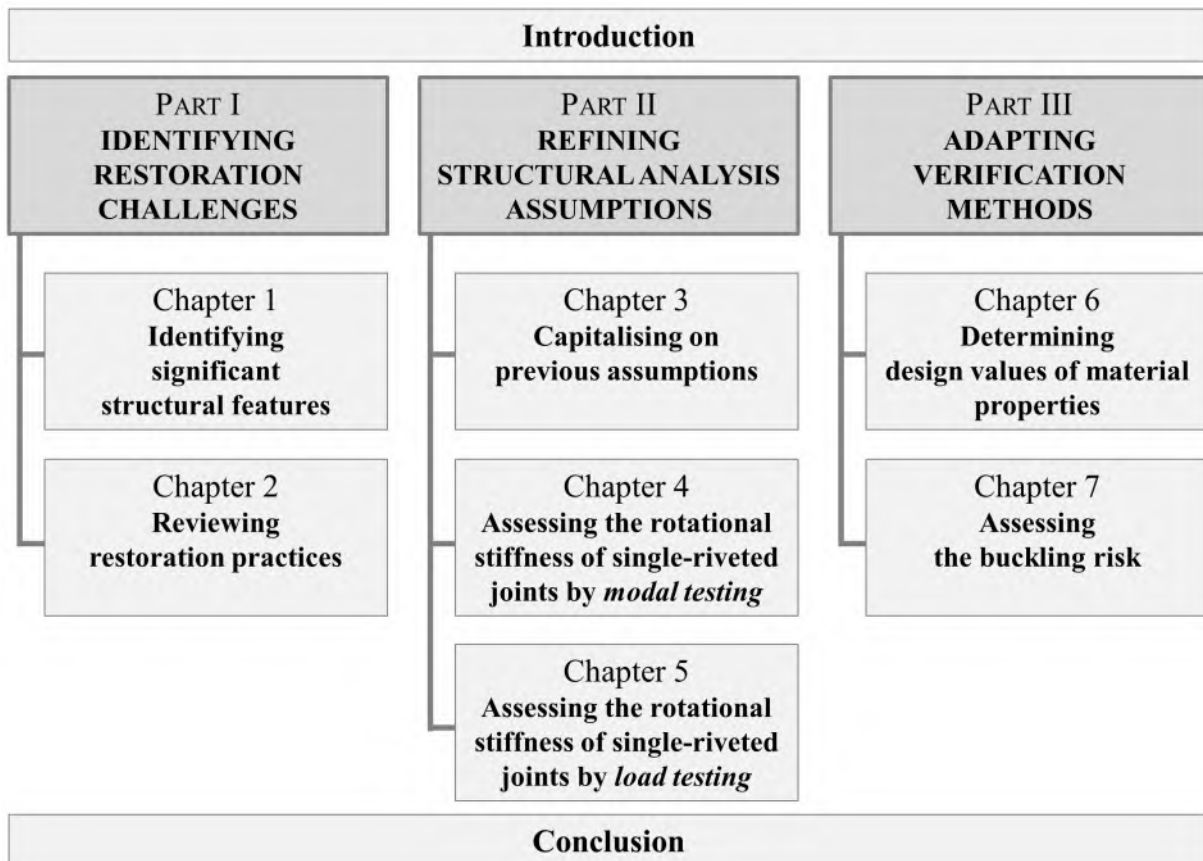


Figure 7 – Outline of the thesis' main parts and chapters.

Chapter 1 discusses the significance of various structural features of train sheds from the perspective of engineering history. It highlights the heritage value of riveted lattice girders and makes out how the structure should be preserved to keep its authenticity. **Chapter 2** gives insight into structural interventions related to train shed restorations. It discusses how architectural decisions impact the metal structure of train sheds. In particular, it shows how strengthening measures affect the structural authenticity of lattice girders.

Chapter 3 capitalises on historical and more recent literature to discuss modelling assumptions for structural analysis. The evolution of structural analysis methods for lattice girders and knowledge regarding the deformation behaviour of riveted connections are critically summarised. A case study is then conducted to illustrate the consequences of historical and recent approaches. **Chapter 4** presents experimental and numerical investigations carried out on a reclaimed riveted lattice girder, aiming to assess the rotational stiffness of single-riveted joints by modal testing. Both the average stiffness of all similar joints and local variations of joint stiffness are studied. **Chapter 5** presents load tests carried out on a twin specimen to validate and complement the results from modal testing.

Chapter 6 discusses how to determine design values for the yield strength of wrought iron and mild steel, based on material surveys, historical archives or literature. **Chapter 7** compares how the buckling risk of iron and steel members was originally taken into account in the design of metal constructions, especially train sheds, and how it is assessed today in accordance with Eurocode 3. It enhances the limitations of the buckling verifications according to Eurocode 3.

The conclusion chapter summarises the main findings regarding riveted lattice girders, enhances the methodological contributions of the thesis and discusses the perspectives for future work.

PART I

**IDENTIFYING RESTORATION
CHALLENGES**

IDENTIFYING SIGNIFICANT STRUCTURAL FEATURES

Chapter 1 discusses the significance of various structural features of train sheds, especially riveted lattice girders, to make out how the structure should be preserved to retain its authenticity. The study confronts the inventory relying on a photographic survey and archival plans with the history of iron and steel construction and the history of railway development.



Detail of a lattice purlin in the train shed of Montauban, France (Picture from SNCF-AREP).

Contents

1.1	Train sheds and heritage recognition	16
1.2	Methodology	17
1.3	Significance of the main “architectural” features	21
1.4	Significance of riveted lattice girders	26
1.5	Conclusion	32

In order to elaborate a sound restoration or transformation strategy, it is essential to determine which structural features are significant from a heritage point of view and need to be preserved or enhanced. Indeed, “authenticity” has become the guiding star of heritage preservation (Mager, 2016). A train shed restored in an “authentic” manner should truthfully convey its “cultural significance” through its “material attributes” (ICOMOS, 2011). However, as Mager pointed out, authenticity remains a blurry concept and must be found and defined anew in each case. The aim of this chapter is, therefore, to discuss what makes up the structural authenticity of train sheds, in order to integrate it as a criterion for heritage-friendly restorations. The chapter starts with some background on the heritage recognition of train sheds and a description of the dataset used for the analyses. It then gives an overview of the specificities of train sheds’ metal roof structures, focusing first on the main “architectural” features. Riveted lattice girders are finally dealt with in particular detail, as they have been largely neglected in the literature until now. Chapters 1 and 2 are derived from a published article (Franz et al., 2023a).

1.1 Train sheds and heritage recognition

In France as in other pioneering countries of metal construction, train sheds built in the 19th and early 20th century were used by railway companies as showcases of their prestige and economic success (Lemoine, 2022, p. 146). Train sheds primarily had the function of covering railway tracks and platforms, but they were also designed to impress travellers. Through their metallic roof structures, they had to be “striking examples of refined technology” (Meeks, 1956, p. 86) and give a taste of the new industrial aesthetics.

Rail passenger transport developed in France from the end of the 1830s. For the structure of the first train sheds built in the 1840s and 1850s, iron was in competition with timber. Metal structures were then prevalent until the end of the 1920s, when reinforced concrete became representative of a new modern age. With very few exceptions, French metallic train sheds were built between 1850 and 1930. Many were destroyed by fire, by war or by necessity, but about 40% have been preserved and are still in service.

The first measures of statutory protection for railway stations were granted in the 1970s, but only for a handful of prestigious mainline stations, mostly in Paris, and for architectural elements related to the station buildings (Smith, 1999, Striffling-Marcu et al., 2022). Today, 72% of French train sheds enjoy some form of heritage protection (Emile et al., 2020). It was primarily thanks to the development of the notion of industrial heritage in France in the 1980s (Gasnier, 2011) that train sheds were considered with new interest and became associated with heritage values. Heritage values formalised by Aloïs Riegl in 1903 (Riegl, 1903) can be used to assess load-bearing structures (Eberhardt et al., 2022)

and industrial heritage (Gasnier, 2019). Train sheds have a strong *use value*, that was continuously present throughout their existence, and from the 1980s they regained their original *symbolical value* and acquired *historical and creative values*, from technical and artistic points of view. However, even though train sheds were acknowledged as engineering feats from the time of their construction, they were mostly studied and valued for their architecture (Meeks, 1956; Krings, 1985; Kanai, 2005). This is why an assessment of the heritage value with a focus on structural aspects is needed.

1.2 Methodology

The study is based primarily on surviving French historic metallic train sheds. It builds upon and extends the survey conducted by the heritage department of AREP. Defining train sheds as structures with a single span, railway stations feature either single sheds or several adjacent sheds. Applying this definition, preserved French metallic train sheds built between 1850 and 1930 constitute a broad dataset of about 90 sheds, distributed across the French mainland as shown on the map in Fig. 1.1. The number 90 differs from the 75 surviving train sheds mentioned by Emile et al., 2020. This is due to the fact that the present study does not count a train shed with multiple spans as just one shed, it counts the spans individually. Moreover, here, only metallic train sheds are considered, excluding train sheds in concrete or timber.

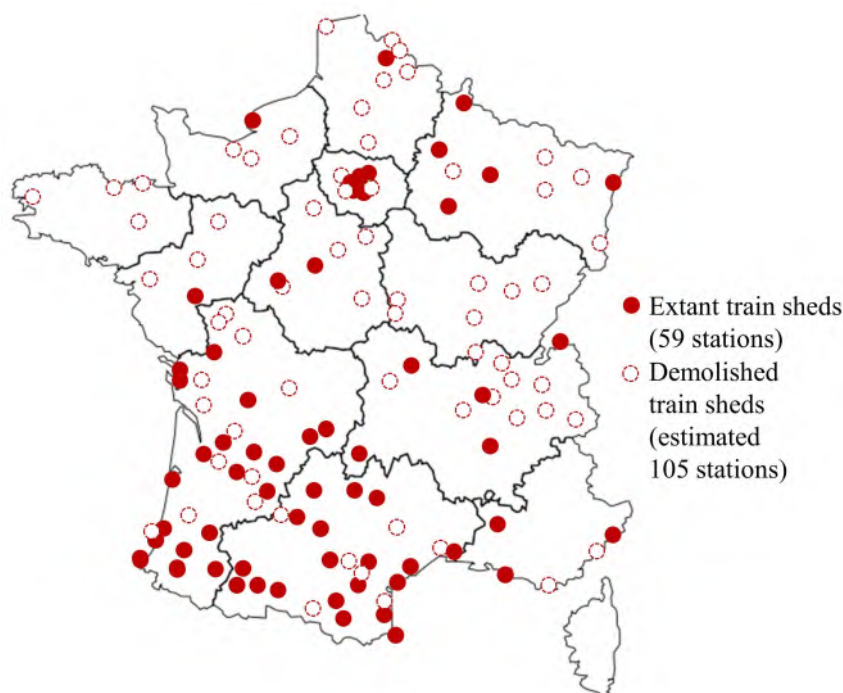


Figure 1.1 – Map of France showing extant and demolished metallic train sheds (Map from SNCF-AREP, heritage department).

To make an inventory of the structural specificities of surviving train sheds, the most useful documents were photographs and historical plans of the metal structure. These documents were mainly gathered from the project server of AREP and also from historical studies of individual train sheds, that had been compiled by AREP’s heritage department since its creation in 1997. However, a lot of interesting archive documents are detained by other entities within SNCF, for example regional engineering offices, which made the gathering of data more difficult. It was possible to obtain relevant historical and more recent archive material from local subsidiaries for eight railway stations. Additionally, historical archive documents were consulted at the national SNCF archive centre in Le Mans. This centre was created in 1995, with the purpose of bringing together all the historical archives of SNCF. Before 1995, the historical archives were kept, at best, in regional archive centres. In the historical studies provided by AREP or other SNCF entities, many of the scanned historical plans were indeed coming from regional SNCF archive centres. However, according to Bowie, 2009, ancient building plans of railway stations used to be kept on-site at the various stations because of continuing operational use, which delayed or prevented their transfer to an archive centre. Given the vast amount of data to be collected, the centralisation process in Le Mans is still ongoing and most of the archives are only summarily inventoried (Zuber, 2009). After two days of consultation of documents related to ten pre-selected railway stations, relevant plans or notes were found only for two of them.

The archival data from surviving train sheds was enriched by technical information or illustrations found in historical sources, especially civil engineering periodicals from the time of construction of train sheds, such as *Nouvelles Annales de la Construction*, *Annales des Ponts et Chaussées* and *Le Génie civil*. These periodicals were readily available from the website Gallica powered by the Bibliothèque nationale de France (« Gallica - Bibliothèque nationale de France », 2023). Translated quotations from historical sources in French or German are marked as [transl.] in the whole manuscript.

Tab. 1.1 provides a detailed list of all surviving metallic train sheds and the available documents that served constituting the database. Train sheds are classified in alphabetical order, according to the name of the corresponding railway station. When one railway station features multiple train sheds, whether joined or not, each shed is described with a distinct additional name, corresponding to the french name used within SNCF. “Halle BV” (BV = “bâtiment voyageur”) designates the shed adjacent to the station building. The year of construction is indicated in the first column. Two categories of relevant documents are listed in the table: [1] historical studies compiled by AREP’s heritage department, or in some cases by other SNCF entities, and [2] historical plans from the time of construction. For many train sheds, there was almost no documentation available. Photographs, even of

poor quality found on the Internet, have made it possible to include almost all the train sheds in the inventory.

Table 1.1 – List of surviving metallic train sheds from the period 1850-1930, with documents gathered as a database for the inventory of structural specificities: [1] historical studies and [2] original plans.

Railway station	Train shed (when multiple)	Year	[1]	[2]
Agen	-	1866	●	●
Angoulême	-	1886	●	
Aurillac	-	1912		
Avignon-Centre	-	1866	●	●
Bar-le-Duc	-	1904	●	
Bayonne	-	1868	●	
Bédarieux	-	1903		●
Bergerac	-	1912		
Béziers	-	1875	●	
Blois-Chambord	-	1890		
Bordeaux Saint-Jean	-	1898	●	●
Brive-la-Gaillarde	Halle BV	1893	●	
Brive-la-Gaillarde	Halle 2	1914	●	
Cahors	-	1885	●	
Capdenac-Gare	-	1884		
Carcassonne	-	1888	●	
Castelnaudary	-	1885		
Castres	-	1896		
Cerbère	-	1884		
Charleville-Mézières	Halle BV	1920	●	
Charleville-Mézières	Halle 2	1920	●	
Charleville-Mézières	Halle 3	1920	●	
Coutras	-	1861		
Cholet	-	1905		
Dax	-	1893	●	
Etampes	-	1879		●
Evian-les-Bains	-	1908		
Foix	-	1902		
Hendaye	-	1880	●	●
La Rochelle	-	1922	●	●
Lannemezan	-	1903		
Le Havre	-	1882		●
Libourne	-	1869		
Lille-Flandres	-	1891	●	

Table 1.1 – *(continued)*

Railway station	Train shed (when multiple)	Year	[1]	[2]
Lourdes	-	1887		
Lyon Perrache	Grande halle	1857	●	
Lyon Perrache	Halle St-Etienne	1885	●	
Marmande	Halle BV	1886		
Marmande	Halle 2	1886		
Marseille Saint-Charles	-	1896	●	
Montauban	-	1903	●	●
Mont-de-Marsan	-	1903		
Montréjeau	-	1900		
Narbonne	-	1888		
Nice-Ville	Halle BV	1867	●	
Nice-Ville	Halle 2	1928	●	●
Niort	-	1856		
Pamiers	-	1903		
Paris Austerlitz	Grande halle	1869	●	●
Paris Est	Hall d'Alsace	1850	●	●
Paris Est	Quai transversal	1931	●	●
Paris Est	Hall Saint-Martin	1931	●	●
Paris Lyon	Hall 1 (côté galerie des fresques)	1897	●	●
Paris Lyon	Hall 1 (côté rue de Bercy)	1897	●	●
Paris Lyon	Hall 1 (Halle du Train Bleu)	1902	●	●
Paris Lyon	Hall 2 (Halle à chiffres)	1927		
Paris Nord	Grande halle	1864	●	
Paris Nord	Halle Eurostar	1864	●	
Paris Nord	Halle Transilien	1864	●	
Paris Saint-Lazare	Salle des pas perdus	1854	●	
Paris Saint-Lazare	Halle 1	1888	●	●
Paris Saint-Lazare	Halle 2N	1888	●	●
Paris Saint-Lazare	Halle 2V	1851	●	●
Paris Saint-Lazare	Halle 3N	1888	●	●
Paris Saint-Lazare	Halle 3V	1853	●	
Paris Saint-Lazare	Halle 4A	1851	●	
Paris Saint-Lazare	Halle 4B	1932	●	
Paris Saint-Lazare	Halle 4C	1843	●	
Paris Saint-Lazare	Halle 4N	1888	●	●
Paris Saint-Lazare	Halle 5N	1888	●	●
Paris Saint-Lazare	Halle 5V	1843	●	

Table 1.1 – (continued)

Railway station	Train shed (when multiple)	Year	[1]	[2]
Paris Saint-Lazare	Quai transversal	1920	●	
Pau	-	1868	●	
Périgueux	-	1860		
Perpignan	-	1896	●	
Puyoô	-	1890		
Rochefort	-	1905	●	
Rodez	-	1906		
Saint-Germain-des-Fossés	-	1902		●
Sète	Halle BV	1913		
Sète	Halle 2	1913		
Strasbourg	Halle BV	1883	●	
Strasbourg	Halle 2	1883	●	
Tarbes	Halle BV	1877		
Tarbes	Halle 2	1877		
Toulouse-Matabiau	Halle BV	1864	●	
Toulouse-Matabiau	Halle 2	1895	●	
Tours	Halle 1	1898	●	●
Tours	Halle 2	1898	●	●
Troyes	-	1895	●	●
Tulle	-	1903		●
Valence-Ville	-	1903	●	●

The significance of the investigated structural features is discussed based on the history of iron and steel construction and railway development.

1.3 Significance of the main “architectural” features

1.3.1 Principles of a roof structure

The principles of historic metallic train sheds are very similar to traditional timber roofs (Fig. 1.2). In plan, the layout of the structure is usually in the form of a rectangle, sometimes slightly distorted, if the station lies in a curve. The primary structural elements are the main roof trusses, which facilitate the span. They usually rest on columns or on the wall of the station building, except for some roof truss typologies starting from the ground. Within the roof trusses, the rafters are the elements following the straight or curved shape of the roof. Purlins are the girders spanning between the roof trusses, in the

longitudinal direction of the train shed. Roof loads, including the weight of the roofing, snow and wind, are either directly transmitted to the purlins or to intermediate elements spanning between the purlins. Additionally, a skylight sometimes follows the ridge of the roof, with a structure supported by the roof trusses. At both extremities of a train shed, glazed gables can also physically close the volume under the roof. Roof trusses, skylights and glazed gables are structural components, yet they were often described in the literature as architectural features, because they outline the architectural form. The discussion around structural specificities starts with those elements.

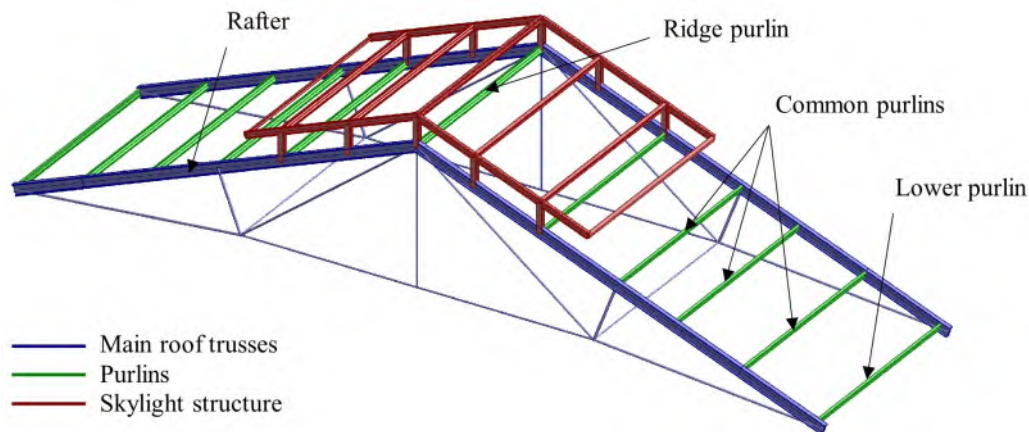


Figure 1.2 – Schematic view of a metallic roof structure with designation of relevant structural elements.

1.3.2 Roof trusses

In the 19th century, the main challenge in the structural design of a train shed concerned the roof trusses. Therefore, both historical and more recent literature tend to reduce the structure of train sheds to their roof trusses. Their typologies have been extensively described classified according to different criteria. A distinction was made between trusses with or without tension ties (Cordeau, 1901), trusses with straight or bent components (de Bouw, 2010) or trusses inspired by the principles of traditional timber trusses or of stone arches (Schädlich, 2015). Many types of roof trusses were developed, and despite mutual influences of European countries, different types were favoured in France, the United Kingdom or Germany (see Fig. 1.3). This was partly due to the nationality of the inventors: the two Frenchmen Polonceau and de Dion for the eponym trusses, the English Turner for the sickle girder, and the German Schwedler for the 3-hinged arch (Kanai, 2005). Regarding surviving French train sheds, the heritage department of AREP identified that four main types of roof trusses prevailed: Polonceau trusses, de Dion trusses, triangulated trusses and arches (Fig. 1.4a). Arched roofs are a minority in France, double-pitched roofs are the rule. Polonceau trusses, the stages of development of which can be witnessed through the various sheds at the Gare Saint-Lazare in Paris (Belhoste, 1999),

were by far the most popular, because they were rational and economic (Holzer, 2010). They were easy to calculate and necessitated less material. However, the prevalence of Polonceau trusses decreased with time. Thanks to the widespread distribution of basic rolled profiles from the 1870s, riveted triangulated trusses became more economic than Polonceau trusses that required the manufacturing of special components for their radial struts and for the connections of struts and ties. Also, the tension ties of Polonceau trusses were deemed unaesthetic, cluttering up the interior space, so that other alternatives such as triangulated trusses or de Dion trusses were favoured (Lemoine, 1986, p. 76). Polonceau trusses are still represented in about half the extant sheds (Fig. 1.4b). As opposed to France, many German train sheds were built with arches starting from the ground, featuring 2 or 3 hinges, and no tension chord (Weller et al., 2006). The 3-hinged arch was the dominant system in German train sheds until World War I, because it was statically determinate, thus easy to calculate, and could cover very large spans.

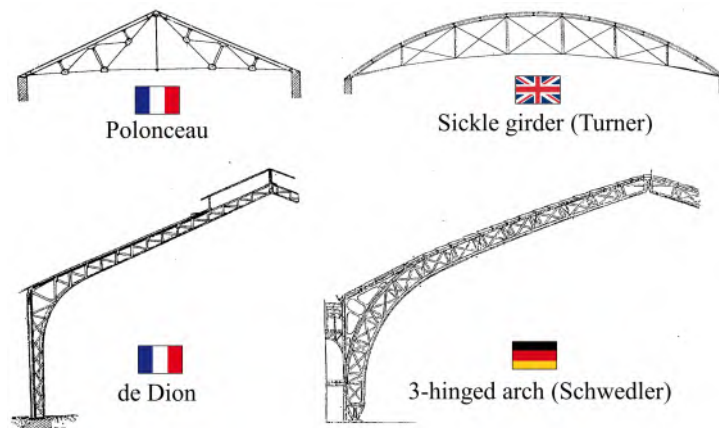


Figure 1.3 – Examples of roof truss typologies favoured in different countries, with the name of their inventor (Pictures from Cordeau, 1901, pp. 222–333).

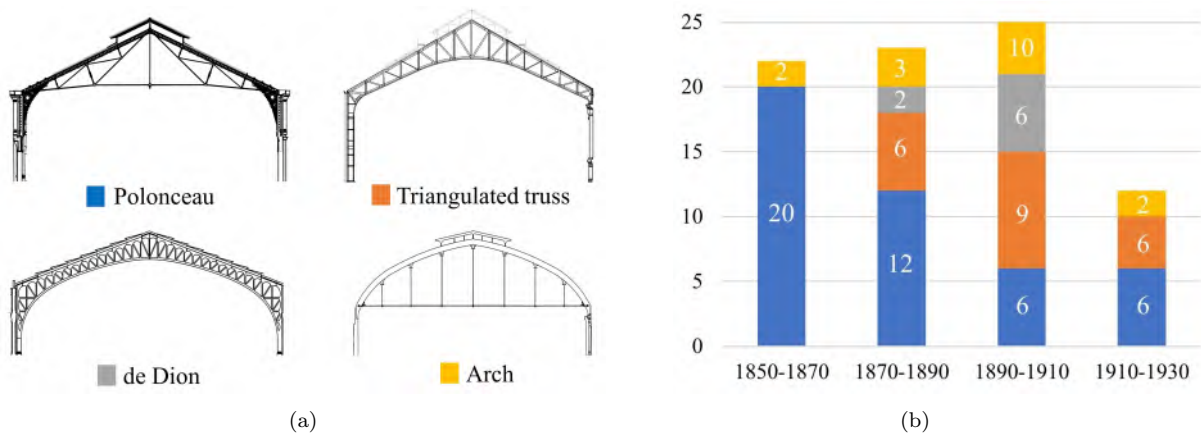


Figure 1.4 – (a) Typologies of roof trusses used for French train sheds (Drawings from SNCF-AREP, heritage department); (b) Number of sheds of each type built in France in 20-year periods ranging from 1850 to 1930.

Within France, some regional preferences existed regarding roof truss typologies, due to the system of private railway companies. Railway stations were distributed throughout the country according to the star-shaped network centred on Paris, defined in 1842. From the beginning of passenger transport, the lines of national interest were conceded to private companies. At the end of the 1850s, six major companies emerged, which did not merge until the creation of SNCF in 1937 (Lemoine, 2022, p. 58). The map on Fig. 1.5 shows surviving railway stations with metallic sheds, according to the company they were built by (by order of creation: Compagnie du Paris-Orléans, Compagnie des Chemins de fer du Nord, Compagnie du Midi, Compagnie des chemins de fer de l'Est, Compagnie des chemins de fer de l'Ouest, Compagnie du PLM (Paris-Lyon-Méditerranée). The railway companies were commonly referred to with their short name, as “le Paris-Orléans”, “le Nord”, etc.).

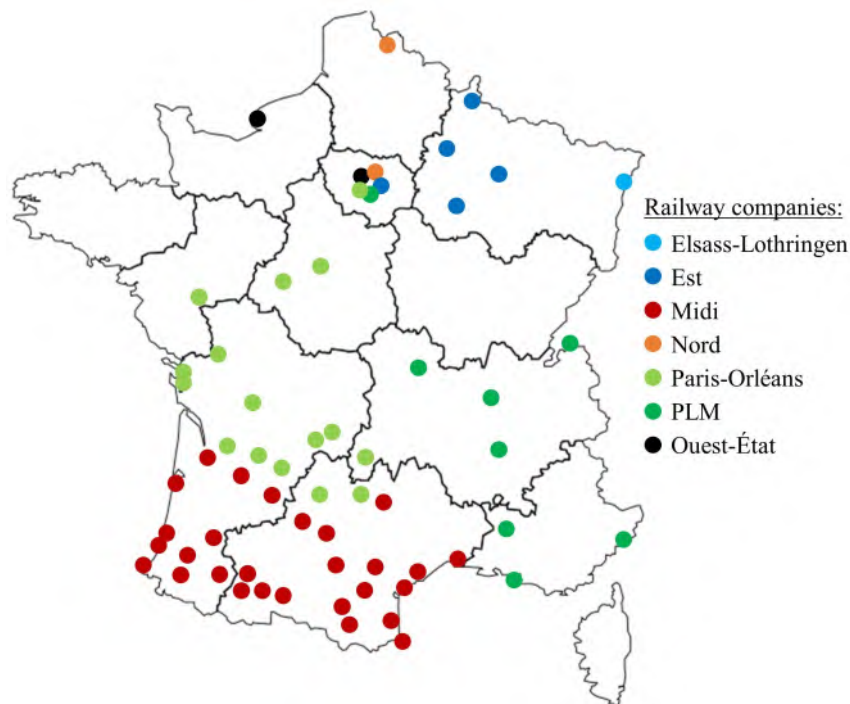


Figure 1.5 – Map of surviving railway stations with a metallic shed, according to their original railway company (Map from SNCF-AREP, heritage department).

For the sake of speed of execution and profitability, each company built series of similar station buildings and train sheds on their network, which contributed to creating a territorial identity (Lemoine, 2022, p. 157). Roof trusses constituted a major architectural feature and were, therefore, key to this territorial identity. As an example, in the South-West of France, the Compagnie du Midi commissioned a series of train sheds with pointed truss arches, with or without tension chord, that is still well-preserved. The train shed of Montauban, from our case study, belongs to this series (Fig. 1.6).

Beyond the type of roof truss, differences between France and other countries are also



Figure 1.6 – Series of similar train sheds (Pictures from SNCF-AREP): (a) Gare de Montauban, full view, Montauban, France; (b) Gare de Bédarieux, full view, Bédarieux, France.

revealed by the spans. Fig. 1.7a shows the largest spans of roof trusses for train sheds built between 1840 and 1940 in France, Germany, the United Kingdom and the United States, according to their date of construction. The dataset was gathered from different sources and comprises railway stations both surviving and demolished: 83 French stations (SNCF data and Kanai, 2005, pp. 205–207), 37 German stations (Krings, 1985; Werner et al., 1992; Weller et al., 2006), 23 English stations and 29 American stations (Meeks, 1956). With a box and whisker chart, Fig. 1.7b underlines the fact that the spans in France were significantly smaller, while the longest spans were built in the United States. This could be interpreted as French designs being more inclined towards delicacy than monumentalism. However, the ratio of height compared to width was higher for French train sheds than English ones: the French had a taste for height as a factor of grandiosity, which could have originated in the French gothic cathedrals (Kanai, 2005, pp. 242–273).

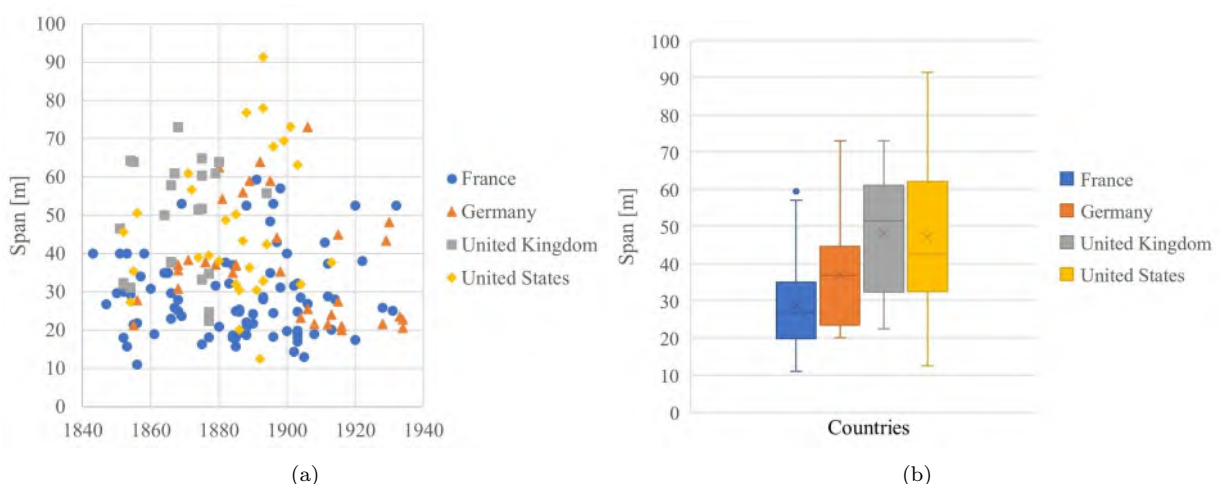


Figure 1.7 – (a) Largest spans featured by sheds of railway stations built between 1840 and 1940 in France, Germany, United Kingdom and United States, according to the date of construction; (b) Statistical distribution represented as box-and-whisker chart.

Regarding heritage assessment, roof truss typologies are useful because their charac-

teristics are easy to gather from photographs or plans and extensive literature is available. They are a good indicator of heritage value, based on criteria such as their span, their degree of ornamentation or whether and how much they conform with main types or not.

1.3.3 Skylights and glazed gables

Next to roof trusses, skylights and glazed gables are structural elements contributing greatly to the architecture of train sheds. While the roofs of train sheds provided shelter against sun and rain, skylights along the ridge (Fig. 1.8a) ensured the evacuation of locomotive smoke and glazed gables (Fig. 1.8b) prevented excessive wind from being engulfed inside the shed. Skylights were commonly used for ventilation purposes in other types of metallic halls such as market and industrial halls (Lemoine, 1986). The structure of glazed gables consisted first of a metallic frame directly supporting the glass panels. The vertical bars of the frame had to transmit the horizontal wind loads to the roof girders on the top and to a trussed girder at the bottom. This bottom girder also supported the weight of the glazing. As skylights and glazed gables had clear functional roles when they were constructed, their preservation is important for the authenticity of train sheds.



Figure 1.8 – (a) Skylight along the ridge (Gare d'Evian, Evian, France) (Picture from SNCF); (b) Glazed gable (Gare de Tours, Tours, France) (Picture from H. Franz).

1.4 Significance of riveted lattice girders

1.4.1 Beams or trusses?

In roof structures, riveted lattice girders were mostly used as rafters or purlins, which are secondary structural elements compared to the main roof trusses. As such, they have been largely neglected by the literature. However, they are key witnesses to the advances and compromises made by iron and steel construction in the second half of the 19th century. The survey of surviving train sheds revealed that about 70% of them feature lattice girders. The *historical*, *scientific* and *technical* values of riveted lattice girders lie

in the fact that they are a blend of rationality and practicality. On the one hand, they were inspired by bridge designs, which benefited from the development of structural analysis, especially truss theory. On the other hand, they were designed as beam equivalents (Rinke et al., 2010). In metal roof structures, riveted lattice girders were a competitor to solid-web girders, made either from rolled sections or from plates riveted together. Rolled sections had the advantage of being easy to manufacture and of making structural calculations straightforward. Riveted solid web girders required more manufacturing effort but offered more flexibility in height. Lattice girders were even more advantageous in terms of design possibilities. Also, they necessitated a lower quantity of material and of rivets and were easy to transport and to assemble on site (Werner et al., 1992, p. 139).

This study considers only lattice girders made of flat and angle bars assembled by single rivets, which were the easiest to manufacture, compared to more complex assemblies. Regarding their dimensions in surviving French train sheds, lattice girders with single-riveted joints are used for purlins with a span ranging from 3.3 m (Gare de Lyon Perrache, halle Saint-Etienne) to 15.4 m (Gare de Marseille St-Charles), but they are mostly used for purlins with a span exceeding 8 m. Lattice rafters in Polonceau trusses are longer, going from 10 m long (Gare d'Evian) to 28 m long (Gare de Paris-Austerlitz). However, considering the single or multiple intermediate supports provided to rafters by compression struts in Polonceau trusses, the free span of lattice rafters ranges from about 5 to 7 m. The geometric slenderness of lattice girders (length-to-height ratio) ranges from about 20 to 30 for lattice purlins and from 10 to 15 for straight lattice rafters. The relative sturdiness of lattice rafters compared to lattice purlins may be due to the fact that purlins work only in bending while rafters also work in compression.

Riveted lattice girders display a wide variety of geometries based on a narrow range of basic elements. The typologies of the web fillings bear witness to the morphological type-based understanding of trusses by designers, as opposed to a structural understanding, as evidenced by Rinke et al., 2013. From the 1850's, truss layouts were classified into formal categories in construction and engineering handbooks, e.g. in Klasen, 1876 or Cordeau, 1901. This facilitated the use of lattice girders as standard components of metal structures. In French train sheds, based on their web geometry, lattice purlins and rafters fall into 4 categories, that can be named after the inventor of the related truss type: the Town type with or without vertical elements (IXI or X-shaped), the Howe or Pratt type (N-shaped), the Warren or Neville type (V-shaped). Examples are displayed on Fig. 1.9a. Fig. 1.9b details the number of surviving sheds featuring lattice girders, differentiated according to their function. A distinction is made between common, lower and ridge purlins as some sheds feature lattice girders only for the ridge or the lower purlins while all other purlins are rolled sections. Fig. 1.9b shows that the X and IXI types are in the majority, despite

representing a more intricate structural system.

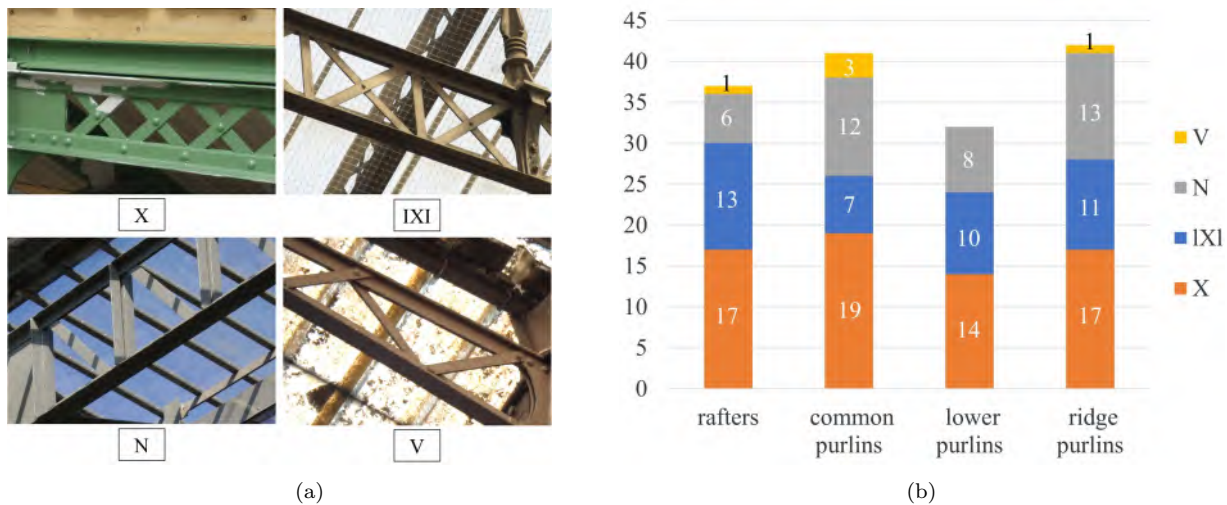


Figure 1.9 – (a) Examples of the 4 types of lattice purlins and rafters: X (Gare de Cerbère, Cerbère, France), IXI (Gare de Paris-Austerlitz, Paris, France), N (Gare d’Etampes, Etampes, France), V (Gare d’Agen, Agen, France) (Pictures from SNCF-AREP); (b) Number of sheds featuring rafters or purlins of each truss type.

In English, the distinction is made between *lattice girders* and *trusses*. The same applies to German, with *Gitterträger* vs. *Fachwerk*. In today’s understanding, *trusses* correspond to triangulated structures with pinned joints, which makes them statically determinate structures. *Lattice girders* are rather seen as girders with web openings. In French however, the same word *treillis* is used for both objects. The name “poutres treillis” used in French to designate “lattice girders” reflects a certain state of confusion. When extrapolated to the scale of bridge girders, lattice girders leave no doubt that they are no trusses, because the web becomes a crisscross of multiple diagonals (Fig. 1.10). The confusion arises at the scale of purlins or rafters, where fewer web members are needed to bind the chords and, therefore, lattice girders take the appearance of a truss. This may point out the *technical* value of riveted lattice girders: those structural components were a miniature transpose of bridge systems, and through this downscaling, their structural nature changed. Therefore, it can be argued that lattice girders used in roof structures are constructs, resulting rather from practical experience than from rational design.

1.4.2 Ornamental role

Riveted lattice girders also have a definite *aesthetic* value. In France, lattice girders were favoured by designers, because they contributed to giving the structure a light appearance and introduced ornamental patterns. In 1863, an engineer wrote in the journal *Nouvelles Annales de la Construction* about rafters in roof trusses: “when a lattice is used [instead of a solid web beam], it is because economy must be sacrificed to ornamentation” (Mathieu, 1863)[transl.]. In 1864, in the journal *Annales des Ponts et Chaussées*, another



Figure 1.10 – Lattice bridge across the Loire - Pont de Varennes-Montsaureau, built in 1917 (Picture by H. Franz).

engineer opposed “the elegance of a well-designed truss” to “the repulsive appearance of a solid web” (Collignon, 1864, p. 159)[transl.]. The ornamental quality of X and IXI type-beams was sometimes enhanced by the addition of non-structural elements at the crossing of diagonals (Fig. 1.11).



Figure 1.11 – Examples of ornamental additions on lattice IXI-type beams: (a) Gare de Blois, Blois, France (Picture by H. Franz); (b) Gare d’Austerlitz, Paris, France (Picture from SNCF-AREP).

Unlike the ones in France, German metallic train sheds seem to have favoured solid-web girders, thus featuring less ornamental structures, which enhanced their engineering quality compared to their architectural one. This idea was supported by the early Austrian architectural theorist Josef August Lux in 1910 in his work *Engineering aesthetics*: “it is the absolute adequacy and utility, the expression of extreme material economy, of strict intellectual discipline, which secures these creations the right to aesthetic recognition” (Krings, 1985, p. 76)[transl.]. In German train sheds, trusses were rather used for monumental purposes – for example to create 3-dimensional arches like in the railway stations of Bremen, Cologne, Dresden and Leipzig.

In the conclusion of his seminal work on the history and the aesthetics of iron structures, Alfred Gotthold Meyer emphasises that “more than with other materials, the [iron] construction becomes the carrier of the effective form with the intrusive logic of its bar systems, which, instead of closed masses, make *the line* essential” (Meyer, 1907,

p. 184)[transl.]. He goes on: “the most important factors of aesthetics are the great curve of the roof arches and the triangular stiffening of the chords with its rhythmic repetitive pattern”. Thus, Meyer seems to attach as much importance to the *outlines* of a structure, drawn by a roof truss or a skylight, than to the *inner lines* drawn by lattice webs.

Given that French engineers valued lattice girders for their aesthetics, it is surprising that they did not experiment more with web patterns. Because lattice girders were regarded as beam equivalents, Vierendeel argued in 1902 that any web pattern could fulfil the role of transmitting the shear force (Fig. 1.12) and that the architecture would benefit from more ornamental patterns than crossed diagonals (Vierendeel, 1902, 752–755). As Vierendeel pointed out, when more refined fillings had been used, they had not been designed as structural web members. It seems that practitioners did not fully exploit the theoretical tools at their disposal in their design work.

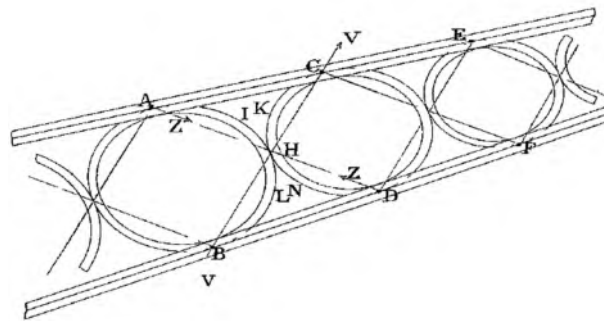


Figure 1.12 – Ornamental and structural web pattern for a lattice girder, suggested by Vierendeel, 1902, Fig. 129.

1.4.3 Construction details

Construction details can contribute to the structural identity of a train shed just as much as the typology of a roof truss. Railway companies regularly employed the same contractors to build several train sheds. Consequently, not only the architectural shape was repeated, but also construction details. This is particularly visible on lattice girders. Taking again the example of the Compagnie du Midi, the contractor Daydé et Pillé built train sheds for at least six railway stations around 1900. When comparing the sheds of Gare de Montauban (our case study) and Gare de Bédarieux, not only the general aspect of their metallic structure is similar (see Fig. 1.6), but several details also appear to be the same. The lattice purlins feature diagonals made out of flat bars with rounded extremities, which is an interesting manufacturing detail. Also, in the three crosses closest to the support, the diagonals pointing downwards towards the support consist of two flat bars instead of one (Fig. 1.13). This last detail was a constructive measure against buckling (see Chapter 7).



Figure 1.13 – Repeated construction details in train sheds built by same contractor Daydé et Pillé (Picture from SNCF-AREP, archive plan from SNCF archives): (a) Gare de Montaubau, detail of a lattice purlin, Montauban, France; (b) Gare de Bédarieux, detail of a lattice purlin from an archive plan, Bédarieux, France.

Gustave Eiffel also worked for the Compagnie du Midi. With his company, Eiffel built train sheds for the railway stations of Toulouse in 1864 and Agen in 1866. Here again, the architecture is very similar between the two sheds. The roof trusses are Polonceau trusses with lattice rafters, which was common at the time. The lattice purlins, however, are very specific to these two sheds. The geometry of their webs corresponds to the Warren (V-shaped) type and the chords are T-sections instead of double angles (Fig. 1.14). Both of these features are unusual in train sheds.



Figure 1.14 – Lattice purlin of the Gare d'Agen, Agen, France (Picture from SNCF-AREP).

Riveted lattice girders also have a *technical* and a *memorial* value through their riveted joints that reflect a practical know-how that has almost disappeared. Rivets were used either to fabricate built-up solid-webbed sections for structural elements such as girders or columns, or to assemble structural elements together. In lattice girders, the single-riveted joints joining chords and web members are single-riveted splice joints under single, double or triple shear. The most common type consists of flat web members assembled between two angles constituting the chords, resulting in a double shear joint. It appears that even the most basic riveted connections offered many possibilities in terms of implementation variants (Fig. 1.15). Compared to bolts, rivets were permanent fasteners and had the advantage of material cheapness and a certain ability to compensate holes misalignment.

However, rivets fell into disuse in the building sector from the 1930s onwards. Bolts became the leading field fastener because of rising labour costs. As to shop fabrication, hot riveting was replaced by the welding technique that generated less additional weight and was more cost effective.

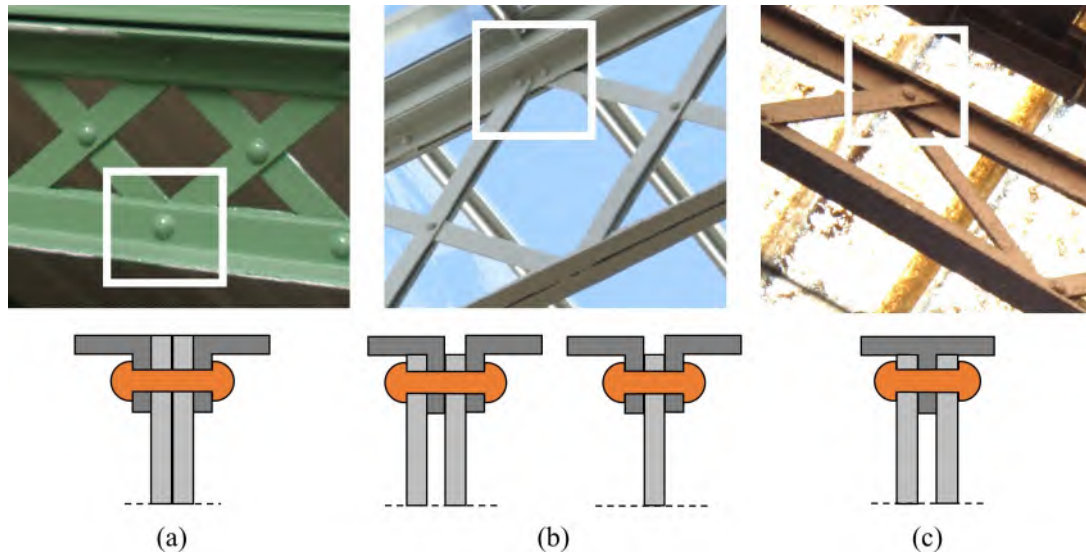


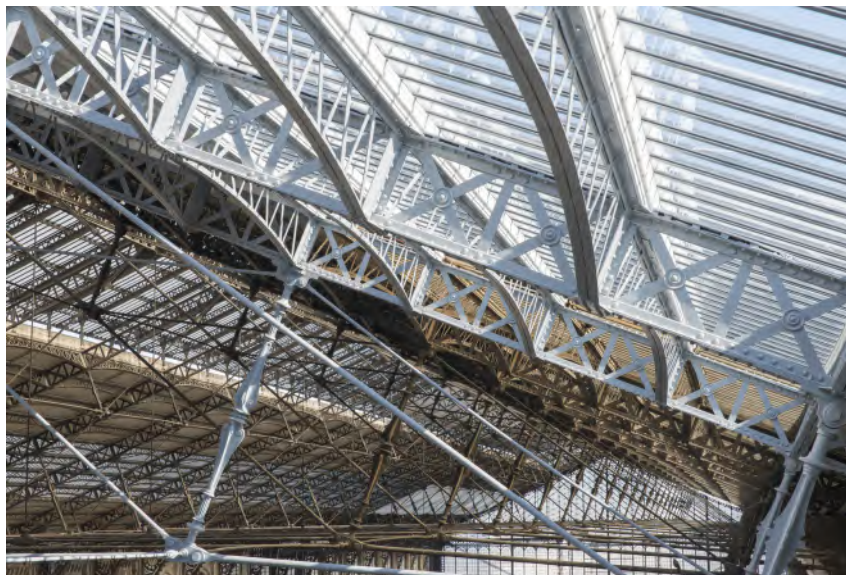
Figure 1.15 – Various configurations of single-riveted joints, with their schematic cross-section: (a) Gare de Cerbère, Cerbère, France; (b) Gare de Montauban, Montauban, France; (c) Gare d’Agen, Agen, France (Pictures from SNCF-AREP).

1.5 Conclusion

Based on an extensive survey of surviving train sheds, this chapter discussed the significance of several structural features of metal structures. The study found that an existing structure benefits from being considered not as an isolated object but as belonging to a family of structures. Roof truss typologies, which are traditionally used to classify the architecture of train sheds, are significant features. They enhance both national preferences, due to the influence of different engineers and different aesthetic tastes in each country, and regional preferences, due to the system of railway companies. However, the study went beyond roof truss typologies, and also underlined the importance of other structural elements outlining the architecture of train sheds, namely skylights and glazed gables. The focus then turned to riveted lattice girders, which bear subtle witness to French construction practice while playing a major ornamental role. Their interest lies not only in the layout of the lattice web, but also in construction details, that can be traced back to the preferences of engineers or contractors. This study helped clarify what conveys structural authenticity in train sheds. The next chapter highlights how its preservation can be integrated into restoration strategies.

REVIEWING RESTORATION PRACTICES

Chapter 2 enhances the impact of restorations on the structure of train sheds. It first traces the evolution of roofing materials, which modify the loading conditions of the structure underneath, and then looks into structural interventions, especially strengthening measures. This overview shall help refine specifications for future restorations.



Railway station Gare d'Austerlitz, Paris, France, under renovation in 2016 (Picture from SNCF-AREP by M. L. Vigneau).

Contents

2.1	Purpose of train shed restorations	34
2.2	Methodology	35
2.3	Roofing materials	35
2.4	Maintenance equipment	46
2.5	Structural interventions	47
2.6	Conclusion	54

Once the heritage value inherent to the structure, especially riveted lattice girders, has been demonstrated, identifying renovation choices leading to structural interventions and how those interventions affect the authenticity is crucial to integrate the preservation of the structure into the renovation strategy. The aim of this chapter is to raise awareness of the impact of train shed restorations on their metallic structure by tracing a history of the restoration practices and shedding light on structural aspects. The evolution of roofing materials in the course of restorations is detailed, stressing the consequences in terms of loading. Structural interventions are then analysed: removal and restoration of skylights and glazed gables, addition of maintenance equipment, and repair and strengthening measures on structural elements.

2.1 Purpose of train shed restorations

Since their construction, preserved train sheds have been regularly restored, every 37 years on average (Emile et al., 2020). Standard restorations involve (Martin-Lebretonchel et al., 2023):

- repairing or replacing the roofing, to restore the water tightness, the luminosity or even the safety;
- repainting the metallic structure to restore the protection against corrosion. In the 20th century, new layers of paint were only added on top of the old ones. In recent restorations, the practice at SNCF has been to strip the metal structure, most often through sandblasting, to get rid of the toxic layer of lead paint that was widely used in the 19th century;
- bringing gutters and downpipes up to standard;
- adding or updating maintenance equipment;
- carrying out structural interventions: repairs, strengthening measures, removal or reconstruction of some parts of the structure.

Until the 1980s, restoration projects focused mainly on maintaining the functional role of train sheds. From the 21st century, train sheds were also acknowledged as a heritage to be preserved. Therefore, recent restorations of train sheds sought to preserve or restore their original appearance. However, architectural choices seem to disregard the potential impact of train shed restorations on their metallic structure. This is also reflected in accounts made in the literature about restorations of historic metallic structures, whether for train sheds or other types of construction. Only some isolated case studies focused on structural interventions and their consequences regarding structural behaviour (Vitzthum et al., 2006; Springer et al., 2012).

2.2 Methodology

For each surviving train shed, information was gathered tracing its life, from its construction to the present day, including intermediary states related to various restorations. The sources of data were the same as for the inventory of structural specificities: AREP's project data, SNCF archives, and historical literature, especially technical periodicals.

When complete, the information gathered for each surviving train shed included: a historical study summarising the life of the corresponding station, a photographic survey, plans and calculation notes for the construction, intermediary restoration projects, and the most recent restoration since 2005, when relevant. There was no train shed for which all this information could be gathered. Consequently, pooling data was extremely valuable, if not necessary, to provide meaningful insights into the history of train sheds. Overall, the study presented in this chapter relies on data gathered from 37 railway stations, corresponding to 43 surviving train sheds. In contrast with the previous chapter, statistics presented in this chapter are based on railway stations rather than on train sheds, because restorations are usually carried out for all train sheds of a railway station at the same time (some exceptions exist, mostly in Paris). The importance of the used dataset varies depending on each study item because of the fluctuating richness of available documentation.

2.3 Roofing materials

Repairing or replacing the roofing was always one of the main purposes of train shed restorations. The impact of roof changes on the metallic structure beneath is imperceptible but significant. The dead loads supported by the structure are modified in an invisible way but have visible consequences in terms of strengthening measures. This section therefore gives an overview of roofing materials used in the original constructions and in restoration projects over time (Fig. 2.1). It also gives an indication of corresponding loads, to highlight the impact on the metallic structure.

From the beginning, train shed roofs had an opaque part and a translucent or transparent part. The ratio between the opaque and the translucent parts was chosen to provide enough luminosity while avoiding a greenhouse effect (Lemoine, 2022, p. 137). This ratio varied a lot amongst different train sheds and was often modified as renovations were undertaken. In the shed of the Gare de Nice, opaque and translucent parts were even inverted in the restoration of 1968. In the following, a clear distinction is made between materials and systems used for the opaque and the transparent parts.



Figure 2.1 – Example of complete replacement of the roofing: aerial view of the restoration of the shed of the Gare de Tulle in 2019, Tulle, France (Picture from SNCF). Right side: old fibre cement panels. Left side: new steel decks and polycarbonate panels.

2.3.1 *Historical evolution of roofing materials*

Throughout the construction period of interest, from 1850 to 1930, the opaque part of original roofs consisted almost always of a zinc roof on timber boarding (see Fig. 2.2a and b) or of corrugated iron sheets. Corrugated iron sheets were lighter and more economical but despite being galvanised, they were sensitive to the corrosive action of locomotive smoke. Some historical sources suggest that railway companies thus preferred zinc roofs protected by their timber boarding (Deharme, 1890; Moreau, 1898). A few train sheds featured slate or tiled roofs.

The translucent part was made of glass, more or less transparent. Archives or periodical articles related to train sheds did not say much regarding the characteristics of the glass. The first train sheds probably used sheet glass made with the cylinder process, following the trend of the famous Crystal Palace built in 1851 (Hollister, 1974; Kefallinos, 2013). The cylinder process consisted of a mass of glass hand-blown into a cylinder, then split open and flattened out. Rolled plate glass was patented in 1847 in England and produced in France by Saint-Gobain from 1854. It was produced by pouring molten glass onto a plate and rolling it into a sheet. Because of its greater thickness, its larger dimensions and its favourable price, it quickly prevailed over sheet glass for the roofing of industrial constructions (Carré, 2010). In 1893, Léon Appert patented wire glass, in France and Germany. Wire glass was produced mechanically, by pouring molten glass, rolling it into a sheet and then rolling wire netting into it. It became a widespread product in the late 1890s (Kefallinos, 2013) and must therefore have been used for the last train sheds built at the beginning of the 20th century (Fig. 2.3a).

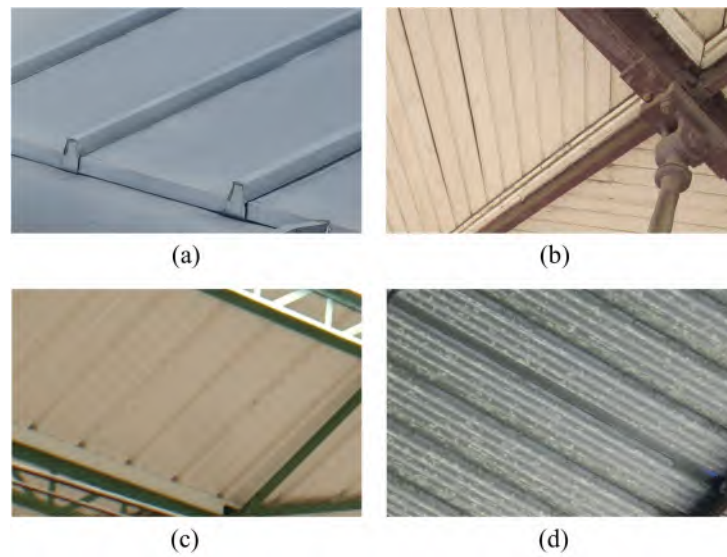


Figure 2.2 – Opaque materials used for roofing (Pictures from SNCF): (a) traditional roll cap zinc roof, seen from above (Gare de Bayonne, Bayonne, France); (b) zinc roof supported by timber boarding, seen from below (Gare de Bayonne, Bayonne, France); (c) steel deck (Gare de Perpignan, Perpignan, France); (d) polyester panels (Gare de Pau, Pau, France).

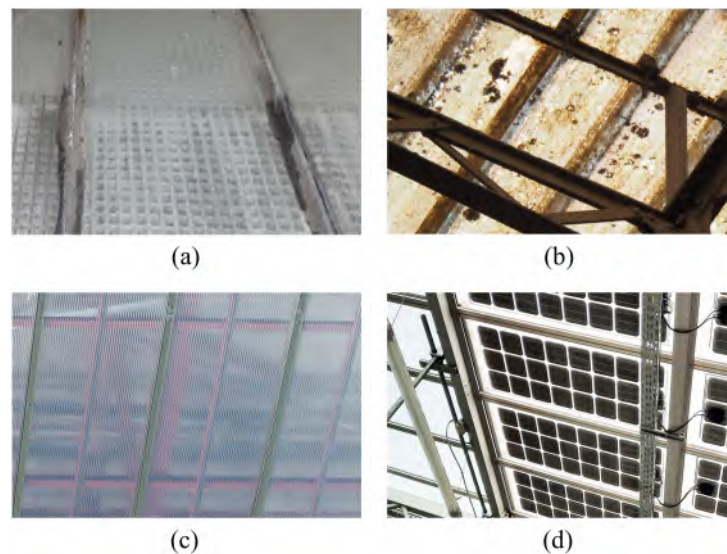


Figure 2.3 – Translucent/transparent materials used for roofing (Pictures from SNCF): (a) wire glass (Gare de Lyon, Paris, France); (b) aged polycarbonate (Gare d’Agen, Agen, France); (c) new polycarbonate (Gare de Tulle, Tulle, France); (d) glass panels with embedded photovoltaic cells (Gare du Bourget, Le Bourget, France).

Little information is available about what happened to roofs of train sheds between the time of their construction and about 1960. However, the survey of historical reports drafted by AREP or other SNCF entities showed that an important wave of train shed restorations took place in the 1970s and 1980s. Tab. 2.1 presents a list of railway stations restored around this time. The dataset accounts for 34 restorations in 33 railway stations (the train shed in Nice was restored twice with a gap of only twenty years). Among the 33 railway stations of the dataset, 28 were renovated between 1970 and 1990. The restoration

dates of the whole dataset range from 1957 to 1995.

Table 2.1 – List of railway stations whose train sheds were restored in the wave of the 1970s and 1980s, with the year of restoration and the materials used for the opaque and translucent roof parts.

Railway station	Year	Opaque roof	Translucent roof
Agen	1970	polyester	polyester
Angoulême	1976	polyester	polyester
Aurillac	1985	steel deck	polyester
Avignon centre	1983	steel deck	polyester
Bayonne	1982	polyester	polyester
Béziers	1974	steel deck	polycarbonate
Blois	1989	zinc	polycarbonate
Bordeaux Saint-Jean	1970	zinc	polyester
Brive-la-Gaillarde	1984	fibre cement	polycarbonate
Cahors	1983	zinc	polyester
Carcassonne	1989	steel deck	wired glass
Dax	1995	zinc	wired glass
Etampes	1971	polyester	polyester
Evian	1957	zinc	wired glass
Hendaye	1980	polyester	polyester
La Rochelle	1972	slates	PVC
Le Havre	1980	slates	polyester
Lille-Flandres	1964	zinc	polyester
Lyon Perrache	1994	steel deck	PVC
Montauban	1971	zinc	polyester
Nice	1968	steel deck	Plexiglas
Nice	1989	steel deck	polycarbonate
Paris Lyon (Hall 1)	1985	tiles	wired glass
Paris Austerlitz	1981	zinc	wired glass
Pau	1965	polyester	polyester
Perpignan	1971	steel deck	polyester
Puyoô	1974	polyester	polyester
Rochefort	1984	slates	Plexiglas
Saint-Germain-des-Fossés	1974	steel deck	Plexiglas
Strasbourg	1984	polyester	polyester
Toulouse	1986	zinc	polyester
Tours	1985	zinc	polyester
Troyes	1985	steel deck	polyester
Tulle	1978	fibre cement	polycarbonate

The restoration wave of the 1970s-1980s was characterised by the replacement of the original materials by cheaper and lighter materials, that were being produced industrially since the middle of the 20th century. Regarding the opaque part of the roofs, slate and tiled roofs were usually preserved but zinc roofs and corrugated iron sheets were often

replaced by steel decks (Fig. 2.2c), polyester panels (Fig. 2.2d), or fibre cement panels. Fig. 2.4a indicates the prevalence of each material. Material alternatives to zinc roofs were easier to implement as they did not require different layers of construction and offered bigger spans. For the translucent part, glass was sometimes preserved, with sheet glass being replaced by wire glass. However, plastic materials, such as polycarbonate, polyester (reinforced with glass fibres), Plexiglas or PVC, were favoured (Fig. 2.4b). Again, their implementation was easier since ribbed or corrugated plastic panels offered much bigger spans than glass panels. Moreover, they had a safety advantage over glass, being less brittle and avoiding the hazard of potential glass shards. Nevertheless, the longevity of translucent plastic materials proved to be much less satisfying than glass (Fig. 2.3b).

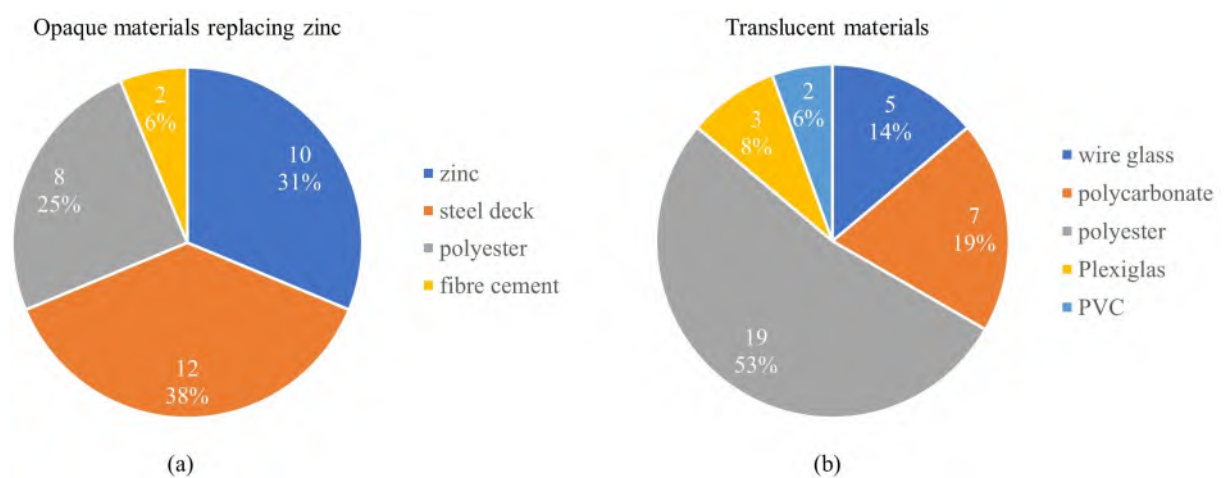


Figure 2.4 – Proportional amounts of roofing materials used in the restoration wave of the 1970s-1980s (the absolute amounts correspond to the number of railway stations in which those roofing materials were implemented).

Since 2005, restoration projects have tended to restore the original roofing, at least for prestigious train sheds. Data was gathered from execution plans and design reports for the restoration of train sheds of 20 stations since 2005 (Tab. 2.2). It appears that, proportionally, the original materials zinc and glass reclaimed their place (Fig. 2.5). Zinc roofs were rebuilt with the traditional roll cap system, even though standing seams are much more common today. Sometimes steel decks were implemented with timber boarding underneath, to preserve the original aspect seen from below. Glazed parts made use of laminated glass. Fixation systems were developed to preserve the existing glazing bars or to replace them with similar profiles, while ensuring waterproofness according to current standards. Even though they restore a sense of authenticity, zinc roofs and glazing are still a minority because they are more expensive than metal decks and plastic panels. Moreover, improvements were made in the manufacturing technology of polycarbonate sheets (Fig. 2.3c), in the form of protection from environmental degradation by UV radiation, so that their suitability as an alternative to glass has increased (Schwartz, 2014). Future

restoration projects might implement glass panels with embedded photovoltaic cells, to exploit the vast surface of train shed roofs for energy production. Such panels have been used for example for a shed of the railway station of Le Bourget newly built in 2008 (Fig. 2.3d).

2.3.2 Weight associated with roofing systems

Opaque roofing

Original zinc roofs were built using the roll cap system. Zinc sheets were fixed on wood rolls with a trapezoidal cross section which were themselves supported by timber boards. In the train sheds for which data was available, the weight of historical or reconstructed roll cap zinc roofs varied between 20 and 40 kg/m² depending on the thickness of the layers of timber boarding beneath the zinc sheets. The first layer of timber boarding, used to fix the wood rolls, had a thickness varying between 18 and 27 mm. Either this layer was left apparent or another layer was added below. This additional layer, between 27 and 34 mm thick, had its boards oriented diagonally. In the original design, this layer was probably meant to contribute to the bracing of the structure. Corrugated iron sheets weighed about 10 kg/m², much lighter than zinc roofs, while slate and tiled roofs were much heavier. Based on Cordeau, 1901, the weight of slate roofs including timber boarding can be estimated at 40 kg/m² and the weight of tiled roofs at 60-100 kg/m² depending on the type of tiles.

In the 1970s-1980s, the opaque polyester panels used to replace zinc roofs or corrugated iron sheets were about 3 kg/m², while fibre cement panels were about 20 kg/m². Steel decks were usually around 7-8 kg/m².

In recent restoration projects since 2005, reconstructed zinc roofs tried to reproduce the original constructive pattern, yielding a similar weight. When steel decks were used, they were the same weight as those used since the middle of the 20th century. However, in some projects, timber boarding was added beneath the steel deck to keep the original aspect from below. The resulting weight was 30 kg/m², and so, compared to a zinc roof, it represented only an economic gain, with no structural benefit. Also the authenticity of this variant is questionable.

The study of the weight of opaque roofing materials shows that the restorations of the 1970s and 1980s tended to reduce the permanent loads supported by the metallic structure of train sheds, while the more recent restorations of the 21st century yielded comparatively higher loads (Fig. 2.6). The study of the weight of glazing materials is now presented to confirm this tendency.

Table 2.2 – List of railway stations whose train sheds were restored since 2005, with the year of restoration and the materials used for the opaque and translucent roof parts.

Railway station	Year	Opaque roof	Translucent roof
Agen	2024	zinc	laminated glass
Bayonne	2013	zinc	laminated glass
Béziers	2020	steel deck	laminated glass
Bordeaux Saint-Jean	2013	zinc	laminated glass
Castelnaudary	2009	steel deck	polycarbonate
Cerbère	2007	steel deck	polycarbonate
Etampes	2015	aluminium deck	polycarbonate
Evian	2010	steel deck	polycarbonate
Hendaye	2013	steel deck	polycarbonate
La Rochelle	2005	zinc	laminated glass
Lyon Perrache (Grande halle)	2010	(not replaced)	polycarbonate
Montauban	2011	zinc	laminated glass
Paris Austerlitz	2015	zinc	laminated glass
Paris Lyon (Halle du Train Bleu)	2022	zinc	laminated glass
Pau	2011	steel deck	polycarbonate
Perpignan	2013	steel deck	polycarbonate
Tours	2012	zinc	polycarbonate
Troyes	2019	steel deck	polycarbonate
Tulle	2019	steel deck	polycarbonate
Valence	2023	zinc	polycarbonate

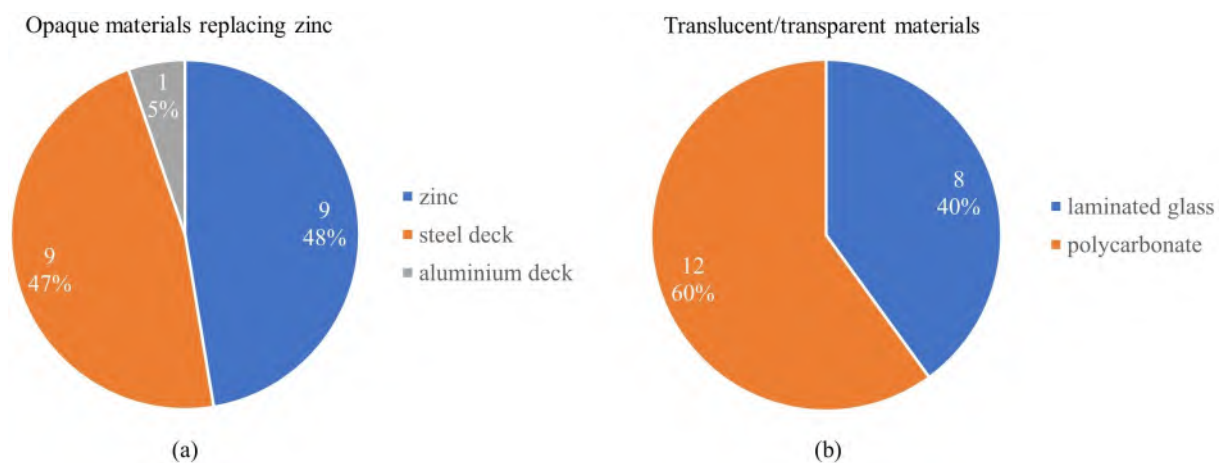


Figure 2.5 – Proportional amounts of roofing materials used in restoration projects since 2005 (the absolute amounts correspond to the number of railway stations in which those roofing materials were implemented).

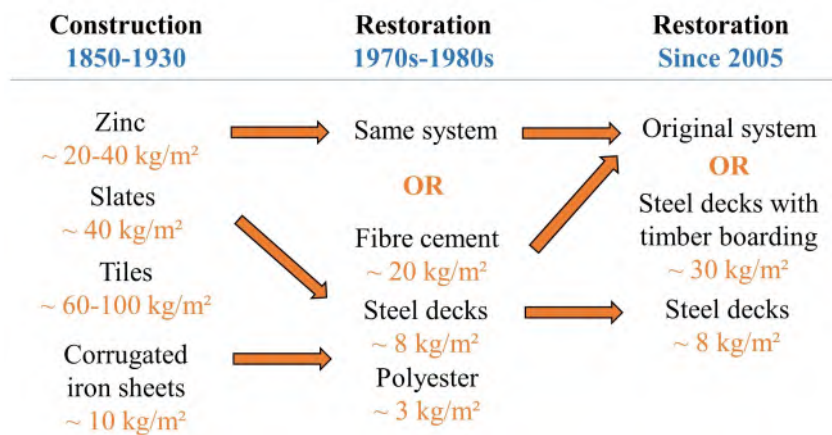


Figure 2.6 – Overview of the evolution of the loads associated with opaque roofing materials.

Glazing

The permanent load associated with roof glazing born by the metallic structure results from the weight of the glazing panels and the weight of their metallic frame. Little data can be found regarding the thickness of original glazing in train sheds built between 1850 and 1930. In the Crystal Palace, sheet glass panels were 2 mm thick, spanning 25 cm. This choice was apparently consistent with the practice of the time, as these dimensions had been used for the glazing of railway stations built in the 1840s in England (Hollister, 1974). In French train sheds, glass panels were about 50 cm wide, so that the glass thickness must have been closer to 4 to 6 mm. These were typical dimensions for sheets of rolled plate glass (Carré, 2010). In Belgium, glass plates used for roof coverings were usually “verre double”, with a thickness of 3-4 mm (Lauriks et al., 2018).

The French journal *Le Génie civil* indicated in 1886 that the new train sheds under construction for the Gare St-Lazare in Paris had a glazed roof using 5 to 6 mm thick glass panels supported by specially designed glazing irons spaced every 58 cm (Boca, 1886). The total weight was then 22 kg/m². Original design reports and plans were available to the authors for the present article on the stations of Bordeaux Saint-Jean built in 1898 and Bédarieux built in 1903. In Bordeaux, the glass panels were 4 mm thick, accounting for 10 kg/m², and the frame was constituted of metallic T-sections 45 mm x 35 mm x 5 mm spaced every 42.1 cm. The total weight was 17 kg/m² then. In Bédarieux, the glass panels were 6 mm thick and the frame was made of T-sections spaced every 41.6 cm, total weight was 22 kg/m² then. From the end of the 19th century, wire glass was employed, with a traditional thickness of 6 to 7 mm (Carret, 1909). Overall, assuming glass panels between 4 and 6 mm thick and a frame weighing a maximum of 10 kg/m², original glazing for train sheds built between 1850 and 1930 weighed about 25 kg/m².

In the restoration wave of the 1970s-1980s, the plastic panels used to replace the glazing led to a significant load reduction, dividing the roof weight by almost ten. The

panels themselves were lighter than glass, but they also offered larger spans, so that the metallic frame structure was removed. A calculation note edited in 1983 for the station Gare de Tours took 2 kg/m^2 as a load assumption for the new polyester panels. For other railway stations, restoration plans indicated the profile of the corrugated polyester panels, for example NERVESCO 1000TS (Gare d'Aurillac, restoration of 1985) or C25 (Gare d'Angoulême, restoration of 1976). The associated weight could be extracted from technical data sheets of today's equivalent products. The weight of plastic panels, whether polyester, polycarbonate or PVC, was about $2\text{-}3 \text{ kg/m}^2$, depending on the thickness of the sheet.

Since 2005, restoration work has kept or re-established the original spacing between glazing irons, whether the translucent part of the roof was renovated with laminated glass or with polycarbonate. The safety glass panels were usually type 44.2 or 55.2, which means an assembly of two glass plates of 4 mm thickness (or 5 mm respectively), with an interlayer of two translucent films of PVB resin of a total thickness of 0.76 mm. These panels weighed 20 kg/m^2 and 25 kg/m^2 respectively, the weight of the interlayer being negligible. Regarding polycarbonate, different products were favoured, either multiwall sheets of 16 mm thickness, weighing $2.5\text{-}3 \text{ kg/m}^2$, or solid sheets of 4 to 6 mm thickness, weighing $5\text{-}7.5 \text{ kg/m}^2$. Precise characteristics of the glazing have been gathered from recent train shed restorations over the last 15 years and are presented in Tab. 2.3. This table shows that the weight of glazed roofs with glass ranged roughly from 30 to 40 kg/m^2 , while the weight of polycarbonate roofs was between 6 and 23 kg/m^2 . The use of multiwall polycarbonate sheets led to a maximum weight of 15 kg/m^2 . Regarding the glazing irons, they were usually made of steel. Two projects used aluminium profiles, probably more expensive, but leading to a substantial reduction in weight. It can also be noted that when rectangular hollow profiles were used, they were lighter than when open T-shaped profiles were used. This is presumably because hollow profiles are more resistant to buckling. The choice of T-shaped profiles over hollow ones could be related to their thinner appearance, closer to the original aspect. However heavier roofs were more likely to require strengthening of the metallic structure.

Finally, glazing can be used to generate energy. Some restoration projects of the last 5 years have included studies to integrate photovoltaics. Two main options exist for photovoltaic glazing: crystalline silicon (c-Si) cells or amorphous silicon (a-Si) cells, encapsulated inside two glass panes with translucent resin. C-Si modules (like the ones presented on Fig. 2.3d) are less translucent than a-Si modules but produce more energy (Casini, 2016). According to some SNCF studies, the weight of such photovoltaic modules would be about 50 kg/m^2 . They have not been implemented yet in restorations.

The study of the weight of transparent or translucent roofing materials confirms and

Table 2.3 – Glazing characteristics and associated weights for recent train shed restoration projects.

Train station	Renovation date	Glazing type	g [kg/m ²]	Glazing irons	Spacing [cm]	g [kg/m ²]	g tot [kg/m ²]
Agen	2024	laminated glass 55.2	25	T 60x60x7	50	14	39
Bayonne	2013	laminated glass 55.2	25	HSS 60x30x2	50	7	32
Béziers	2020	laminated glass 44.2	20	HSS 50x30x3	50	8	28
Montauban	2011	laminated glass 44.2	20	T 60x60x7	40	18	38
Paris Austerlitz	2015	laminated glass 44.2	20	T 60x60x7	50	14	34
Paris Lyon PHV	2022	laminated glass 44.2	20	T WRP 55x55x5..8	45	15	35
Cerbère	2010	multiwall PC 16mm	3	extruded alu profile	40	5	8
Troyes	2021	multiwall PC 16mm	3	HSS 60x30x2.5 (alu)	50.5	3	6
Valence	2023	multiwall PC 16mm	3	HSS 60x40x2 (alu)	50	3	6
Evian	2010	multiwall PC 16mm	3	HSS 60x60x2	50.5	9	12
Hendaye	2013	multiwall PC 16mm	3	HSS 60x40x2	50	9	12
Pau	2011	multiwall PC 16mm	3	HSS 60x60x2	50.5	9	12
Perpignan	2013	multiwall PC 16mm	3	HSS 60x30x2	50.5	8	11
Tours	2012	multiwall PC 16mm	3	HSS 60x60x3	50	12	15
Tulle	2019	multiwall PC 16mm	3	HSS 60x30x2	50	7	10
Etampes	2015	solid PC 4mm	5	T 60x60x7	40	18	23
Lyon Perrache	2010	solid PC 6mm	8	HSS 60x60x2	50	9	17

PC : polycarbonate

HSS : hollow structural steel

WRP: welded reconstituted profile

even enhances the results obtained with opaque materials. The suggested tendency becomes even clearer: through restorations of the 1970s and 1980s, permanent loads supported by the metallic structure of train sheds decreased, while through restorations since 2005, permanent loads increased (Fig. 2.7). This questions the authentic character of recent restorations. They strived to restore the original aspect of the roofing while filling today's requirements in terms of safety and durability. However, by doing so, they overloaded the metallic structure, which led to more strengthening measures. In turn, these strengthening measures harmed the authenticity of the restored train sheds, by modifying the appearance of the structure or by introducing irreversible changes. This applies in particular to our case study, the train shed of Montauban. Tab. 2.3 shows that the glazing characteristics selected for the restored roofing yielded very high dead loads compared to other recent restorations. The question then arises: “should polycarbonate glazing have been favoured instead of laminated glass to minimise structural interventions?”.

2.3.3 A change in perspective?

In France, it seems that heritage-friendly restorations implied restoring the appearance and the materiality of the original roofing. However, this is not a universal practice. The tendency observed for recent restorations of train sheds in France does not necessarily apply to other countries. For example, in 2006, a completely different strategy was adopted for the restoration of the train shed of Dresden in Germany. Instead of restoring the

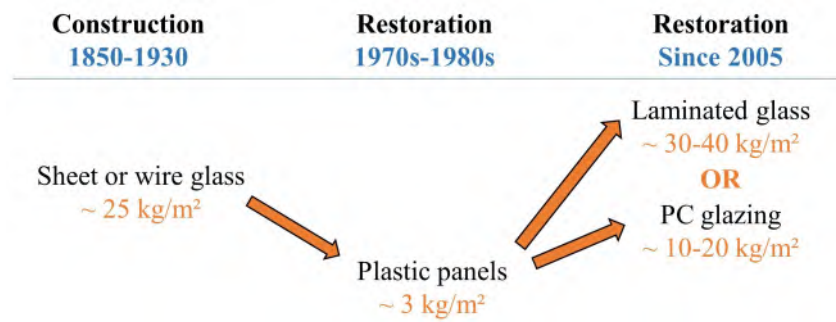


Figure 2.7 – Overview of the evolution of the loads associated with opaque roofing materials.

roofing with original materials, the metallic structure of 1898 was covered with a PTFE-coated glass fibre membrane (Fig. 2.8). The idea was to increase the natural daylight and “reveal” the metallic structure (Vitzthum et al., 2006). The notion of “revealing” was biased. Since the membrane decreased the dead loads but generated high compression loads in the existing arches, the load-bearing system was deeply modified and it was rather the architecture than the structure that was revealed. These radically different choices enhance the importance of defining what is meant by “preserving” the structure or the authenticity of the building.



Figure 2.8 – Dresden Hauptbahnhof, built in 1898, after renovation in 2006, Dresden, Germany (Picture from Wikimedia Commons by Kolossos).

It could be argued that the authenticity of historic metallic train shed structures lies in their functional role and their power to impress, relying on state-of-the-art construction techniques. These are indeed the qualities that inspired the new generation of metallic train sheds built in the 21st century, like the railway station of Orléans (Fig. 2.9).



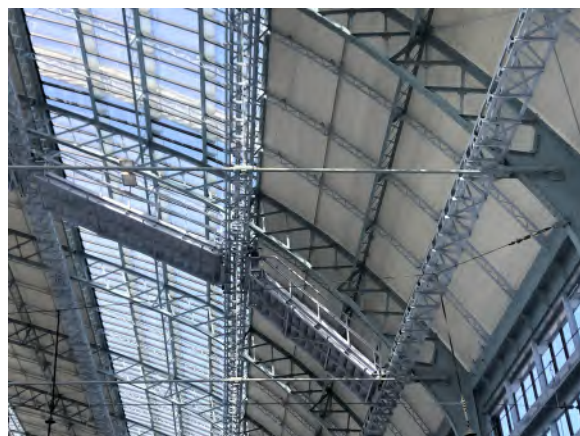
Figure 2.9 – Gare d'Orléans, built in 2009, Orléans, France (Picture from SNCF-AREP by D. Boy de la Tour).

2.4 Maintenance equipment

Like the roofing, maintenance equipment installed on existing structures may have an impact in terms of loading. In the course of restoration projects, equipment was added to train sheds, to provide more safety for the workers carrying out inspection and maintenance tasks. Some equipment such as lifeline systems have negligible weight, but maintenance platforms must usually be taken into account. This type of equipment installed over the roof is discrete and does not have any impact on the aspect of the train shed for passengers (Fig. 2.10a). A counterexample is given by the stairs that were added below the roof surface in the railway station of Bordeaux Saint-Jean in 1928, with a relatively massive railing system to allow the stairs to move in the longitudinal direction (Fig. 2.10b).



(a)



(b)

Figure 2.10 – Maintenance equipment added on the course of restoration projects in the train shed of Bordeaux Saint-Jean, Bordeaux, France (Pictures from SNCF and by H. Franz): (a) Maintenance platform and lifeline system over the roof, added in 2016 (Picture from SNCF); (b) Metallic stairs and rails below the roof, added in 1928.

Such invasive measures were avoided in more recent restoration projects. However, in the restoration of Bordeaux Saint-Jean in 2016, the stairs and rails of 1928 were left in place, thus endorsing a profound modification of the original aspect. Even if maintenance equipment contributes to the preservation of the structure, it is important to consider its direct structural impact to select the most appropriate type of equipment and its location.

2.5 Structural interventions

Structural interventions covered in this section are all operations that directly concern the structure: removing or adding, repairing or strengthening structural elements. Some interventions, like the ones on skylights and glazed gables, result merely from architectural or economical considerations. Repairs and strengthening measures are due to structural requirements. Even though structural interventions are visible, they are not easily noticeable. New steel elements blend in with the old ones on account of uniform paint. Thus, this section draws attention on a variety of structural interventions and discusses their impact on the authenticity.

2.5.1 Skylights and glazed gables

Removal and reconstruction

In the course of restoration projects in the 20th century, skylights were often removed. A historical note from the SNCF archives dating back to 1981 indicated that skylights were mandatory installations when trains were still powered by steam but were no longer needed after the end of steam locomotives (CNAH, 1981). Their removal could moreover minimise subsequent maintenance expenses, because the metallic structure would then be better protected from the weather. There are also a few examples of modified skylights. In the railway station of Etampes, the original double-pitched skylight built in 1911 was replaced in the second half of the 20th century by a curved skylight made of curved polycarbonate panels, thus eliminating any waterproofing problems at the ridge. The original metallic structure of the skylight was removed. In the restoration projects since 2005, skylights have usually been reconstructed with dimensions close to the original, for heritage reasons but also for the purpose of ventilation. The new metallic structures were built according to the current construction practice, using bolted or welded rolled sections.

The original glazed gables lost their prevalence in the 20th century. Sometimes glass panels were replaced by plastic panels, but in many cases, broken glass panels were simply removed, while the metallic frame or at least the bottom trussed girder were left in place. In some cases, the metallic structure of the glazed gables was removed completely. This

results in very different impressions of originally similar structures: in the railway station of Bordeaux Saint-Jean, the glazed gables with their glazing were completely preserved and renovated in 2017 (Fig. 2.11a), while in Bédarieux, only the bottom girders and some vertical bars were preserved (Fig. 1.6b), and in Montauban, the gable structure was completely removed (Fig. 1.6a). In some railway stations, the structure of the extreme roof trusses, deprived of glazing, was modified, as in the station of Carcassonne in the 1960s (Fig. 2.11b). Only the bottom girders of the glazed gables were preserved. New metallic struts, reminiscent of the geometry of the Polonceau roof trusses inside the shed, were added to transmit the load of the higher roof.



Figure 2.11 – Glazed gables restored or modified: (a) Gare de Bordeaux Saint-Jean, Bordeaux, France; (b) Gare de Carcassonne, Carcassonne, France (Pictures from SNCF-AREP by D. Boy de la Tour and C. Lebreton).

Influence on wind loads

Wind loads started to be taken into account in design calculations around 1840 (Holzer, 2006) and were integrated in design regulations in Europe starting from 1880 (Schueremans et al., 2018). In France the first design regulations regarding train sheds were released in 1902 (« Circulaire du ministre des travaux publics aux préfets du 25 janvier 1902 (Halles à voyageurs et à marchandises des chemins de fer) », 1904) and recommended the assumption of a wind load of 150 kg/m^2 , in a direction inclined 10 deg to the horizontal. This assumption, that does not reflect any real aerodynamical behaviour, had already been developed in the 1850s. Wind uplift was not considered in design practice until the 1930s, even though this phenomenon had been highlighted by Navier almost a century before (Holzer, 2006). The integration of wind uplift in the structural assessment of train sheds built between 1850 and 1930 led to strengthening measures for some structural elements, as the reversal of the sign of wind loads sometimes caused elements designed in tension to work in compression and thus be exposed to buckling.

Beyond the evolution of regulations, the effect of wind uplift was physically increased by the removal of glazed gables, as wind would then act on both the upper and lower

surfaces of the roof. According to today’s Eurocode regarding wind actions (EN 1991-1-4, 2005), train shed roofs can usually be regarded as “canopy roofs” because two or three of their sides are open (*ibid* §7.2.9(2)). The removal of glazed gables means a reduction of the degree of blockage φ of the wind as defined for the design of “canopy roofs” (EN 1991-1-4 2005) from about $\varphi = 0.5$ (50% of the gable surface is closed) to $\varphi = 0$. For wind blowing in the longitudinal direction, this leads to an increase of the estimated wind force of 40%.

Maintaining, removing or reconstructing the skylights and the glazed gables has therefore an influence not only on the architectural appearance but also on the structural authenticity. Removing or modifying those substructures changes the loading conditions related to wind. Thus, it modifies the structural behaviour and the functionality of train sheds, namely ensuring a good ventilation while protecting from wind gusts.

2.5.2 Repair or replacement of structural elements

The main pathology of the metal structure of train sheds is corrosion. In restoration projects since 2005, when the section of some structural elements was too seriously reduced because of corrosion, those elements were either repaired or replaced. Repairs often consisted in locally adding metallic plates. Fig. 2.12 shows the example of local riveted repairs of roof truss chords in the railway station of Troyes, after restoration in 2021. In the last decades, the hot riveting process has been re-introduced in renovation practice, to restore existing riveted structures in which the riveted connections are an integral part of the heritage value (Collette, 2014). Also, driven rivets are favoured to replace damaged or missing rivets, because high-strength bolts necessitate to ream the holes in situ to be fitted in (D’Aniello et al., 2011). There are only a few experienced riveting teams in each country still able to drive rivets. As an example, the SNCF has its own riveting team, dedicated to the repair of old metallic railway bridges.

When damaged areas are too large, structural elements tend to be replaced, with new elements as close to the original as possible. For example, in the train shed of Montauban, some purlins were heavily corroded, especially their top chord (Fig. 2.13a). They were then replaced (Fig. 2.13c), keeping a similar aspect to the original preserved purlins (Fig. 2.13b).

2.5.3 Strengthening measures

Whether it was because of the effective increase in the dead loads of the roof or because design criteria became stricter, strengthening measures were often carried out during restoration projects. Little data could be found regarding restoration projects of the 20th century. Apart from the addition of bracing systems, the strengthening measures



Figure 2.12 – Local repairs of roof truss chords with added riveted plates in the train shed of Troyes renovated in 2021, Troyes, France (Pictures from SNCF).

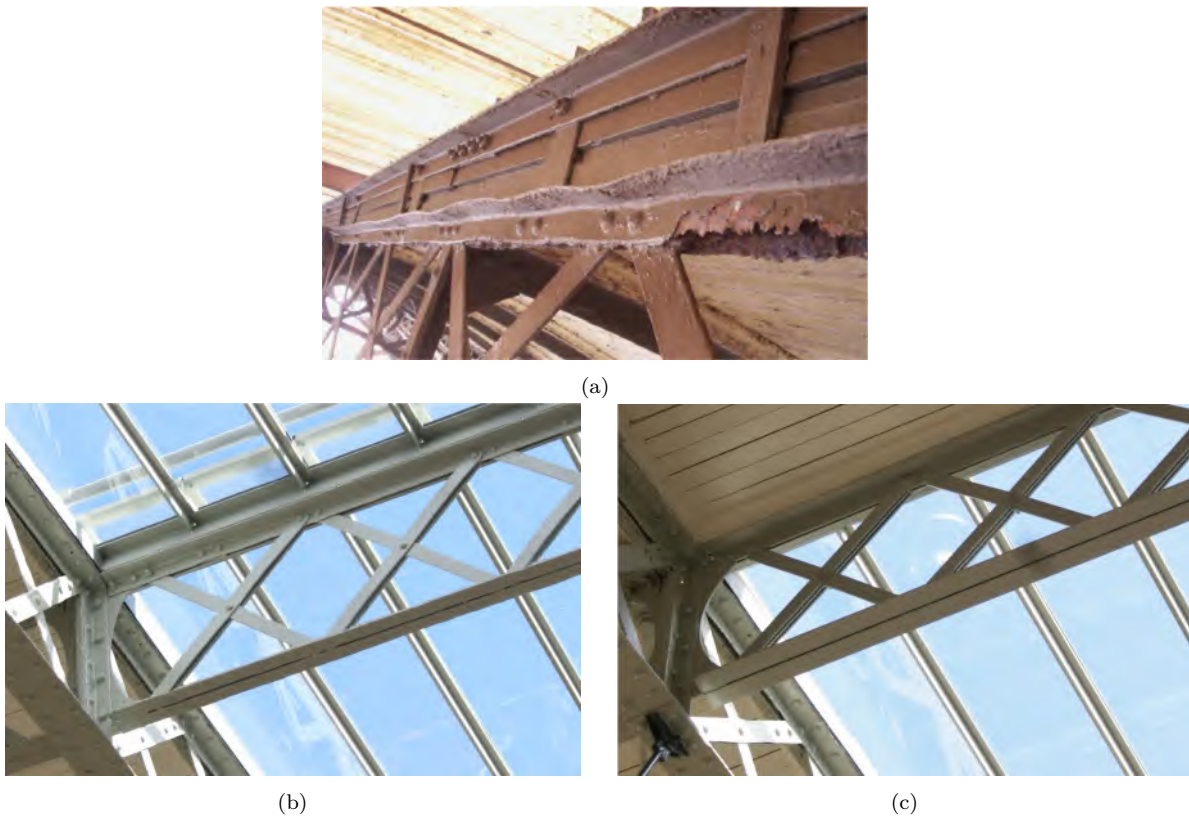


Figure 2.13 – Replacement of purlins in the train shed of Montauban, France (Pictures from SNCF): (a) Corroded purlin in 2007 before restoration; (b) Original non-corroded repainted purlin after restoration of 2011; (c) Corroded purlin replaced by a new purlin after restoration of 2011.

implemented seemed to disregard the original functionality and the visual impact. In Bordeaux Saint-Jean, around 1980, the lattice rafters of the skylight were reinforced with tension ties, transforming them into underspanned beams (Fig. 2.14a). This strengthening measure modified the functionality of the rafter, from a beam working in bending to a compression element. In Paris Austerlitz, the lattice purlins supporting the skylight were reinforced in 1983 with added diagonals (Fig. 2.14b). The original lattice purlins had only

diagonals pointing upwards towards the middle of the span, thus working in compression. The added diagonals made of corner plates transformed the original lattice girders into girders with crossed out sections, thus changing their aspect considerably. Furthermore, the new diagonals worked in tension and had a much larger section than the original diagonals, so that the latter probably did not contribute to the bearing capacity anymore. These examples of strengthening measures went against the idea of authenticity: beyond being visually invasive, they modified the structural behaviour of the reinforced girders.

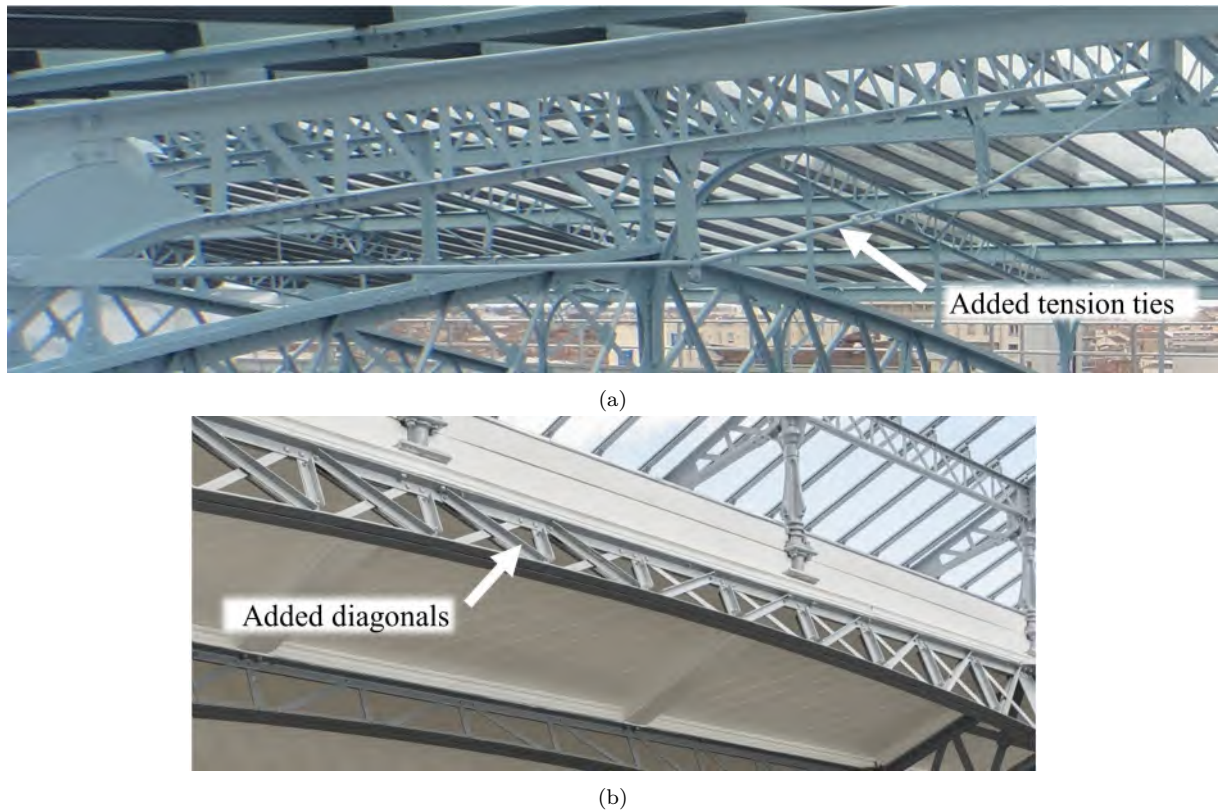


Figure 2.14 – Invasive strengthening measures of the end of the 20th century (Pictures: SNCF). (a) Gare de Bordeaux Saint-Jean: underspanned lattice rafters, Bordeaux, France; (b) Gare de Paris-Austerlitz: diagonals added to lattice purlins, Paris, France.

In restoration projects since 2005, strengthening measures have been less invasive. Amongst recent restorations, execution plans regarding interventions on the metal structure were obtained for 16 railway stations. 11 restorations out of the 16 involved strengthening measures, which were analysed for this study. The interventions could be classified in two categories: interventions increasing the section of existing structural elements, or interventions adding elements to the structure (Tab. 2.4).

Lattice purlins and rafters were often reinforced by increasing the section of their web or chord members, to prevent them from buckling. Flat or L-shaped plates were added to the original elements with welds or bolts (Fig. 2.15a and b). Welds were visually better integrated than bolts but did not obey the principle of reversibility recommended

Table 2.4 – List of railway stations restored since 2005, with the year of restoration, the indication whether strengthening measures were implemented or not, and if relevant, the type of interventions: [1] increasing the section of existing structural elements or [2] adding elements to the structure.

Railway station	Year	Reinforced?	[1]	[2]
Bayonne	2013	yes	●	●
Béziers	2020	yes		●
Bordeaux Saint-Jean	2013	yes	●	
Cerbère	2007	yes	●	●
Etampes	2015	no		
Evian	2010	no		
Hendaye	2013	yes	●	
La Rochelle	2005	yes		●
Lyon Perrache (Grande halle)	2010	no		
Montauban	2011	yes	●	●
Paris Austerlitz	2015	yes	●	
Paris Lyon (Halle du Train Bleu)	2023	no		
Pau	2011	yes		●
Perpignan	2013	yes		●
Tours	2012	yes	●	●
Troyes	2019	no		

for the restoration of heritage structures (ICOMOS, 2003). Bolts created holes in the existing elements, while welds probably induced residual stresses. These variants did not significantly change the load distribution in the existing elements. On the contrary, in the railway station of Cerbère, HEA100 rolled steel sections were added on top of the lattice purlins to create a new cross-section far more rigid than the original one and with a displaced neutral fibre (Fig. 2.15c). The restoration of the railway station of Béziers in 2020 took it a step further by adding new tubular purlins on top of the original ones and structurally independent from them, thus completely deactivating them. This solution favoured the preservation of the aspect of the structure over its structural functionality (Fig. 2.15d).

As an alternative to the increase of existing sections, added structural elements also aimed at preventing buckling issues. In some projects, tension rods were added to link the purlins together, either at the level of the top chord or through the web. These tension rods had thin circular or L-shaped sections (Fig. 2.16a). To provide buckling restraints for the bottom chord of lattice girders, small brackets were sometimes added (Fig. 2.16b).

Overall, the survey of strengthening measures in the eleven recent restoration projects providing relevant data showed that no intervention type stands out. The strengthening measures carried out were extremely varied, both in their principle and their constructive implementation. It appears that there is no common practice as to how the metallic structure of train sheds should be reinforced.



Figure 2.15 – Interventions increasing the cross-section of existing elements or replacing them (Pictures from SNCF-AREP). (a) Welded flats, Gare de Montauban, Montauban, France; (b) Bolted flats on existing diagonals, Gare d’Hendaye, Hendaye, France; (c) Added rolled steel section on top of existing lattice purlin, Gare de Cerbère, Cerbère, France; (d) Added tubular purlins effectively replacing the existing ones, Gare de Béziers, Béziers, France.

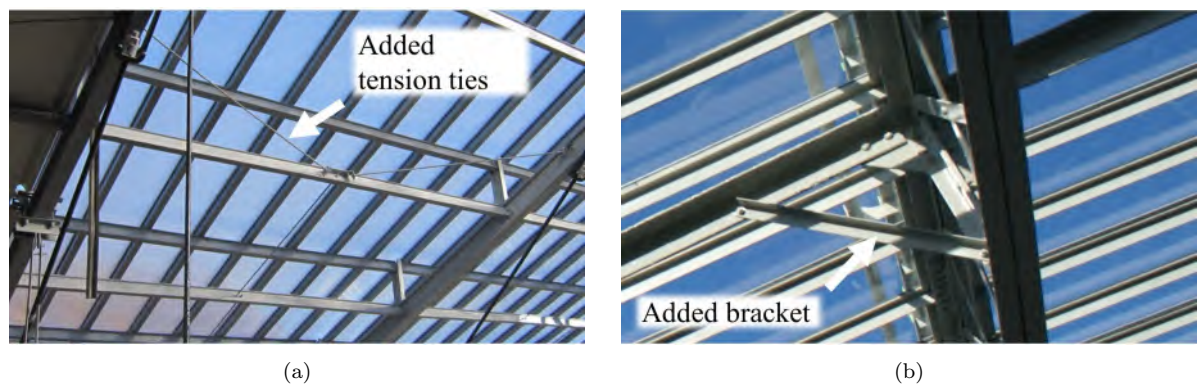


Figure 2.16 – Interventions adding structural elements to provide buckling restraints (Pictures from SNCF-AREP). (a) Tension ties between purlins, Gare de Pau, Pau, France; (b) Bracket restraining the bottom chord of a lattice purlin, Gare de Montauban, Montauban, France.

Strengthening measures from the two last decades strived to remain discrete. In Montauban, lattice purlins were reinforced both by brackets to restrain the bottom chord (Fig. 2.16b) and by additional welded flats on the most compressed diagonals (Fig. 2.15a) - the structural principle of these reinforcements is presented on Fig. 2.17. These strengthening measures are very less visible, because the brackets were connected to existing secondary rafters. Still, their impact on the authenticity of the original structures is non-negligible and welded flats are not reversible. In other train sheds like Cerbère or Béziers, the addition of new purlins on top of the original ones changes the load distribution or even deactivates some structural components. This loss of functionality also means a loss of authenticity.



Figure 2.17 – Principle of the strengthening measures implemented on the lattice purlins of the train shed of Montauban, France.

The less discrete variants, involving sections reinforced by bolted plates or added structural elements, can profoundly change the appearance of the structure when they accumulate. The restoration of the train shed of Perpignan provides a representative example (Fig. 2.18). The end result of the restoration is aesthetically satisfying (Fig. 2.18b). However, when compared to the original structure, it can be noticed that the restored structure, with added brackets and tension ties, has lost some of its lightness (Fig. 2.18c). This results in a loss of authenticity, as lightness was a key characteristic of metallic structures in the 19th century.

2.6 Conclusion

Based again on an extensive survey of surviving train sheds, this chapter provides a critical insight into the evolution of restoration practices for train sheds and their consequences on the preservation of the metal structure. Until the 1980s, the choice of roofing materials and the elaboration of structural interventions disregarded the preservation of the original appearance. Since 2005, in the framework of the restoration program carried out by SNCF, train sheds have been restored with a definite sensitivity towards heritage preservation. Roofing materials and techniques have strived to reproduce the original impression, removed skylights were reconstructed, repairs and strengthening measures stayed discrete. However, this chapter demonstrated that current restoration practices have led

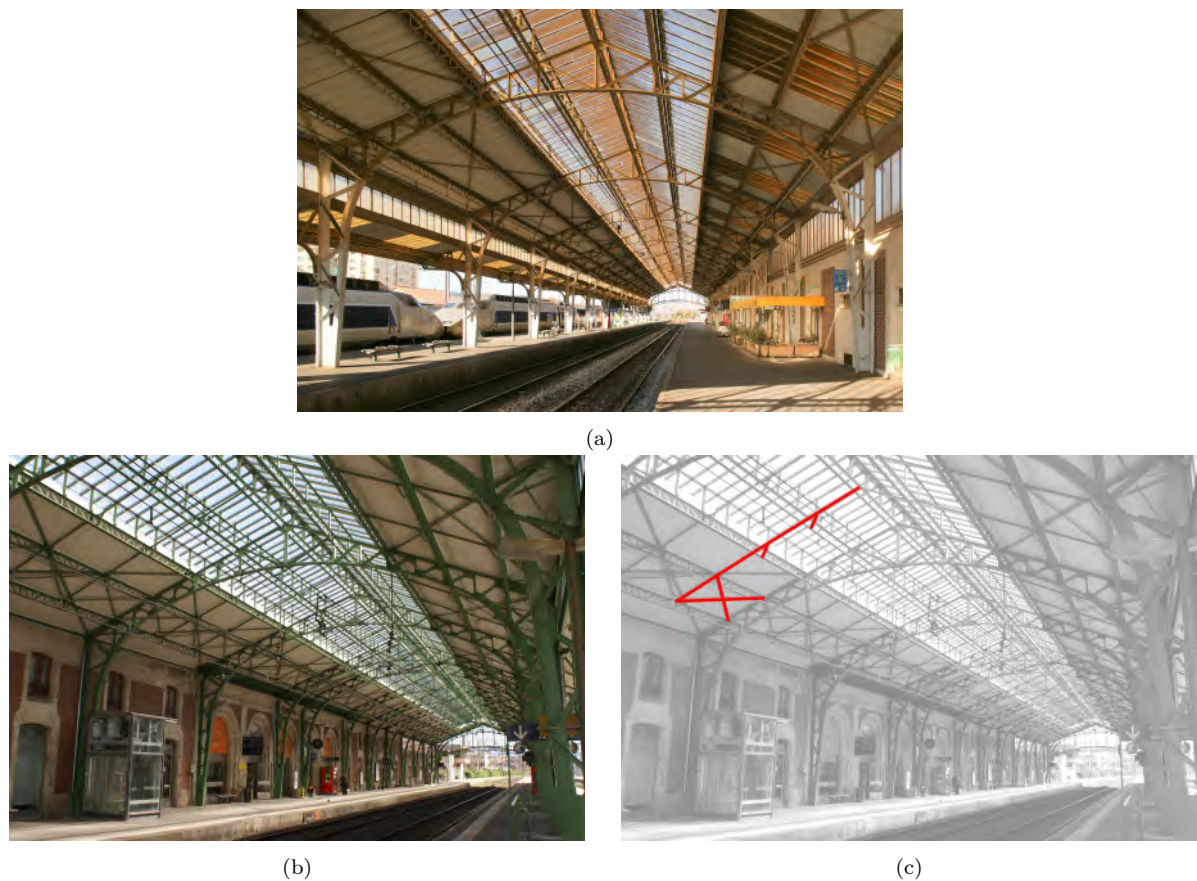


Figure 2.18 – Gare de Perpignan, built in 1896, Perpignan, France (Pictures from SNCF-AREP by D. Boy de la Tour and A. Striffling). (a) Before and (b) after restoration of 2013; (c) Strengthening measures added in the restoration of 2013, highlighted in red.

to an increase in the permanent loads supported by the structure, which has made further structural interventions necessary. It was also shown that the strengthening measures carried out were extremely varied, both in their principle and their constructive implementation. This suggests that an optimisation of strengthening measures could be possible by comparing criteria such as their structural efficiency, their ease of implementation, their visual impact or their “authenticity”. Some strengthening measures, despite being visually well integrated, significantly changed the load distribution in existing structural members, or even deactivated them. There is no perfect strengthening measure. However, being aware of the qualities and drawbacks of the various existing options is essential to refine criteria for successful heritage-friendly restorations.

A paradox emerged: even though the heritage value of train sheds relies strongly on their engineering qualities, restoration projects focused on preserving mainly their functionality and, more recently, on restoring the architecture. Strengthening measures are the mere consequence of renovation strategies that seem to disregard how to best preserve the structure itself. A change of perspective might be apt: for the structure to serve the architecture, restoration should serve the structure. With this in mind, the discussion

regarding acceptable retrofitting interventions on old iron and steel structures from a heritage point of view should be enriched by extending it to other types of structures than train sheds and by comparing the French practice with other countries.

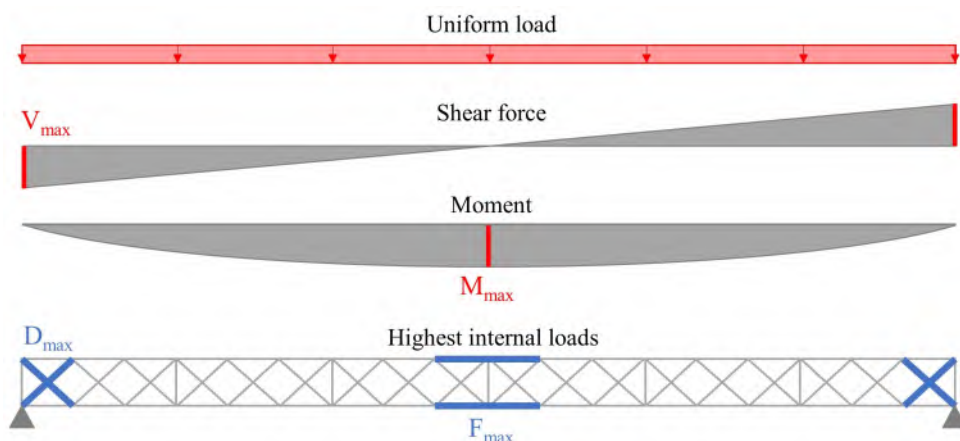
Chapters 1 and 2 enhanced what shall be preserved in train sheds, for what reasons, and what trade-offs are possible to favour the preservation of the metal structure. The topics explored in Part I are usually dealt with by construction historians and heritage architects. The discussions suggest that the engineering point of view is also of interest. Part II, on the opposite, deals with issues that traditionally fall within the remit of engineers: “how to refine modelling assumptions to improve structural assessment?”. Nevertheless, historical insights are used to identify critical parameters.

PART II

**REFINING STRUCTURAL
ANALYSIS ASSUMPTIONS**

CAPITALISING ON PREVIOUS ASSUMPTIONS

Chapter 3 capitalises on historical and more recent literature to discuss modelling assumptions for structural analysis. The evolution of structural analysis methods for lattice girders and knowledge regarding the deformation behaviour of riveted connections are critically summarised. A case study is then conducted to illustrate the consequences of various assumptions.



Principle of analytical calculations to assess the highest internal loads in a lattice girder under uniform load.

Contents

3.1	Historical structural analysis methods	60
3.2	Joint modelling	64
3.3	Discussion based on the case study	71
3.4	Conclusion	75

Structural analysis is a step of the design or assessment procedure that determines how external loads, such as gravity or wind, are transmitted through the structure and distributed among its various components. It is performed before the verification stage and provides engineers with the internal forces and stresses they need for design checks. Modelling assumptions, especially boundary conditions, are decisive for the results. In lattice girders, the freedom of movement in the web-to-chord riveted connections is a key factor in determining whether those structures behave like trusses or not. To avoid arbitrary or conservative assumptions, it is essential to capitalise on existing knowledge, i.e. to gain critical insight into previous interpretations. This chapter first looks into historical design intentions regarding lattice girders by tracing the evolution of structural analysis methods. It then reviews historical and recent literature on the behaviour of riveted connections. The consequences of various interpretations on the results of structural analysis are finally discussed using the case study of a lattice purlin in the train shed of Montauban.

3.1 Historical structural analysis methods

3.1.1 Theory of trusses for triangular systems

In the 19th century, the theoretical developments regarding the structural analysis of trusses had a tremendous impact on the design of metal structures, encouraging rationalisation and standardisation instead of pragmatic overlays of structural components (Rinke et al., 2013). The analytical methods applying to trusses understood as triangulated structures with pinned joints still permeate our perception of trussed frameworks.

According to Timoshenko, 1953, the first useful contribution regarding the analysis of trusses was due to Whipple in 1847. Whipple proposed design methods for trusses such as the one shown in Fig. 3.1, assuming that the diagonals could only work in compression, thus yielding a statically determinate system. His analytical method, the “method of joints”, consisted of writing the equilibrium at each joint of the truss consecutively, starting from the supports (Timoshenko, 1953, p. 185). His graphic method corresponded to drawing the parallelogram of forces at each joint.

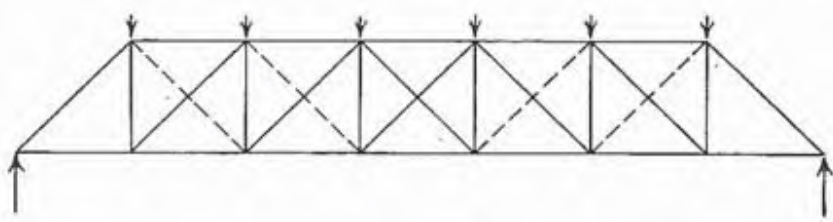


Figure 3.1 – Truss analysed by Whipple in 1847 after Timoshenko, 1953, p. 185.

In 1862, Ritter developed a simplified analytical method for when the internal axial forces needed to be calculated only in some specific truss members (Timoshenko, 1953, p. 190). His “method of sections” worked by cutting through the whole truss at a single section and using global equilibrium to solve for the unknown axial forces in the intersected members.

In 1851, Culmann was the first to set out a theory of graphical analysis of trusses, and went on to systematically develop graphical analysis methods applicable to all kinds of structures, which he published in 1866 (Timoshenko, 1953, pp. 190–194). Graphic statics was improved in 1864 by Maxwell, who developed a theory of reciprocal figures, thus rationalising the diagrams of forces so that the force in each member would appear only once. In 1872, Cremona further developed Maxwell’s theory and the Cremona diagram became the incarnation of graphical analysis (Kurrer, 2018, p. 456).

The design methods developed for truss structures were advantageous because of their simplicity. Until the beginning of the 20th century, those methods were widely used to design roof trusses or truss bridges. However, lattice purlins or rafters were designed using different methods. As they were supposed to behave as beams, they were also designed as such.

3.1.2 Structural analysis methods for lattice girders

Navier’s bending theory

In his seminal work on beam theory, first published in 1826, Navier tackled the bending problem of “pieces formed by several parts joined together”, particularly the assembly of two parallel bars (Navier, 1833, 328–329)[transl.]. Navier proposed a mathematical formulation of their bending moment resistance, considering that the resistance of the parallel bars was equivalent to that of a beam with a hollow core (Fig. 3.2). This approach was valid if the relative sliding between the parallel bars was effectively prevented, for example, “if the bars [were] joined together by a system of transverse pieces and crosses” [transl.]. However, Navier’s theory allowed the calculation of cross-sections only for the top and bottom chords of lattice girders.

Schwedler’s truss theory

In 1851, Schwedler proposed his own “truss” theory, which broadly applied to trusses with various types of filling. In this sense, it is not a theory restricted to trusses defined as statically determinate triangulated structures. Schwedler was the first to derive the differential equations for the shear force using the example of a simply supported beam (Kurrer, 2018, p. 449). Applying his idea to a lattice girder with crossed diagonals, he

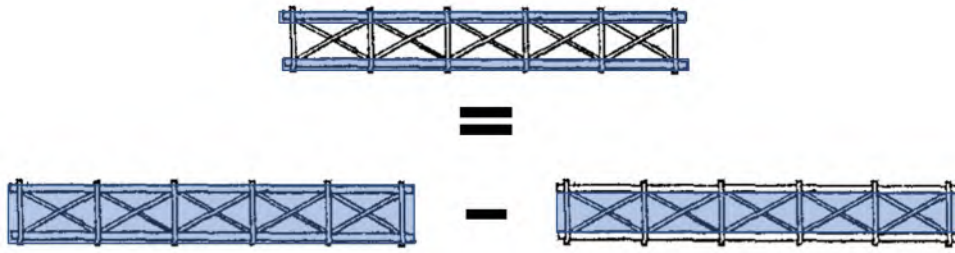


Figure 3.2 – Navier’s bending theory applied to lattice girders (diagram derived from (Navier, 1833, Fig. 94)).

proposed formulas for the axial forces in the diagonals (Schwedler, 1851, 162–167). In a unit cell containing one cross (Fig. 3.3), these forces were described as responsible for transmitting the shear force, corresponding to the incremental moment over the length of the cell. When the chords were parallel, the axial force D in the diagonals of the cell ranging from x to $x + \Delta x$ wrote:

$$D = \frac{1}{2 \sin \alpha} \frac{\Delta M}{\Delta x} \quad (3.1)$$

Where α is the angle between the diagonals and the horizontal and ΔM is the incremental moment.

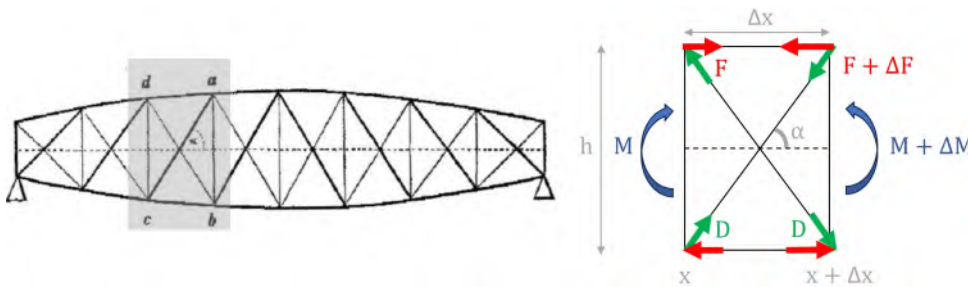


Figure 3.3 – Lattice girder with crossed diagonals used by Schwedler as a case study (Schwedler, 1851, p. 162) and corresponding diagram of forces in the case of parallel chords.

Schwedler’s approach relied on several assumptions. Crossed diagonals should not interact at their crossing point, and they should have identical cross-sections. Furthermore, the vertical load was supposed to be evenly distributed between the top and the bottom chords. This load distribution was ensured by the vertical web members.

Despite Schwedler’s contribution to the shear force, the design of web members in lattice girders used in roof structures seems to have retained secondary importance compared to the design of the chords, way until the end of the 19th century. The consequence can be witnessed in some design reports and technical journals. In the design report drafted by the contractor Daydé et Pillé for the train shed of Bordeaux Saint-Jean in 1896, cross-sections were calculated only for the chords of lattice purlins, not for their crossed diagonals (Daydé et Pillé, 1896). In 1888, the journal *Le Génie civil* illustrated

the new train sheds of Gare Saint-Lazare in Paris. It depicted the detailed cross-sections of the lattice rafters from the Polonceau roof trusses, providing information only about their chords, not their web members (Richou, 1888). This negligence was maybe due to Schwedler's publication being explicitly dedicated to bridge girders through its title, even though it could apply to any lattice girder. Schwedler's theory was spread in France quite rapidly, but again, at first, the application focused on bridge girders (Collignon, 1864). It can be assumed that lattice purlins or rafters, having a secondary role compared to the main roof trusses, were more likely to be calculated following Navier's simple approach, though it was incomplete. When they were not calculated, cross-sections attributed to web members must have resulted from practical experience.

Résal's synthetic approach

Towards the end of the 19th century, some engineers like Résal managed to merge Navier's and Schwedler's theories in a practical way, with synthetic formulas applicable to various types of web patterns (Résal 1892, 577–583). Following Résal's approach, the moment and shear force were determined treating the lattice girder as a continuous beam. Considering a lattice girder with two parallel chords of identical cross-section, the maximum stresses in the chords σ_c and in the diagonals σ_w could then be computed as:

$$\sigma_c = \frac{M_{\max}}{I_c} \frac{H}{2} = \frac{M_{\max}}{A_c h} \frac{H}{h} \quad (3.2a)$$

$$\sigma_w = \frac{V_{\max}}{2A_w \sin \alpha} \quad (3.2b)$$

Where I_c is the moment of inertia of the girder for in-plane bending, A_c is the cross-section of each chord, A_w is the cross-section of the diagonals, h is the lever arm between the chords, H is the total height of the lattice girder (Fig. 3.4), α is the angle between the diagonals and the horizontal, and M_{\max} and V_{\max} are the maximum moment and shear force respectively.

It is interesting to note that Résal's formulas yield higher stresses than the one that would be derived from Schwedler's approach. This is mainly because in Schwedler's theory, the forces in the chords and diagonals are calculated cell by cell, while Résal computes the loads assuming a continuous beam. Furthermore, the maximum stress in the chords σ_c corresponds to Navier's theory. According to Schwedler, estimating the maximum axial force in the chords as M_{\max}/h , the stress σ_c would write:

$$\sigma_c = \frac{M_{\max}}{A_c h} \quad (3.3)$$

Thus, Navier’s approach yields an estimated stress in the chords higher than Schwedler’s by a ratio of H/h (Fig. 3.4).

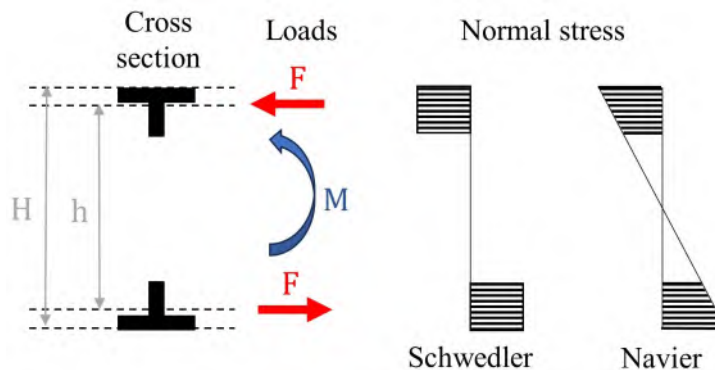


Figure 3.4 – Calculation of the stress distribution in the chords of a lattice girder according to Schwedler and Navier.

This historical study of structural analysis methods applicable or applied to lattice girders enhanced the approximations related to the original design, which should be kept in mind when re-assessing those structures. The next section focuses on joint modelling. In the 19th century, engineers were already aware of a discrepancy between the assumed behaviour of riveted joints and analytical models elaborated for truss-like structures. Today, reviewing historical and recent literature on riveted connections may help improve structural assessment.

3.2 Joint modelling

3.2.1 Pinned, rigid or semi-rigid

In the last decades of the 19th century, some engineers acknowledged that the models used to calculate trusses, relying on the assumption that the joints between chords and web members were pinned, did not reflect the as-built reality of riveted iron or steel trusses. The theory of secondary stresses was developed from the 1870s, allowing to take into account the effect of rigid joints or eccentricities at connection nodes. In 1872, Winkler estimated that secondary stresses, due to additional bending moments resulting from those effects, could amount to up to 30% of primary stresses resulting from truss theory (Kurrer, 2018, p. 797). However, in practice, secondary stresses in lattice girders were not calculated. They were not mentioned in the design report for the train shed of Bédarieux (Daydé et Pillé, 1902). This gap between theory and practice may be due to the fact that the transition from theoretical developments to teaching in engineering schools across Europe and to implementation in practice took time, even more so with language barriers (Schueremans et al., 2018).

In the second half of the 20th century, new computational tools have been developed, which enabled physical understanding to be transposed easier and more accurately into modelling. The finite element method (FEM) allowed numerical simulation to become a pillar of structural design, alongside theory and experimentation (Kurrer, 2018, p. 847). FEM relieved engineers from the load of time-consuming analytical calculations. However, the drawback of numerical models is that they tend to set aside the reflection on what they represent. When a lattice girder is modelled, the question does not arise whether it behaves like a truss or like a beam: the software decides, depending on the input modelling assumptions. As formulated by Argyris, one of the founding fathers of modern FEM, in 1965: “the computer shapes the theory” (Kurrer, 2018, p. 848).

A great source of differences in the structural analysis of trusses between the 19th century and today is that designers used to “choose” whether a web member participated in bearing the load, whether it worked in compression or in tension, and they calculated accordingly. Conversely, today, without prejudging how the system is supposed to behave, our numerical models put all the elements on an equal footing and the distribution of the loads is done according to the rigidity of the components. Therefore, the modelling assumptions behind a numerical model are essential - typically the freedom of movement of riveted joints in lattice girders. “Until the 1920s, we tried to build as we calculated. Since then, relying on increased experience, we have tried to calculate as the constructively designed structure requires” (Werner et al., 1992, p. 56) [transl.].

Many studies from recent literature have focused on riveted truss structures. In finite element models, each truss member is usually reduced to its longitudinal axis using beam elements. The assumptions made for the modelling of the riveted connections vary a lot. Joints are assumed to be rigid or pinned depending on what “feels” realistic based on the geometry. For example, Buitrago et al., 2021 analysed a riveted Pratt-type truss bridge for which the diagonals were modelled as fully connected to the chords, because the connections looked relatively bulky and involved multiple rivets. In contrast, Braathen Granhaug et al., 2018 studied another riveted truss bridge with a similar pattern, but where diagonals were connected to the chords through gusset plates. Riveted connections were then considered rigid for in-plane rotations and pinned for out-of-plane rotations. de Bouw, 2010 investigated roof truss structures in which the diagonals were connected to the chords with single-riveted joints. Pinned joints were then introduced in the model for both in-plane and out-of-plane rotations. Fig. 3.5 displays several riveted connections in truss-type structures, with various degrees of complexity. For the connection in Fig. 3.5a, assuming diagonals to be fully connected to the chords for both in-plane and out-of-plane rotations feels appropriate. For the connections in Fig. 3.5b and even more so in Fig. 3.5c, the choice between rigid and pinned seems more arbitrary. Because of its consequences

on the load distribution and on the predicted buckling behaviour, a refined knowledge of the joints' behaviour is necessary.

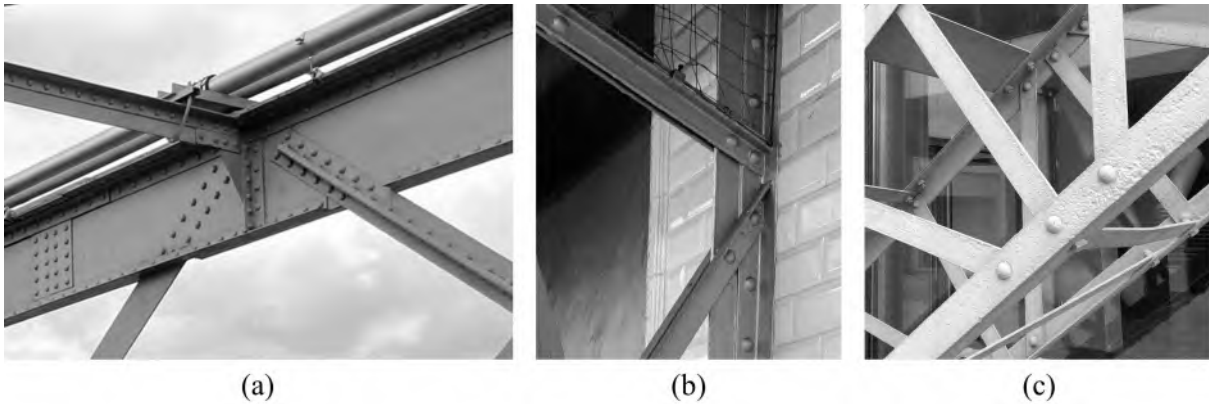


Figure 3.5 – Riveted connections in truss-type structures: (a) Lattice bridge across the Loire - Pont de Varennes-Montsaureau; (b) Roof truss in the metro station Duplex, Paris, France; (c) Outer structure of the former Sudac factory, Paris, France (Pictures by H. Franz).

While in conventional structural analysis, joints are considered either perfectly rigid or perfectly pinned, the reality is usually in-between: connections are semi-rigid. The study of semi-rigid connections started in the first quarter of the 20th century and intensified from the 1950s onwards, focusing mostly on joints in steel frame structures, typically beam-column connections (Celik et al., 2022). When structural analysis stays in the elastic domain, semi-rigid connections can be described by a linear moment rotation curve, whose slope is the rotational stiffness of the joint (Fig. 3.6). The joints can then be represented by rotational (spiral) springs between the ends of two connected members (Maquoi et al., 1998, pp. 22–23). The classification of a joint as rigid, pinned, or semi-rigid does not depend on the absolute value of its rotational stiffness. The relevant parameter is the ratio between the rotational stiffness k_r of the joint and the bending stiffness EI/L of the connected member, where L and EI are its length and rigidity. This ratio is sometimes called the *stiffness indice* R in the literature (Palacio-Betancur et al., 2019):

$$R = k_r \frac{L}{EI} \quad (3.4)$$

In the case of a pinned connection, R is equal to 0, while in the case of a rigid connection R is tending towards the infinity. To model a near-hinged connection, R must be small, while to model a near-rigid connection, R must be large (Fig. 3.7). In its part dedicated to the design of joints, Eurocode 3 proposes boundary values to classify beam-column connections or column bases in frames (EN 1993-1-8, 2005, §5.2.2.5). No boundaries exist in the literature regarding riveted joints in truss structures, especially single-riveted joints in lattice girders. Therefore, in-depth investigations are crucial to improve the structural assessment of riveted lattice girders. A distinction needs however to be made between the

in-plane and the out-of-plane rotational stiffness. As riveted lattice girders are usually designed to experience in-plane loads, the in-plane rotational stiffness of the joints has an influence on the distribution of internal loads. In contrast, the out-of-plane rotational stiffness has little influence on the results of structural analysis. It is nevertheless a decisive parameter for the assessment of the out-of-plane buckling risk, which is the prime weakness of riveted lattice girders.

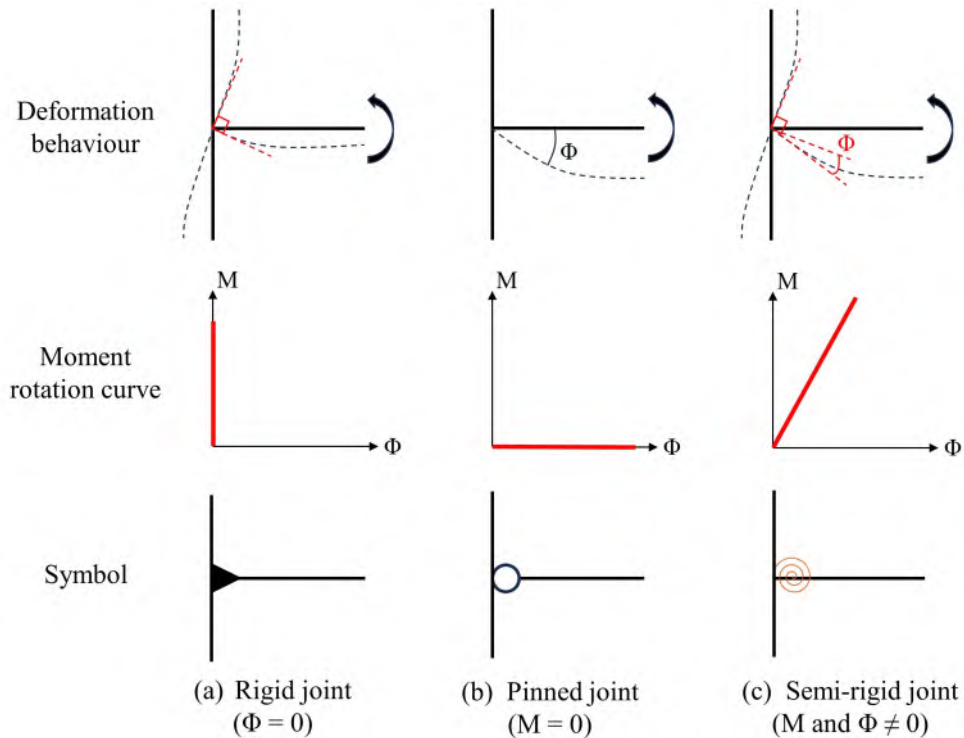


Figure 3.6 – Classification of joints according to their stiffness and corresponding modelling in the case of elastic analysis (derived from Maquoi et al., 1998, pp. 22–23).

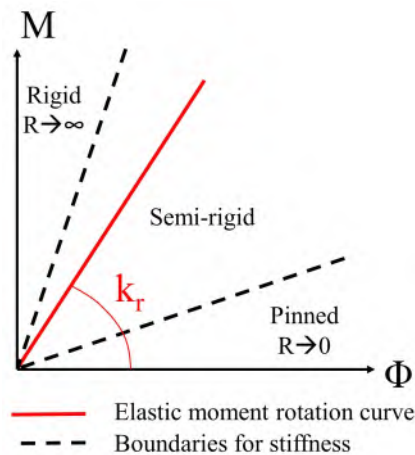


Figure 3.7 – Stiffness classification boundaries (derived from Maquoi et al., 1998, p. 83).

3.2.2 *Understanding of riveted connections*

Since the 19th century, research on riveted connections has mainly focused on assessing their load-bearing capacity when working under shear. Collette, 2014 provides an extensive overview of studies conducted from the mid-19th century to the early 2010s. Pioneering experiments were conducted in 1838 by the British William Fairbairn on the strength of riveted connections assembling wrought-iron plates (Fairbairn, 1850). Other investigations followed, both in Europe and the US, revealing the different failure mechanisms of riveted splice joints subjected to shear loading: plate tension (net section), rivet shear, and plate bearing (around the rivet hole). The developed design methods, which were based on failure modes, i.e. on the behaviour under ultimate loads, disregarded the frictional resistance induced by the rivet clamping force. However, there was a debate on whether to consider riveted connections as friction-type or shear-type fasteners. Some engineers argued that under service loads, the frictional strength was sufficient to take up the shear loading (e.g. Clark, 1850). From the 1880s onward, it was finally agreed to neglect the contribution of the frictional strength, mostly because of the high variability in the magnitude of the clamping force.

Riveted connections made by hot riveting are indeed very sensitive to the manufacturing process. The residual tensile force in the rivets results from the driving temperature during the hot riveting process (Lepretre et al., 2016), which cannot be accurately controlled. Thus, the residual force has been shown to be effectively largely scattered, especially for short grip lengths - the grip length being the total thickness of the assembled plates (Leonetti et al., 2020). Overall, the bandwidth of the rivet pre-stress is in the range 20-220 MPa, with an average value of about 100 MPa (D’Aniello et al., 2011). It is low compared to the clamping force of about 600 MPa in high-strength friction-grip bolted joints (Åkesson, 2010, p. 32). Even though the clamping force in rivets is relatively low, its role in the deformation behaviour of riveted joints under service conditions, that is in their stiffness, cannot be dismissed as was its influence on their strength.

In the last decades, some studies focused on assessing the stiffness of riveted connections, mostly because of its influence on their fatigue strength. Studies from the literature dealt with the shear stiffness of simple splice joints (D’Aniello et al., 2011; Gallegos Mayorga, 2016; Jost, 2012) or with the rotational stiffness of more complex bridge connections (Al-Emrani et al., 2003; Imam et al., 2007). To understand the contribution of friction to the stiffness, it is of interest to consider a typical load-deformation curve for a single-riveted splice joint subjected to shear (Fig. 3.8a). The behaviour can be decomposed as follows (Åkesson, 2010):

Stage I: The load is transmitted between the plates through static friction: the joint behaves as a friction-type fastener and is very rigid.

Stage II: The static frictional strength is overcome and the load is transmitted through dynamic friction: the connected plates slip on one another.

Stage III: The rivet shank enters into contact with the internal surface of the rivet hole. The load is transmitted both by friction between the plates and by shearing of the rivet and bearing in the plates around the rivet hole.

Stage IV: Plastic strains develop. The ultimate strength is a function of either the tensile strength of the plates, the bearing capacity or the rivet shear strength.

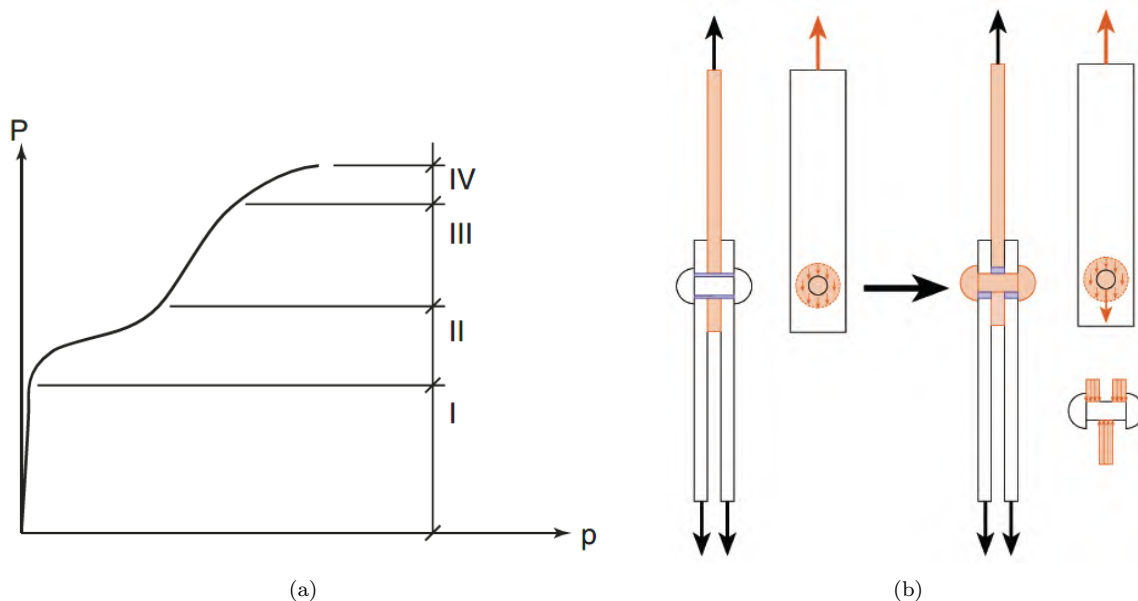


Figure 3.8 – (a) Characteristic load-deformation behaviour of a riveted joint (Åkesson, 2010); (b) stress state in stage I and II (left) and in stage III (right)(Gallegos Mayorga, 2016).

Fig. 3.8b represents the activated parts of the assembly and the associated stress states, first in stages I and II and then in stages III and IV. This working scenario implies that for shear loads of moderate magnitude, riveted joints are slip-resistant. The amount of shear load that can be transferred by friction in stage I and stage II depends both on the clamping force and on the static and dynamic friction coefficients of the plates. Experimental investigations on riveted lap shear connections showed that, in practice, stage I is more or less pronounced. Gallegos Mayorga, 2016 observed sliding between the plates right from the application of the load, while, for some of their specimens, D’Aniello et al., 2011 obtained a sudden slip only after a certain degree of elastic deformation. Overall, the stiffness of riveted joints may correspond only to the stiffness of the joined plates, if static friction is working, or also to the sliding between the plates, if static friction is overcome and some clearance exists between the rivet and the hole.

For the assessment of riveted lattice girders, it is rather the rotational stiffness of riveted joints than their shear stiffness that is decisive. Numerical studies from the literature on riveted connections usually use finite element models of the connection itself, where the

clamping force can be applied on the rivets as an input. However, in contrast with studies on the shear stiffness, the existing literature tends to discard or disregard the effect of the clamping force of rivets on the rotational stiffness of riveted connections. Al-Emrani et al., 2003 examined the behaviour of double angle stringer-to-floor-beam connections in riveted railway bridges and showed numerically that the rotational stiffness of double-angle stringer-to-floor-beam connections is primarily a function of the geometry, in particular the distance between the rivets and the fillet of the angle (Fig. 3.9). The magnitude of the clamping force in the rivets was found to have only a marginal effect on the rotational stiffness of the connections. This was confirmed by Imam et al., 2007. Also, Sarou et al., 2023 developed analytical models and simplified numerical models to determine the compressive stiffness of L-stubs, which can be used to model the rotational behaviour of bolted or riveted double web angle connections. In these models, bolts and rivets are treated the same way, the rivet clamping force is neglected. Minor et al., 2019 presented a numerical study on the rotational stiffness of truss joints from the main girder of an old riveted bridge. They established a linear relationship between the rotational stiffness of the connection and the number of rivets of the connection. No clamping force was integrated in the model.

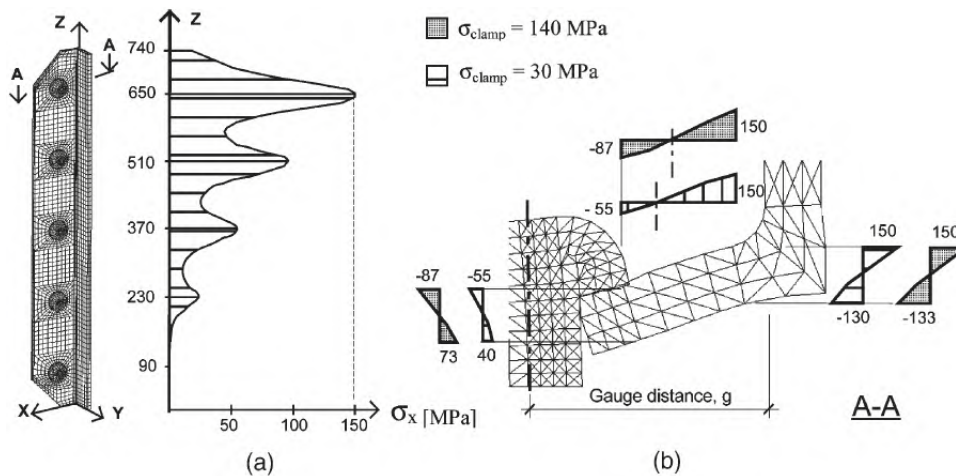


Figure 3.9 – Distribution of bending stresses in a riveted angle from a stringer-to-floor-beam connection (Al-Emrani et al., 2003).

The review of literature on riveted connections enhanced that the clamping force has an influence on the deformation behaviour of riveted connections but its influence on rotational stiffness may be negligible compared to geometrical parameters. In the case of single-riveted joints, where the rivet itself plays a central role, the variability of the clamping force may still be responsible for scattered joint behaviours within a lattice girder. A numerical study investigating the influence of the clamping force on the rotational stiffness of single-riveted joints (in-plane or out-of-plane) is missing.

3.3 Discussion based on the case study

The consequences of various possible modelling assumptions on the stress distribution in lattice girders are now illustrated using the case study of a lattice purlin in the train shed of Montauban. This train shed was built in 1903 by the steel construction company Daydé et Pillé and retrofitted in 2012 by SNCF. The structural assessment report from the 2012 restoration, drafted in 2010 by the contractor Constructions Saint-Eloi, was made available by AREP. This report helped validate the geometry of the structure. The original design report was not available from the archives of SNCF for the train shed of Montauban, but for the very similar train shed of Bédarieux, built by the same contractor in the same year (Daydé et Pillé, 1902). This report was used to derive the historical loads and compare the design principles of these train sheds with common practice at the time of construction. An extract of the report is presented in the Appendix.

3.3.1 Geometry

The primary structural components of the train shed of Montauban are trussed arches spanning 24.8 m. Between those trussed arches, placed every 12 m, lattice purlins span in the longitudinal direction. Lattice purlin n°4 (Fig. 3.10a) was chosen as a case study because it was the purlin experiencing the highest load, according to the original design report of Bédarieux. It is inclined by $\beta = 14^\circ$ from the vertical to follow the slope of the roof. Its total height H is 640 mm, while the lever arm h between the chords is 610 mm. The chords are double-angle irons 60 mm x 60 mm x 6 mm. The web members are crossed diagonals made of 50 mm x 6 mm flats, inclined by $\alpha = 42.5^\circ$ compared to the horizontal. Only the three most compressed diagonals on each side of the purlin are constituted of double flats (Fig. 3.10b, (c) and (d)).

3.3.2 Historical loads

In the historical design report of Bédarieux, Daydé et Pillé considered the following loads:

- Dead loads g :
 - Self-weight of the purlin (and some additional structural components), estimated 35 daN/m along the purlin;
 - Weight of the roofing 30 daN/m² (on the basis of the zinc roof, but applied also to glazed surfaces);
- Snow $s = 60$ daN/m²;
- Wind $w = 200$ daN/m² at an angle of 10° to the horizontal.

Only two load combinations were considered: $g + s$ (dead loads + snow) and $g + w$

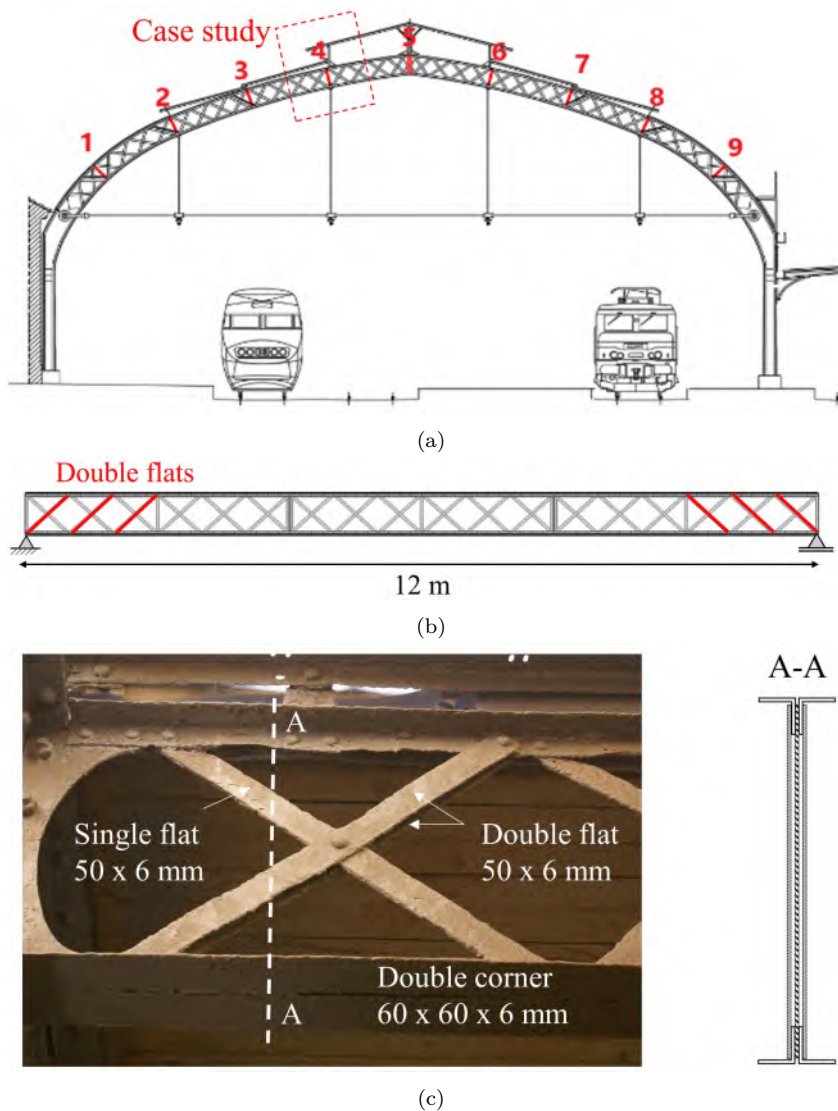


Figure 3.10 – Geometrical details for the case study: (a) elevation view of the train shed; (b) elevation view of the studied lattice purlin n°4; (c) photograph of crossed diagonals near the support (before renovation - picture from SNCF) with a cross section of the lattice purlin.

(dead loads + wind). Loads tangential to the roof were not transmitted to the purlins. The width of influence of the purlin along the roof slope is $e = 2.8$ m. On purlin n°4, $g + s$ yielded the highest normal loads, that is in the plane of the lattice girder. Thus, the resulting uniform load in the plane of the purlin is 280 daN/m.

3.3.3 Structural analysis

The lattice purlins of the train shed of Bédarieux were designed following Résal's approach (see Section 3.1.2). The extract of the original design report presented in Fig. A.2 of the Appendix displays the calculations carried out for the ridge purlin. Under uniform load, the maximum axial force in the chords F_{max} is obtained at mid-span of the girder, while the maximum axial force in the diagonals D_{max} is near the supports (Fig. 3.11). For

the purlin from our case study in Montauban, bearing a uniform design load of 280 daN/m, Résal's approach yields a maximum axial force in the chords $F_{max} = M_{max}/h = 8217$ daN and a stress $\sigma_c = 7.38$ daN/mm² (using Eq. (3.2)) in the net section, that is without the rivet hole. The maximum axial force in the diagonals is $D_{max} = 1253$ daN, which corresponds to $\sigma_w = 6.14$ daN/mm², also in the net section, when considering only single diagonals. By comparison, Schwedler's approach yields $F_{max} = 8166$ daN and $\sigma_c = 6.94$ daN/mm² for the chords and $D_{max} = 1168$ daN and $\sigma_w = 5.73$ daN/mm² for the diagonals.

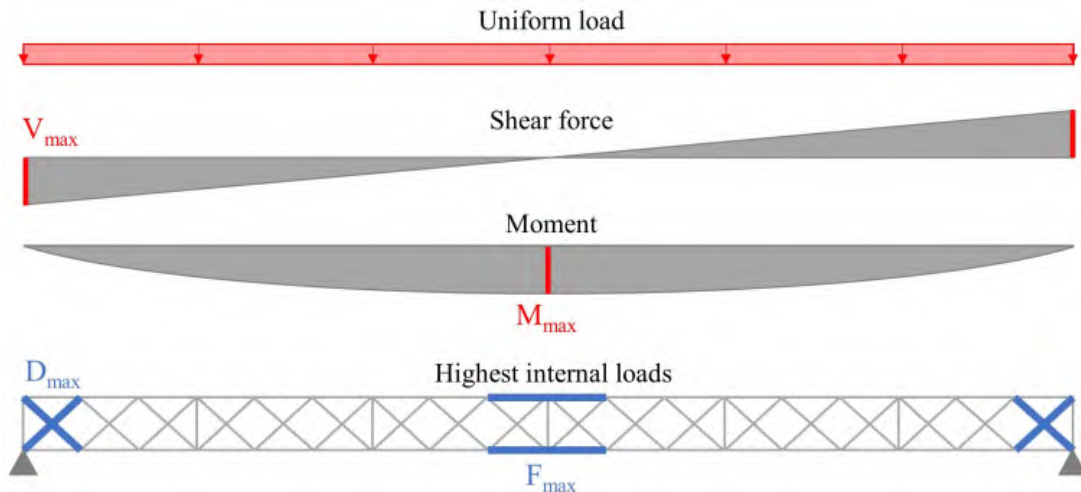


Figure 3.11 – Distribution of internal loads following Résal's approach for a lattice purlin of the train shed of Montauban under uniform loading. Location of the most stressed chord and diagonal sections.

Let us now compare those values with the results obtained from finite element (FE) models using first-order analysis. For this case study, the FE models of the lattice purlin were built with the commercial structural engineering software Robot, version 2022 (« Autodesk - Robot Structural Analysis », 2024), to be in the same operational conditions as a structural engineer who needs to assess an existing structure. A first FE model (FE1) of the lattice purlin was built, in which all diagonals were attributed the same cross section and were modelled as truss elements. The diagonals could then transmit only axial forces, which corresponds to the historical assumptions of truss theory. However, the chords were modelled as continuous beam elements (Bernoulli-type), and the load was applied as a uniform load on the top chord. The chords were divided into segments of about 160 mm and the diagonals into segments of about 120 mm, which ensured convergence. Under these modelling assumptions, the maximum axial force in the chords was found to be $F_{max} = 8176$ daN and the maximum axial force in the diagonals $D_{max} = 1259$ daN. These values are in fair agreement with the approximate results from Résal's approach. One difference with Résal is that in a vertical section of the girder, the bottom chord experiences a higher axial force than the top chord, which is reminiscent of a truss-like behaviour, where the top and the bottom chord are not exactly symmetrical in terms of

load distribution. The other difference with Résal is that, in the FE model, the chords experience bending moments in addition to axial forces (Fig. 3.12). At mid-span of the girder, those moments induce an increase of about 10% of the stresses in the net section of the bottom chord.

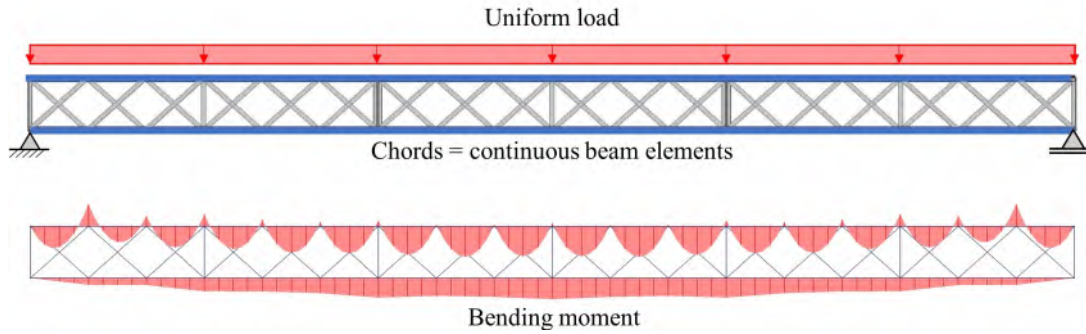


Figure 3.12 – Bending moment distribution in the chords when the chords are modelled as continuous beam elements and the load is applied as a uniform load on the top chord.

The FE model was then modified (FE2) to take into account that the three compressed diagonals were made out of double flats, instead of single flats. The maximum axial force in the most compressed diagonals consequently became 1371 daN, meaning it increased by 9%.

Finally, in a last model FE3, the diagonals were converted to beam elements, able to transmit bending moments. The riveted joints at their extremities were modelled as rigid, both in the in-plane and out-of-plane directions. Also crossed diagonals shared a node at their crossing point, in accordance with the as-built reality where diagonals are joined by a rivet in their midst. The distribution of axial forces was not affected much. In the chords, the secondary stresses due to the additional bending moments were found to be negligible. In contrast, in the diagonals, the secondary moments led locally to a significant increase of the secondary stresses. In the most compressed diagonal, with a double flat cross section, the stress in the net section increased by 25%, which is close to the estimate of 30% made by Winkler in 1872. Tab. 3.1 provides an overview of the results.

Table 3.1 – Comparison of internal loads and stresses obtained from various analytical and FE models. FE1: diagonals modelled with truss elements, all as single flats. FE2: diagonals modelled with truss elements, with differentiated cross sections (single vs. double flats). FE3: diagonals modelled with beam elements, with crossing node, with differentiated cross sections.

		Schwedler	Résal	FE1	FE2	FE3
F_{max}	[daN]	8166	8217	8176	8176	8223
D_{max}	[daN]	1168	1253	1259	1371	1367
σ_c	[daN/mm ²]	6.94	7.38	7.61	7.61	7.67
σ_w (single diag.)	[daN/mm ²]	5.73	6.14	6.17	-	-
σ_w (double diag.)	[daN/mm ²]	2.86	3.07	3.09	3.36	4.23

These results show that, when the diagonals were designed using Résal's approach, the analytical calculations provided a good estimate of the stresses. However, if the clamping force is such that riveted joints are indeed rigid for in-plane rotations, secondary stresses are non-negligible. It could be that the original design, assuming pinned connections, was thus not always on the safe side - depending in how large the security margin was in the selected design criteria. When assessing roof structures today, the significance of secondary stresses lattice girders depends on how much they influence the buckling behaviour. In this regard, the joints' flexibility regarding out-of-plane rotation, which does not play a role in the load distribution resulting from normal loads, is actually the decisive parameter.

3.4 Conclusion

Riveted lattice girders used in roof structures between 1850 and 1930 tell an interesting story about the design practice of this period. The structural analysis methods used to design them as beam equivalents were a compilation of Navier's bending theory and Schwedler's truss theory. Engineers such as Résal strived for practicality, which led to underestimating some stresses - especially if riveted joints exhibit a rigid behaviour for in-plane rotations. A literature review on riveted connections showed that the assumptions made in finite element models of truss structures regarding the rotational stiffness of riveted connections vary extremely. Recent research aiming to assess the stiffness of riveted joints has revived the debate about the role of the clamping force and the resulting friction in the structural behaviour. Some studies investigating the rotational stiffness of some typical riveted connections underlined the prevalent influence of the geometry over the clamping force. This questions whether the rotational stiffness of riveted connections differs from bolted connections because of the mechanical properties of rivets or rather because of the geometrical properties specific of old riveted connections. In any case, single-riveted joints in lattice girders still need to be investigated. Chapters 4 and 5 focus on their out-of-plane rotational stiffness because of its dominant influence on out-of-plane buckling, which was responsible for many reinforcements in recent train shed restorations.

ASSESSING THE ROTATIONAL STIFFNESS OF RIVETED JOINTS BY MODAL TESTING

Chapter 4 presents the experimental and numerical investigations aiming to assess the out-of-plane rotational stiffness of single-riveted joints in lattice girders. Modal-based indicators are proposed to identify the average stiffness of all similar joints. An indicator is also developed to detect local variations of joint stiffness.



Principle of vibration tests on the tested lattice girder (Picture by H. Franz).

Contents

4.1	Applications and techniques of modal testing	78
4.2	Proposed methodology	88
4.3	Results and discussion	100
4.4	Conclusion	111

Riveted lattice girders with typical single-riveted joints were reclaimed from a demolition site. A modal testing campaign was carried out on one of the girders to assess the out-of-plane rotational stiffness of the single-riveted joints by a non-destructive method. This chapter first describes the principles of modal testing, with a focus on the applications for civil engineering structures, and gives an overview of the existing techniques, insisting on the ones that were selected for testing the lattice girder. Then, the proposed methodology is detailed for the experiments and the associated numerical modelling. Finally, the results arising from the comparison of the measured and the predicted modal behaviour are presented. They first concern the average joint stiffness in the tested lattice girder and then the effect of local variations of the joint stiffness. Most of the results presented in this chapter have been previously published in preliminary conference papers (Franz et al., 2022b; Franz et al., 2023b) and in a journal (Franz et al., 2024a).

4.1 Applications and techniques of modal testing

4.1.1 *Applications of modal testing for civil engineering structures*

Modal testing consists in measuring and then analysing the vibration properties of a structure or of a structural component or assembly. It was first applied around 1940 to aircraft structures and really developed from the 1970s, expanding to multiple fields in mechanical and civil engineering (Silva, 1999). In civil engineering, modal testing is used for a range of purposes:

- assessing the susceptibility of an existing or new structure to vibrations, when subjected to dynamic loading;
- identifying the structural properties or the stress state of an existing structure;
- structural health monitoring.

Regarding the identification of structural properties, modal testing has in particular been used to investigate semi-rigid connections in steel structures. Many studies focused on steel frames with semi-rigid supports or beam-to-column connections (Türker et al., 2009). Other studies aimed to estimate the actual behaviour of joints in truss-type structures. Szopa et al., 2020 studied a three-dimensional bolted truss structure constituting a simplified physical model of an electric pylon. They used modal testing to identify the rotational stiffness of single-bolted connections, around the bolt axis. Luong, 2018 developed a methodology based on vibration measurements providing information about the joint flexibility of semi-rigid joints in iron and steel roof truss structures. She tested her approach with an in-situ experiment on a historic Polonceau truss, displaying various typologies of bolted joints connecting tension members and compression struts. She showed that the joint flexibility was closer to the rigid condition than the common assumption

of hinged joints and explained these findings by the presence of friction and possible corrosion damages.

Regarding structural health monitoring, vibration-based methods were primarily developed for use on large and expensive structures such as bridges and offshore platforms, to detect damages typically related to corrosion or fatigue (Rytter, 1993). Most classical vibration-based damage assessment methods rely on changes in the natural frequencies or the mode shapes (Carden et al., 2004). The measurement of natural frequencies is easy and usually requires only one sensor, so changes in natural frequencies were used for damage detection in many applications, such as monitoring the tension of pre-stressed cables (Robert, 1993). However, the use of natural frequency shifts was mostly successful for small simple laboratory structures with only single damage locations, such as a cantilever beam with a single crack (Carden et al., 2004). Contrary to natural frequencies, mode shapes can help localise and assess damages. More generally, they can be used to detect local variations of stiffness or mass compared to the expected distribution. Mode-shape-based damage assessment methods can, therefore, also be seen as “local” system identification methods.

4.1.2 Principles and techniques of modal testing

When modal testing is used for the identification of structural properties, the principle is to measure a structure’s vibration properties in order to validate or update a finite element model of the structure. This model can then be used to predict the structure’s behaviour, both static and dynamic. The different steps of vibration-based structural identification can be broken down as follows:

- collecting data;
- processing the digital signals;
- extracting modal parameters and estimating mode shapes;
- updating a finite element model to obtain a sufficient level of correlation with experimental results.

Data collection

The key challenges of data collection consist in choosing the excitation source and the measurement technique. Modal testing techniques can be classified according to the type and function of the excitation source, as (i) *input-output* or *experimental modal analysis* (EMA); (ii) *output only* or *operational modal analysis* (OMA); and (iii) *combined experimental-operational modal analysis*, also called operational modal analysis with exogenous input (OMAX) (Reynders, 2012). In EMA, the structure is excited by one or several artificial dynamic forces and both the excitation and the response of the struc-

ture are recorded. The modal parameters are extracted from the measurements, in the frequency range of interest. To test large structures in operational rather than laboratory conditions, OMA was developed to extract the modal parameters from the dynamic response to the ambient excitation of a structure, due for example to wind or traffic. In OMAX, an artificial force is used as an excitation in operational conditions. OMA is usually favoured for large civil engineering structures because excitation forces applied in EMA techniques, typically by an impulse hammer, do not provide enough energy to obtain a recordable response. For lattice girders, which are lightweight structures, an impulse hammer remains a convenient excitation source. Thus, for our study, EMA was favoured.

In EMA, different excitation sources can be used. Shakers provide a continuous excitation yielding forced vibrations of the structure. Impulse hammers constitute another popular method and yield free vibrations of the structure. The frequency range effectively excited by a hammer depends on the mass of the hammer head and the stiffness of the hammer tip. The softer the tip is, the narrower the excited frequency range. It is important to choose the tip so that the excited frequency range is wide enough, but not too wide so that excitation energy does not get wasted in vibrations outside the range of interest. Nevertheless, applying excitation using a hammer has some drawbacks. It is difficult to ensure repeatability as the position and the orientation of the hammer relative to the surface may vary. Also, caution must be applied to avoid multiple impacts or “hammer bounce” (Ewins, 2000).

The response of the structure is estimated from measured vibration data, typically acceleration and displacement measurements. The collection of vibration data can be carried out through contact or contactless solutions. Contact-based methods rely on sensors integrated into the monitored structure. The most widespread technique is based on accelerometer measurements. Accelerometers have the advantage of providing a relatively high precision and a large frequency bandwidth. However, the full-scale characterisation of a structure usually requires a large number of such sensors, leading to wiring issues and an addition of mass. When choosing accelerometers, several points of attention need to be considered. The mass of accelerometers must stay below 10% of the mass of the structural members on which they are placed. The frequency bandwidth must correspond to the frequency range of interest: piezoelectric accelerometers can provide a much wider frequency bandwidth than capacitive accelerometers but are not suitable if the frequencies of interest are low. The sensitivity of accelerometers, that is the ratio between the electrical signal and the measured physical parameter, must ensure that the sensors do not saturate at the time of impact while providing a high enough precision. The fixation system of the accelerometers on the structure must be able to resist shocks: if an impulse hammer is used, magnet assemblies must be preferred to beeswax (Thomas et al., 2007).

The wide deployment of contact-based sensors such as accelerometers or strain gauges in realistic engineering structures is limited by the requirement of cumbersome and expensive installation and maintenance of sensor networks and data acquisition systems. To avoid those drawbacks, non-contact measurement methods relying on radar and optical imaging technologies, such as laser instruments or cameras, have been developed in the last two decades. However, those methods provide an alternative favouring high-displacement and low-frequency vibrations (Feng et al., 2018).

Digital signal processing

Many mathematical methods were developed to process the measured vibration data, either in the frequency or in the time domain (Reynders, 2012). In the frequency domain, the vibration response can be described by frequency response functions (FRFs). The tested structure is reduced to a certain number of degrees of freedom (DOFs), corresponding to displacements or rotations at selected measurement locations. A frequency response function represents the harmonic response X_j in one of the degrees of freedom j , caused by a harmonic force F_k applied at a different degree of freedom k :

$$\alpha_{jk}(\omega) = \left(\frac{X_j}{F_k} \right) \quad \text{when} \quad \forall m \neq k, F_m = 0 \quad (4.1)$$

Using FRFs corresponds to a deterministic system description, that is only one type of description amongst a myriad of other possible descriptions (Reynders, 2012). In the field of modal testing, system identification based on FRF measurements is sometimes considered only as a preliminary step before more sophisticated parametric identification techniques are implemented (Antoni et al., 2007).

Current FRF measurement techniques are extensively based on the discrete Fourier transform (DFT) owing to its very efficient computation using the fast Fourier transform (FFT) algorithm. To obtain consistent estimates of the FRF, the computation of the FFT of the digital signals is completed by various smoothing or averaging operations (Antoni et al., 2007). Digital signals have a random character due to a certain level of noise. To calculate the frequency spectrum of those signals, spectral densities are used. While the Fourier transform of a signal describes the signal amplitude along the frequency range, the power spectral density (PSD) describes a quantity squared that corresponds to an energy content.

The power spectral density S_{ff} of the excitation and the cross-spectral density of excitation and response S_{xf} can be computed as a multiplication of Fourier transform

and Fourier transform conjugates:

$$\begin{aligned} S_{ff}(\omega) &= F(\omega).F^*(\omega) \\ S_{xf}(\omega) &= X(\omega).F^*(\omega) \end{aligned} \quad (4.2)$$

Where $F(\omega)$ and $X(\omega)$ are the FFT transforms of the excitation (input) and the response signal (output) respectively, and $F^*(\omega)$ is the conjugate of $F(\omega)$.

The PSD estimate generated from one set of sampled time-domain data can be volatile. When the excitation signal is a random stationary noise, estimates of the PSDs are usually computed using an average from individual PSDs based on different time segments of the original data. The Welch's procedure, using overlapped windowed segments, has become a standard (Antoni et al., 2007). Nevertheless, when the excitation signal is an impulse, this procedure is not necessary.

Based on the PSDs, the FRF can be estimated. Several estimators of the FRF exist. Ewins, 2000 proposed an estimator having the advantage of eliminating the bias due to noise on the output:

$$H(\omega) = \frac{S_{xf}(\omega)}{S_{ff}(\omega)} \quad (4.3)$$

To verify the quality of the measurements, the coherence $\gamma^2(\omega)$ can be calculated based on the PSDs:

$$\gamma^2(\omega) = \frac{|S_{xf}|^2}{S_{xx}S_{ff}} \quad (4.4)$$

$\gamma^2(\omega)$ is comprised between 0 and 1. If the measurements are well made, the coherence should be close to unity.

The estimates of the Fourier transforms and their derivatives are obtained with a spectrum range $0-\omega_{\max}$ and a resolution $\Delta\omega$:

$$\begin{aligned} \omega_{\max} &= \frac{\omega_s}{2} = \frac{1}{2} \left(\frac{2\pi N}{T} \right) \\ \Delta\omega &= \frac{\omega_s}{N} = \frac{2\pi}{T} \end{aligned} \quad (4.5)$$

where T is the period during which the measurement was made, ω_s is the sampling rate and N is the resulting number of discrete values in the recorded signal. The sampling rate must be large enough to avoid ‘‘aliasing’’, a phenomenon in which high frequencies appear as low frequencies. Shannon's theorem indicates that the sampling rate should be at least twice the highest frequency of the signal, to avoid aliasing. In practice, according to Thomas et al., 2007 the frequency of acquisition f_s should be taken equal to 10 times the highest frequency, to get enough measurement points. The measurement period should be chosen such that the response signal has just died away by the end of it, to

avoid “leakage” problems. Spectral leakage occurs when the signal transformed by the DFT contains a non-integer number of periods. If the incomplete periods have very small amplitudes compared to the complete ones, the leakage, in which spectral energy “leaks” to neighbouring frequency components of the real frequency, is limited.

Modal parameter extraction

Modal parameter extraction is a major step of modal analysis. It is a curve-fitting procedure aiming to match the theoretical expression of individual FRFs with the measured data. The coefficients in the theoretical expression of the FRF thus determined are directly related to the modal properties. There are several forms of FRF according to the nature of the measured response: displacement, velocity or acceleration. When considering the acceleration, the FRF is called inertance. When considering the displacement, the FRF is called receptance and can be expressed explicitly in a series form:

$$\alpha_{jk}(\omega) = \sum_{r=1}^M \frac{\phi_{jr}\phi_{kr}}{\omega_r^2 - \omega^2 + i\eta_r\omega_r^2} = \sum_{r=1}^M \frac{{}_r A_{jk}}{\omega_r^2 - \omega^2 + i\eta_r\omega_r^2} \quad (4.6)$$

where M is the number of considered modes, ω_r and η_r are the natural frequency and the damping ratio of mode r , ϕ_{jr} is the modal displacement of DOF j in mode r and ${}_r A_{jk}$ is the modal constant, also referred to as residue. ω_r , η_r , ${}_r A_{jk}$ are called modal parameters.

Many methods of modal parameter extraction exist. Some extract parameters for a single mode at a time (SDOF methods) or several (MDOF methods). Some operate on a single FRF, that is on a SISO (single input single output) dataset, others on a set of FRFs which have been measured simultaneously at several response points, under one or multiple points of excitation. Those datasets are called SIMO (single input multiple outputs) and MIMO (multiple inputs multiple outputs) respectively. Multi-FRF methods applying to SIMO data are sometimes called global methods (Ewins, 2000).

The “line-fit” method (Ewins, 2000) is an SDOF method, operating on the frequency domain, that can be applied both on SISO and SIMO datasets. SDOF methods are founded on the main assumption that in the vicinity of resonance, the behaviour of the system is dominated by a single mode. Mathematically, it means that the expression of the receptance as in Eq. (4.6) can be written as:

$$\alpha_{jk}(\omega)_{\omega \rightarrow \omega_r} = \frac{{}_r A_{jk}}{\omega_r^2 - \omega^2 + i\eta_r\omega_r^2} + {}_r B_{jk} \quad (4.7)$$

where ${}_r B_{jk}$ is constant. This assumption implies that the modes are sufficiently distinct over the considered frequency range.

The line-fit method, also called “inverse” method, relies on the idea that the plot of

the inverse FRF of a purely SDOF system in the complex (Nyquist) plane is a straight line, from which parameters can be extracted easily. To use this interesting feature, the term ${}_r B_{jk}$ is removed from Eq. (4.7) by introducing a fixing frequency Ω and considering $\alpha_{jk}(\omega) - \alpha_{jk}(\Omega)$. Two successive linear regressions are then conducted and yield values of the modal parameters.

Mode shape estimation

Once the residue is computed for all the measurement points, mode shapes can be derived. The computed residues are usually complex numbers, due to damping. The majority of damping in real structures is concentrated at the joints between components of a structural assembly, which usually results in a non-linear damping distribution. However, test-derived mode shapes can be assimilated to real mode shapes under certain conditions, which makes their comparison with mode shapes produced by theoretical or numerical analysis easier. When the structure vibrates in a real mode, all parts of the structure reach their maximum deflection at the same time in the vibration cycle. In a complex mode, each part reaches its maximum deflection at a different instant in the vibration cycle - which translates into different phases for each measurement point. A test-derived mode shape can be considered close to real if the relative phases between all measured elements are near-0° or near-180°. The complexity of a mode shape can be graphically displayed by plotting all measured elements of the eigenvector on a polar plot. The more points are aligned, the closer the measured mode shape is to a real mode (Ewins, 2000).

To convert a test-derived mode shape to a pure real mode, the procedure is as follows (Fig. 4.1):

1. fitting a straight line to all eigenvector elements on the polar plot (linear regression on the imaginary vs. real parts) and deducting the global phase θ of the mode from its slope.
2. rotating all complex elements of the eigenvector by the angle $-\theta$ (multiplying by $\exp^{-i\theta}$).
3. Option 1: taking the modulus of each element and assigning a plus or minus sign depending on whether the measured residual phase angle is within $\pm 10^\circ$ of 0° or 180° respectively.

Option 2: taking the real part of each element.

When large structures are tested and the number of sensors is limited, it is usual to measure the DOFs of interest in different setups. The data from the different setups then needs to be merged to obtain a complete mode shape. Data merging strategies fall into categories depending on whether the merging is performed before or after modal identification (Reynders et al., 2009). If the number of setups is not too large, the classical

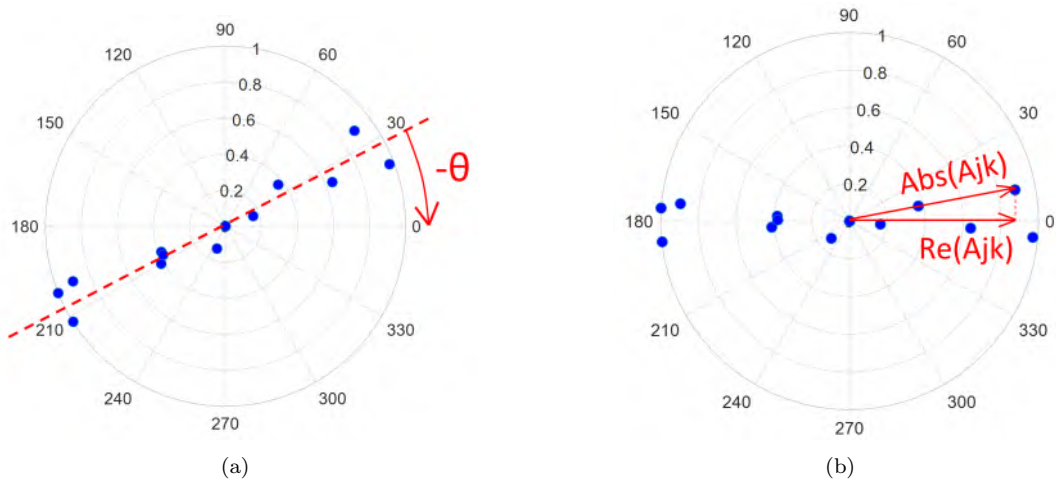


Figure 4.1 – Polar plot of the modal constants measured for one mode. Complex-to-real conversion: (a) setting the average mode phase to zero; (b) using the modulus or the real part of each element.

approach consists in first processing the data from the different setups separately and then merging the data to combine the different parts of the mode shapes. This is typically the approach used when experimental tests are conducted as roving response tests with a single excitation reference. Some of the sensors stay at the same location in all the setups and are used as reference sensors for data merging. This classical approach consists in:

1. selecting one setup as the reference setup.
2. re-scaling the mode shapes of the other setups using the reference DOFs of the reference setup (least-squares method).
3. merging the re-scaled partial mode shapes.

After complete real mode shapes have been derived, they are often normalised to allow a comparison with numerical or analytical mode shapes. There are two most common ways to normalise the measured mode shapes: mass-normalisation and 1-scaling. For mass-normalisation, it is necessary to measure the point FRF at the excitation position H_{kk} , in addition to the transfer FRFs at the response points of interest. The mass-normalised modal displacement at point j for mode r is then, according to Eq. (4.6):

$$|\phi_{jr}| = \frac{|{}_r A_{jk}|}{\sqrt{|{}_r A_{kk}|}} \quad (4.8)$$

The advantage of mass-normalised eigenvectors is that they allow to build a modal model, that is to construct the mass matrix, the stiffness matrix, and the damping matrix of the system. However, a mathematical model is not always needed. To compare numerical and experimental mode shapes, the following procedure can be followed:

1. scaling each experimental eigenvector so that its largest element has a magnitude of 1.

2. scaling each numerical eigenvector to obtain the best fit with the corresponding experimental eigenvector (least-squares method).

One advantage of this 1-scaling method is that the FRF at the excitation point does not need to be measured. Thus the risk of saturation for an accelerometer placed right at the excitation point can be avoided.

Finite element model updating

Finite element (FE) model updating is the process of calibrating the parameters of a numerical FE model based on vibration test data, to reduce the discrepancy between numerical and experimental results.

Either direct or iterative methods can be used. The direct methods directly update the stiffness and mass matrices, but the updated system matrices have little physical meaning. The iterative methods update the physical properties of the finite element model, such as material properties, geometrical measures and support conditions, and edge towards a satisfactory model by minimising objective functions (Ribeiro et al., 2012). Objective functions measure the agreement between experimental and numerical results, depending on selected uncertain parameters and based on selected features of the vibration behaviour. The results and performance of model updating depend on the chosen objective function(s), the optimisation method and the choice of parameters to be modified (Zabel et al., 2009). It is recommended to conduct preliminary sensitivity analyses to retain only the most erroneous and sensitive parameters.

To define objective functions, the first step is to select a residual vector containing the difference between measured and predicted structural behaviour for each mode or in a broader sense, characterising the discrepancy between measured and predicted structural behaviour. Secondly, weights are attributed to each term of the residual vector, depending on the importance of each mode. Finally, the objective function can be defined as the sum of weighted squared or absolute terms of the residual vector (Link, 1999).

Residuals can be formed for example by frequency response errors, by eigenfrequency errors or by mode shape errors. When the residual is based on differences between experimental and predicted eigenfrequency, each term, corresponding to a mode r can be defined as (Szopa et al., 2020):

$$P_r = \frac{|f_{r,\text{num}} - f_{r,\text{exp}}|}{f_{r,\text{exp}}} \quad (4.9)$$

Considering M modes, an objective function can then be defined as:

$$\Phi = \frac{1}{M} \sum_{r=1}^M w_r P_r, \quad (4.10)$$

where w_r are the weights attributed to each mode.

Regarding mode shape errors, the modal assurance criterion (MAC), developed in the 1970s, estimates the degree of correlation between two mode shape vectors. It provides a measure of the least-squares deviation of the points from the straight-line correlation (Ewins, 2000). Given a set of M_{exp} experimental modes and a set of M_{num} predicted (numerical or analytical) modes, a MAC matrix of size $M_{\text{exp}} \times M_{\text{num}}$ can be computed, with each term writing:

$$\text{MAC}_{j,k} = \frac{|\{\phi_{k,\text{exp}}\}^T \{\phi_{j,\text{num}}\}|^2}{(\{\phi_{k,\text{exp}}\}^T \{\phi_{k,\text{exp}}\}) (\{\phi_{j,\text{num}}\}^T \{\phi_{j,\text{num}}\})} \quad (4.11)$$

where $\{\phi_{k,\text{exp}}\}$ is the experimental mode shape vector of mode k and $\{\phi_{j,\text{num}}\}$ is the predicted mode shape vector of mode j . The exponent T indicates a transposed vector. When two sets of mode shape vectors are perfectly correlated, the diagonal terms of the MAC matrix should edge towards 1 and the other terms should edge towards 0. As the MAC is a statistical computation depending on the number of elements in the modal vectors, MAC values are meaningful only if the modal vectors encompass a sufficient number of degrees of freedom (Allemang, 2003).

The terms of the MAC matrix can be used individually as objective functions, or be combined to yield a single objective function. For example, Szopa et al., 2020 proposed an objective function (or “quality criterion”) derived from the sum of all diagonal terms of the MAC matrix. For each mode r , they first defined L_r :

$$L_r = 1 - \text{MAC}_{r,r} = 1 - \frac{|\{\phi_{r,\text{exp}}\}^T \{\phi_{r,\text{num}}\}|^2}{(\{\phi_{r,\text{exp}}\}^T \{\phi_{r,\text{exp}}\}) (\{\phi_{r,\text{num}}\}^T \{\phi_{r,\text{num}}\})} \quad (4.12)$$

Then, they proposed the objective function:

$$\Phi = \frac{1}{M} \sum_{r=1}^M m_r L_r, \quad (4.13)$$

where M is the number of considered modes and m_r are weights selected depending on the importance given to each mode. With this definition, the updating of parameters in the model aims to obtain Φ close to 0.

Regarding the solving algorithms for the optimisation of objective functions, several

methods were developed, such as gradient-based methods, response surface methods and genetic algorithms (Ribeiro et al., 2012).

Detection of local variations

To detect local variations of stiffness or mass compared to the expected distribution, mode-shape-based methods are better suited than frequency-based methods. A reduction of MAC value (see Eq. (4.11)) may be an indication of damage or local variation. However, the effectiveness of MAC as an indicator is limited because it is insensitive to small changes or small magnitudes (Allemang, 2003). The most classical parameter attempting to identify which measurement degrees-of-freedom contribute negatively to the correlation between two sets of mode shapes is the coordinate modal assurance criterion (COMAC)(Ewins, 2000). To avoid biases linked to the definition of modal vectors, the enhanced coordinate modal assurance criterion (ECOMAC) was developed (Hunt, 1992). The ECOMAC between two sets of mode shapes, typically numerical and experimental mode shapes, is defined as:

$$\text{ECOMAC}[\text{set1},\text{set2}](j) = \frac{\sum_{r=1}^n |\phi_r^{\text{set1}}(j) - \phi_r^{\text{set2}}(j)|}{2n} \quad (4.14)$$

where $\phi_r^{\text{set1}}(j)$ and $\phi_r^{\text{set2}}(j)$ are the components of the mode shape vector of mode r at measurement point j for two sets of data, and n is the number of modes taken into account. Other mode-shape-based methods rely on the study of mode-shape curvature or modal strain energy.

4.2 Proposed methodology

The previous section presented a wide range of sophisticated techniques developed for modal testing. The progress made in digital signal processing and modal parameter extraction contributed to reducing experimental biases and increasing the precision of measured modal properties. However, the most classical and simple methods can still provide satisfactory results under certain conditions. SDOF extraction methods are widely used as a preliminary investigation tool, but when the measured modes are sufficiently distinct, their validity can be considered acceptable. Straightforward methods have the advantage of readily providing the experimenter with a pertinent overview of the modal properties of the system. This is the philosophy of the methodology proposed hereafter.

4.2.1 Experiments

Test specimen

Several riveted metallic lattice girders were collected from a demolition site. They belonged to the roof structure of platform sheds, built in 1930 at the railway station Gare de l'Est in Paris, from which a small part was dismantled in 2021 (see Fig.4.2). Two of the lattice girders had the same geometry and visual inspection revealed neither apparent defects in the joints nor damage to the material. They were therefore selected as test specimens, one for modal testing and the other for load testing. The similarity of the geometry between the two girders was verified with tape and calliper measures. They are 3300 mm long Pratt-type cantilevers, with a height varying from 190 mm at their tip to 340 mm at the support (see Fig. 4.3). The bar sections were taken from original plans and verified by measurements with a calliper. The reclaimed lattice girders were covered with several layers of paint, amongst which a layer of lead paint, with its distinct orange colour. The thickness of the paint prevented precise measurements. However, on the girder used for load testing, the paint was locally removed to install gauges on some diagonals and the top chord. Calliper measurements on the naked sections could then validate the sections from the historical plans. Also the comparison of measurements on painted and stripped elements helped estimate the thickness of the paint at about 0.9 mm.

The chords are made of double L45x45x5 angles, while the web members are made of 40x7 flats. The diagonal and vertical web members are connected to the chords by single rivets of 12 mm diameter. The last cell at the tip of the lattice cantilever is filled with a 7 mm thick gusset. Horizontal wing plates served to connect edge beams. At the support of the cantilever, 7 mm gusset plates transmit the loads from the chords to a vertical 68 cm high double L60x60x6 angle. This double angle was originally connected to the web of the main longitudinal girder of the platform shed with two rows of 9 bolts of 16mm diameter. The top chord was also connected to the top chord of the main girder through a horizontal gusset plate and 4 bolts.

The platform sheds were built in 1930 at the same time as the main train shed of the Gare de l'Est. A material survey was carried out in 2016 by the firm A-Corros based on 8 samples of the metallic structure of the train shed. The material was characterised through chemical and metallographic analyses and its mechanical properties were measured with tensile tests. The survey yielded that the structure was made of mild or extra-mild steel, with a carburization level below 0,2%, featuring a mean elastic modulus $E = 210$ GPa. The material constituting the lattice girders of the platform sheds can be assumed to be of the same nature. However, the steel used for the platform sheds may have been of lesser quality, so the value retained for the elastic modulus in the following study is 200 GPa,

in line with recommendations from the literature for mild steel (Brandes, 2008).



Figure 4.2 – Original setting of the research object: the platform sheds of the station Paris Gare de l'Est. Source: SNCF-AREP.

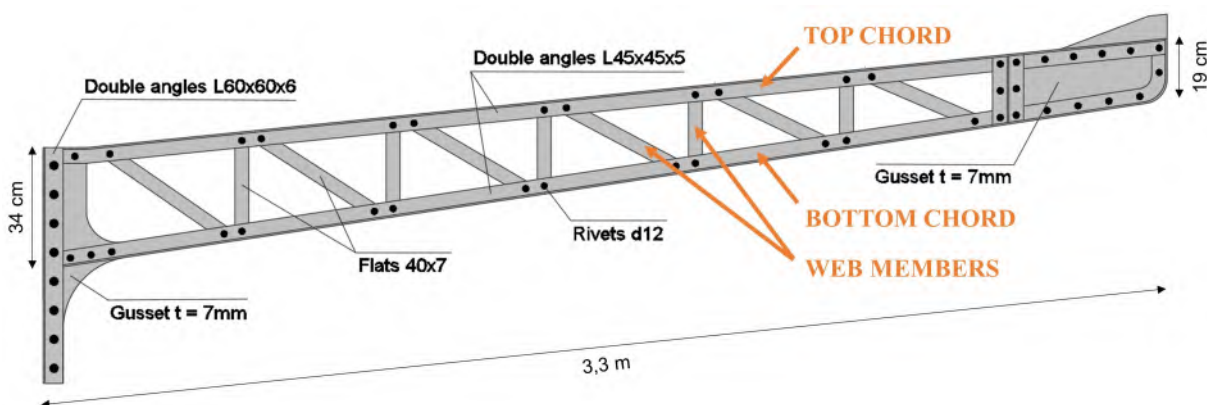


Figure 4.3 – Elevation drawing of the tested lattice girder specimen.

Experimental setup

Fig. 4.4a gives a view of the laboratory setup for modal testing. To preserve the structural system, the original support conditions of the cantilever were reproduced. An assembly of welded steel plates was designed and manufactured as an intermediary to anchor the lattice girder on a concrete wall, with pre-existing anchoring positions (Fig. 4.4b). The cantilever was fixed on the welded steel plates through bolts. Bolt holes were drilled in the support plates with the cantilever in position so that the holes would perfectly match the position of the holes in the historic cantilever.

The structure was excited using an impulse hammer PCB 086D05 with a sensitivity of 0.23 mV/N, a mass of 0.32 kg and an extra soft tip, resulting in a frequency range of 150 Hz. To retrieve the structure's response, 12 capacitive accelerometers, 7 single-axis and 5 tri-axis were used. Their sensitivities ranged from 100 to 1000 mV/g and their



Figure 4.4 – Experimental setup in the laboratory: (a) global view; (b) fixation system of the girder; (c) girder instrumentation.

frequency bandwidth was at least 0-100 Hz. They were fixed to the girder with magnets glued on 3D-printed plastic supports, designed to fit the accelerometers (see Fig. 4.4c).

To obtain satisfactory mode shapes, 30 measurement points were defined, 11 on the top chord, 11 on the bottom chord and 8 on distinct web members. On the web members, the accelerometers were placed at mid-span. On the chords, the accelerometers were placed either close to connection points or in the middle of chord segments between two connection points. This distribution aimed to capture local deformations if relevant. Accelerations were measured only in the out-of-plane direction. Tri-axis accelerometers could have measured accelerations also in the vertical direction, but vertical modes were not relevant to provide information on the out-of-plane rotational stiffness of the joints. Tri-axis accelerometers were used to complement the batch of single-axis accelerometers available in the laboratory. Three sensor setups were tested (see Fig. 4.5):

1. a “top chord” (TC) setup with 11 accelerometers on the top chord and 1 accelerometer on the bottom chord.
2. a “bottom chord” (BC) setup with 11 accelerometers on the bottom chord and 1

accelerometer on the top chord.

3. a “web members” (WEB) setup with 8 web members equipped with 1 accelerometer at mid-length and 4 accelerometers on the top and bottom chords. The accelerometers located on diagonals were the single-axis ones because their weight was lower than the tri-axis ones. Thus their weight remained below 10% of the weight of each web member, which is the rule-of-thumb usually recommended in practice to avoid mass loading effects.

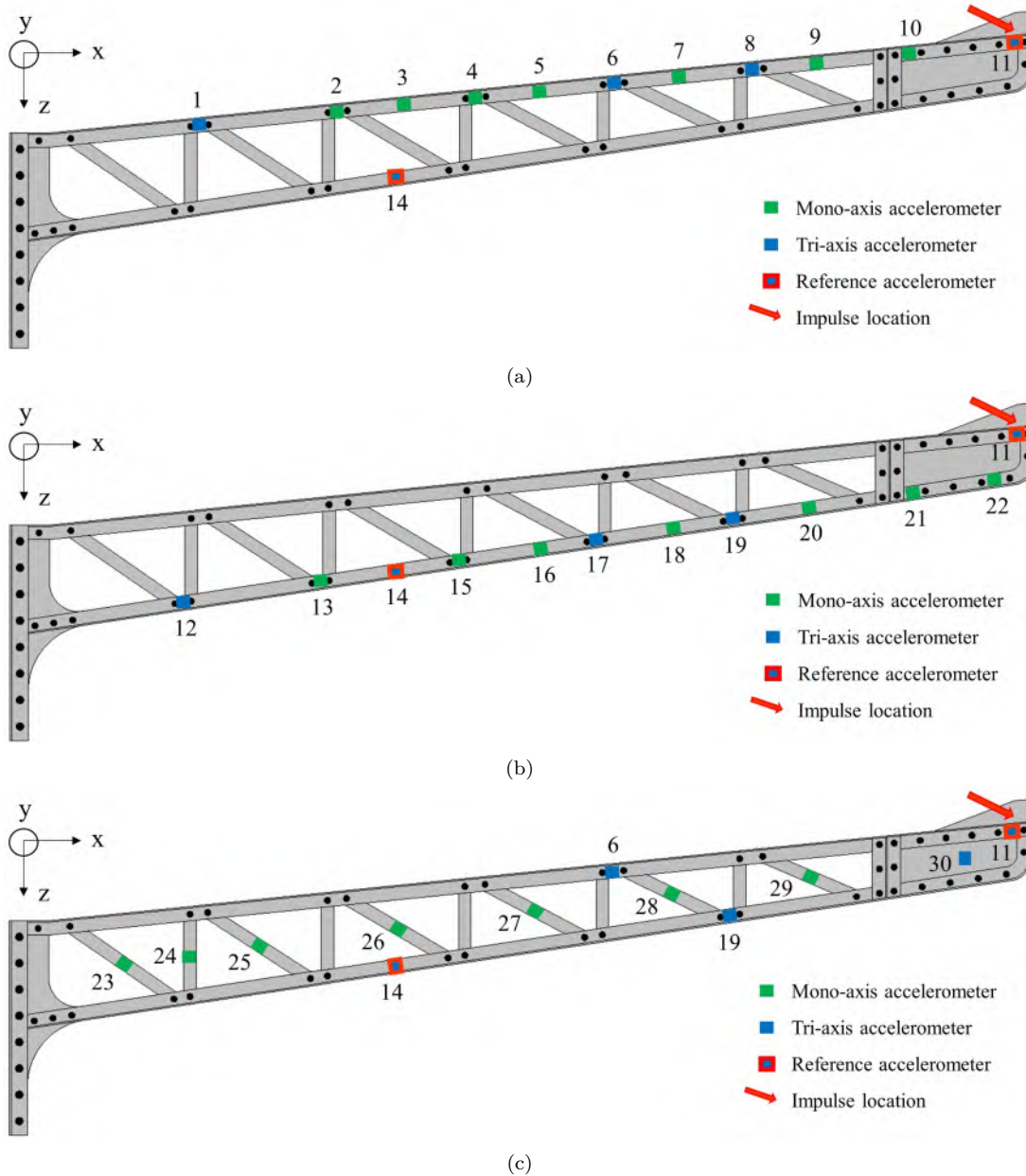


Figure 4.5 – Sensor setups: (a) TC setup; (b) BC setup; (c) WEB setup.

The two accelerometers at points 11 and 14 were present in all setups, to be used as references. In each setup, the same test was repeated 7 times to get accurate results. The

beam was excited with one horizontal impulse at the tip of the top chord. Data acquisition was performed with the HBM Quantum X system, with a module MX1615B and a module MX1601B, and the associated software catman. An anti-aliasing lowpass filter with a cut-off frequency of 500 Hz was applied previous to acquisition. The signals were recorded with a frequency of acquisition of 4800 Hz. The maximum considered frequency being 100 Hz, due to the bandwidth of the used accelerometers, a lower frequency of acquisition of 1200 Hz would probably have also yielded satisfactory results. The recording time was 2.5 seconds. After this time, out-of-plane accelerations decayed to near zero (see Fig. 4.6). The resulting sampling resolution was 0.4 Hz (see Eq. (4.5)). The first mode being expected around 3 Hz, this sampling resolution was considered sufficient.

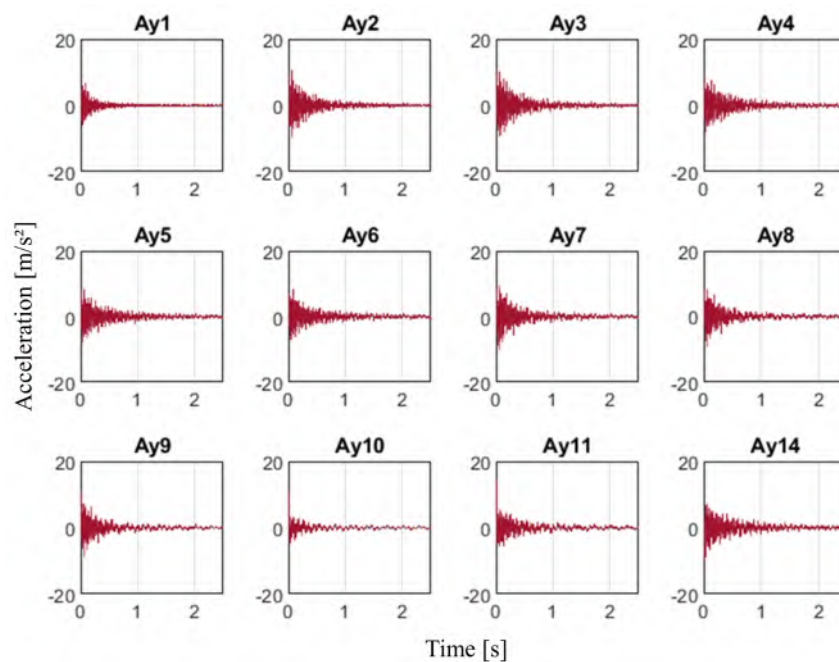


Figure 4.6 – Output acceleration signals from the accelerometers in the TC setup. Ay_i is the acceleration measured at point i in the horizontal y -direction.

System identification

For each test, the excitation and response signals were transformed from the time domain to the frequency domain using FFT. The power spectral density S_{ff} of the excitation and the cross-spectral density of excitation and response S_{xf} were computed according to Eq. (4.2). As each test was repeated 7 times, the spectral densities were averaged out. The FRF was estimated from Eq. (4.3). Modal parameters were extracted using the “line-fit” method (Ewins, 2000), through an adapted existing Matlab code that was developed over the years in the SMC laboratory (Hondermarck, 2007, Dia, 2020). This “SDOF” method could be used because the modes were sufficiently distinct.

Experimental modal parameters were extracted for the first six modes observed on

the FRFs resulting from the measurement of out-of-plane accelerations, in the frequency range below 100 Hz (see Fig. 4.7). A good coherence was measured around the peaks. The measured frequencies result from an average over all the measurement points and all tests (Table 4.1).

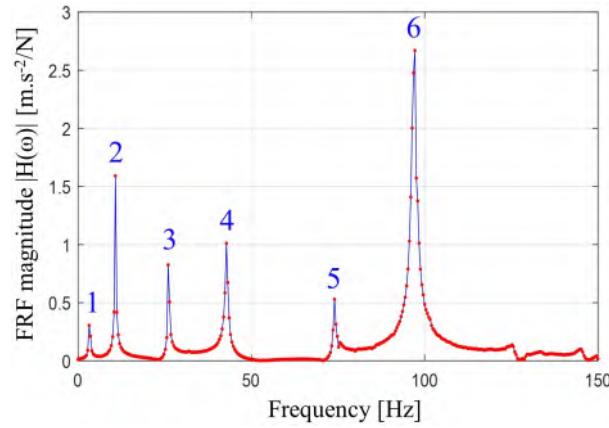


Figure 4.7 – Inertance magnitude at point 17 in the BC setup.

Table 4.1 – Average frequencies of the first six experimental modes, identified through the measurement of out-of-plane accelerations.

Exp. mode #	Average f [Hz]
1	3.37
2	10.88
3	26.17
4	42.92
5	74.09
6	97.29

Relying on the small-displacement assumption, the modal displacements derived from the measurements were assumed to be purely horizontal following the y -axis. The measured mode shapes thus correspond only to a projection of the three-dimensional mode shapes. Modal displacements were normalised following a 1-scaling procedure: they were re-scaled so that the maximum amplitude of the top or the bottom chord was equal to 1. Fig. 4.8 presents the measured modal displacements for the first six modes, plotted along the global horizontal x -axis. The graphical display is equivalent to a top view of the deformed structure.

Estimation of the measurement uncertainty

There exists a range of sources of error associated with experimental testing (Mottershead et al., 1993):

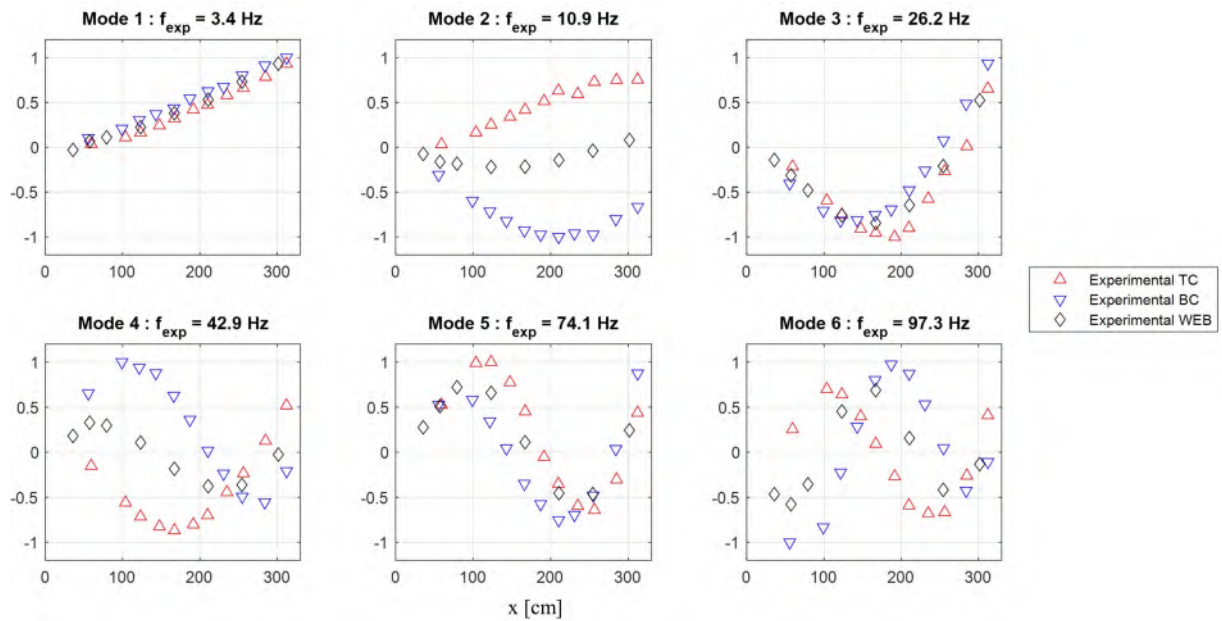


Figure 4.8 – Measured modal displacements after 1-scaling for the first six modes.

- limitations of the measuring tools and A/D converters: electronic systems introduce low instrument noise levels. Transverse motion and base bending of accelerometers are common sources of error in test data. Also, errors in the natural frequencies are commonly due to the mass of roving accelerometers. According to their datasheets, the used accelerometers had a measurement uncertainty of 1.6%, while the impulse hammer had a measurement uncertainty of 3.8% (corresponding to a 95% confidence level, with a coverage factor of 2).
- human error during testing (operator-related): each impulse might have a slightly different location or direction;
- FRF estimation from time signals: errors can arise as a result of aliasing, spectral leakage and linearisation of non-linear effects;
- modal parameter extraction: the curve-fitting process requires manual intervention by the user.

The uncertainty on the measured natural frequencies and FRF magnitude was estimated in two ways: first based on the values obtained from different sensors, and second based on the values obtained from repeated tests.

Estimation 1 (based on measures of the frequency for all accelerometers): In each sensor set-up, 12 accelerometers yield a measurement of the frequency for each mode. All three sensor set-ups combined therefore provide 36 measurements of the frequency for each mode. From the standard deviations presented in Tab. 4.2, the frequencies were measured with a precision of ± 0.4 Hz, which is below 5%.

Estimation 2 (based on test repetition): For three sample accelerometers, 2, 4 and 11, in the “TC” setup, the modal parameters were extracted from the FRF-estimator computed

Table 4.2 – Estimate of the measurement uncertainty (in terms of absolute (abs.) and relative (rel.) standard deviation SD) for the frequency f , from the measurements of all accelerometers.

Exp. mode	Avg. f	f SD	f rel. SD
#	[Hz]	[Hz]	[%]
1	3.37	0.12	3.6
2	10.88	0.37	3.4
3	26.17	0.10	0.39
4	42.92	0.06	0.13
5	74.09	0.20	0.27
6	97.29	0.24	0.25

individually for each test. For each accelerometer and each mode, the uncertainty on the frequency and the magnitude were computed. The level of error between the tests was found to be similar for all accelerometers, but dependent on the modes. The relative error, that is the ratio between the standard deviation and the mean value, was higher for the lower modes. According to the results presented in Tab. 4.3, the frequencies were measured with a precision of ± 0.1 Hz. This error is lower than the one estimated with the previous method, so we retain that the error on the frequency is the highest one: ± 0.4 Hz. Regarding the FRF-magnitude, the error was found to go beyond 20% for the two first modes, so the mode shapes for those modes must be considered with care. The error on the FRF-magnitude for the higher modes was estimated to about 10%, which is acceptable.

Table 4.3 – Estimate of the measurement uncertainty (in terms of absolute (abs.) and relative (rel.) standard deviation SD) for the frequency f and the FRF-magnitude $|H(\omega)|$ for each mode, estimated from the outputs of 7 repeated tests for 3 sample accelerometers.

Exp. mode	f abs. SD	f rel. SD	$ H(\omega) $ rel. SD
#	[Hz]	[%]	[%]
1	0.12	3.3	20.5
2	0.07	0.6	21.5
3	0.03	0.1	7.3
4	0.08	0.2	4.6
5	0.05	0.1	13.8
6	0.06	0.1	6.0

4.2.2 Finite element modelling

A finite element model of the lattice girder was built to calibrate parameters based on vibration test data, as presented in Section 4.1.2. The main parameter of interest was the rotational stiffness of the riveted joints.

Finite elements

The finite element model was built with the software MARC (« HEXAGON - Marc », 2023). The chords and web members were modelled using beam elements, while only the gussets at both ends of the girder and the vertical angles at the support were modelled using shell elements (see Fig. 4.9).

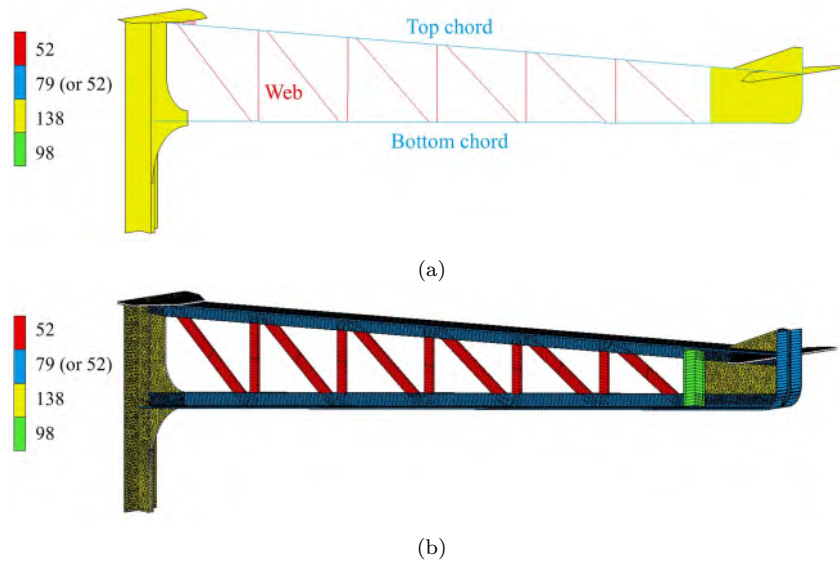


Figure 4.9 – View of the finite element model, with associated element types (from MARC’s element library): (a) outline display style; (b) expanded display style.

The chords and web members fulfil the Bernoulli conditions in terms of aspect ratio in the out-of-plane direction (i.e. length-to-thickness ratio above 10). The assumption behind this verification is that the reference length for the chords corresponds to the wavelength of the highest studied mode, which was about 3.1 m. In MARC’s element library (MARC 2018.1, 2018), the basic Bernoulli elements with two nodes are type 52. When the beam elements were modelled using type 52, the torsional stiffness factor, corresponding to the St Venant torsional constant, had to be entered manually and was computed for each section with the formulas for thin-walled open sections and solid rectangles (Hugues et al., 2011). As an alternative to type 52, the chords could be modelled with 2-node thin-walled elements including warping as an additional degree of freedom at each node (type 79 from MARC’s element library). Type 79 was not relevant for the web members as warping is negligible for solid sections. So the chords were modelled either with type 52 or type 79, and the web members were modelled with type 52.

The gussets at both ends and the vertical angles at the support were modelled with triangular 3-node shell elements (type 138 from MARC’s element library). The short vertical angles connecting the end gusset to the rest of the girder were modelled together

as Timoshenko beam elements (type 98 from MARC's element library).

Material properties

The elastic modulus of the mild steel constituting the girder was taken equal to 200 GPa. The volumic mass was assumed to be $\rho = 7850 \text{ kg/m}^3$, in line with the recommendations of the current Eurocodes for the self-weight of steel (EN 1991-1-1, 2003). In addition to the mass density as an intrinsic property of the material, the weight of the rivets, the accelerometers and the 1 mm-thick layer of paint had to be taken into account. Riveted connections were modelled without modelling the rivets themselves. The weight of the rivets was estimated from their number and size. They represented about 2.5% of the weight of the girder modelled without rivets. Additionally, the mass of the accelerometers was not negligible. The weight of each sensor, including its fixation system, was 29g for single-axis accelerometers and 127g for tri-axis accelerometers. The weight of all sensors represented 1.0% of the total weight. Finally, the weight of the paint had to be included. Assuming a volumic mass of 1000 kg/m^3 for the paint, the 0.9 mm-thick paint layer accounted for an increase of 4 to 5% of the original weight of the lattice girder. Overall, as an approximation, the mass distribution was considered uniform, and the equivalent density of the beam was estimated to be $\rho = 8450 \text{ kg/m}^3$.

Given the uncertainty on the assumed material properties, a sensitivity analysis was carried out to assess the impact of their variations on the modal behaviour. For the parametric study, the Young modulus E was varied in the range [190 200 210] GPa, while the volumic mass ρ was varied in the range [8300 8450 8500] kg/m^3 . The results are presented in Section 4.3.2.

Boundary conditions

At the cantilever support, the displacements of the surfaces of the vertical angles facing the wall were fixed, as well as for the horizontal surface of the top gusset plate. It was acknowledged that this would result in a more rigid support condition than in reality. The effect of introducing more flexible support conditions through elastic foundations was evaluated and is discussed in Section 4.3.2.

At the connection between chords and web members, two distinct nodes were preserved. Local coordinate systems were defined at each connection, with the z-axis going along the web member, and the x-axis pointing in the out-of-plane direction (see Fig. 4.10). The connecting nodes were tied for all degrees of freedom (DOF) except for DOF 5 corresponding to the out-of-plane rotation. For DOF 5, the connection was modelled with a spring of varying stiffness k_r . To model the extreme case of a hinged connection ($k_r = 0$), the connecting nodes were left independent from each other for this DOF, with

no coupling condition. To model the other extreme case of a perfectly rigid connection ($k_r = \infty$), the nodes were tied for this DOF. Intermediate stiffness values were defined based on the stiffness indice R (see Eq. (3.4)), with R varying approximately between 0.01 and 100. The same rotational stiffness k_r was assigned to all connections, even though web members had varying lengths. This approximation was made to ease the parametric study presented in the following. As a consequence, to obtain roughly $R = 0.01$ and $R = 100$ for all the web members, k_r was taken equal to 10^4 N.mm/rad and 10^8 N.mm/rad respectively. $k_r = 10^6$ N.mm/rad was tested as an intermediary case. It is acknowledged that the same joint stiffness does not offer the same degree of restraint to all web members. It means that a certain type of riveted joint, with given properties, would not have the same influence on the behaviour of the connected web members, depending on their length.

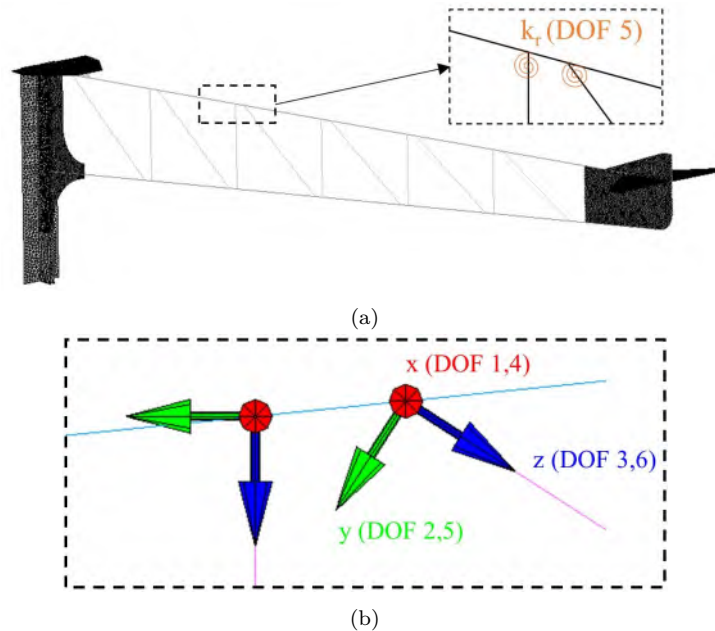


Figure 4.10 – (a) Connections modelled with rotational springs for DOF 5; (b) Detail of local coordinate systems at the connections.

Reference model

As an initial model for the updating procedure, a reference model was defined with a specific set of modelling assumptions amongst those discussed above (see Tab. 4.4). In this model, the beam elements for the chords were type 79, while web members were type 52. The mesh size was about 10 mm both for line and surface elements, yielding 9446 elements and 5489 nodes. The elastic modulus was taken equal to 200 GPa and the equivalent volumic mass equal to 8450 kg/m^3 . The support conditions were fully rigid. Regarding riveted connections between the chords and the web members, the connection nodes were tied for all 6 degrees of freedom so that the reference model featured perfectly

rigid connections. For this model, the CPU time to compute the first 10 modes was inferior to 5 seconds.

Table 4.4 – Set of modelling assumptions used for the reference model.

Parameters	Value
Chord elements	Type 79
Web member elements	Type 52
Mesh size	10 mm
E	200 GPa
ρ	8450 kg/m ³
Support conditions	Fully rigid
Connections	Nodes tied for all 6 DOFs

4.3 Results and discussion

4.3.1 Comparison of experimental results with the reference model

Experimental results were first compared with the modal properties of the numerical reference model. In the frequency range of interest 0-100 Hz, in which 6 modes had been identified experimentally, the reference model yielded 7 modes: 6 out-of-plane modes that could be fairly paired with the experimental ones, and 1 in-plane mode, that could not be accounted for with the presented experimental setup. Tab. 4.5 displays the average values of the frequencies measured for the 6 modes identified experimentally and the frequencies of the corresponding numerical modes, as well as the resulting quality criteria P_r from Eq. (4.9).

Table 4.5 – Comparison of the experimental results with results from the numerical reference model: experimental frequencies (Exp. f) and corresponding numerical frequencies (Num. f) obtained with the reference model, quality criteria P_r and L_r .

Exp. mode	Exp. f	Num. f	P_r	L_r
#	[Hz]	[Hz]	[%]	[%]
1	3.37	3.49	3.73	0.18
2	10.88	11.21	3.03	0.84
		24.81		
3	26.17	27.60	5.47	1.52
4	42.92	46.62	8.62	2.14
5	74.09	80.35	8.44	4.44
6	97.29	106.15	9.10	11.52

grey: in-plane mode

The numerical frequencies are up to 10% higher than the experimental ones, as expected for this model with conservative stiff boundary conditions at the cantilever support.

Fig. 4.11 presents a comparison of numerical and experimental eigenfrequencies and mode shapes, for the six first out-of-plane modes. Experimental mode shapes were 1-scaled and numerical mode shapes were then re-scaled to obtain the best fit between the numerical and experimental mode shapes of the chords.

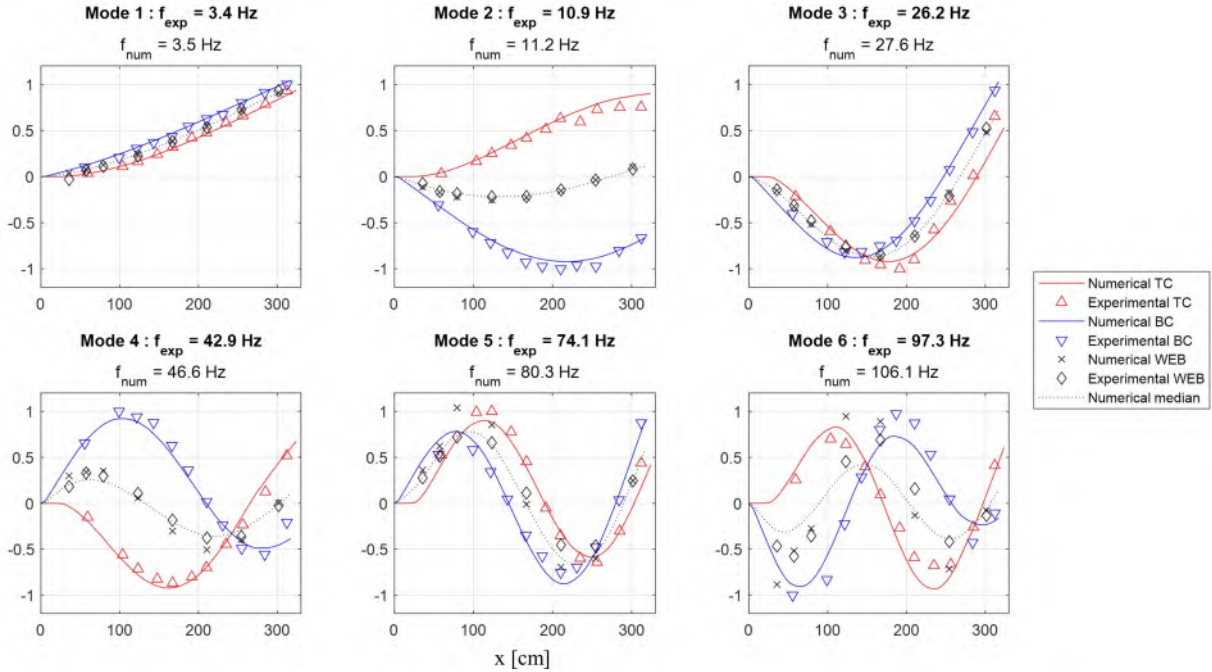


Figure 4.11 – Comparison of experimental mode shapes and corresponding numerical mode shapes obtained with the reference model.

The mode shapes were found to be in very good agreement for the first four modes, both graphically and quantitatively. L_r values were computed following Eq. (4.12) and are presented in Tab. 4.5. Real discrepancies appeared for modes 5 and 6. In Fig. 4.11, the numerical median between the top and bottom chords' displacements is plotted as a dotted line. It enhances that in mode 5, the numerical mode shape exhibited large web member deformations, while in the experimental mode shape, web member deformations remained closer to the median. Fig. 4.12 provides a visualization of the numerical mode shape of the 5th out-of-plane mode. In mode 6, the fitting between experimental and numerical mode shapes is overall less satisfactory.

These results showed that the reference model provided an acceptable level of agreement with the measured data, regarding frequencies and mode shapes, especially for the first four modes. It was therefore a good reference to carry out sensitivity analyses on some modelling parameters.



Figure 4.12 – 3d-view and top view of the deformed and original states of the structure for the 5th mode, obtained with the numerical reference model (fully rigid connections). The colours correspond to different quantities of out-of-plane displacements along the z -axis.

4.3.2 Preliminary sensitivity analyses

Preliminary sensitivity analyses were carried out to evaluate idealisation and discretisation errors. The influence of different modelling parameters was evaluated: the mesh size, the element types for the chords, the material properties (Young modulus and volumic mass), and the support conditions.

Element types

In section 4.2.2, it was mentioned that the chords could be modelled with elements type 52 (simple Bernoulli) or with elements type 79 (including warping). When the chords were modelled with elements type 52 instead of type 79 like in the reference model, the obtained frequencies were closer to the measured frequencies (Tab. 4.6). However, the agreement of the obtained numerical mode shapes with the test-derived mode shapes was not satisfactory, especially from mode 4 onward, as can be seen from Fig. 4.13. L_r values presented in Tab. 4.6 quantify the discrepancies. It was concluded that elements type 79 allowed to more accurately represent the vibration behaviour, based on the agreement between experimental and numerical mode shapes. Regarding the frequencies, it was actually good that the frequencies obtained with elements type 79 were higher than the measured frequencies because the support conditions in the reference model were knowingly more rigid than in reality.

Mesh size

The influence of the mesh size when refined from 10 mm to 1 mm in the reference model was studied. Tab. 4.7 shows that the obtained frequencies did not converge. When the chords were modelled with type 52 instead of type 79, a convergence was obtained. It seemed that the lack of convergence was related to the formulation of element type

Table 4.6 – Comparison of the numerical frequencies and L_r values for the modes paired with the experimental ones, when the chords are modelled with elements type 79 or type 52.

Exp. mode #	Exp. f [Hz]	Type 79 f [Hz]	Type 52 f [Hz]	Type 79 L_r [%]	Type 52 L_r [%]
1	3.37	3.49	3.48	0.18	0.16
2	10.88	11.21	10.37	0.84	1.20
3	26.17	27.60	26.53	1.52	2.98
4	42.92	46.62	40.48	2.14	5.38
5	74.09	80.35	75.92	4.44	15.44
6	97.30	106.15	94.05	11.52	32.59

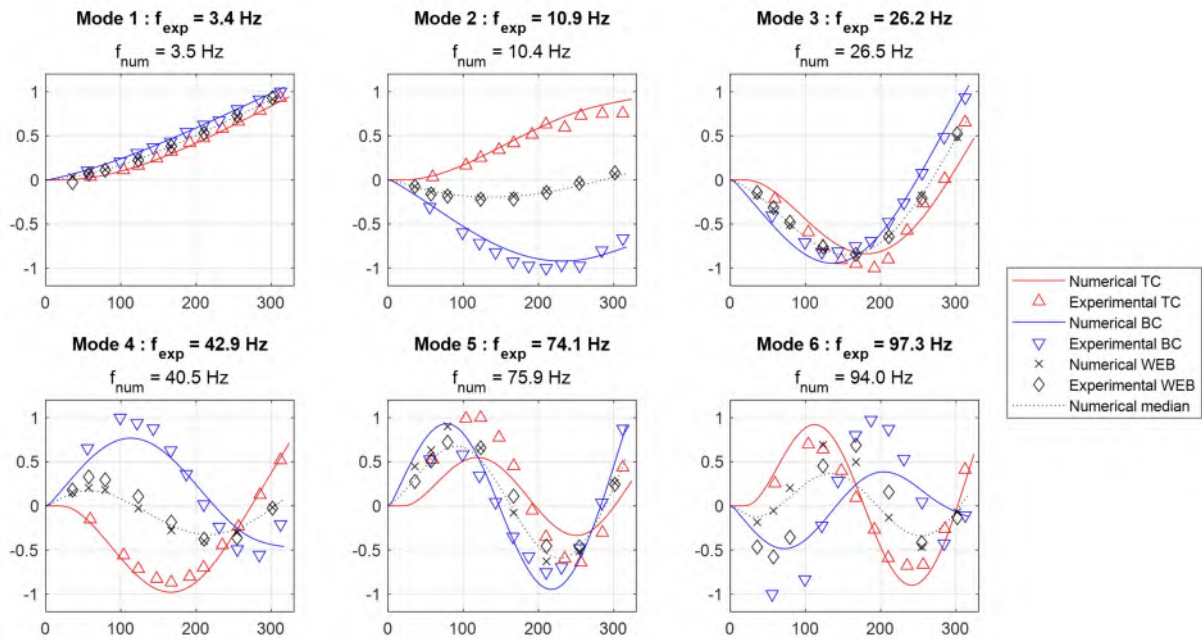


Figure 4.13 – Comparison of experimental mode shapes and corresponding numerical mode shapes obtained with the model where the chords are modelled with elements type 52 instead of 79.

79. However, even though the frequencies did not converge, their variations were deemed acceptable, as the variations did not exceed 10 % when the mesh was refined by a factor 10. Also, the mode shapes remained stable. As a consequence, it was decided to maintain the numerical model with elements type 79 and mesh size 10 mm as the reference model.

Material properties

It was admitted that the uncertainty on the Young modulus E was situated in the range 190-210 GPa, while the uncertainty on the volumic mass ρ was estimated between 8300 and 8600 kg/m³. The influences of E and ρ can be studied together, as the frequencies depend on the parameter ρ/E . Table 4.8 shows that the resulting uncertainty on the frequency of each mode was a constant $\pm 3.4\%$ compared to the reference model. Regarding the mode shapes, the considered variation of material properties had no influence.

Table 4.7 – Comparison of the numerical frequencies obtained for different mesh sizes.

Exp. mode #	10 mm f [Hz]	5 mm f [Hz]	2 mm f [Hz]	1 mm f [Hz]
1	3.49	3.54	3.58	3.60
2	11.21	11.48	11.78	11.93
3	27.60	27.75	27.87	27.96
4	46.62	48.38	50.44	51.60
5	80.35	81.07	81.88	82.33
6	106.15	109.59	113.79	114.87

Table 4.8 – Comparison of the numerical frequencies obtained for different input material properties.

Exp. mode #	$E = 200$ GPa $\rho = 8450$ kg/m ³ f [Hz]	$E = 190$ GPa $\rho = 8600$ kg/m ³ f [Hz]	$E = 210$ GPa $\rho = 8300$ kg/m ³ f [Hz]	Δf [Hz]
1	3.49	3.37	3.61	± 0.12 (3.4%)
2	11.21	10.84	11.60	± 0.38 (3.4%)
3	27.60	26.66	28.53	± 0.94 (3.4%)
4	46.62	45.04	48.20	± 1.58 (3.4%)
5	80.35	77.62	83.07	± 2.72 (3.4%)
6	106.15	102.56	109.75	± 3.60 (3.4%)

Support conditions

In the reference model, the displacements were fixed in all directions on the support surfaces. The effect of more flexible support conditions was studied, by replacing the fixed displacements with elastic foundations. For example, on the vertical surfaces, the nodes were connected to horizontal axial springs in the x -direction with a stiffness $k = 10$ N/mm. The displacements remained fixed in the y and z -directions. On the horizontal gusset plate, four nodes, corresponding to the axis of the four bolts connecting the gusset plate to the anchoring plate, were connected to axial springs in all three directions, with a stiffness $k = 10^4$ N/mm. Tab. 4.9 shows that the proposed adapted support conditions yield frequencies closer to the experiments, but slightly less satisfactory mode shapes. Contrary to material properties, the range of plausible stiffness values for the springs used to model the support conditions was unknown, so the effect of support conditions was not fully apprehended. For the reference model, assuming fully rigid conditions was preferred to setting uncertain stiffness values, so that the numerical frequencies could be expected to be above the experimental frequencies.

Table 4.9 – Comparison of the numerical frequencies and L_r values for the modes paired with the experimental ones, when the support conditions are modelled as fully rigid (REF) or with an elastic foundation (E. F.).

Exp. mode #	Exp. f [Hz]	REF f [Hz]	E. F. f [Hz]	REF L_r [%]	E. F. L_r [%]
1	3.37	3.49	3.28	0.18	0.32
2	10.88	11.21	10.96	0.84	1.01
3	26.17	27.60	27.12	1.52	1.24
4	42.92	46.62	46.17	2.14	2.73
5	74.09	80.35	79.24	4.44	4.88
6	97.30	106.15	103.79	11.52	16.21

4.3.3 Assessment of the average rotational stiffness of the riveted joints

The preliminary sensitivity analyses allowed to estimate the bias resulting from modelling choices in the reference model. It could then be used as an initial model in the updating procedure regarding the parameter of interest, the rotational joint stiffness k_r . Tab. 4.10 presents the obtained frequencies for different values of k_r . The maximum considered frequency was chosen as the frequency of the 6th out-of-plane mode of the reference model ($f=106.15$ Hz). As reducing k_r from the infinite (perfectly “rigid” connection) to zero (perfectly “hinged” connection) decreased the overall rigidity of the structure, the expected frequencies corresponding to the experimental modes had to be lower than 106.15 Hz.

Table 4.10 – Frequencies of the numerical modes in the frequency range [0-106.15] Hz.

Num. mode #	k_r [N.mm/rad]				
	∞ (rigid)	10^8	10^6	10^4	0 (hinged)
1	3.49	3.49	3.46	3.42	3.41
2	11.21	11.21	11.08	10.99	10.99
3	24.81	25.05	25.03	25.01	25.00
4	27.60	27.59	27.44	27.22	27.21
5	46.62	46.60	45.93	44.38	44.31
6	80.35	80.32	78.72	74.23	73.99
7	106.15	106.07	97.50	79.85	79.60
8			104.72	85.96	85.11
9				87.06	87.14
10				93.89	93.64
11				95.57	95.29
12				105.82	105.50

Considering the frequencies of the first five out-of-plane modes, it seems from Tab. 4.10

that the model with hinged connections provides a better agreement with the measured frequencies presented in Tab. 4.1. However, it must be remembered that the support conditions of the numerical model were stiffer than reality, potentially yielding higher frequencies. The frequencies of the first modes were therefore not considered a reliable indicator in this study. Also, the model with hinged connections provides satisfactory results only up to the 5th out-of-plane mode. For higher frequencies, obvious discrepancies appear.

Tab. 4.10 highlights one important effect of lowering the out-of-plane rotational joint stiffness: in the models with lower stiffness k_r , several additional modes came out. Those modes were dominated by the deformations of one or several web members. Despite measurement points being located on web members in the WEB setup, those modes were not observed experimentally. The horizontal dashed line in Tab. 4.10 shows the limit above which it was not possible to attribute numerical modes to experimental ones. For example, in the model with $k_r = 10^6$ N.mm/rad, the modes 7 and 8 had close frequencies and mode shapes, and they were not in satisfactory agreement with the experimental 6th mode. Thus the presence or absence of additional modes compared to the modes identified experimentally is an indicator suggesting that the models with higher stiffness k_r are in better agreement with the experiments.

Tab. 4.11 presents the values calculated for L_r . Those values decrease when the stiffness increases. L_r is then another indicator suggesting that the model with rigid connections best represents the experiments. The increase of L_r when k_r decreases was mostly due to larger web deformations in the numerical model. As an example, the numerical mode shape of mode 5 obtained with the “hinged” model is presented in Fig. 4.14. From the comparison with Fig. 4.12, it is conspicuous that the web deformations become out-of-proportion.

Table 4.11 – Quality criteria L_r [%] comparing numerical and experimental mode shapes for different values of k_r .

Exp. mode #	k_r [N.mm/rad]				
	∞ (rigid)	10^8	10^6	10^4	0 (hinged)
1	0.20	0.20	0.25	0.32	0.32
2	0.83	0.83	0.95	1.07	1.07
3	1.50	1.51	1.72	2.36	2.39
4	2.12	2.13	3.22	5.01	5.07
5	5.23	5.33	14.19	44.87	45.36
6	13.1	13.53			

In this section, it was shown that attributing a lower rotational stiffness k_r to the riveted joints of the lattice girder yielded a less good agreement between numerical and

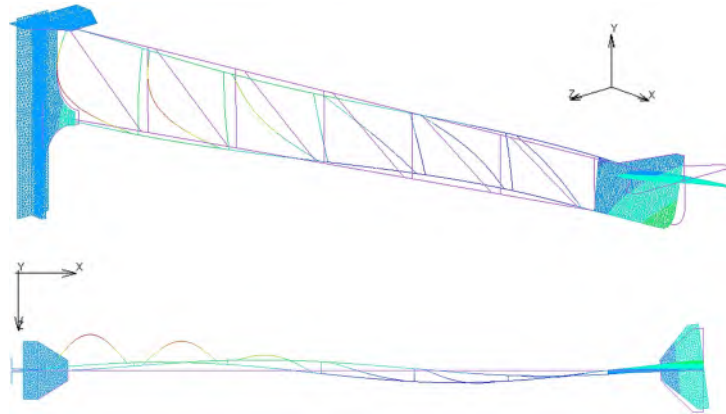


Figure 4.14 – 3d-view and top view of the deformed and original states of the structure for the 5th mode, obtained with the “hinged” numerical model. The colours correspond to different quantities of out-of-plane displacements along the z-axis.

experimental results than with the numerical reference model with perfect rigid joints. Two indicators were proposed to lead to this conclusion. The first indicator is the presence or absence of additional numerical modes, dominated by the vibration of web members. The second indicator is more quantitative and relies on the quality criteria L_r , derived from the MAC matrix, measuring the gap between numerical and experimental mode shapes.

4.3.4 Effect of local variations of the joint stiffness

In section 4.3.3, the same rotational stiffness was attributed to all riveted joints. It was assumed that the structure was healthy and that all riveted joints were nominally identical. However, in reality, the level of pre-stress is likely to vary amongst the rivets, either because of initial variations during riveting operations or because of ageing. Different clamping forces probably induce variations of the rotational stiffness amongst riveted joints (see Section 3.2). An investigation was therefore carried out to assess the effect of local variations of the joint stiffness on the modal behaviour. The study aimed to predict whether a riveted joint presenting a lower rotational stiffness than the other joints of a lattice girder could be detected by modal analysis and to determine which modal-based indicator could be used for detection. Such a joint, with a reduced rotational stiffness, could be described as “faulty”. The investigation is therefore similar to a damage detection procedure. For this purpose, “damages” were numerically introduced into the finite element model of the structure, by locally attributing a lower stiffness to some riveted joints. Only single-damaged models were analysed, in which only one riveted joint was released. Three specific cases were tested, corresponding to introducing hinges or springs with a low rotational stiffness at three different riveted joints. The tested joints were selected to be representative: they were located at the end of either vertical or diagonal web members, close or far from the cantilever support (see Fig. 4.15).

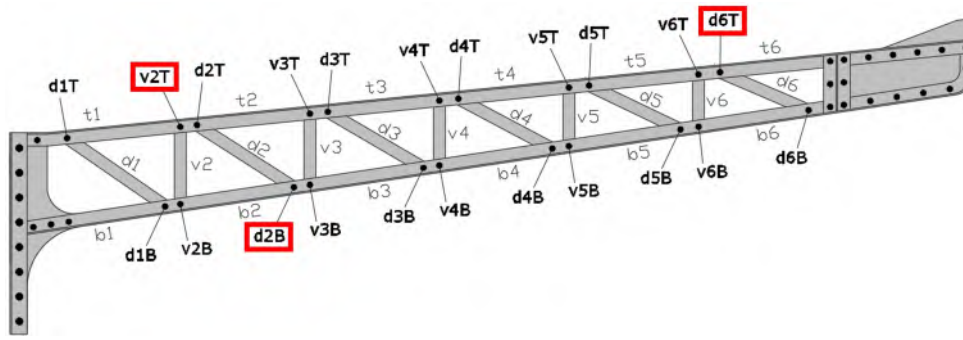


Figure 4.15 – Location of the riveted joints that were loose numerically.

Need for a refined indicator

First, single-damaged models were built, in which one riveted joint (v2T, d2B or d6T) was modelled as a hinged connection ($k_r = 0$) while all other riveted joints were modelled as rigid connections. No significant change compared to the reference model could be observed with the indicators used in section 4.3.3. The computed modes stayed the same, with similar frequencies and mode shapes. No additional mode appeared. The quality criteria L_r did not vary significantly either.

As L_r is a quantity indicating the global correlation of two sets of mode shapes, for one mode, it is understandable that this quantity is little affected when only one connection exhibits a different behaviour. It was, therefore, necessary to find a mode-shape-related parameter indicating for each measurement point the local variation of correlation between the experimental and numerical results, taking into account several chosen modes.

ECOMAC between single-damaged models and the reference model

The effectiveness of the ECOMAC (see Eq. (4.14)) was tested by comparing the mode shapes derived from the numerical reference model, where all joints are rigid, and the mode shapes derived from a single-damaged model. As an example, Fig. 4.16 presents the values of $\text{ECOMAC}[\text{num}^{\text{SD}}, \text{num}^{\text{ND}}]$ obtained from the comparison of a single-damaged model (num^{SD}), where the rotational restraint was released ($k_r = 0$) at joint d2B, and the reference model with no damage (num^{ND}). Those values were computed for the components of the mode shapes corresponding to the location of measurement points in the experiments. The first six out-of-plane modes were taken into account.

A clear peak could be observed at measurement point 25, which corresponded to the sensor placed on web member d2, connected to the bottom chord by joint d2B. Similar results were obtained when releasing the rotational restraint at v2T and d6T: peaks appeared at measurement points 24 and 29 respectively. Thus it seemed that the ECOMAC was capable of identifying the web member connected to a released joint. This result was in line with the common assumption used by damage detection methods relying

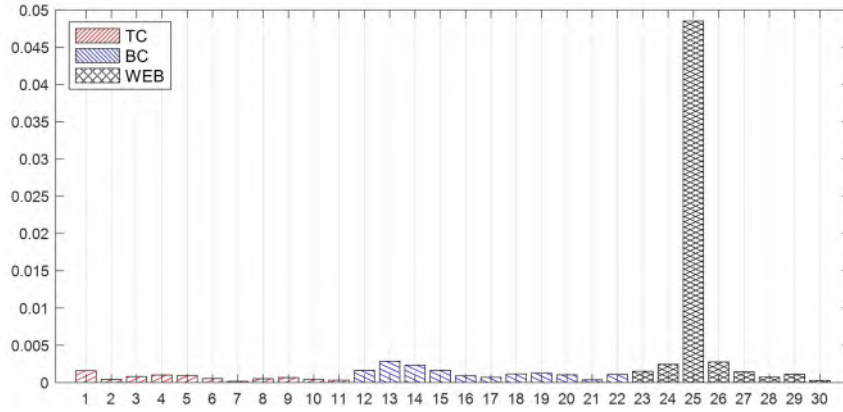


Figure 4.16 – ECOMAC[num^{SD}, numND] ($n = 6$) between the single-damaged model (d2B - $k_r = 0$) and the reference model with all joints rigid.

on mode-shape related parameters: damage is located at the location or the vicinity to where the change of mode shape function is the greatest (Maia et al., 2003).

ECOMAC between single-damaged models and the experiments

After validating that the ECOMAC could localise a defect introduced in a numerical model, the study aimed to verify whether the ECOMAC was capable of detecting a local discrepancy between the single-damaged models and the experimental results from the tested structure. Assuming the tested lattice girder was healthy, the computation of the ECOMAC between the experimental mode shapes and the numerical mode shapes derived from a single-damaged model could be expected to yield a peak as in the comparison of the single-damaged model with the reference model. However, this was not the case. Fig. 4.17 presents the values of ECOMAC[num^{SD}, exp] obtained from the comparison of the single-damaged model (num^{SD}), where the rotational restraint was released ($k_r = 0$) at joint d2B, with the experiments (exp). Taking into account the first six out-of-plane modes ($n = 6$), the values of ECOMAC appeared to be relatively evenly distributed over the measurement points. This was probably due to the many sources of discrepancy between the experiments and the numerical modelling, prevailing over the value attributed to the stiffness of one individual riveted joint. The ECOMAC therefore had to be adapted.

Introduction of a differential ECOMAC $\Delta\xi$

To filter out the “noise” created by the various sources of discrepancy other than the joint stiffness, it was decided to calculate a differential ECOMAC. This new index, noted $\Delta\xi$, is the difference between the ECOMAC obtained from the comparison of the experiments and a damaged model, and the ECOMAC obtained from the comparison of the experiments and the reference model:

$$\Delta\xi[\text{num}^{\text{SD}}, \text{num}^{\text{ND}}](j) = \text{ECOMAC}[\text{num}^{\text{SD}}, \text{exp}](j) - \text{ECOMAC}[\text{num}^{\text{ND}}, \text{exp}](j) \quad (4.15)$$

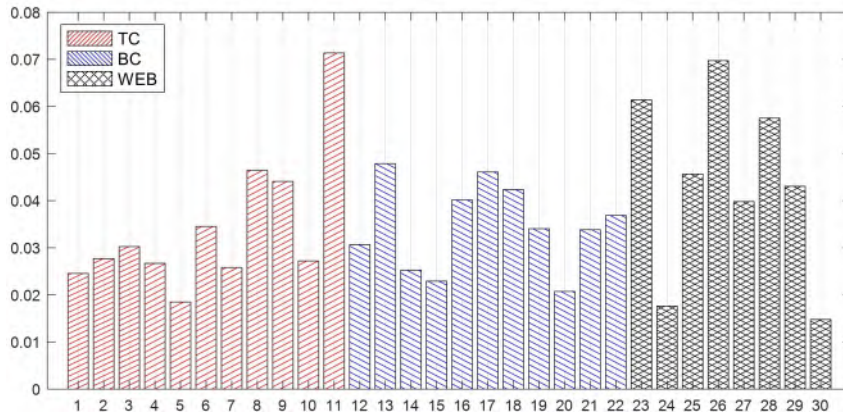


Figure 4.17 – ECOMAC[num^{SD}, exp] ($n = 6$) between the single-damaged model (d2B - $k_r = 0$) and the experiments.

Fig. 4.18 presents the differential ECOMAC between the ECOMAC[num^{SD}, exp] calculated for the model damaged at joint d2B ($k_r = 0$) and the ECOMAC[numND, exp] calculated for the reference model. A clear increase of the ECOMAC stood out at measurement point 25, corresponding to the sensor placed on diagonal d2, connected to the bottom chord by joint d2B. A positive peak meant that locally the experimental mode shapes showed a larger discrepancy with the damaged model than with the reference model. It confirmed that the tested structure was healthy. It seemed that the differential ECOMAC would allow to detect and localise a riveted joint with a lower rotational stiffness: the parameter $\Delta\xi$ was capable of identifying the web member connected to this joint, which narrowed the localisation down to only two riveted joints. Similar results were obtained when the rotational restraint was released at joints v2T and d6T. Peaks of $\Delta\xi$ were then obtained at measurement points 24 and 29 respectively.

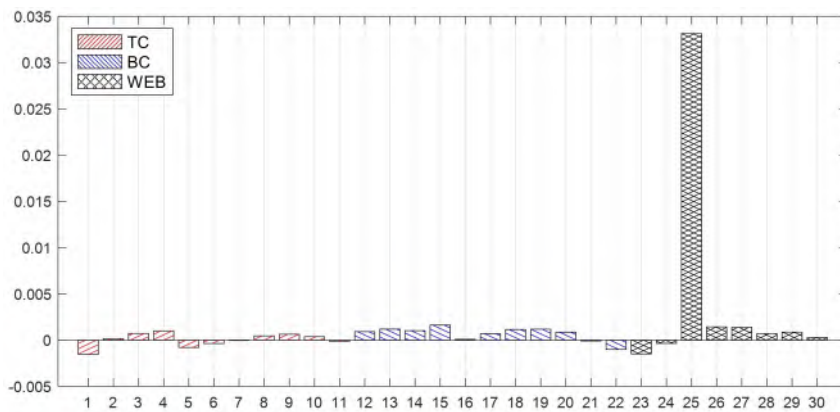


Figure 4.18 – $\Delta\xi$ [num^{SD}, numND] ($n = 6$) for the single-damaged model (d2B - $k_r = 0$).

Further simulations were conducted to evaluate the sensitivity of the criterion $\Delta\xi$. It was concluded that taking into account the first four or five out-of-plane modes ($n = 4$ or $n = 5$) was optimal to obtain unequivocal peaks. $n < 4$ is not representative enough and $n = 6$ introduces extra noise. Also, it was shown that it was necessary to establish a

threshold defining what “significant” peaks were, depending on which reduction of joint stiffness was considered as damage.

Based on $\Delta\xi$, a damage detection procedure could be developed, consisting in comparing vibration measurements from a potentially damaged riveted lattice girder with a range of single-damaged numerical models. To assess riveted joints from a lattice girder with an approach derived from $\Delta\xi$, it would be necessary to have only one measurement point on each diagonal. The drawback of mode-shape-based methods for damage detection is the necessity of having measurements from a large number of locations (Carden et al., 2004). For on-site detection, the method could be implemented through a roving excitation on the diagonals, with only a few sensors located on the chords. More details were provided in Franz et al., 2024a.

4.4 Conclusion

A modal testing methodology was developed to assess the single-riveted joints in a steel lattice girder. The main investigation aimed to evaluate their out-of-plane rotational stiffness k_r to help better predict the buckling behaviour of riveted lattice girders. An experimental modal analysis was conducted and the results were confronted with modal properties obtained from finite element models. In the models, the chords and web members were modelled using beam elements and the web-member-to-chord connections were represented by kinematic conditions. In particular, the out-of-plane rotation of the joints was controlled by rotational springs.

A reference model with rigid joints ($k_r = \infty$) was built, yielding a satisfactory agreement with the experiments. The uncertainty related to various modelling assumptions (element types, mesh size, material properties, support conditions) was estimated and discussed. A parametric study was then conducted, taking the joint stiffness k_r at the web member ends as a parameter. It was shown that decreasing k_r results in a less good agreement between numerical and experimental results. This conclusion was based on two indicators. The first indicator is the presence or absence of additional numerical modes, dominated by the vibration of web members. The second more quantitative indicator is the quality criteria measuring the gap between numerical and experimental mode shapes.

The single-riveted joints of the tested lattice girder seemed to be best represented using rigid connections. This result would induce a decrease in the estimated buckling risk based on an eigenvalue analysis. However, the results obtained with the tested lattice girder need to be confirmed by further numerical and experimental investigations. It is necessary to verify to which family of single-riveted joints these results apply, in terms of geometry. Riveted lattice girders with different connection geometries (rivet size, chord

sections, diagonal sections) should be tested. Numerically, finite element models of the lattice girders, using shell elements for the chords and web members, could be built. The rivets could be modelled by pre-stressed beam elements through the rivet holes, while contact conditions between chords and web members would be applied around the rivet holes. The rotational stiffness would then be derived from the model's behaviour as an output, instead of being an input like in the beam models with spring connections.

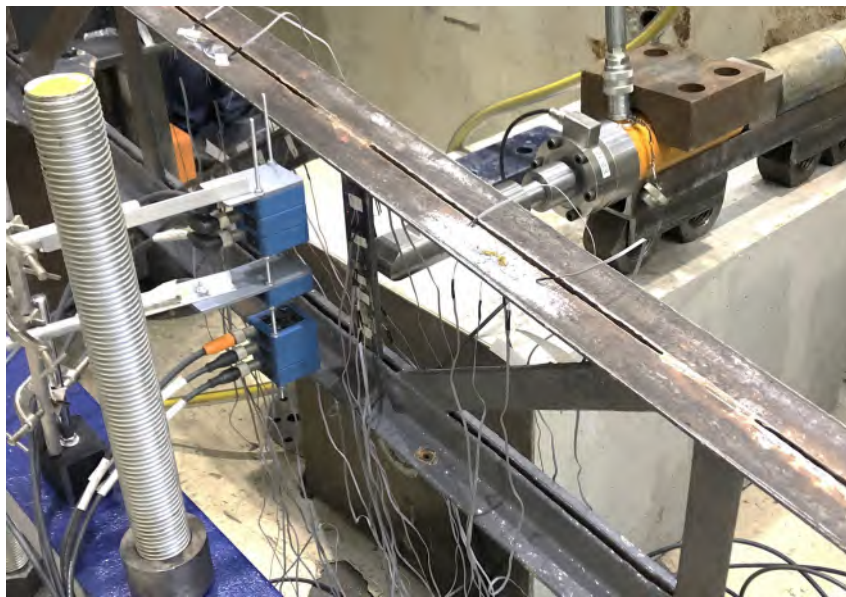
Furthermore, the model-based indicators proposed to assess the stiffness of riveted joints were determined in laboratory conditions, with controlled support conditions and no external loading. Stress-stiffening effects on the modal behaviour were neglected. Further experimental investigations should be conducted on *in situ* lattice girders, using more sophisticated modal testing techniques.

Finally, a numerical study was conducted to assess how the modal behaviour evolves when the rotational joint stiffness is not uniform. This study can help predict the ability of modal analysis to detect “faulty” riveted joints, with a lower rotational stiffness than the majority of the joints in the considered girder. The indicator $\Delta\xi$ was derived from the enhanced coordinate modal assurance criterion ECOMAC to compare the agreement between the experimental mode shapes and numerical mode shapes from a reference model with rigid joints and a series of single-damaged models, with one riveted joint having a reduced stiffness. It was shown that $\Delta\xi$ is able to localise the web members connected to “damaged” joints. However, this numerical study was predictive and requires experimental validation. Further experimental investigations could involve progressively replacing the rivets of the tested lattice girder with bolts with different levels of pre-stress. It would help establish a relationship between the rivet clamping force and the resulting rotational joint stiffness.

Chapter 4 allowed us to gain insight into the behaviour of single-riveted joints using a non-destructive method that could be implemented outside the laboratory, in operational conditions. Chapter 5 relies on classical load testing methods, that are limited to the laboratory but can help validate and extend the knowledge gained from modal testing.

ASSESSING THE ROTATIONAL STIFFNESS OF RIVETED JOINTS BY LOAD TESTING

Chapter 5 presents the experimental and numerical investigations aiming to assess the rotational stiffness of single-riveted joints based on quasi-static experiments. These experiments allow to validate the joint stiffness derived from modal tests and to understand the contribution of the rotational restraint provided by the joints compared to the restraint provided by the chords.



Load testing experiment on a riveted lattice girder (Picture by H. Franz).

Contents

5.1	Proposed methodology	114
5.2	Results and discussion	119
5.3	Conclusion	128

A load testing campaign was carried out on a lattice girder identical to the one used as a specimen for modal testing. The quasi-static experiments aimed to assess the rotational stiffness of riveted joints. The vibration experiments suggested that the single-riveted joints exhibited a rigid behaviour regarding out-of-plane rotations. The first aim of the quasi-static experiments was to validate the rotational stiffness measured by modal testing and to define a validity domain: do the riveted joints feature the same rotational stiffness under dynamic and quasi-static loading? Is the semi-rigid behaviour of the joints linear? The second aim was to further explore the behaviour of web-to-chord connections, by sharpening the understanding of the rotational restraint experienced by web members at web-to-chord connections. What is the contribution of the stiffness of the chords compared to the stiffness of the joints in the rotational end-restraint provided to web members? This chapter presents two series of tests that were conducted by applying a horizontal load in the out-of-plane direction, generating global or concentrated load distributions. Load tests were conducted under elastic conditions, staying way below the critical load to avoid buckling failure and be able to conduct several series of tests on the same specimen. Experimental results are derived from the measurements of deformations and displacements and compared to finite element modelling and analytical predictions.

5.1 Proposed methodology

5.1.1 Test specimen

The tested lattice girder was a twin girder of the one used for the vibration experiments. Both girders originally belonged to the same platform shed. Tape and calliper measures ensured that the geometry was the same. As for the previous girder, visual inspection revealed neither apparent defects in the joints nor damage to the material. Consequently, the two girders were nominally identical. Of course, they could not be rigorously identical, for example due to material inhomogeneity or variations inherent to the hot riveting process. However, the behaviour of both lattice girders and especially their riveted joints was expected to be similar.

5.1.2 Experimental setup

Similarly to the vibration experiments, an assembly of welded steel plates was designed and manufactured as an intermediary to anchor the lattice girder, this time on an existing prestressing table. The cantilever was fixed on the welded steel plates through bolts and was mounted upside down so that the tip of the girder pointed towards the floor. This made the different parts of the girder easier to access for instrumentation. For the sake of coherence with the naming system used for vibration experiments, all the members of

the girder keep the same name. Consequently, as the girder was installed upside down, the top chord (TC) is at the bottom and the bottom chord (BC) is at the top in this experimental setup (Fig. 5.1).

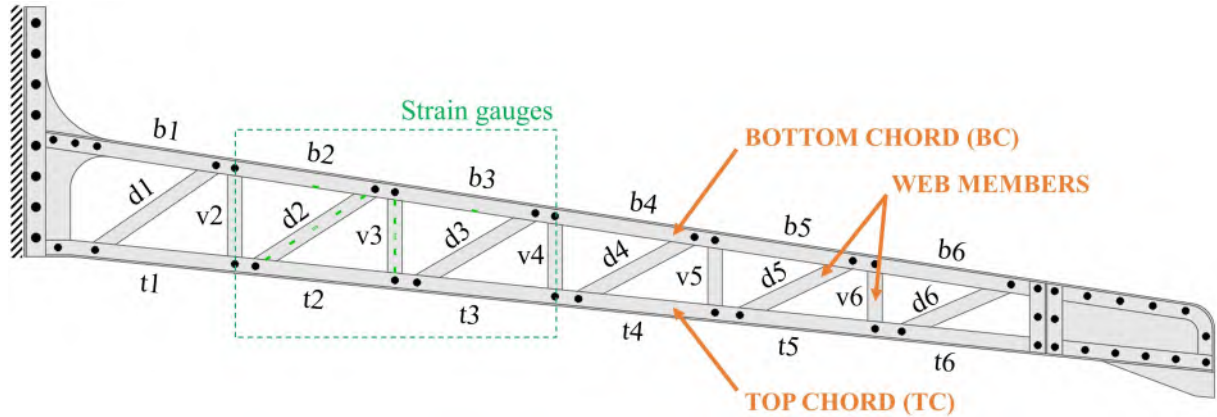


Figure 5.1 – Naming system for the chord and web members of the tested lattice girder. Strain gauges were concentrated around d2 and v3.

Two series of tests were conducted with varying points of load application, points of measurement of the displacements and boundary conditions. The load was applied with a load jack SR.20.100.S, with a capacity of 198 kN, and was measured by a force transducer AEP/TC4 with a capacity of 2.5 kN. The displacements were measured with 7 lasers having a capacity of 20 mm and a resolution of 10 μm . In addition, 30 strain gauges with a maximum elongation of 2% were installed on two web members, d2 and v3, and some neighbouring chord members (Fig. 5.1 and Fig. 5.2).

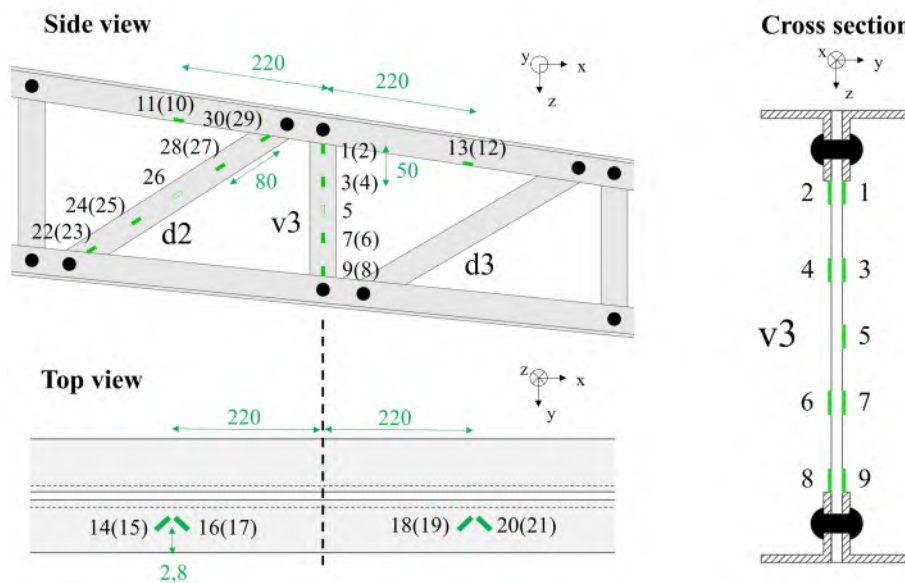


Figure 5.2 – Gauge positions for the load tests (distances in mm).

On web members d2 and v3, the strain gauges were arranged in pairs on two opposite sides of the flat, except at mid-span, to make it possible to apply a load at this point.

To install the gauges, the lead paint was locally removed on d2, v3 and the chord BC through thermal stripping. The naked steel surfaces were then ground out and cleaned to ensure satisfactory bonding conditions.

Tests were carried out in two setups, designed to assess the contribution of the rotational stiffness of the joints and the rotational stiffness of the cantilever support on the out-of-plane deformation behaviour of the lattice girder. In the global setup “G_hor” (Fig. 5.3), a horizontal load was applied at the tip of the girder, and the horizontal displacement was measured along the girder at the mid-span of several web members by lasers L2 to L7 (Fig. 5.4).

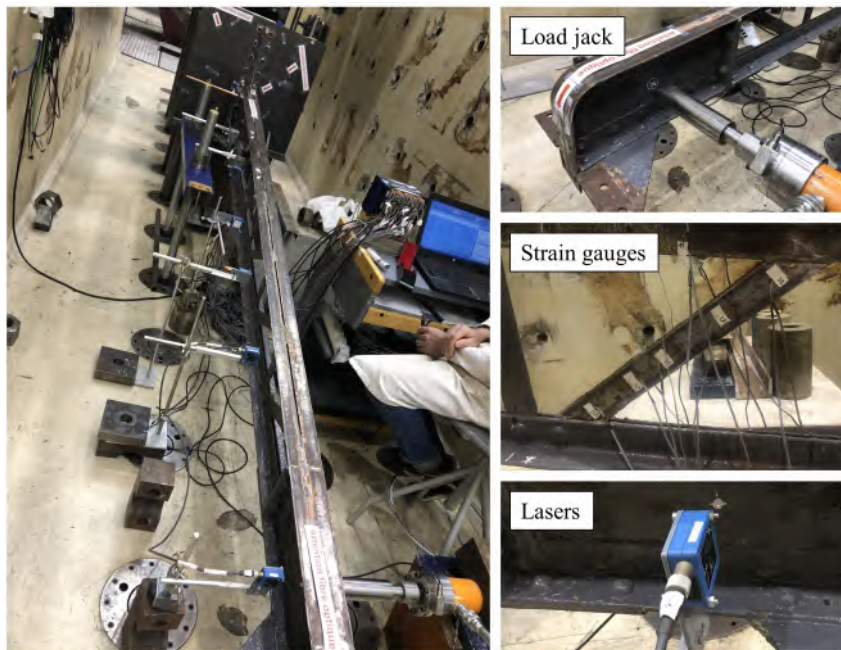


Figure 5.3 – Global setup G_hor. Left: global view of the setup. Right: zoom on instruments.

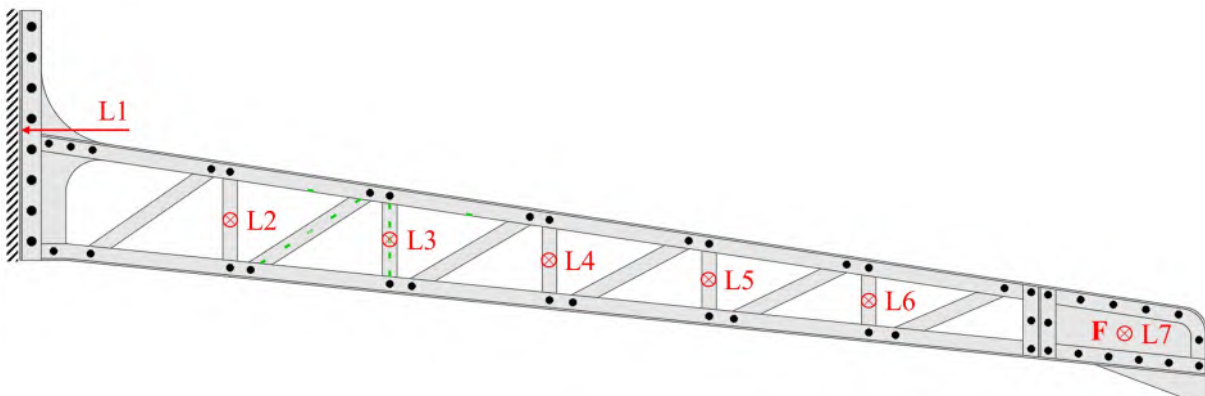


Figure 5.4 – Global setup G_hor. F is the point of application of the load. L1 to L7 give the position and the direction of the lasers.

Laser L1 was measuring the displacement of the anchoring plate, to verify that displacements stayed close to zero. The load was increased until 200 N, based on preliminary

numerical investigations ensuring that the girder would stay in the elastic domain and presented no buckling risk, and then released.

In the local setup “L_v3”, a horizontal load was applied at the mid-span of web member v3 (Fig. 5.5). The horizontal displacement was measured along v3 by the seven lasers. The load was increased until 1200N, again based on preliminary numerical investigations, and then released. To isolate the behaviour of the loaded web member from the global behaviour of the girder, lateral restraints were added in the vicinity of the loaded web member, to restrain the displacement and the rotation of the chords. The lateral restraints were effected by building props, spanning between the side walls and the chords. The props were positioned as close as possible to the loaded web member, the space being constrained by the otherwise cumbersome instrumentation equipment. The props were positioned in a way that they exerted a certain level of rotational restraint against the torsion of the chords. However, it was estimated to be negligible compared to the torsional stiffness of the chords.

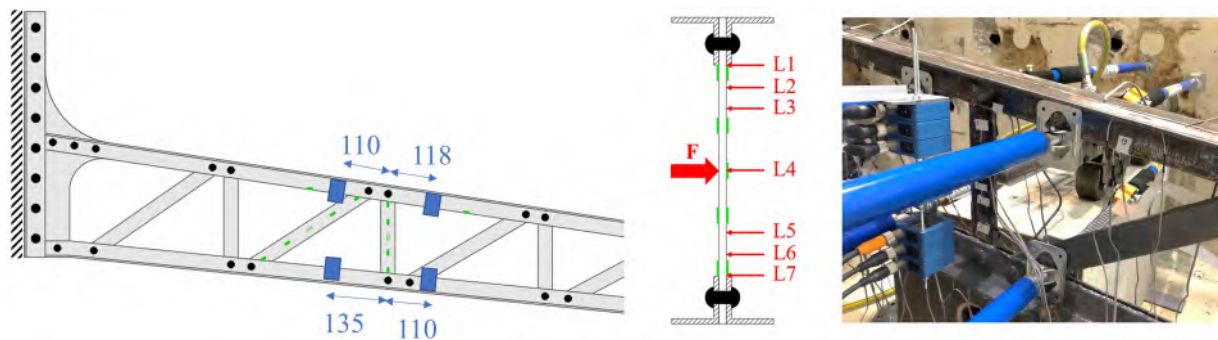


Figure 5.5 – Local setup L_v3. Left: elevation view with the position of the props (distances in mm). Center: cross section at v3. F is the point of application of the load. L1 to L7 give the position and the direction of the lasers. Right: picture of the experimental setup.

5.1.3 Preprocessing of the experimental data

The load jack was activated manually, resulting in an unsteady force increase with time. The frequency of acquisition was 50 Hz. To obtain usable results, all the measured values (force, displacements, strains) were smoothed with a moving average of 100 data points. Each test was repeated 3 times. To obtain displacements and strains for a given value of the applied force, the displacement and strain values from 3 repeated tests were averaged out.

The strain gauges placed on v3 were arranged in pairs on two opposite sides of the flat. Only gauge 5 was single because it was placed opposite the point of application of the load in test series L_v3. For each strain gauge i placed on v3, the measured deformations ϵ_i corresponded to axial deformations. They were converted to axial stresses using the elastic law $\sigma_i = E\epsilon_i$, with $E = 200$ GPa. Those axial stresses σ_i resulted from the combination of

tensile or compressive stresses due to the axial force and bending stresses due to the out-of-plane bending moment at the gauge's position. Fig. 5.6 shows the stress distribution typically expected over the thickness of web member v3 and the decomposition of stresses derived from the measurements of a pair of gauges (i, j) . The stresses σ_i and σ_j derived from the measurements of a gauge pair (i, j) write:

$$\sigma_{i,j} = \sigma_{N(i,j)} \pm \sigma_{M(i,j)} = \frac{N_{(i,j)}}{A} \pm \frac{M_{(i,j)}}{I_z} \frac{e}{2} \quad (5.1)$$

Where $\sigma_{N(i,j)}$ is the axial stress due to the axial force $N_{(i,j)}$ in the section in line with the gauge pair (i, j) , $\sigma_{M(i,j)}$ is the bending stress due to the out-of-plane bending moment $M_{(i,j)}$ (around the weak axis of the section), e is the thickness, A is the cross-section area and I_z is the moment of inertia around the weak axis. The cross-section of v3 is a rectangle with a width $b = 40$ mm and a thickness $e = 7$ mm. Thus, $I_z = be^3/12$.

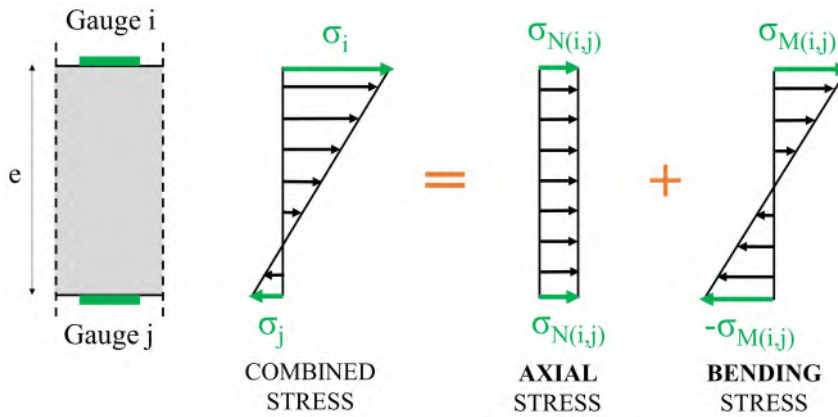


Figure 5.6 – Expected stress distribution over the thickness of web member v3 and decomposition of stresses derived from the measurements of a pair of gauges (i, j) in line with the considered cross-section.

Based on Eq. (5.1), the bending moment $M_{(i,j)}$ in a section in line with a pair of gauges can be computed as:

$$M_{(i,j)} = (\sigma_i - \sigma_j) \frac{I_z}{e/2} \quad (5.2)$$

The chosen sign convention was such that the moment would be positive when the side opposite the load jack in setup L_v3 was in tension. By convention, positive bending stresses on the side of gauges 1, 3, 5, 7 and 9, i.e. opposite the application of the load in test series L_v3, thus correspond to a positive bending moment.

Given the loading in both test setups G_hor and L_v3, the axial force in v3 was close to zero so that the measured stresses resulted almost only from the bending moment. Therefore, the measurements from the single gauge 5 provided a fair estimate of the bending moment at mid-span of web member v3.

The measurements from gauges 10 to 30 have not been used for the discussion pre-

sented in the following.

5.1.4 Finite element modelling

The reference numerical model was the same as in Chapter 4, except for the rotational stiffness of the joints equal to $k_r = 10^8$ Nmm/rad (nearly rigid connections instead of perfectly rigid connections). A new mesh convergence study was conducted, considering this time the results of static analysis instead of modal analysis. Testing the L_v3 setup, it was found that the mesh size of 10 mm was satisfactory. When the mesh was refined below 10 mm, the maximum deflection and the bending moment of v3 at mid-span remained stable. The lack of convergence observed for the results of modal analysis thus did not transpose to static analysis.

For the setup L_v3, the props were modelled as local restraints at one node. The axial stiffness of the props was estimated based on their approximate section and their length. So the props were represented by horizontal axial springs in the out-of-plane direction, linked to the ground, with a stiffness $k_y = 3 \times 10^4$ N/mm.

5.2 Results and discussion

5.2.1 Validation of the rotational stiffness of the joints

Global tests with a horizontal load (G_hor series)

The displacements measured for the force $F = 200$ N by lasers L2 to L7, as well as the bending moments derived from the strains measured on v3, were compared to numerical results from several finite element models (see Fig. 5.7). The displacements obtained from the numerical reference model were much lower than the measured displacements, suggesting that this model was too rigid compared to the reality. The parameter k_r corresponding to the rigidity of the joints was reduced from $k_r = 10^8$ Nmm/rad to $k_r = 10^6$ Nmm/rad, with almost no effect on the displacements. The support conditions were then adjusted, as they were in Section 4.3.2. The modelling of an elastic foundation yielded a much better agreement for the displacements. In contrast, the numerical bending moments along v3 remained unsatisfactory for all models, which may be due to modelling biases and reveals that support conditions could be further refined in the model. Indeed the linear bending moment along v3 is due to a constant shear force created by differential displacements between the top and the bottom chord. These differential displacements can be related to the particular geometry of the lattice girder, with two chords that are not parallel, but also to different restraint conditions for the top and the bottom chords close to the cantilever support.

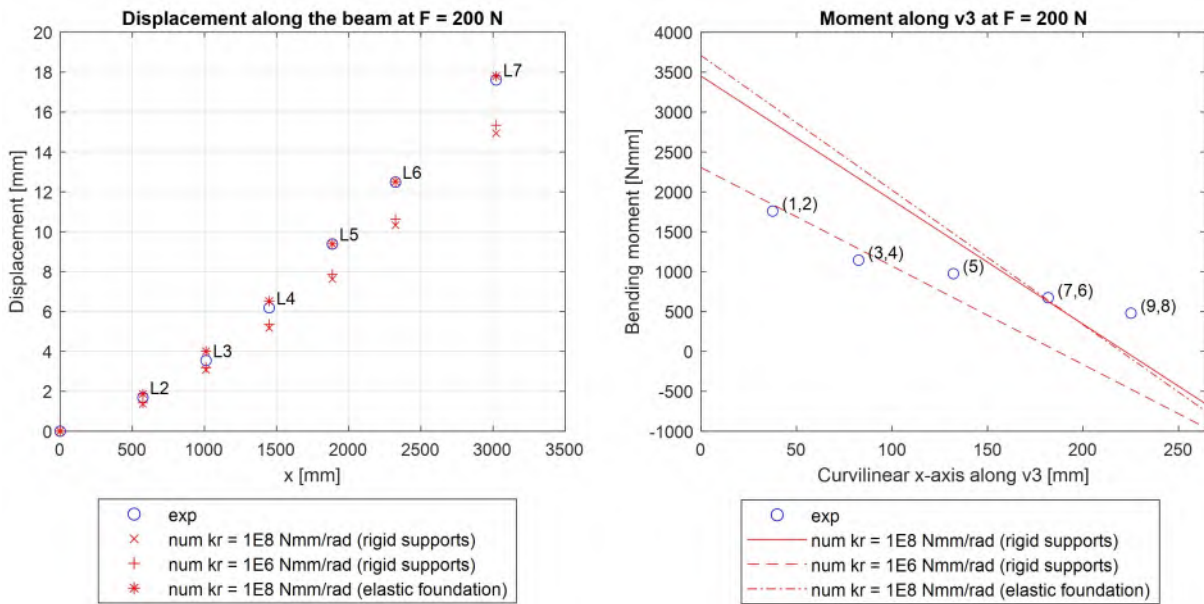


Figure 5.7 – Comparison of the experimental displacements and bending moments from the tests in the G_hor setup with the results from several numerical models: the reference model with $k_r = 10^8$ Nmm/rad and rigid supports, a model with $k_r = 10^6$ Nmm/rad and rigid supports, and a model with $k_r = 10^8$ Nmm/rad and an elastic foundation. The labels of the experimental data points correspond to the lasers (L2 to L7) and the gauge numbers.

However, the exploitation of G_hor results leads to the conclusion that the rotational stiffness of the joints has little influence on the global behaviour of the lattice girder. A variation of k_r does not make a large difference in the global displacements of the girder. Its influence can be seen at a more local scale, for example on the bending moments along a web member. At a global scale, the stiffness of the supports prevails over the joint stiffness regarding the out-of-plane behaviour. This confirms the results obtained by modal testing. k_r variations had little effect on the mode shapes of the lower modes, which were global mode shapes dominated by the deformation of the chords. Only mode shapes dominated by the deformation of web members were sensitive to k_r .

Local tests on web member v3 (L_v3 series)

For the setup L_v3, a comparison between experimental and numerical results was done for the displacements and the bending moments along web member v3. Fig. 5.8 displays a comparison of the results obtained for a force $F = 100$ N from the experiments, the reference numerical model with $k_r = 10^8$ Nmm/rad and the same model with $k_r = 10^6$ Nmm/rad. The reference model yields a good agreement with the experimental measurements. k_r values above 10^8 Nmm/rad do not significantly improve this agreement. In contrast, when k_r is decreased in the numerical model, large discrepancies appear, suggesting that lower values of the joint stiffness are further from reality. The local load tests thus suggest the same conclusion as modal testing: the riveted joints seem to ex-

hibit a rigid behaviour. More quasi-static tests, on other web members and with different positions of the prop, should be carried out and analysed to confirm this finding.

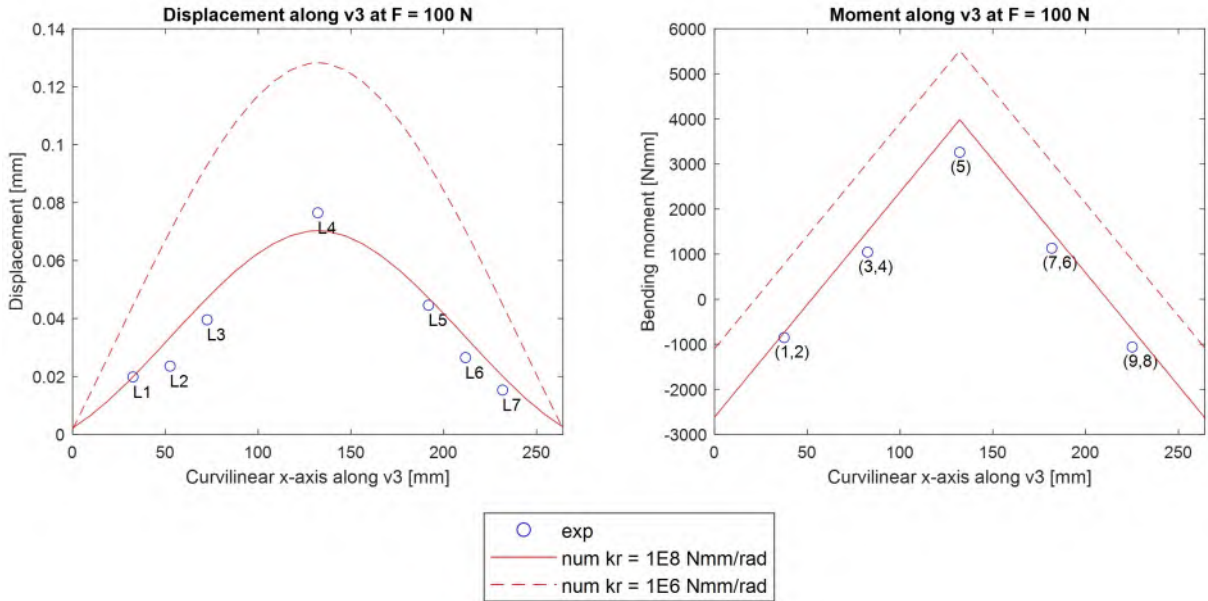


Figure 5.8 – Comparison of the experimental displacements and bending moments from the tests L_v3 with the results from the corresponding numerical model with $k_r = 10^8$ Nmm/rad and $k_r = 10^6$ Nmm/rad. The point labels refer to lasers (L1 to L7) and gauges (1 to 9).

5.2.2 Measurement and modelling of the apparent rotational stiffness

Plotting moment-rotation curves

So far, the joint stiffness has been estimated by updating numerical models based on experimental measurements. Thanks to the local bending tests L_v3 , the rotational stiffness at the extremities of $v3$ was also measured directly by plotting moment-rotation curves. For each web-to-chord connection, the measurement point was set to be the intersection between the neutral axis of the web member and the neutral axis of the chord, which corresponds to a connection node in the numerical models.

In the setup L_v3 , the web member $v3$ was loaded by a force applied at mid-span. The expected moment diagram along the loaded web member was constituted of two slopes:

$$\begin{aligned} \text{For } 0 \leq x \leq L/2 : M(x) &= A_1x + B_1 \\ \text{For } L/2 < x \leq L : M(x) &= A_2x + B_2 \end{aligned} \quad (5.3)$$

Where L is the length of web member $v3$, and A_1 , B_1 , A_2 and B_2 are coefficients depending on the applied load. Each slope A_1 and A_2 could be determined by two pairs of gauges. Thus, for each selected value of the applied force, the moment at a joint was computed by linear extrapolation (Fig. 5.9).

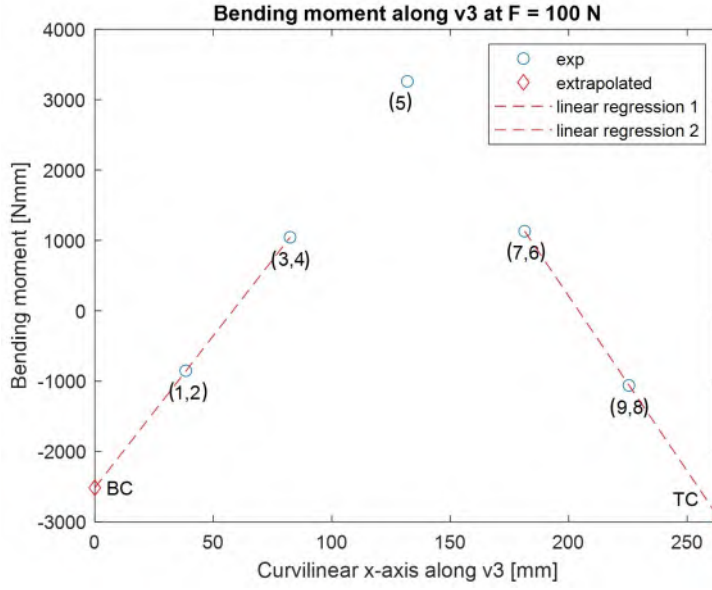


Figure 5.9 – Linear extrapolation based on measured moments to compute the moment at the extremities of the loaded web member (label BC: connection between v3 and bottom chord BC; label TC: connection between v3 and top chord TC).

Regarding the rotation, it was measured by taking the derivative of a curve fitted to the measured displacements. The curve fitting process relied on the equations for the moment derived from gauge measurements. Under small deformations, the moment is theoretically proportional to the second derivative of the displacement:

$$M = EIy'' \quad (5.4)$$

Where E is the modulus of elasticity and I is the out-of-plane moment of inertia of v3 cross-section. Based on Eq. (5.3), the displacement curve was thus expected to correspond to two third-order polynomials:

$$\begin{aligned} \text{For } 0 \leq x \leq L/2 : y(x) &= A_1 \frac{EI}{6} x^3 + B_1 \frac{EI}{2} x^2 + C_1 x + D_1 \\ \text{For } L/2 < x \leq L : y(x) &= A_2 \frac{EI}{6} x^3 + B_2 \frac{EI}{2} x^2 + C_2 x + D_2 \end{aligned} \quad (5.5)$$

Consequently, the curve-fitting process consisted in adjusting only the coefficients C_1 , D_1 , C_2 and D_2 . The fitted displacement curves for several values of the load are presented in Fig. 5.10. The results are satisfactory and prove that the analytical model relating the displacements and the moments reflects well the coherence between the measured displacements and the measured deformations. However, the chosen curve-fitting process does not guarantee a perfect continuity of the displacement and its derivative at $L/2$.

Once the coefficients of Eq. (5.5) are determined, the rotation angles at the extremities of v3 can be deduced from the first-order derivative of the displacement y' . Only the

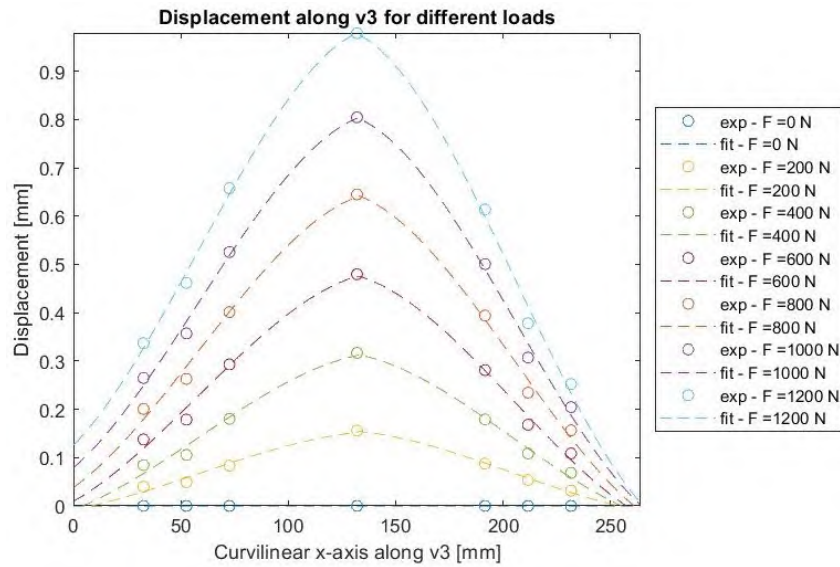


Figure 5.10 – Curve fitting on the measured displacements for the tests L_v3 with a piecewise third-order polynomial, for values of the applied force ranging from 0 to 1200 N with a step of 200 N.

rotation angles resulting from the deformation of v3 are of interest. The contribution of a rigid body motion of v3 must be removed. Thus, the angle corresponding to the inclination θ_R of the web member due to the differential displacements of the top and bottom chord was subtracted from y' (Fig. 5.11).

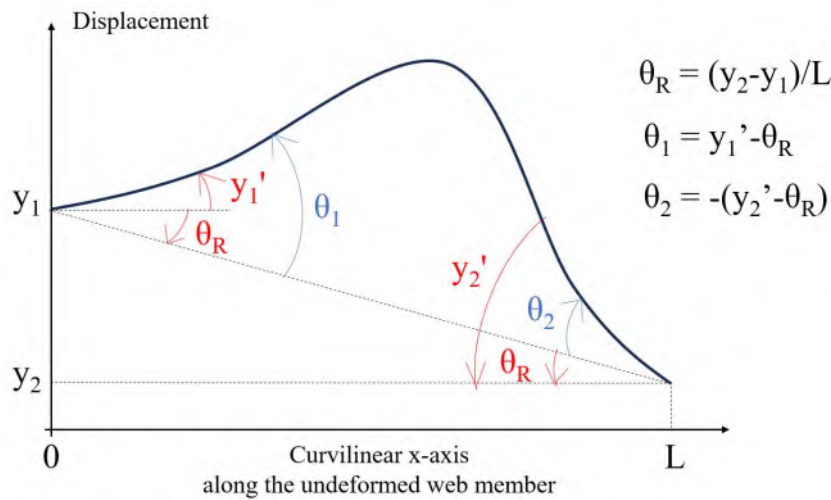


Figure 5.11 – Correction of the first-order derivative of the displacement to obtain the rotation angle due only to the deformation of v3. θ_R is exaggerated.

The moment-rotation curves at the two extremities of v3 were traced based on sample moments and rotations corresponding to selected force values, ranging from 0 to 1200 N with a step of 100 N (Fig. 5.12). Both curves appear to be linear, which means that web-to-chord connections exhibit a linear semi-rigid behaviour. The slope of each moment-rotation curve corresponds to the rotational stiffness measured at each extremity of v3. The measured stiffness values, approximately on the order of 10^6 to 10^7 Nmm/rad, are

smaller than the joint stiffness estimated at around 10^8 Nmm/rad or higher through the comparison of experimental data with numerical models. This is because experimental moment-rotation curves yield an apparent stiffness, resulting not only from the joint stiffness, but also from the rotational restraint provided by the chords. A mechanical model is proposed in the following section to explain the difference between joint stiffness and apparent stiffness, and also to understand the difference between the apparent stiffness measured at the top and the bottom chord.

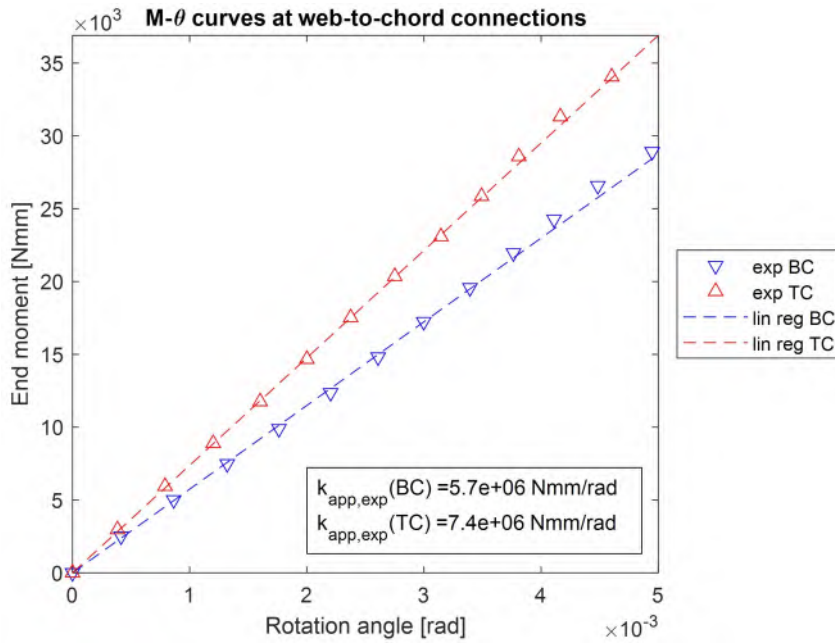


Figure 5.12 – Moment rotation curves at the ends of v3.

Mechanical model

The restraint exerted at the end of a web member can be modelled by two rotational springs connected in series (Fig. 5.13a). One spring corresponds to the joint stiffness k_r that was given as an input in the numerical models. The other spring k_c is a combination of the out-of-plane flexural stiffness of the chord and its torsional stiffness. Indeed, the out-of-plane bending moment transmitted by the web member to a chord can be decomposed in an out-of-plane bending moment and a torsional moment in the chord (Fig. 5.13b).

Depending on the angle between the web member and the chord, the contribution of the bending stiffness versus the torsional stiffness of the chord varies. The decomposition of the rotation angle is mathematically more complex. Therefore, we relied on the literature to obtain an analytical expression of k_c . Lee, 2013 conducted a study on the buckling behaviour of web members in open web steel joists. He derived a hand calculation procedure to estimate the resisting out-of-plane rotational stiffness k_c at web member

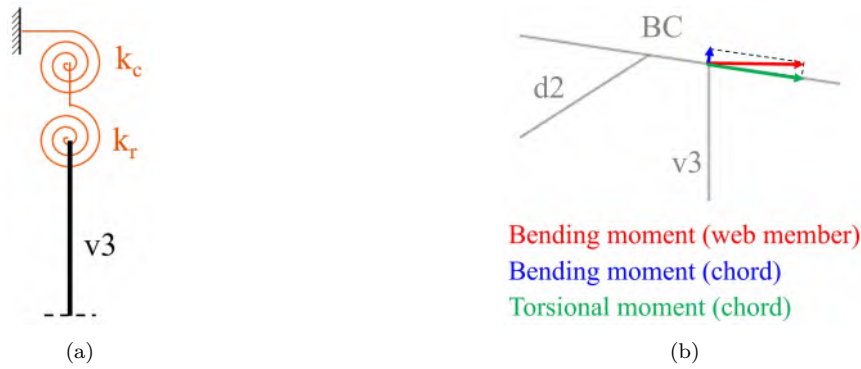


Figure 5.13 – Mechanical model for the riveted connection: (a) series of rotational springs; (b) decomposition of the out-of-plane bending moment in the web member as the sum of the out-of-plane bending moment and the torsional moment in the chord.

extremities, assuming perfectly rigid joints (Lee, 2013, p. 37):

$$k_c = \alpha - \frac{\beta}{\gamma} \quad (5.6)$$

$$\begin{aligned} \alpha &= \sum_{j=1}^n [k_{\text{bending},j} \cos^2 \phi_j + k_{\text{torsion},j} \sin^2 \phi_j] \\ \beta &= \sum_{j=1}^n [k_{\text{bending},j} \cos \phi_j \sin \phi_j - k_{\text{torsion},j} \cos \phi_j \sin \phi_j]^2 \\ \gamma &= \sum_{j=1}^n [k_{\text{bending},j} \sin^2 \phi_j + k_{\text{torsion},j} \cos^2 \phi_j] \end{aligned} \quad (5.7)$$

$$\begin{aligned} k_{\text{bending},j} &= \frac{4E_j I_j}{L_j} \\ k_{\text{torsion},j} &= \frac{G_j J_j}{L_j} \end{aligned} \quad (5.8)$$

Where E_j , G_j , I_j , J_j , L_j are the elastic modulus, the shear modulus, the out-of-plane moment of inertia, the Saint-Venant torsion constant and the node-to-node length of each neighbouring member j of the truss. ϕ_j is the angle measured counter-clockwise from the web member to the neighbouring member j (or equivalently, the smallest positive angle between the web member and the neighbouring member of interest). Fig. 5.14 represents a graphical interpretation of Lee's geometrical parameters, applied to the tested lattice girder. Eq. (5.7) translates that the rotational restraint provided by each neighbouring member is a combination of its out-of-plane bending stiffness $k_{\text{bending},j}$ and its torsional stiffness $k_{\text{torsion},j}$. The importance of the contribution of each term depends on the angle ϕ_j between the web member and the neighbouring member j .

Several modifications were made to adapt Eq. (5.8) to the tests L_v3 carried out on the lattice girder. First, it was considered that the neighbouring web members did not

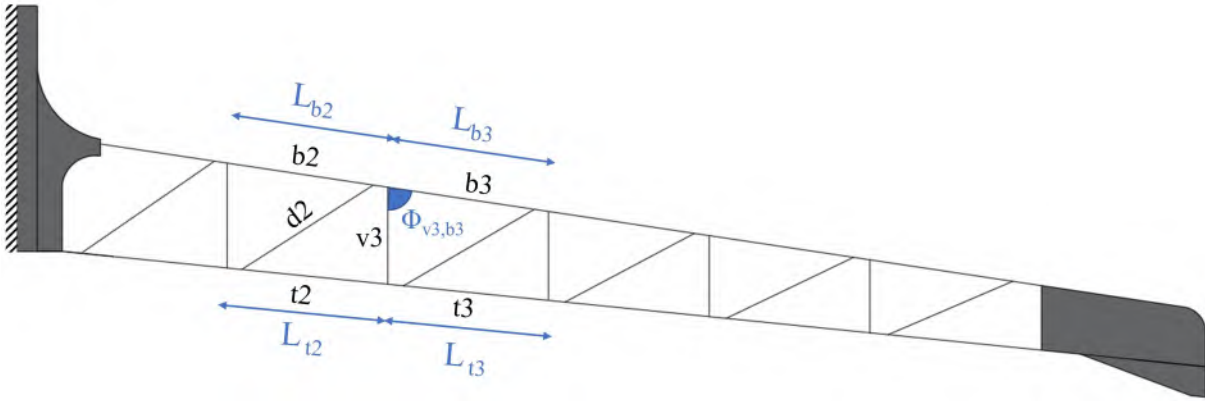


Figure 5.14 – Geometrical parameters used for the stiffness calculations proposed by Lee, 2013 after the formulas Eq. (5.7) and (5.8).

contribute to any rotational restraint, because of their low out-of-plane moment of inertia and torsional constant. For example, at the connection between $d2$, $v3$ and the top chord, it was assumed that $d2$ and $v3$ have no mutual influence on each other. Secondly, the length of each chord segment was not taken equal to the length of a cell. The length L_j corresponds to the length between the loaded web member and a support. Two different lengths were defined for the bending stiffness and the torsional stiffness. Regarding bending, the supports were provided by the props, so the lengths to be considered corresponded to distance between the web-to-chord connection and the prop (see Fig. 5.15). Regarding torsion, the props did not provide sufficient rotational restraint to be considered as supports. The retained lengths were then assumed to be the lengths between the web-to-chord connection and the vertical gussets at each extremity of the riveted lattice girder. Finally, factor 4 in the first terms of α , β and γ was removed, as it corresponded to clamped supports. As a result, Eq. (5.8) was transformed into:

$$\begin{aligned} k_{\text{bending},j} &= \frac{E_j I_j}{L_{\text{bending},j}} \\ k_{\text{torsion},j} &= \frac{G_j J_j}{L_{\text{torsion},j}} \end{aligned} \quad (5.9)$$

The apparent stiffness k_{app} obtained from moment-rotation curves results from k_c and k_r working in series:

$$k_{app} = \frac{1}{\frac{1}{k_c} + \frac{1}{k_r}} \quad (5.10)$$

Table 5.1 summarises the parameters used for the analytical computation of k_c and presents a comparison of the resulting analytical stiffness $k_{app,ana}$ with the experimental stiffness $k_{app,exp}$. k_r was taken equal to 10^8 Nmm/rad. The analytical stiffness values are in reasonable agreement with the experimental values. However, it appears that exper-

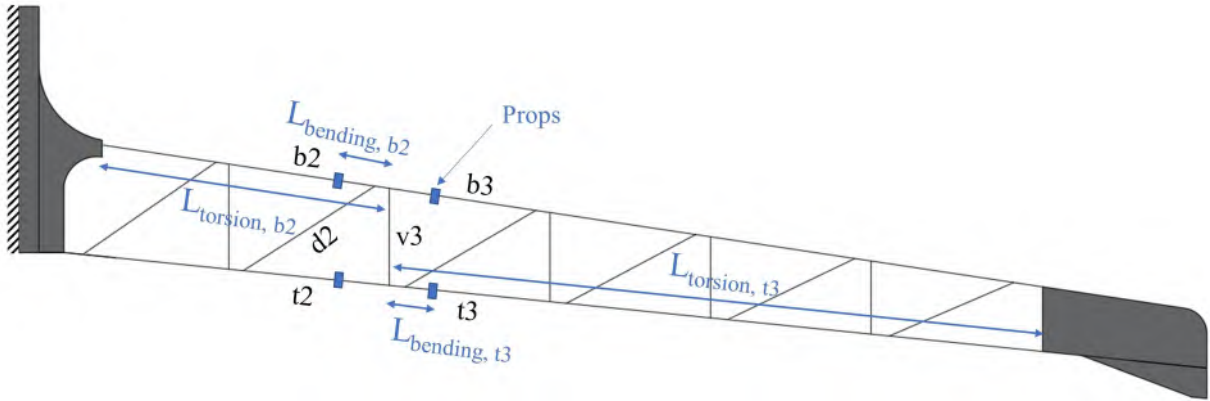


Figure 5.15 – Adapted geometrical parameters used for the stiffness calculations after the formulas Eq. (5.7) and (5.9), taking into account the boundary conditions in setup L_v3. L_{bending} and L_{torsion} were represented only for b2 and t3.

imentally, $k_{\text{app,exp}}(BC) < k_{\text{app,exp}}(TC)$, while analytically, $k_{\text{app,ana}}(BC) > k_{\text{app,ana}}(TC)$. This can be explained by the fact that in the analytical model, the difference in restraint provided by TC or BC to v3 is only due to a difference in the inclination of TC and BC. The angle between BC and v3 is smaller than the angle between TC and v3. Thus, the contribution of the bending stiffness of BC at the connection v3-BC is larger than the contribution of the bending stiffness of TC at the connection v3-TC. Because the bending stiffness of the chords is much larger than their torsional stiffness, this results in $k_{\text{app,ana}}(BC) > k_{\text{app,ana}}(TC)$.

Table 5.1 – Parameters used for the analytical computation of k_c and comparison of the resulting analytical stiffness $k_{\text{app,ana}}$ with the experimental stiffness $k_{\text{app,exp}}$.

		v3-BC	v3-TC
$\Phi_{\text{v3/chord,left}}$	[°]	98.6	84.2
$\Phi_{\text{v3/chord,right}}$	[°]	81.4	95.8
$L_{\text{bending,left}}$	[mm]	110 ± 10	135 ± 10
$L_{\text{bending,right}}$	[mm]	118 ± 10	110 ± 10
$L_{\text{torsion,left}}$	[mm]	800 ± 100	840 ± 100
$L_{\text{torsion,right}}$	[mm]	1800 ± 100	1790 ± 100
k_c	[Nmm/rad]	$(1.6 \pm 0.2) \times 10^7$	$(7.3 \pm 0.6) \times 10^6$
$k_{\text{app,ana}}$	[Nmm/rad]	$(1.4 \pm 0.1) \times 10^7$	$(6.8 \pm 0.5) \times 10^6$
$k_{\text{app,exp}}$	[Nmm/rad]	5.7×10^6	7.4×10^6

In the experiments, the supports provided by the props were not perfectly rigid, so the support conditions of the lattice girder as a whole did play a role in the restraint provided by each chord. The fixing conditions of TC are more rigid than the fixing conditions of BC, because TC is maintained by a horizontal gusset bolted directly to the anchoring plate, while BC is fixed to a vertical gusset that was not designed to resist out-of-plane bending. So, understandably, the restraint provided by TC is stiffer than the one provided by BC: $k_{\text{app,exp}}(BC) < k_{\text{app,exp}}(TC)$.

The proposed mechanical model has the merit of underlining the contribution of the bending stiffness and the torsional stiffness of the chords in the rotational end-restraint provided to web members. However, the analytical formulas are obviously limited in their capacity to reflect measurements. We need to repeat the analytical development of the formulas for computing k_c proposed by Lee, 2013, who relied on Matlab's Symbolic Math Toolbox. Also, an optimisation procedure could be carried out to find sets of geometrical parameters ($L_{\text{bending},j}$, $L_{\text{torsion},j}$) yielding the best agreement with the measured apparent rotational stiffness. The winning sets of parameters could then be confronted with a physical interpretation. Also, moment rotation curves could be plotted based on results from the finite element model of the lattice girder or reduced models around the tested web member with clearer boundary conditions. This could help understand if the limitations of the analytical approach are due to the complex boundary conditions at the cantilever support.

5.3 Conclusion

A load test campaign was carried out on a lattice girder twin to the one used as a specimen for the vibration tests. Two series of tests were carried out in two different setups. In setup G_hor, the lattice girder was submitted to a horizontal load at its tip. The comparison of the measured displacements along the girder with displacements predicted by a finite element model confirmed two results from the modal testing campaign. First, the out-of-plane rotational stiffness of the joints has little influence on the global out-of-plane deformation behaviour of the girder. Second, the support conditions of the cantilever cannot be considered rigid and play a dominant role in the global behaviour.

In setup L_v3, a load was applied at the mid-span of web member v3 and intermediary support conditions were added via props to isolate v3 from the cantilever support. The comparison of measured displacements and bending moments along v3 with results from numerical models confirmed that the best agreement is obtained when the riveted joints are modelled as rigid or almost rigid ($k_r = 10^8$ Nmm/rad). This suggests that the riveted joints feature the same rotational stiffness under dynamic and quasi-static loading.

Additionally, moment rotation curves were traced at both ends of v3 based on the measurements of test series L_v3. The rotations were estimated by taking the derivative of a piecewise polynomial fitted to the measured displacements. The obtained moment rotation curves were close to straight lines, so the semi-rigid behaviour of the connections appeared to be linear. The rotational stiffness derived from the slopes of the linear moment rotation curves was inferior to the assessed rotational stiffness of the joints. A mechanical model was proposed to explain the contribution of the bending and the torsional stiffness

of the chords to the rotational end-restraint provided to web members. Analytical values of the apparent rotational stiffness were found to be in reasonable agreement with the experimental values. However, the analytical procedure presents a range of limitations due to the complexity of the specimen geometry and the experimental setup. It does not properly account for differences between riveted connections with the top chord and the bottom chord.

The results of the presented tests need to be further analysed and validated. The bending moments measured along web member v3 in the global setup G_hor presented large discrepancies with the moments obtained from the numerical model. As was done for the modal testing campaign, a parametric study should be conducted to assess the impact of several modelling assumptions on the predicted behaviour. As the support conditions were found to have a major influence on global behaviour, special focus could be dedicated to refining them. Regarding the local tests, other configurations should be analysed. A series of complementary tests were actually already carried out, where the load was applied also on d2, and the props were placed at varying distances from the loaded web members, v3 or d2. A future study will hopefully be able to analyse the results of those tests and use them to improve the finite element modelling and the analytical mechanical model. Also, the measurements from the gauges that were left out of the analysis so far should contribute to a better overview.

Overall, Part II proposed several ways to refine modelling assumptions. Chapter 3 brought together a historical study and a review of recent literature to cast light on the various possible assumptions regarding the behaviour of riveted connections and the consequences on the predicted load distribution and buckling behaviour of lattice girders. This helped characterise the uncertainties that may be responsible for discrepancies between the original design and the assessment of the existing structure. Chapter 4 and 5 aimed to remove certain uncertainties by means of experimental and numerical investigations. Part III moves on to discussing design criteria, focusing first on the resistance derived from material properties and then on the assessment of the buckling risk.

PART III

**ADAPTING VERIFICATION
METHODS**

DETERMINING DESIGN VALUES OF MATERIAL PROPERTIES

Chapter 6 discusses how to derive design values for the yield strength of wrought iron and mild steel. Two sources of information on the material are analysed: historical archives and material sampling. The literature review regarding historic metal structures in general is compared with the specific case of train sheds.



Top: specimen for material testing (Picture from the survey of the station Gare de Marseille St-Charles by A-Corros, 2017). Bottom: historical design report of the train shed of Bédarieux, 1902.

Contents

6.1	Historical perspective on iron and steel varieties	134
6.2	Historical “design resistance”	136
6.3	Material sampling and characteristic values	143
6.4	Conclusion	153

Following structural analysis, the verification stage of structural assessment consists of carrying out design checks that compare the internal loads or stresses with an allowable limit or “design resistance”. This resistance depends on the capacity of the material. When designing a new steel structure today, engineers estimate the capacity of steel using nominal values of the yield strength f_y provided by the Eurocodes (EN 1993-1-1, 2005, §3.2). Even though Eurocode 3 is used also to assess historic metal structures, it does not deal explicitly with historic materials such as wrought iron or mild steel. Thus, when assessing an existing iron or steel structure, engineers face uncertainties regarding which nominal value of the yield strength to use. They usually fall back on two types of sources: the analysis of historical archives or of material samples of the structure. Historical archives, such as design reports or drawings, can indicate the stress limit, the so-called “working stress”, used for the original design. Material testing can provide measurements of mechanical properties taken from samples of the existing structure. In both cases, the values cannot be used directly as design values of the material strength for structural verification. Therefore, this chapter focuses on how to determine design values of material properties, using the example of wrought iron and mild steel in train sheds.

The chapter begins by providing a historical background on iron and steel varieties. Then, it traces the evolution of working stresses used in France for wrought iron and mild steel, enhancing discrepancies between values recommended in the literature or regulations and the ones effectively used in practice. It goes on to examine the results from tensile tests on wrought iron and mild steel specimens, obtained both from the literature and samples of train shed structures. Finally, the discussion gives critical insight into the possibilities and the limitations of both types of sources. Portions of the presented study have been published as a book chapter (Franz et al., 2023c) and a conference paper (Franz et al., 2022a).

6.1 Historical perspective on iron and steel varieties

The production of pig iron using charcoal furnaces dates back to the Middle Ages. In 1709 in England, the ironmaster Darby introduced blast furnaces heated with coke, produced by the pyrolysis of mineral coal. The heating temperature increased and better quality *cast iron* could be produced (de Bouw et al., 2009). The first coke foundry in France was built in Le Creusot in 1781-1785 (Lemoine, 1986, p. 14). The puddling process was invented around 1780 in England, but the first puddling furnace was not introduced in France until 1818, again at Le Creusot (Schädlich, 2015, p. 32). Puddling consists of bringing together pasty masses of iron and impurities, known as slag, heated in low furnaces, and rolling them into bars. Hammering partially eliminates the slag. As a result

of the rolling process, *wrought iron* has a fibrous structure. In 1855, the English inventor Bessemer developed a process for refining cast iron that oxidised undesirable elements with air, making it possible to produce *steel* economically. The slag, which was less dense than the metal, separated from the iron by flotation. This process was improved by the chemist Thomas in 1877, who modified the converter from cast iron to steel by essentially changing its coating from acidic to basic. The first Thomas converter was installed in France at Le Creusot in 1879. At the same time, in 1864, the Martin brothers and Siemens proposed a process that had the advantage of being able to reuse scrap metal and produce better-quality steel. But the Siemens-Martin process, like the Bessemer process, required ores with a low phosphorus content, which were less common in France than in England. The Thomas process, therefore, remained predominant in France and Belgium until steel production using an electric furnace began to develop in the early 20th century (de Bouw et al., 2009).

Overall, in 19th-century metal construction, the three main types of materials derived from iron ore were cast iron, wrought iron and steel. Cast iron has the highest percentage of carbon, between 2 and 6% (Bates, 1984, p. 8). Its microstructure is characterised by a uniform matrix with lamellar graphite inclusions dispersed in different orientations (Fig. 6.1a). It is a hard, brittle material, but can be easily moulded and resists compression well. In train sheds, it was therefore mainly used for decorative elements, and for elements working predominantly in compression, such as columns and struts in Polonceau trusses. Wrought iron, obtained by refining cast iron, also contains carbon but at a very low level (less than 0.05%) (Moy et al., 2009). It features a fibrous structure with a variable density of long parallel slag lines in the rolling direction (Fig. 6.1b). Wrought iron works well in traction. Finally, steel contains slightly more carbon than iron, as well as other elements that can alter its properties (manganese, nickel, chromium, etc.). Still, mild or extra-mild steels (also called soft or extra-soft), which were used for profiles and plates in metal constructions, have a relatively low carbon concentration, staying below 0.25% (de Bouw et al., 2009). Mild steels of the late 19th century have fairly coarse iron grains of variable size with a majority of small irregularly shaped slag particles (Fig. 6.1c). Mild steels of the early 20th century have smaller, homogeneous grains thanks to better control of the manufacturing process (Kühn et al., 2008; STRRES, 2014). Steel has a higher hardness and greater ductility than wrought iron. Those materials have, however, many properties in common and were used for the same purposes. Mild steel progressively took over wrought iron at the end of the 19th century. Wrought iron and mild steel were used to fabricate the flat and angle bars assembled to make riveted lattice girders - which is why the following study focuses on those two materials.

The names iron and steel are not unambiguous. Several terms such as wrought iron,

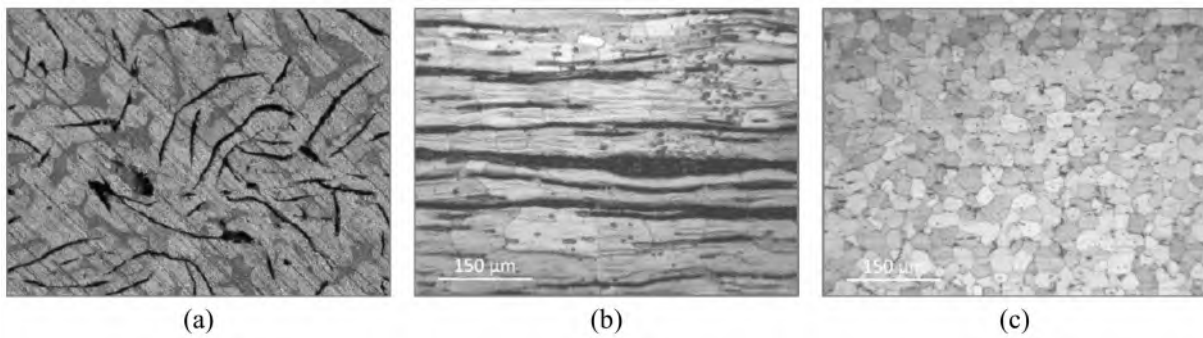


Figure 6.1 – Characteristic microstructures of (a) cast iron, (b) wrought iron and (c) mild steel. (a) Picture from the material survey of the station Gare d’Angoulême carried out by A-Corros in 2012 (scanning electron microscope view, x100); (b) and (c) Pictures from the material survey of Marseille St-Charles Station carried out by A-Corros in 2017 (optical microscope view, x280).

ingot iron and ingot steel have coexisted, and their use depended on the author (Werner et al., 1992, p. 37). The distinction between iron and steel was sometimes based on chemical characteristics (particularly carbon content), sometimes on the manufacturing process. This problem was highlighted by many engineers in the 19th century, for example: “puddling and fusion can at will produce iron and steel, but by giving them different structures and properties; it is therefore important to know, not only what is the hardness of the metal we are dealing with, but also what is its origin”(Considère, 1885, p. 579)[transl.]. However, some simplifications were admitted: “as puddling is used mainly to produce soft metal and fusion has hitherto been used mainly to make hard metal, the word iron, without a qualifier, always refers to wrought iron and the word steel, used alone, refers to steel produced by fusion”(Considère, 1885, p. 579)[transl.]. A large range of iron and steel varieties can be distinguished in the nomenclature (de Bouw et al., 2009). Still, in line with common practice in structural assessment, this study restricts itself to the distinction between wrought iron and mild steel (obtained by fusion).

6.2 Historical “design resistance”

In the 19th century, the safety concept for designing metal structures consisted in comparing the stresses resulting from the loads with a “working stress”, which was a fraction of the ultimate strength of the material. No safety factors were used on the loading side, only on the resistance side. They accounted for uncertainties such as calculation errors, material inhomogeneities, imperfections related to manufacturing and construction, dimensional errors, etc. Schueremans et al., 2018 summarised design practices for iron and steel structures in 19th century Western Europe, mostly based on official regulations. However, the choice of working stress depended a lot on the experience and theoretical knowledge of the designers and the risk-willingness of the project owners or contracting authorities. Early regulations actually gave little guidance (Werner et al., 1992, p. 72).

The gap between design criteria recommended in the literature or regulations and the ones effectively used in practice remains widely unexplored. Therefore, an extensive survey of the French literature of the 19th century and the beginning of the 20th century is used to trace the evolution of French design criteria for wrought iron and mild steel. Beyond regulations, the survey draws on construction treatises, civil engineering periodicals and reports from the French Society of civil engineers. Some case studies of the literature highlighted the working stresses effectively used for single constructions, such as the Garabit viaduct in France (Schueremans et al., 2018) or a dome in the Vienna Hofburg (Hochreiner et al., 2019). In order to provide a more representative illustration of the working stresses used in practice, this study develops insight into the design criteria used for train sheds, based on historical design reports from SNCF archives.

6.2.1 Recommendations from historical literature and regulations

From the first half of the 19th century, the limit of 6 kg/mm² became the default working stress for iron, for elements working in tension. The unit kg/mm², sometimes noted only “k”, was the unit commonly used in the 19th century. 1 kg/mm² corresponds to 1 daN/mm² or 10 MPa. The value of 6 kg/mm² was first recommended by Navier in 1826 (Navier, 1833, p. 118). He was imitated by Poncelet in 1829 and Morin in 1853 (Poncelet, 1841, pp. 356–357, Morin, 1853, pp. 52–53). According to Vierendeel, who published a monograph on iron and steel construction in 1902, it was thanks to Poncelet and Morin that the limit of 6 kg/mm² was adopted by the French administration and became widely used in practice (Vierendeel, 1902, p. 404).

Authors often defined the working stress as a fraction of the ultimate strength or yield strength of the material. The ultimate strength is the stress at which fracture occurs when the material is subjected to tensile forces. The yield strength is theoretically the stress at which the material begins to deform irreversibly. As the start of plastic deformation was hard to clearly establish experimentally, the yield strength was more difficult to measure than the ultimate strength. For this reason, the ultimate strength remained for a long time the reference to define the working stress (Brune, 1888, p. 13). In 1826, Navier defined the working stress based on an average ultimate strength of 40 kg/mm² obtained from a comprehensive review of tensile tests conducted by other scientists. His safety factor of about 6, leading to a working stress of 6-7 kg/mm², became standard thereafter (Navier, 1833, pp. 19–34).

Recommended working stresses depended on the load combination used to calculate the stresses in the structure. Dead loads result from the weight of the construction, live loads correspond to the weight of trains, vehicles or pedestrians and climatic loads include snow and wind. In today’s Eurocodes, dead loads are called “permanent actions” while live

loads and climatic loads are grouped under the name of “variable actions”. “Accidental actions” refer to explosions or impacts (EN 1990, 2002). In the literature of the 19th century, the words “permanent”, “variable” and “accidental” were used in a much less straightforward manner. Holzer, 2006 also showed that the refinement of load assumptions varied depending on their nature. Several authors defined the working stress as a limit for “permanent” stresses (Bresse, 1857, p. 220) but then some applied this working stress to examples including climatic loads (Ardant, 1840, pp. 84–87) or accidental loads (Collignon, 1869, pp. 546–547, Brune, 1888, pp. 13–14). Navier indicated a limit of 6 to 7 kg/mm² for dead loads and 8 to 10 kg/mm² for stresses resulting from dead and “accidental” loads, without detailing their nature. The limit was set higher for combinations including several types of loads because they generated a lower level of uncertainty for the maximum calculated stress.

Other references were more explicit regarding load assumptions. The working stress of 6 kg/mm², recommended by the first French regulation on metallic road bridges published in 1869 and its revision published in 1877, applied to stresses resulting from dead loads and live loads (Regnauld, 1870, pp. 539–543). In 1886, Flamand mentioned a formula for the working stress proposed by Séjourné:

$$\sigma_{\text{lim}} = \frac{6}{1 - 0,4 \frac{\sigma_{\text{min}}}{\sigma_{\text{max}}}} \text{ kg/mm}^2 \quad (6.1)$$

σ_{min} was the minimum stress and σ_{max} the maximum stress in the considered element, depending on load combinations (Flamand, 1886, pp. 227–230). Vierendeel calculated that with this formula the working stress varied between 6 kg/mm² if the dead load was close to zero and 10 kg/mm² for permanent loads only. In the case of “light-weight roof structures, for which the dead load is low compared to accidental loads related to wind, snow or people”[transl.], the working stress would lie between 6 and 7 kg/mm² (Vierendeel, 1902, pp. 405–407). The regulation for metallic bridges released in 1891 also gave formulae calculating the working stress depending on the ratio between live and dead loads, leading to values between 6 and 9 kg/mm² (Résal, 1892, pp. 526–534). The first regulation for train sheds, released in 1902, recommended a working stress for iron of 8 kg/mm², corresponding to load combinations including dead load, snow and wind (« Circulaire du ministre des travaux publics aux préfets du 25 janvier 1902 (Halles à voyageurs et à marchandises des chemins de fer) », 1904). The next revision of the regulation on metallic bridges, published in 1915, introduced a wider range of load combinations including live loads, snow, wind and temperature (Résal, 1917, pp. 109–140).

The working stress of 6 kg/mm² for iron was a default value. This limit could be

increased according to the type of structure, the quality of the material or the experience of the contractor. Poncelet stated that “contractors specialised in the construction of iron suspension bridges, guided by a long experience and sure of a consistent manufacturing”[transl.] may use a higher stress limit (Poncelet, 1841, p. 357). Regulations also explicitly allowed engineers to choose higher working stresses according to their individual judgement. Brune stated that “the safety load commonly accepted for iron is of 6 kg/mm² for public constructions, 8 kg/mm² for private constructions, and 10 kg/mm² for industrial constructions”(Brune, 1888, p. 15)[transl.]. Ardant indicated working stresses between 6 and 12 kg/mm² “depending on the quality” of the material (Ardant, 1840, p. 103). Morin allowed a working stress of 8 kg/mm² for roof trusses, arguing that the rigidity of connections and the friction of girders on their supports, which were not considered for determining the stresses, played in favour of stability. Moreover, Morin stated that roof trusses were made of “selected materials” (Morin, 1853, p. 402). The same idea was presented in the “General study on iron roof structures” of the periodical *Nouvelles Annales de la Construction* in 1863, thus recommending working stresses between 8 and 10 kg/mm² (Mathieu, 1863).

In the 1880s, authors began to propose working stresses for steel. The recommended values in the theoretical literature varied more than those for iron, which may be due to fluctuations in the carburization level of the steel. Flamand suggested applying Séjourné’s formula to steel, with a 50% increase compared to iron (Flamand, 1886, p. 220). The International Congress for construction processes, gathered in Paris during the World Exhibition of 1889, favoured an increase of 40% (Vierendeel, 1902, pp. 414–416). Brune recommended working stresses between 6 and 10 kg/mm² for iron and 15 and 20 kg/mm² for steel (Brune, 1888, p. 15). Résal gave working stresses between 5 and 8 kg/mm² for iron and between 7 and 9 kg/mm² for steel (Résal, 1892, p. 532). The formulae in the bridge regulation of 1891 led to working stresses between 8 and 12 kg/mm² for steel. The train shed regulation of 1902 prescribed 10 kg/mm². Novat stayed more conservative with recommended working stresses between 7 and 10 kg/mm² (Novat, 1900, p. 28). In 1909, Flamand cited both Séjourné’s formula and the regulation of 1891, thus clearly showing that engineers remained free in their choices (Flamand, 1909, pp. 243–248). The bridge regulation of 1915 prescribed that stresses resulting from dead and live loads should not exceed 12 kg/mm² while stresses including also the effect of wind should stay below 12.5 kg/mm² (Résal, 1917, pp. 112, 118). In 1917, Résal stated that in practice a working stress of 12 kg/mm² for steel was commonly used.

Tab. 6.1 summarises the sources discussed above and indicates in which engineering school the authors were teaching, to enhance the potential impact of their knowledge in practice.

Table 6.1 – List of sources used to establish the evolution of working stresses of iron and steel between 1820 and 1930. Year: date of publication of construction treaty or lecture notes. *In italics*: regulations.

Year	Author	Engineering school	σ_{lim} (iron) [kg/mm ²]	σ_{lim} (steel) [kg/mm ²]
1826	NAVIER C.-L.	Ecole des Ponts et Chaussées	6-10	-
1840	ARDANT P.-J.	Ecole d'Application de l'Artillerie et du Génie (Metz)	6-12	-
1841	PONCELET V.-J.	Ecole d'Application de l'Artillerie et du Génie (Metz)	6	-
1853	MORIN A.	Conservatoire des Arts et Métiers	6-8	-
1857	BRESSE J.	Ecole des Ponts et Chaussées	6	-
1863	MATHIEU E.	-	8-10	-
1869	COLLIGNON E.	Ecole des Ponts et Chaussées	5-6	-
<i>1869</i>	<i>Circulaire du 15 juin 1869 relative aux épreuves à faire subir aux ponts métalliques destinés aux voies de terre</i>		<i>6</i>	<i>-</i>
<i>1877</i>	<i>Circulaire du 9 juillet 1877 relative aux épreuves des ponts métalliques</i>		<i>6</i>	<i>-</i>
1886	FLAMANT A.	Ecole Centrale des Arts et Manufactures, Ecole des Ponts et Chaussées	6-7	9-10.5
1888	BRUNE E.	Ecole des Beaux-Arts	6-10	15-20
<i>1891</i>	<i>Circulaire du 29 août 1891 relative aux épreuves des ponts métalliques</i>		<i>6-9</i>	<i>8-12</i>
1892	RESAL J.	Ecole des Ponts et Chaussées	5-8	7-9
1900	NOVAT J.	Société d'enseignement professionnel du Rhône	6-8	7-10
<i>1902</i>	<i>Règlement du 25 janvier 1902 sur les halles à voyageurs et à marchandises des chemins de fer</i>		<i>8</i>	<i>10</i>
1909	FLAMANT A.	Ecole Centrale des Arts et Manufactures, Ecole des Ponts et Chaussées	6-9	8-12
<i>1915</i>	<i>Circulaire du 8 janvier 1915 relative aux épreuves des ponts métalliques</i>		<i>-</i>	<i>12-13</i>
1928	ARAGON E.	-	6-8	8-12

6.2.2 Working stresses used in practice for train sheds

Original design reports of surviving train sheds have been gathered and design criteria used for the calculations compared with commonly recommended working stresses at the time of their construction. The working stresses used for the design of nine train sheds built between 1852 and 1931 were collected, either from original design reports preserved in the archives of SNCF (see Archival sources) or from articles of the periodical *Annales des Ponts et Chaussées* (Secrétariat de la commission des Annales, 1855; Sévène, 1871). This journal regularly published short technical and economic data as well as technical drawings regarding major structures such as train sheds. Tab. 6.2 presents the collected values of the working stress, or of the maximum calculated stress when the working stress was not explicitly indicated.

Fig. 6.2 graphically brings together the working stresses obtained from the literature and the values used for train shed designs. The bars show the lower and upper limit for the working stress proposed by various authors, while the dots indicate the working stresses used for specific train sheds. These charts highlight that the default working stress for iron stayed quite constant throughout its period of use, while the upper limit fluctuated, and that the working stress recommended for steel varied much more than for iron. They also reveal that the working stress values used for train sheds were mostly above the upper limit recommended in the literature.

Table 6.2 – List of train sheds for which working stresses were collected. *: maximum stress (working stress not explicitly indicated). APC: Annales des Ponts et Chaussées.

Year	Train shed	Contractor	Source	σ_{lim} (iron) [kg/mm ²]	σ_{lim} (steel) [kg/mm ²]
1852	Paris St-Lazare (hall Flachot)	Joly	APC, 1855	7.6*	-
1868	Bayonne	Rigolet	SNCF arch., 1868	9.53*	-
1869	Paris Austerlitz	Schneider	APC, 1871	6	-
1879	Hendaye	A. Moisant	SNCF arch., 1880	6	-
1892	Marseille St-Charles	Sénès et Arnal	SNCF arch., 1892	-	14.38*
1898	Bordeaux St-Jean	Daydé et Pillé	SNCF arch., 1896	-	13
1902	Bédarieux	Daydé et Pillé	SNCF arch., 1902	-	11
1908	St Germain des Fossés	<i>unknown</i>	SNCF arch., 1908	-	12.62*
1931	Paris Gare de l’Est	Schmid, Bruneton, Morin	SNCF arch., 1929	-	13

6.2.3 Discussion

The review of historical literature showed that authors of construction treatises or technical papers, who were often also professors in renowned engineering schools and practising engineers, recommended working stresses based either on experiments or on their practical knowledge. The limits varied among authors, according to the load assumptions, the type of structure, or the quality of the material, and regulations followed the global trend. When comparing these approaches with the design criteria used in practice for nine train sheds, it appears that overall, designers chose working stresses higher than recommended. So, not only was the safety concept in the 19th century different from the Eurocodes’, but the safety factors from this period cannot be directly related to objective characteristics of a structure. Thus, deducing a characteristic yield strength from a working stress in order to assess an existing structure according to the Eurocodes is a hazardous process.

However, historical design notes are not useless. An original design report can provide

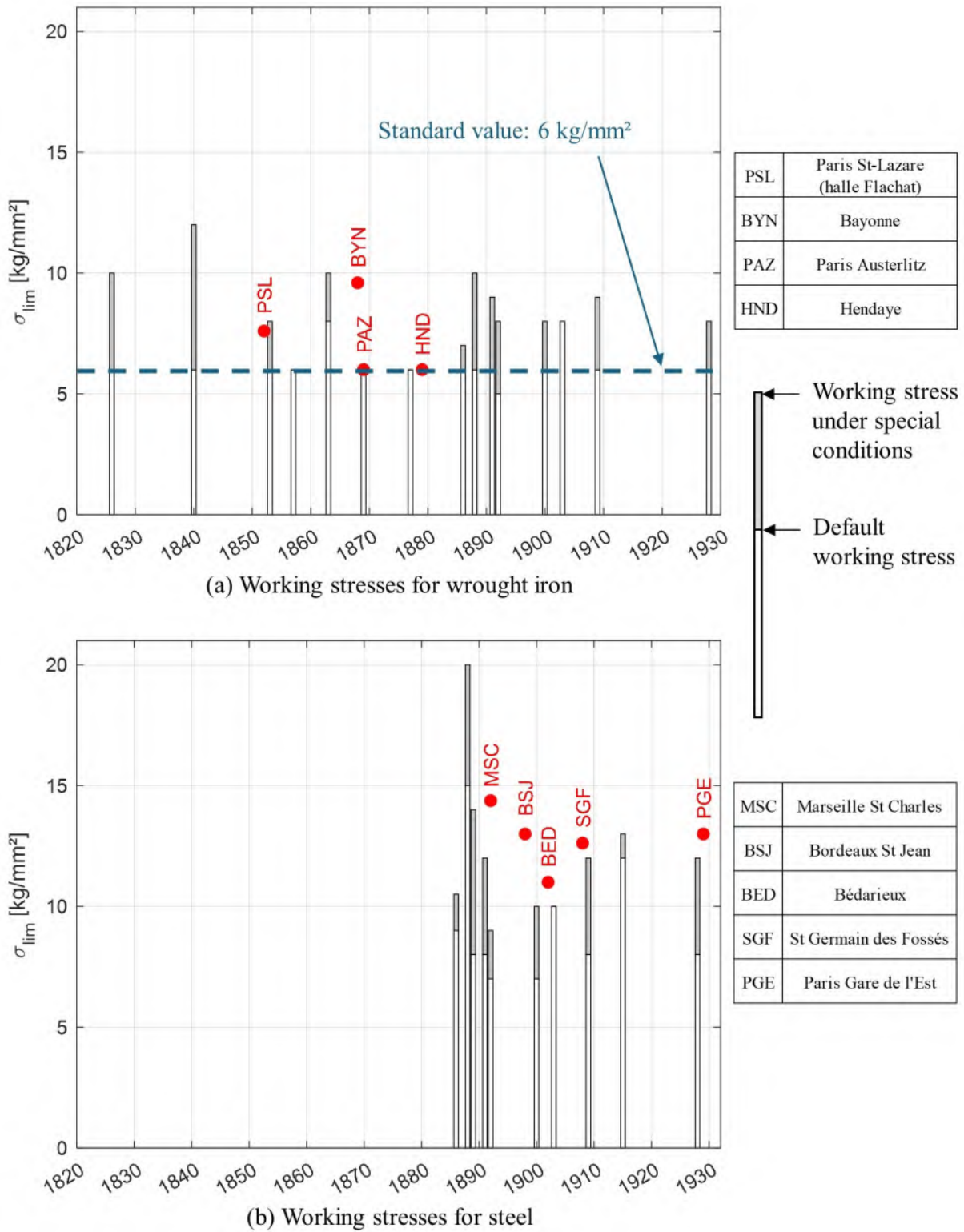


Figure 6.2 – Evolution of the working stresses recommended in the literature for (a) wrought iron and (b) steel between 1820 and 1930, compared with working stresses used for train sheds.

information on the elements which, *a priori*, have large load reserves or those which have been designed as accurately as possible. In addition, the comparison of the chosen working stress with the recommendations of the literature provides information about the quality of the used material. For example, in a design report drafted in 1892 for the train shed in Marseille St-Charles, some elements are designed with a stress of up to 14.38 kg/mm². This high value is well above the values recommended for mild steel in the literature and regulations of the time. This suggests that the steel used for this train shed was of superior quality and that its mechanical properties are, therefore, particularly good.

The presented debate among engineers regarding working stress values not only gives insight into the evolution of design criteria but also into the role of the designer within the design process. What is surprising is that, while most narratives of the history of structures see an increasing influence of mechanical models and design procedures throughout the 19th century, the design practice still relied on an engineer as an experienced individual making deliberate design decisions. This apparent duality of a growing science and determinism on one side and an explorative practice and individual engineering agency on the other is a fascinating aspect of that period. However, it is hardly compatible with our standardised engineering practice today. Therefore, to re-assess a structure, it seems more suitable to derive design values from standardised test results regarding material properties than to adapt them from historical design values.

6.3 Material sampling and characteristic values

6.3.1 Definition of characteristic values according to the Eurocodes

In the Eurocodes, structural design relies on the verification of limit states. A distinction is made between ultimate limit states (ULS) referring to the structural safety and serviceability limit states (SLS) affecting the functionality, appearance or user comfort. In the ultimate limit state STR concerning internal failure or excessive deformation of the structure, the design value of the effect of actions E_d shall not exceed the corresponding design resistance R_d (EN 1990, 2002, §6.4.2(3)). The design approach in the Eurocodes is semi-probabilistic. Material properties and loads are considered random variables with associated probability distributions, and partial safety factors are derived from probabilistic considerations. However, these factors are applied deterministically in design calculations.

In Eurocode 3 intended for the design of steel structures, the design resistance R_d of a cross-section or a structural member can be expressed as (EN 1993-1-1, 2005, §2.4.3):

$$R_d = \frac{R_k}{\gamma_M} \quad (6.2)$$

Where R_k is the characteristic value of the particular resistance and γ_M is the global partial factor for this particular resistance. R_k depends on the characteristic value X_k of the relevant material property, such as the yield strength. As a convention set by current standards, the measurements of the yield strength of steel correspond to the stress at 0.2% deformation under tensile stress. In all Eurocodes, by default, where a low value of material or product property is unfavourable, the characteristic value is defined as the 5% fractile value (EN 1990, 2002, §4.2(3)). Therefore, the nominal value of the yield strength f_y to be used in designing or assessing a steel structure based on Eurocode 3 is a characteristic value such that only 5% of material samples of the structure, if tested, may have a lower strength (Fig. 6.3). γ_M accounts for uncertainties in the resistance model and for unfavourable deviations of a material property from its characteristic value due, for example, to discrepancies between test results and the behaviour of the material in the structure. According to the French national annex of EN 1993-1-1, 2005, $\gamma_M = 1.0$ for the verification of the resistance of cross-sections and the buckling resistance of structural members.

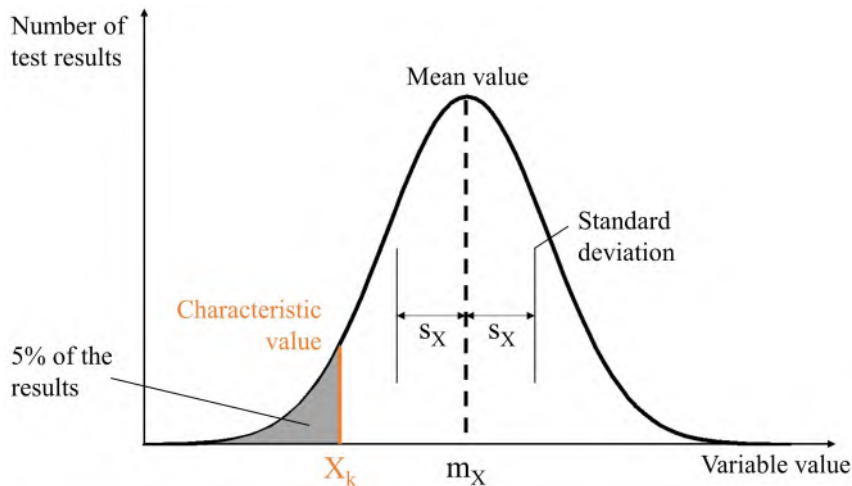


Figure 6.3 – Definition of the characteristic value after Eurocode 0 based on the probability distribution of the considered variable, determined from a certain number of tests.

Eurocode 0 provides (non-mandatory) guidance on how to derive a characteristic value from test results (EN 1990, 2002, Annex D.7.2). The characteristic value can be calculated from the following expression:

$$X_k = m_X (1 - k_n V_X) \quad (6.3)$$

Where m_X is the mean value obtained from the dataset, V_X is the coefficient of variation, and k_n is a coefficient provided by (EN 1990, 2002, Tab. D1), assuming a normal distribution. k_n depends on the number n of performed tests and on whether V_X is known from prior knowledge or not. When V_x is unknown, then it can be estimated from the sample

as $V_X = s_X/m_X$, where s_X is the standard deviation.

6.3.2 Test results from the literature

The tensile test has always been regarded as the standard test to ensure the quality of steel and other metals and thus to guarantee the safety of steel structures (Brandes, 2008). Timoshenko, 1953 gave a historical overview of experimental studies conducted in the 19th century on mechanical properties of materials, such as the ultimate or the yield strength. However, it is difficult to take advantage of test results obtained in this period because material properties depend on the specimen shape and the test conditions. In the Eurocodes, the safety factor γ_M and the definition of the characteristic value correspond to standardised tests performed under specified conditions (EN 1990, 2002, §4.2(4)). It is, therefore, not easy to deduce a value from information in old documents that corresponds to today's test results (Brandes, 2008). Moreover, the nomenclature of materials tested in the 19th century is ambiguous, so historical test results cannot always be clearly attributed to iron and steel types as we understand them today. Finally, inadequate recording and the repetition of results in different sources without giving full credit makes it difficult to compare the tests or to analyse them statistically (Bussell, 2014, p. 68). As a consequence, it has been common practice to take samples from existing iron and steel structures to carry out tensile tests in accordance with the standards.

An effort has been made by researchers and some guideline authorities to collect data from tensile tests carried out on various metal structures and analyse them to derive meaningful characteristic values of material properties. Regarding wrought iron, the British standards BD21 “Assessment of Highway Bridges and Structures” edited in 1984 compiled over 500 tests carried out on bridge samples and analysed by the British railways. They consequently recommended a characteristic yield strength $f_y = 220$ MPa for wrought iron (Bussell, 2014, p. 74). In 2008, the Joint Research Centre (JRC) of the European Commission published a report on the assessment of existing steel constructions, focusing on the fatigue of old bridges. Based on test results from the literature, corresponding to the properties of specimens from riveted bridges, they derived a characteristic yield strength $f_y = 203$ MPa at +10°C (Kühn et al., 2008, p. 31). Moy et al., 2009 merged the results from tensile tests carried out on samples from almost 30 wrought iron bridges in the United Kingdom. From their dataset of 329 tensile tests, they calculated characteristic values for material properties using the formula given in British Standard BS2846-3 “Guide to statistical interpretation of data”, 1975. The study of Moy et al., 2009 yields a characteristic value of the yield strength along the grain $f_y = 198$ MPa. O’Sullivan, 2013 also compiled the results from 550 tensile tests on wrought iron specimens, relying partly on the same database as Moy et al., 2009 and partly on his own

testing campaign, dealing with bridge samples as well. Compared to Moy et al., 2009, this study enhanced that different structural component types possess different characteristic material properties. The distinction was made between plate iron, square and round bars, angles and tees, bolts and rivets, and rolled beams. For lattice girders, the category “angles and tees” is the most relevant, as such profiles were used for the chords. The available tensile test data for angles and tees yielded a characteristic yield strength $f_y = 200$ MPa (O’Sullivan, 2013, p. 161).

Recent testing campaigns compared the strength of wrought iron samples along the grain (i.e. in the rolling direction) and across the grain (Gallegos Mayorga, 2016; O’Sullivan, 2013) and showed that the yield strength and the ultimate strength are about 15% lower across the grain. However, for assessing lattice girders, the yield strength along the grain is the only one of interest, as rolled profiles were produced with the grain of the material in their longitudinal direction.

Regarding mild steel, the British standards BD21 “Assessment of Highway Bridges and Structures” edited in 1984 recommends $f_y = 230$ MPa for pre-1955 steel (Bussell, 2014, p. 73). The 2008 report from the JRC confirms this value (Kühn et al., 2008, p. 31). Brandes, 2008 also mentions a large testing campaign of more than 900 tests carried out in Leipzig, Germany, in 2000, on samples of wrought-iron and mild-steel constructions from 1840-1938. The available information about this data is, however, incomplete.

Overall, the literature suggests characteristic values of the yield strength $f_y = 200$ MPa for wrought iron (220 MPa in some sources) and $f_y = 230$ MPa for mild steel. These values should be treated with caution, however, as they cover materials produced over a long period of time, and correspond only to bridge samples.

6.3.3 Test results from train shed samples

Since 2005, samples have been taken from the metal structure of French train sheds in more than twenty railway stations in order to assess the nature and the properties of the materials. Material sampling was carried out in the framework of the general survey of train sheds prior to their restoration. In general, the survey of old metal structures aims to describe the health of the structure, in particular the degree of corrosion, to study the paint systems with a view to stripping them, and to characterise the materials (Memet et al., 2021). Material sampling allowed, first of all, to determine or confirm the nature of the materials by chemical analysis, which gives the content of chemical elements (iron, phosphorus, etc.) and metallographic analysis, which reveals the microstructure of the samples (Fig. 6.1). Mechanical properties were determined from tensile tests. Indeed, most material surveys of train sheds involved only one to three tensile tests, but for large train sheds, especially in Paris, a larger number of tests on up to ten samples were carried

out. Test results providing measurements of the yield strength f_y , the ultimate tensile strength f_u and the ultimate elongation A have been gathered and are presented in Tab. 6.4 (mild-steel specimens) and Tab. 6.5 (wrought-iron specimens). In total, the dataset contains yield strength measurements from 28 wrought-iron samples and 40 mild-steel samples. As some of the data is incomplete, the number of ultimate strength and ultimate elongation measurements is slightly lower. Fig. 6.4 shows graphically the distribution of values for yield strength, tensile strength and ultimate elongation, according to the date of construction of the sampled train shed.

Firstly, it appears that wrought iron was the predominant material until around 1880, when mild steel started taking over. There was a period of overlap in the use of the two materials until the end of the 19th century. The results also reflect the extreme dispersion in mechanical properties, both from one structure to another and within the same structure. This is highlighted, for example, by the results obtained from 12 samples taken from the roof structure of two halls built in 1931 at Gare de l'Est in Paris. Finally, mild steel does not appear to have significantly better properties than wrought iron in terms of strength. In contrast, the improvement in ductility, embodied by the ultimate elongation, is quite clear.

Statistical analysis

The extent of the dataset made it statistically relevant to derive a characteristic value of the yield strength for wrought iron and mild steel using EN 1990, 2002, Annex D.7.2 and Eq. (6.3). V_X is supposed unknown. The analysis yields characteristic values $f_y = 213$ MPa for wrought iron and $f_y = 225$ MPa for mild steel (Tab. 6.3). These values are in good agreement with the characteristic values derived from bridge samples in the literature. What's more, the coefficients of variation V_X also correspond to the ones from Moy et al., 2009 for wrought iron ($V_X = 0.12$) and Brandes, 2008 for mild steel ($V_X = 0.15$).

Table 6.3 – Calculation of the characteristic value of the **yield strength** for wrought iron and mild steel, based on material sampling from train sheds, using EN 1990, 2002, Annex D.7.2.

	Wrought iron	Mild steel
Number of tests n	28	40
Mean m_X [MPa]	269	297
Standard deviation s_X [MPa]	33	42
Coefficient of variation V_X	0.12	0.14
k_n	1.73	1.73
Characteristic value X_k [MPa]	213	225

Table 6.4 – Test results from *mild-steel* specimens taken from French train sheds (n.a.: not available).

Railway station	Train shed	Number of tests	f_y [MPa]	f_u [MPa]	A [%]
Angoulême	-	2	294	391	32.3
			291	366	30.3
Bordeaux St-Jean	-	5	314	396	36
			n.a.	264	21
			255	327	14
			299	413	31
			223	354	44
Evian	-	2	242	356	36
			323	446	31
La Rochelle	-	1	322	393	35
Marseille St-Charles	-	1	255	377	29
Montauban	-	1	296	n.a.	n.a.
Paris Lyon	Hall 1 (GHV)	1	257	363	30
Paris Lyon	Hall 1 (Halle du Train Bleu)	2	306	421	25
			292	385	35
Paris Est	Quai transversal	8	303	390	33
			407	482	22
			297	386	30
			316	372	34
			306	401	31
			374	433	28
			320	407	29
			412	439	28
Paris Est	Hall Saint-Martin	4	342	459	31
			315	418	30
			286	415	28
			240	370	35
Paris St-Lazare	Halle 1	10	250	355	18.7
	Halle 1		234	354	29.1
	Halle 2N		243	350	15.2
	Halle 2N		284	375	19.2
	Halle 3N		302	404	28.8
	Halle 3N		282	376	9.8
	Halle 4N		332	410	17
	Halle 4N		272	356	35.3
	Halle 5N		316	363	31.6
	Halle 5N		329	418	30.1
Tulle	-	3	269	n.a.	n.a.
			281	n.a.	n.a.
			276	n.a.	n.a.
Perpignan	-	1	334	393	35

Table 6.5 – Test results from *wrought-iron* specimens taken from French train sheds.

Railway station	Train shed	Number of tests	f_y [MPa]	f_u [MPa]	A [%]
Agen	-	2	248	349	14
			285	399	17
Bayonne	-	1	309	408	18
Béziers	-	2	261	376	30
			236	365	27
Hendaye	-	1	255	370	23
Lyon Perrache	Grande halle	1	257	352	12
Paris Austerlitz	Grande halle	7	268	365	13
			244	343	12
			230	329	16
			272	379	14
			281	352	10
			261	378	14
			245	366	27
Paris Est	Hall d'Alsace	4	399	438	2
			253	388	24
			299	409	11
			256	367	19
Paris Lyon	Hall 1 (GHV)	3	226	300	8
			293	424	20
			254	374	24
Pau	-	1	287	343	10
Perpignan	-	4	255	344	39
			259	323	7
			273	379	14
			263	353	20
Tours	-	2	280	393	15
			291	404	19

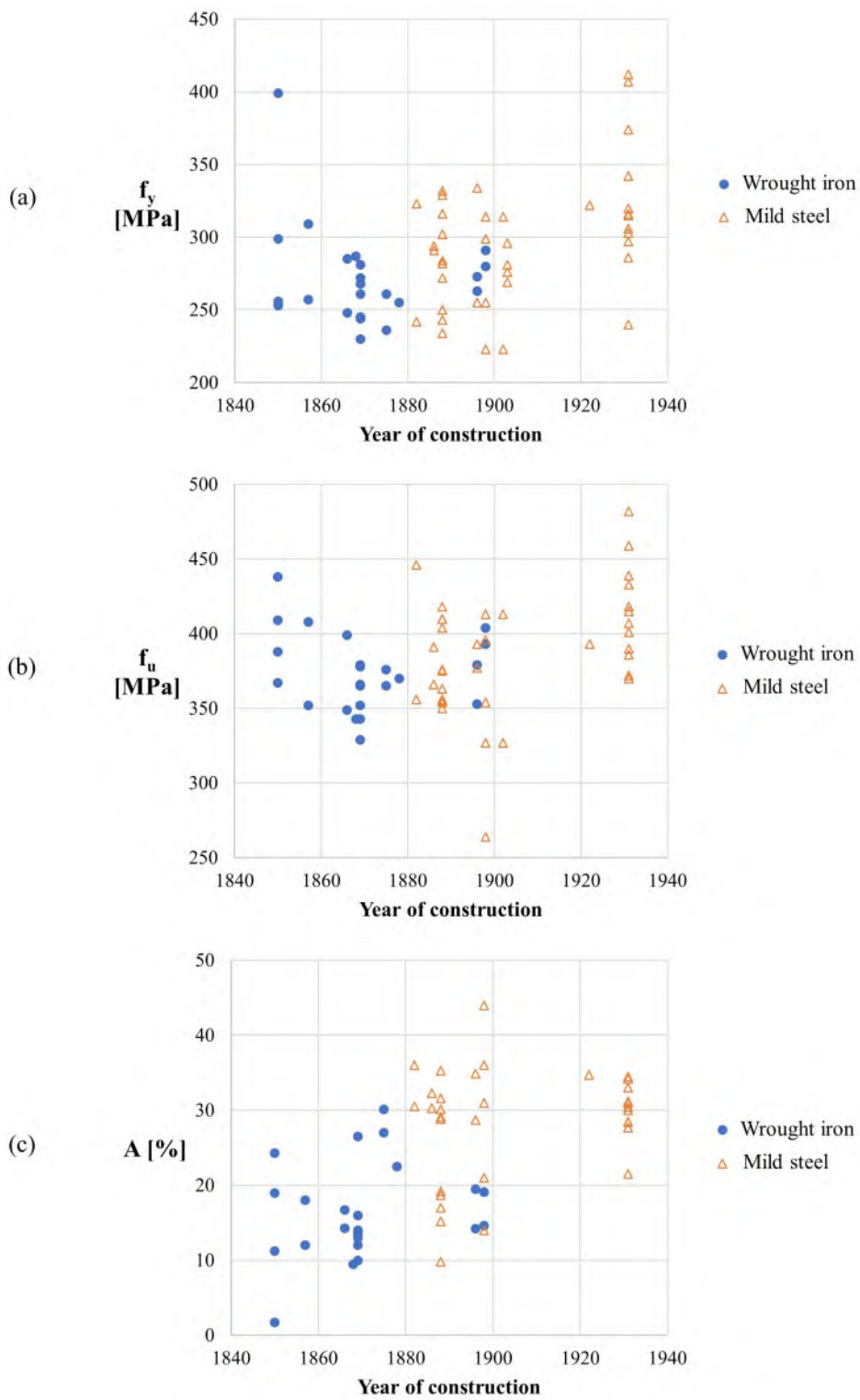


Figure 6.4 – Results of tensile tests on train shed samples as a function of their year of construction: (a) yield strength f_y ; (b) ultimate tensile strength f_u ; (c) ultimate elongation A .

Adopted strategy for design

In practice, when an engineer receives the results of tensile tests carried out on samples of the existing structure to be assessed, nominal values of the yield strength are rarely derived using statistical calculations. The survey of assessment reports related to the train shed restorations since 2005 showed that two approaches prevail. In some cases, the nominal yield strength is taken as the lowest value from the sample test results. This might seem conservative, but it is not, as the characteristic value shall correspond to the 5% fractile. When the lowest value from 2 or 3 tests is selected, there is a high chance that all test results are actually above the 5% fractile. In most cases, however, engineers simply consider that the test results are in agreement with the predicted behaviour from modern S235 steel and accordingly assign $f_y = 235$ MPa. This, for sure, is not conservative, because the characteristic yield strength of S235 is higher than the characteristic values of wrought iron and mild steel obtained both from the literature and the statistical analysis of test results from train shed samples.

6.3.4 Discussion

Because of the knowledge that wrought iron and mild steel feature variable material properties, it is common practice to carry out material sampling on existing metal structures in order to obtain structure-specific or even member-specific data. However, due to its destructive nature, material sampling affects the integrity of the structure, which may locally weaken it and also harm its authenticity. The usefulness of material testing is therefore open to debate.

The current Eurocodes clearly set boundary conditions for the determination of characteristic values. When only a few tests are performed, which is the case for train sheds, a statistical interpretation is possible only by using extensive prior information (EN 1990, 2002, Annex D6). As the next generation of Eurocodes shall become more tailored to assessing existing structures, the technical specification XP CEN/TS 17440, 2020 “Assessment and retrofitting of existing structures” supplies more detailed provisions on how to supplement the available prior information with new results, i.e. how to update data. Prior information corresponds to known statistical parameters describing the distribution of basic variables derived from a population of comparable structures (XP CEN/TS 17440, 2020, §7.1(5)). Given an available prior probability distribution and statistical data from new observations, posterior “updated” distributions can be derived, e.g. by applying a Bayesian method (Tanner, 2021). Brandes, 2008 suggests more specifically determining the mean value of the updated distribution based on the structure-specific data and the standard deviation from the available prior distribution.

However, the use of updated data has practical limitations. First, even when combining sample test results with prior information, the sample size shall provide a statistically significant and representative basis for updating parameters (XP CEN/TS 17440, 2020, §7.1(5)). So, again, when only 2 or 3 samples are tested like for most train sheds, they do not provide enough information to update prior probability distributions. Second, the notion of “comparable structures” is very much open to interpretation and makes it difficult to select appropriate prior information. Most of the available data concerns metal bridges. The distinction between wrought iron and mild steel bridges may not be fine enough to obtain meaningful homogeneous statistical populations. If it is, can the probability distributions derived from literature be used for structures other than bridges? The analysis of train shed samples suggests that the metals used for those structures are of similar quality to bridges. This may be due to the fact that train sheds were also prestigious and strategic constructions. However, clear criteria regarding relevant prior information for updating data are missing. Finally, like in the 19th century, there is a gap between theory and practice. The mathematical procedures to update data may be familiar to some researchers, but, in practice, structural engineers are not trained to use the results of material tests correctly.

For all these reasons, it might be more advisable to directly use characteristic values recommended by the literature for wrought iron and mild steel. Regarding bridges, the JRC report clearly states that a sufficiently large database is already available and that material tests should be carried out only in the rare cases where the statistical values available for the material in question lead to results that are too conservative (Kühn et al., 2008, p. 28). The 1984 edition of the British standard BD21 “Assessment of Highway Bridges and Structures” also warned that sampling of material from a particular structure will not necessarily give a more reliable estimate of strength than the prescribed value, due to the inherent variability of the materials and the limitations of statistical interpretations when using only a small number of samples (Bussell, 2014, p. 74). This argument applies also to structures other than bridges.

Brandes, 2008 argue that the results of few tensile tests are rather intended to give an impression of whether any special features are to be expected. Tensile test results could then be of similar use to working stresses obtained from historical archives: they may indicate whether the material of the assessed structure is of particularly good or bad quality. However, the gain in information does not appear to be significant in relation to the damage caused to the structure. Some alternatives have been proposed to measure material properties without deteriorating the structure. Material testing methods have been developed to carry out tensile tests using very small specimens, which limits the impact on the structure (van Es et al., 2023). Those testing procedures still need to

be standardised. As an alternative to tensile tests, hardness tests have the advantage of being non-destructive and easy, so a large number of measurements can be carried out on a given structure. Hardness values can be empirically correlated with the material's strength properties but the results of the conversion are not reliable enough (Brandes, 2008). So, for now, standardised tensile tests seem the only practical option when material testing is deemed necessary. However, relying on knowledge from the literature, material testing can often be avoided.

6.4 Conclusion

When an existing iron or steel structure needs to be assessed, the definition of appropriate design values of material properties is essential to determine the load-bearing capacity of the structure in accordance with our current standards. As the Eurocodes do not provide nominal values for the yield or the ultimate strength for wrought iron and mild steel, it is up to structural engineers to select meaningful values. Because wrought iron and mild steel are known to have variable properties, it is tempting to derive design values from structure-specific data, that is either from original design reports related to the structure or from material sampling. However, the comparison of historical and recent literature with data about historical working stresses and material test results for train sheds showed that structure-specific data does not necessarily convey usable information. Working stresses cannot be used for verification in accordance with the Eurocode because the safety concepts have evolved too much. Test results often lack statistical significance. As a consequence, the best practical approach, for now, seems to rely on recent literature to obtain characteristic values of yield strength, typically $f_y = 200$ MPa for wrought iron and $f_y = 230$ MPa for mild steel. The upcoming generation of Eurocodes will explicitly apply to the assessment of existing structures. The standardisation of data updating procedures, combined with the development of alternative test methods, will hopefully help improve the practice of material sampling and refine the information available on wrought iron and mild steel.

Design values of material properties are useful to check both the resistance of cross-sections and the buckling resistance of structural members. The next chapter focuses specifically on assessing the buckling risk, which is responsible for most strengthening measures of riveted lattice girders.

ASSESSING THE BUCKLING RISK

Chapter 7 compares how the buckling risk of iron and steel members was originally taken into account in the design of metal constructions, especially train sheds, and how it is assessed today in accordance with Eurocode 3. The various approaches are compared using a case study.



Lattice purlin with buckled web members in the train shed of the railway station of Le Havre, France (Picture from SNCF-AREP).

Contents

7.1	Historical design against buckling	156
7.2	Assessment of the buckling risk according to Eurocode 3	164
7.3	Discussion based on the case study	170
7.4	Conclusion	178

When reviewing assessment reports of historic metallic train sheds, buckling stands out as the main reason for failed design checks. The prediction of the out-of-plane buckling risk for riveted lattice girders (see Fig. 4 in the introduction chapter) was responsible for most strengthening measures carried out in recent train shed restorations. This is due to the fact that riveted lattice girders, like many components of historic metal structures, feature individual members with relatively high slenderness. At low slenderness, the load-carrying capacity of iron or steel members is governed by their cross-sectional resistance. With increasing slenderness, buckling becomes decisive. However, the buckling design resistance of a compression member depends on modelling assumptions and design criteria. In the recent assessment reports of metallic train sheds, the buckling risk of riveted lattice girders was estimated by checking members individually after first-order analysis, using the standard procedures proposed in EN 1993-1-1, 2005 and assuming conservative buckling lengths. The picture on the cover page of this chapter features a lattice purlin from a French train shed, with buckled web members. This case is actually an exception. Routine visual inspections carried out by SNCF on train sheds rarely evidence excessive deformations. Strengthening measures against buckling are, therefore, always preventive - but are they necessary? This chapter aims to critically discuss the buckling risk for lattice girders. The chapter first gives insight into how buckling was taken into account in the original design. This historical study has been published in a conference paper (Franz et al., 2022a). Then, the chapter examines how buckling can be assessed today in accordance with EN 1993-1-1, 2005. Finally, the various approaches and associated modelling assumptions are compared using the case study of a lattice purlin in the train shed of Montauban, whose behaviour was already investigated in Chapter 3.

7.1 Historical design against buckling

7.1.1 *Evolution of the state of knowledge on buckling*

The first studies on the buckling of compressed members date back to the 18th century. Originally, compressed members were referred to more restrictively as “columns”, columns being the structural components typically subjected to axial compression forces. Around 1730, Van Musschenbroeck carried out experiments from which he concluded that the resistance of a column did not only depend on the material, but also on its geometry. In 1744, Euler developed an analytical formulation of the “critical” load that a column with pinned ends could admit without bending (Nowak, 1981, pp. 6–10):

$$N_{cr} = \pi^2 \frac{EI}{L^2} \tag{7.1}$$

Where L is the length of the column and EI is its bending stiffness. The term EI was broken down only later into the elastic modulus E of the material, as defined by Young in 1807, and the moment of inertia of the cross-section I , correctly formulated by Coulomb in 1773. In 1820, Duleau derived the critical load for compressed members with different boundary conditions - free, pinned or fixed (Nowak, 1981, pp. 22–24). Eq. (7.1) becomes:

$$N_{cr} = \pi^2 \frac{EI}{L_{cr}^2} \quad (7.2)$$

Where L_{cr} is the so-called “effective” length, which depends on the boundary conditions of the compressed member. When the member has pinned ends, the effective length L_{cr} is equal to the system length L . When the same member has fixed ends, the effective length is half the system length. The deformed shapes of compressed members due to buckling in some of the standard cases examined by Duleau, well-known today as Euler cases, are displayed in Fig. 7.1. The effective length can be grasped as the length the column would have to be if it were to buckle as a pinned-pinned column.

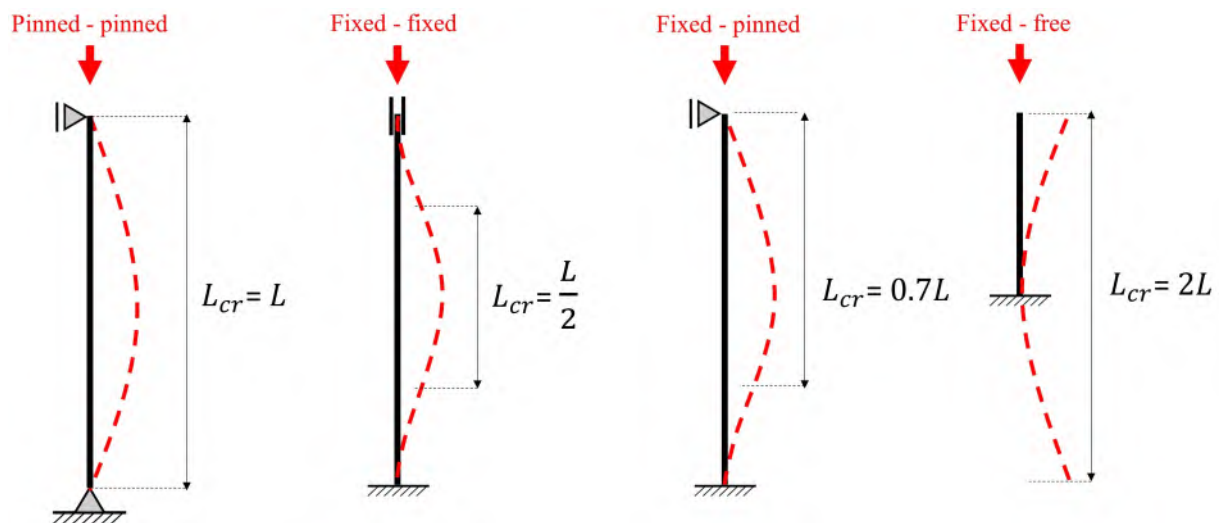


Figure 7.1 – Influence of the end conditions of a compressed member on its buckling shape and effective length.

Euler’s formula was a major contribution to the understanding of buckling. However, further experiments, such as Hodgkinson’s in 1840, showed that instabilities occurred for compressive loads much lower than the critical load calculated by Euler. The idealised assumptions behind Euler’s theory were unravelled progressively. Firstly, Euler assumed that bars were perfectly straight, with a load applied in a perfectly centred manner. The influence of geometrical imperfections (eccentricity of the load or initial curvature) was described only at the beginning of the 19th century, for example by Young in 1807 and Navier in 1826. Secondly, Euler’s formula necessitated bars to remain elastic. In 1826, Navier defined ranges of slenderness for which Euler’s formula was valid, but Lamarle

was the first in 1845 to link this validity domain to the yield strength. The first theories of inelastic buckling were proposed by Engesser and Considère in 1889. Finally, Euler’s theory was valid only for a homogeneous material. The fluctuation of the strength within the section, as well as the residual stresses, were accounted for from the 1950s onwards (Nowak, 1981, pp. 21–25, 84, 144–148, 291–300).

Based on Eq. (7.2), the “critical” stress σ_{cr} a compressed member can experience without buckling writes:

$$\sigma_{cr} = \frac{\pi^2 E}{\left(\frac{L_{cr}}{r}\right)^2} = \frac{\pi^2 E}{\lambda^2} \quad (7.3)$$

Where $r = \sqrt{I/A}$ is the radius of gyration, depending on the moment of inertia I and the section A of the bar, and $\lambda = L_{cr}/r$ is the slenderness. As an alternative to Eq. (7.3), many authors strived to propose an estimate of the stress limit before buckling that would be more in line with experimental data. Instead of defining the equilibrium like Euler, they conceptualised the maximum axial stress of a compressed member as a combination of compression and bending. The bending stress was derived by assuming geometrical imperfections or by assimilating it to a stress due to the critical load. The resulting formula yielded:

$$\sigma_{lim} = \frac{a}{1 + b\lambda^2} \quad (7.4)$$

Where λ is the slenderness, and a and b are constants, whose values could vary depending on ranges of slenderness. The first author to give such a formula was Tredgold in 1822. In the 1850s, several authors such as Schwarz, Gordon and Rankine proposed different approaches leading to a similar result. This formula was convenient to use and became very popular in the following decades, known mostly as Rankine’s formula (Nowak, 1981, pp. 71–98). Usually, the coefficient a at the numerator corresponds to the working stress used for designing cross-sections or elements in tension.

Euler’s formula was rehabilitated in the 1880s, thanks to the experiments of Bauschinger and Tetmajer in Germany and Considère in France. They proved Euler’s theory right for very slender elements when the experimental setup accurately reflected theoretical boundary conditions. Tetmajer proposed abandoning the unification of all results into a single formula, as Rankine’s formula attempted to do. For intermediate slenderness values, Tetmajer described the maximum stress as a function of slenderness using a straight line, which became widely used in German-speaking countries (Nowak, 1981, pp. 106–127).

7.1.2 Design criteria against buckling in France

As theoretical and empirical approaches regarding buckling were very diverse, the buckling design criteria recommended in construction handbooks varied accordingly. In France, the first reference on which designers probably relied for their design of iron columns is Navier's *Résumé des Leçons* from 1826. For large slenderness values, Navier recommended using Euler's formula with a safety factor of 4 to 5. For smaller slenderness values, he gave isolated experimental stresses (Navier, 1833, pp. 259–160). In 1840, Ardant indicated working stresses for some individual slenderness values, not associated with any formula (Ardant, 1840, p. 103). In 1851, Love submitted a memorandum to the French Society of Civil engineers in which he presented the experiments of Tredgold and Hodgkinson. Based on those experiments, he proposed a Rankine-type formula, which, according to Buchetti in 1888, became prevalent in France until the end of the 19th century. Love did not recommend any safety factor but Buchetti indicated that Love's formula was to be reduced by a safety factor of 6 (Love, 1851; Buchetti, 1888, pp. 210–216). The first bridge regulations from 1869 and 1877 did not mention buckling. They recommended a working stress of 6 kg/mm² for iron, both in tension and in compression. At the end of the 1880s, several authors such as Flamand and Résal proposed Rankine-type formulas with different constants (Flamand, 1886, pp. 443–445; Résal, 1892, pp. 507–511). Brune preferred the use of Euler's formula with a reduced modulus of elasticity $E = 80$ GPa instead of 210 GPa (Brune, 1888, pp. 183–197). The 1891 bridge regulation was the first to require that “elements in compression be not exposed to buckling” but it did not indicate any method on how to ensure it (Résal, 1892, p. 530). The same line was adopted by the 1902 train shed regulation. In 1915, the new regulation for bridges finally favoured a Rankine-type formula but it stayed quite vague, as it left engineers free to decide which constants to use (Résal, 1917, pp. 210–211).

To help visualise the discrepancies between the empirical formulas proposed by different authors, the formulas of each author were all converted to the same format $\sigma_{\text{lim}} = f(\lambda)$, where σ_{lim} is the working stress for a compressed member, including the safety factor, and λ is the slenderness derived from the buckling length of the member, depending on its boundary conditions and the geometry of the cross section. This format allows to gather formulas derived from various experiments, on bars with different cross section types and boundary conditions. Fig. 7.2 thus displays the working stress σ_{lim} proposed by several authors for elements working in compression, as a function of their slenderness λ . The legend indicates whether the analytical representation of working stresses for each author was derived from Euler's formula (Eq. (7.3)) or from Rankine's formula (Eq. (7.4)).

contractor pointed out that the maximum stress had been kept “voluntarily low”.

For diagonal members in trusses, some authors argued that constructive measures were enough to ensure buckling safety. Collignon and Brune declared that truss diagonals were not exposed to buckling thanks to their clamped riveted connections (Collignon, 1869, p. 563; Brune, 1888, p. 222). For elements in compression, other than columns, Novat recommended cross-sections shaped like an X, a T, a U or an L to avoid buckling (Novat, 1900, p. 241).

Lattice girders used in train sheds for purlins or rafters also provide examples of constructive solutions. In some train sheds, one can observe differentiated cross-sections between truss bars in compression and in tension. For example, in the ridge purlin truss of Gare d’Etampes, the diagonals in tension feature flat sections while the vertical bars in compression have a double L section (Fig. 7.3a). As a common strategy to resist buckling, bars in compression were given a larger inertia than the bars in tension.

In lattice girders with diagonals crossing each other, diagonals pointing upwards from the supports towards the centre of the beam usually work in compression while the diagonals pointing downwards work in tension. Compression diagonals therefore have a larger cross-section. In the purlins of Gare de Montauban, compression diagonals consist of a double layer of flat plates while the tension diagonals only feature single flat plates (Fig. 7.3b). In the lower purlins of Hall St-Etienne in Gare de Lyon-Perrache, the compression diagonals close to the supports are reinforced by additional riveted plates (Fig. 7.3c). Moreover, the intersection with tension diagonals provides another local stabilisation measure.

However, as the compressed web members were not formally verified against buckling by calculations, it is understandable that these elements are problematic in a new assessment of the structure with current design methods. Next to the buckling of compressed web members, the out-of-plane buckling of the compressed chord is also a decisive failure mechanism of lattice girders which was not considered at all in the original design. The lateral-torsional buckling of beams, which was long understood as due to the buckling of the compressed flange, was studied intensively only from the 1930s (Werner et al., 1992, p. 55).

7.1.4 Efficiency of lattice vs. solid-web girders

The previous sections have highlighted the gaps in the understanding of the flexural buckling of compressed elements and its lack of consideration in calculations until the 20th century. However, engineers were at least aware of this failure mechanism and took it into account in their design, if only through constructive measures and practical know-how. In the meantime, another buckling phenomenon, namely shear buckling, remained well

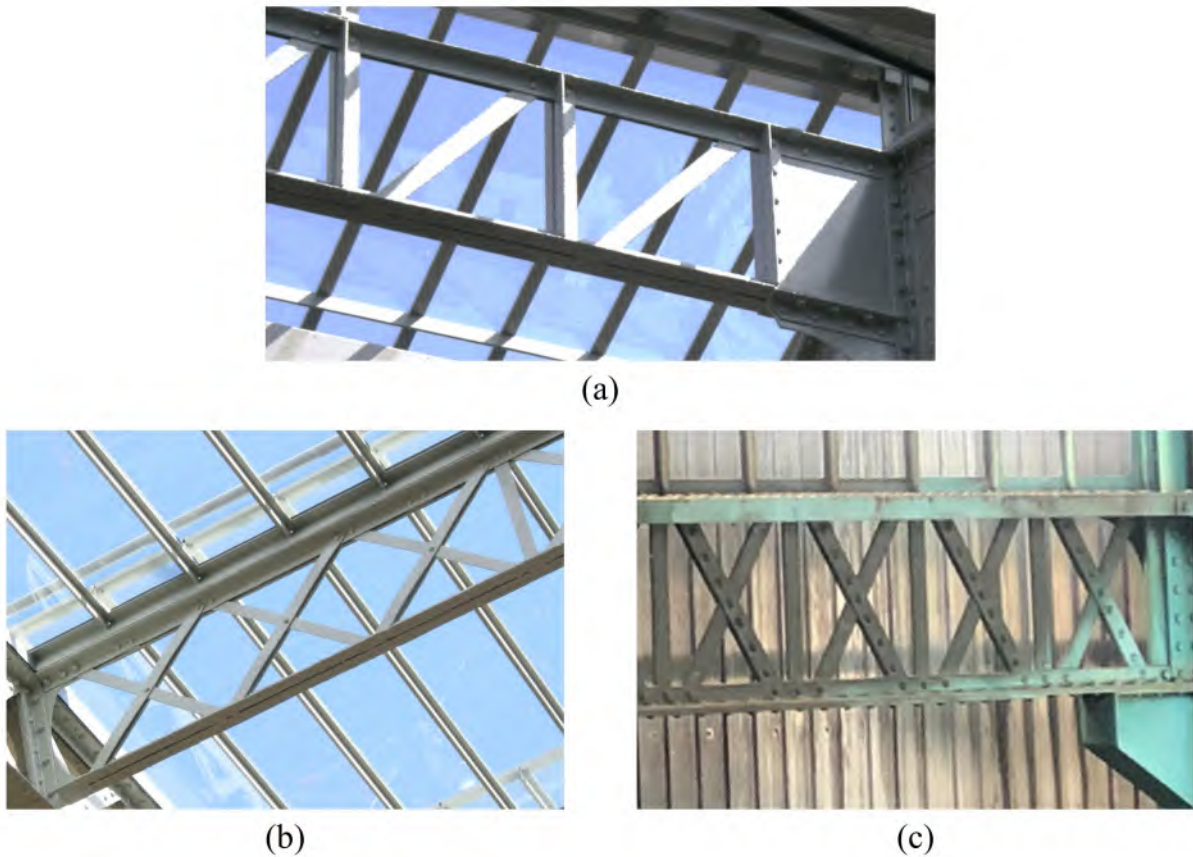


Figure 7.3 – Compressed web members exhibiting stiffer cross sections than tensioned web members: (a) Gare d'Etampes, Etampes, France; (b) Gare de Montauban, Montauban, France; (c) Gare de Lyon Perrache, Lyon, France. (Pictures from SNCF-AREP).

outside the scope of designers' concerns, which led to some misconceptions regarding the advantages and drawbacks of lattice vs. solid-web girders. Shear buckling is responsible for the instabilities of plates, typically web plates of solid-web girders. This section will show that the ignorance of this phenomenon could be one of the main reasons why lattice girders were said to be favoured by designers for their aesthetics (see Section 1.4), despite their lack of efficiency when compared to solid-web girders. Several authors indeed argued that the volume of a lattice web was at least twice the volume of a solid web (Collignon, 1864, pp. 157–158; Brune, 1888, pp. 224–225). If this were true, a lattice girder would use much more material than a solid-web girder with the same load-bearing capacity and thus come at a greater cost. The proof was as follows.

In a lattice girder, the optimised section of the diagonals is such that $\sigma_w = \sigma_{\text{lim}}$ where σ_w is the maximum calculated stress in the diagonals and σ_{lim} is the working stress. Considering a portion dx of a lattice girder, with diagonals inclined by an angle α to the horizontal, the length of the diagonal segments equals $dx/\cos \alpha$, so that their volume writes:

$$\mathcal{V}_w^{\text{lattice}} = 2A_w \frac{dx}{\cos \alpha} = \frac{V_{\text{max}}}{\sigma_{\text{lim}} \sin \alpha} \frac{dx}{\cos \alpha} = 2 \frac{V_{\text{max}}}{\sigma_{\text{lim}}} \frac{dx}{\sin 2\alpha} \quad (7.5)$$

Where A_w is the cross-section of the diagonals and V_{\max} is the maximum shear force in the lattice girder (see Eq. (3.2)). Considering a portion dx of the same girder, but replacing the lattice web with a solid web, optimised so that the stress in the web plate is also $\sigma_w = \sigma_{\lim}$, the volume of the web plate writes:

$$\mathcal{V}_w^{\text{solid}} = \frac{V_{\max}}{\sigma_{\lim}} dx \quad (7.6)$$

Consequently, in the most favourable configuration, where the diagonals are inclined by 45° , the volume of the lattice web is twice the volume of a solid web. This demonstration yields a result that feels counter-intuitive because it contains two main errors.

The first error is to assume that the resistance of the diagonals, working in tension or compression, is the same as the resistance of the solid web plate working in shear. Some authors acknowledged this misconception around the turn of the 20th century. For example, Novat recognised that the shear resistance τ_{\lim} was lower than the resistance in tension σ_{\lim} by a ratio of 0.8, which led him to conclude that a lattice web would rather use 1.6 times more material than a solid web (Novat, 1900, p. 243). The proposed ratio of 0.8 is still higher than what is recommended today in Eurocode 3, where the computation of the shear resistance involves dividing the limit of elasticity by $\sqrt{3}$ (EN 1993-1-1, 2005, §6.2.6(2)). This corresponds to a ratio of 0.58. The ratio of volume of the lattice web compared to the volume of the solid web would then drop to 1.15.

The second error is to disregard the shear buckling phenomenon for the solid web. Again, bridge designers were aware of stability problems related to thin-walled structures. As early as 1850, the design team of the Britannia wrought-iron tubular bridge used web stiffeners to prevent buckling. However, unlike for the buckling of compressed bars, a sound theoretical basis was lacking until Timoshenko's analytical study on the shear buckling of isotropic rectangular plates in 1907 (Zureick, 2023). Shear buckling remained completely out of scope in construction handbooks in the 19th and beginning of the 20th century. Consequently, the optimisation of a solid web could lead to a plate thickness that would be unacceptable according to our current standards. In the case of the lattice purlin of Montauban, with a lattice web constituted of 50 mm x 6 mm flat diagonals, a solid web having the same volume as the lattice web would have a thickness of 1.3 mm. The resulting ratio h_w/t_w (height over thickness) is then worth 483, way above the limit of 72 recommended by Eurocode 3 to avoid shear stiffeners (EN 1993-1-1, 2005, §6.2.6(2)).

The erroneous statement, echoed by several engineers, that a lattice web is at least twice the volume of an equivalent solid web, underlined that lattice girders were used *despite* their efficiency. The discussion showed that their use instead of solid-web girders, which was almost a matter of taste, was actually also a sound choice from the structural

point of view. This is in line with our perception today that trusses are rather efficient and economical structures. Nevertheless, the buckling safety of lattice girders, when assessed using our current methods, is often considered insufficient. To minimise retrofitting operations, it is necessary to examine the different approaches and assumptions leading to such an assessment.

7.2 Assessment of the buckling risk according to Eurocode 3

Eurocode 3 proposes several approaches to assess the buckling risk. The preferred practical approach is the “buckling curve approach”, but alternative possibilities are also available: the “general method” or advanced numerical simulations, relying on second-order analysis with imperfections. This section presents the various approaches and enhances how they can be applied to riveted lattice girders.

7.2.1 Buckling curve approach

The buckling curve approach consists of carrying out a structural analysis determining the internal load distribution, followed by the verification of the buckling resistance of individual members using buckling curves (Tankova, 2018, p. 9). According to EN 1993-1-1, 2005, §6.3.1, the design check for a compression member consists in verifying:

$$N_{Ed} \leq N_{b,Rd} \quad (7.7)$$

Where N_{Ed} is the design value of the compression force and $N_{b,Rd}$ is the design buckling resistance of the compression member. $N_{b,Rd}$ is defined as a fraction of the cross-sectional resistance in tension:

$$N_{b,Rd} = \frac{\chi A f_y}{\gamma_{M1}} \quad (7.8)$$

Where χ is the reduction factor for the relevant buckling mode, A is the section area, f_y is the characteristic value of the yield strength (see Chapter 6) and γ_{M1} is a partial safety factor (in France, $\gamma_{M1} = 1.0$). The buckling curves provide values of χ depending on the slenderness and the expected level of imperfections. The Eurocode defines a non-dimensional slenderness $\bar{\lambda}$ as:

$$\bar{\lambda} = \sqrt{\frac{A f_y}{N_{cr}}} \quad (7.9)$$

Where N_{cr} is the critical load. Imperfection factors α are prescribed depending on the geometry of the cross-section. The code thus proposes five buckling curves $\chi = f(\bar{\lambda})$, corresponding to various imperfection factors (Fig. 7.4).

The buckling curve approach is applied to the stability design not only of uniform

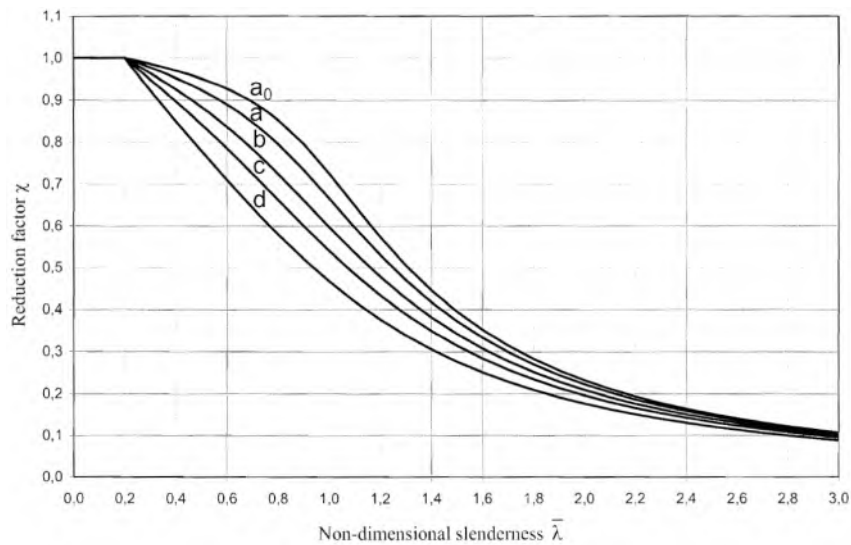


Figure 7.4 – Buckling curves prescribed by EN 1993-1-1, 2005 depending on the cross-section geometry.

columns (members in compression subjected to flexural or torsional buckling - EN 1993-1-1, 2005, §6.3.1) but also of uniform beams (members in bending subjected to lateral-torsional buckling - EN 1993-1-1, 2005, §6.3.2). The design of beam-columns, loaded both in bending and compression, is based on an interaction approach (EN 1993-1-1, 2005, §6.3.3).

The buckling curves were established in the 1970s, relying on an extensive experimental programme carried out on modern steelwork specimens and associated theoretical developments and reliability assessments (Tankova, 2018, pp. 26–29). The reason for this new experimental campaign was the need for harmonisation, given the diversity of existing regulations on buckling in the various European countries and the difficulty of reaching a consensus on a single theoretical approach. Also, unlike previous buckling experiments, the test conditions aimed not to be idealised but, on the contrary, to be as realistic as possible, in order to encompass all possible imperfections. Test specimens were ordered from several manufacturers in different countries, and the straightness of the bars was checked only visually. The experimental results did not make it possible to distinguish the influence of different types of imperfection (out-of-straightness, residual stresses, load eccentricity), but on the contrary to bring together their effects for practical use (Nowak, 1981, pp. 307–311).

The experimental programme comprised more than a thousand column tests, covering a variety of cross-sections (I and H, hollow and T sections...) and fabrication procedures (welded and rolled sections) (Tankova, 2018, p. 27). However, those modern steel specimens may not feature the same imperfections as wrought-iron and mild-steel rolled sections from the 19th century. Our conclusion is that the validity of the buckling curves proposed in Eurocode 3 for assessing old iron and steel structures can, therefore, only be

admitted.

7.2.2 Estimation of the critical load

Analytical and numerical approaches

As the imperfection factor is provided by the Eurocode depending on the cross-section geometry, the remaining unknown for determining the reduction factor χ is the critical load N_{cr} . For uniform members with ideal boundary conditions and subjected to a uniform axial force, typically the Euler cases from Fig. 7.1, N_{cr} can easily be determined analytically. Extensive research has been conducted to derive formulas for the effective length of members with more complex and varied boundary conditions than the Euler cases, or rather for the effective length factor defined as $K = L_{cr}/L$ (Aristizabal-Ochoa, 1994). Let us take the example of a member with both ends fixed in displacement. When the ends are pinned, the effective length is equal to the member length, so $K = 1$. When the ends are fixed, $K = 1/2$. When end-connections are semi-rigid, neither perfectly rigid nor perfectly pinned, K lies between 1/2 and 1. Newmark, 1949 proposed a formula giving the effective length factor depending on the stiffness indice R (see Eq. (3.4)) of the end connections. In the particular case where both connections have the same stiffness, the effective length factor writes:

$$K = \frac{\frac{\pi^2}{R} + 2}{\frac{\pi^2}{R} + 4} \quad (7.10)$$

However, even the most advanced formulas necessitate first being able to analytically represent the end conditions of a member, which is difficult when the member is part of a more complex structure. This is why N_{cr} is often determined using finite element modelling and a linear buckling analysis (LBA). In LBA, the behaviour of the structure is analysed based on linearised equations of equilibrium, assuming small displacements and linear material behaviour. The analysis predicts the critical load factor α_{cr} at which the structure becomes unstable in a given buckling mode. α_{cr} is a dimensionless parameter that indicates the ratio of the buckling load to the applied load. Given the design value N_{Ed} of the axial force in a member, the critical load N_{cr} for this member is obtained from the critical load factor corresponding to the lowest buckling mode where this member becomes unstable:

$$N_{cr} = \alpha_{cr} N_{Ed} \quad (7.11)$$

No matter whether N_{cr} is obtained analytically or numerically, it depends strongly

on the modelling assumptions regarding boundary conditions. For example, an isolated member with fixed ends can withstand four times the critical load of the same member with pinned ends, according to Eq. (7.2). The uncertainty on the behaviour of the connection and the resulting modelling assumptions can thus be responsible for a variation in the estimated critical load by a factor of 4 (Fig. 7.5).

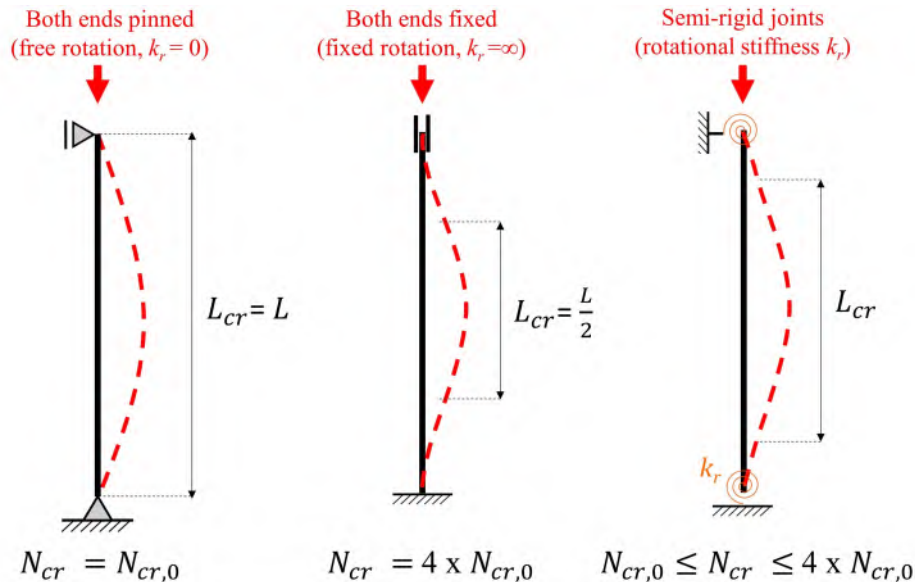


Figure 7.5 – Influence of the end conditions of a column on its effective length and the critical load.

In its informative Annex BB, Eurocode 3 provides guidance regarding effective lengths to be assumed for the flexural buckling of members in triangulated and lattice structures. Regarding out-of-plane buckling, it recommends, by default, to take the buckling length of chord and web members equal to the system length, that is $L_{cr} = L$, unless a smaller value can be justified by analysis (EN 1993-1-1, 2005, Annex BB.1). This is why several experimental campaigns were carried out on steel trusses in the literature.

Experimental studies on steel trusses

Many experiments were conducted on different types of steel trusses with the aim of characterising their buckling behaviour and deriving realistic buckling lengths for prediction purposes. Test specimens were often loaded until failure.

Regarding the buckling of web members, Yost et al., 2004 tested open web steel joists having single angles with crimped ends for web members and found that the effective length factor could be reduced from $K = 1$ (pin-ended condition) to $K = 0.8$. Since the welded connections were assumed to be rigid, the K -factor smaller than 1 underlines the influence of the flexibility of the chords on the rotational restraint experienced by web members. Zaharia et al., 2006 investigated cold-formed steel trusses focusing on the rotational stiffness of the bolted connections. Tests were conducted separately on typical

joint specimens and on a full-scale truss. Empirical formulas were derived for the joint stiffness and the buckling length of web members. Somma et al., 2023 carried out push-out tests on steel lattice girders made of welded reinforcement bars for composite concrete slabs. They also showed how the weld stiffness at the connection between the chords and the diagonals influenced the buckling length of the web bars.

Regarding the buckling of the chords, some studies focused on the effect of lateral restraints, while others enhanced the restraint provided by the web members. Jankowska-Sandberg et al., 2013 investigated the stability of a steel truss girder with hollow section members, depending on the points of application of the load and the lateral bracing system. They concluded that one important factor for the stability of the chords is the type of lacings and their rigidity versus chord rigidity. Patnaik et al., 2003 tested trusses also made from hollow structural sections, with one point load applied at mid-span on the top chord. They showed that the effective length factor K for in-plane buckling was close to 1 but that for out-of-plane buckling K could be reduced to 0.65.

The presented studies relied on full-scale truss specimens loaded until failure or on typical joint specimens. This requires a series of identical specimens, which is difficult to obtain in the case of historic riveted lattice girders. This is why the experimental strategy favoured in Chapters 4 and 5 was to determine the rotational stiffness through non-destructive tests. The buckling behaviour can then be predicted via calibrated numerical models and LBA.

Potential of LBA for lattice girders

In riveted lattice girders, the decisive buckling modes concern out-of-plane buckling of either web members or one of the chords (see Fig. 4 in the introduction chapter). Web members are more prone to out-of-plane buckling than in-plane buckling because they are made of flats with their weak axis corresponding to out-of-plane bending. For the chords, out-of-plane buckling is more critical than in-plane buckling because the in-plane effective length is usually much shorter than the out-of-plane effective length. In-plane, the chords are maintained by web members so that the effective length is about the size of one cell of the web pattern. Out-of-plane, by default, buckling is considered to be constrained only by the supports at both ends of the girder or other lateral restraints.

In Chapters 4 and 5, single-riveted joints in lattice girders have been shown to exhibit a rigid behaviour for out-of-plane rotations. This does not mean that the effective length for out-of-plane buckling of web members can be divided by two. Chapter 5 has evidenced that the end restraint experienced by a web member depends not only on the joint stiffness but also on the bending and torsional stiffness of the chords. In this case, LBA perfectly qualifies to obtain the buckling modes corresponding to the out-of-plane buckling of web

members and the associated critical load factors α_{cr} . LBA was used for example by Lee, 2013 to derive the critical load for web members in open web steel joists, where the welded connections could be assumed to be rigid in the out-of-plane direction.

Regarding the chords, taking the effective length for out-of-plane buckling equal to the full system length is conservative for two reasons. First, the chords have a non-uniform axial force distribution. The design value of the axial force N_{Ed} is reached only in some segments of the chords. Second, due to the rigidity of single-riveted joints in the out-of-plane direction, the compressed chord experiences, to some extent, lateral restraints provided by the web members when the other chord is otherwise restrained. The effect of this type of restraint, corresponding to multiple elastic supports along the length of the compressed chord, was studied by Wen et al., 2020 to understand the buckling behaviour of the upper chords in aluminium half-through truss bridges. Again, LBA can be used to derive the critical load for the compressed chord of a lattice girder.

7.2.3 Second-order analysis with imperfections

Determining the critical load using LBA allows for a less conservative assessment of the buckling risk for a member in compression. However, as was shown in Chapter 3, the web members and the chords may experience in-plane bending moments due to the continuity of the chords and the in-plane rotational stiffness of the riveted joints. Out-of-plane bending moments may also occur for example due to gravity loads when the lattice girder is slanted, like the purlins in Montauban (see Fig. 3.10a). The stability of lattice members should then be checked based on the interaction approach from EN 1993-1-1, 2005, §6.3.3. However, the interaction factors are established based on ideal moment distributions that hardly reflect the distributions observed in lattice girders.

The available alternative possibilities for the design of non-standard cases are the General Method given in EN 1993-1-1, 2005, §6.3.4 or advanced numerical simulations. The applicability of the general method, however, is limited and the results have been shown to be unreliable (Tankova, 2018, p. 159). The real alternative then seems to perform a so-called geometrically non-linear elastic analysis with imperfections (GNIA). In this method, LBA is first conducted to obtain the shape for the buckling mode of interest. This shape is then used as initial imperfection shape for a second-order analysis. The amplitude of the initial local bow imperfection for a given member is prescribed by the Eurocode depending on the relevant buckling curve (EN 1993-1-1, 2005, Tab. 5.1). When equivalent geometric imperfections are correctly defined, the buckling check may be substituted by a simple stress check. In practice, this method is not much used because it is time-consuming, requires the correct definition of the initial imperfections in shape and magnitude, and its reliability depends on the experience of the user (Tankova, 2018, p. 9).

In the next generation of Eurocodes, Eurocode 3 will have a new part specially dedicated to design assisted by finite element analysis (prEN 1993-1-14, 2023), which clarifies the conditions for using the various available possibilities for buckling design.

7.3 Discussion based on the case study

The case study of a lattice purlin in the train shed of Montauban, which was investigated in Chapter 3 for the sake of comparing structural analysis assumptions, is now used to illustrate the differences between historical verification methods and design checks according to Eurocode 3. Before going into calculations, the findings from previous chapters relating to this case study are summarised.

7.3.1 *Summary of findings from previous chapters*

The train shed of Montauban was built in 1903 by the steel construction firm Daydé et Pillé for the railway company Compagnie du Midi. Daydé et Pillé actually built a series of several similar train sheds for this railway company around the turn of the 20th century. This series of train sheds is characterised by its pointed truss arches (see Chapter 1, Fig. 1.6), which could have been designed by either the chief architect of the railway company or by Daydé et Pillé. However, it is not only the typology of the main roof trusses that distinguishes this series of train sheds, but also constructive detailing. The web layout of lattice purlins and rafters, as well as the rounded ends of diagonals, for example, are most probably due to Daydé et Pillé. Also, most interestingly, in the very similar train sheds of Montauban and Bédarieux, the lattice purlins have diagonals made of single flats except for the three most compressed diagonals at each extremity (Fig. 1.13). These compressed diagonals feature double flats instead of single flats. This constructive measure against buckling testifies to solid engineering know-how.

The train shed of Montauban was retrofitted in 2012 by SNCF. The transparent part of the existing roofing was made of polyester panels that had been installed during the last renovation of 1971. To restore the original appearance of the transparent roofing made of sheet or wire glass, polyester panels were replaced with laminated glass panels supported by glazing irons every 40 cm. This led to an increase in the dead load from originally about 25 kg/m² to 38 kg/m² (see Chapter 2, Fig. 2.7. and Tab. 2.3). This architectural choice is partly responsible for the strengthening measures that were carried out in 2012. The lattice purlins were reinforced against out-of-plane buckling by increasing the cross-section of the most compressed diagonals through additional welded flats and by adding brackets as lateral restraints for the bottom chord (see Fig. 2.17).

The case study conducted in Chapter 3 focused on the lattice purlin of Montauban's

train shed experiencing the highest historical load (lattice purlin n°4 in Fig. 3.10a). A structural analysis was carried out using various possible modelling assumptions to assess their influence on the stress distribution. Two historical approaches were compared, as well as three different finite element models (see Tab. 3.1). In the last finite element model FE3, yielding the highest stresses, the diagonals were modelled with beam elements instead of truss elements, taking also into account the crossing node between two diagonals.

In the model FE3, riveted joints were modelled as rigid out-of-plane. This assumption does not make a difference in stress distribution but in the assessment of the buckling length. The riveted joints of the studied lattice purlin are very typical: flat web members assembled between two angles constituting the chords using one rivet. In Chapters 4 and 5, the out-of-plane rotational stiffness of such riveted joints was assessed through experimental investigations conducted on lattice girders featuring this joint type. Those experiments suggest that the considered riveted joints exhibit indeed a rigid behaviour regarding out-of-plane rotations.

Before moving on to buckling risk assessment, Chapter 6 discussed relevant design values of the yield strength for calculations according to Eurocode 3. The original design report of Bédarieux's train shed indicated that the working stress used for design was $\sigma_{lim} = 11 \text{ kg/mm}^2$, which corresponds to 110 MPa. However, this value cannot be used for assessment purposes. For the renovation of Montauban's train shed, a tensile test was conducted only on one sample, yielding $f_y = 296 \text{ MPa}$ (see Tab. 6.4). The review of the literature and the discussion on material sampling suggest that this value alone is not significant. Instead, $f_y = 230 \text{ MPa}$ should be used, the material being mild steel.

In this chapter, the attention shifts to verification methods and the resulting working ratios. The working ratio ρ of a member can be calculated as the calculated stress divided by the working stress when following the historical safety concept or as the design load divided by the design resistance when using Eurocode 3. For the sake of simplicity, the case study is restricted to working ratios obtained for the diagonals of the lattice purlin. The verification of the chords is left out.

7.3.2 Original design checks under historical loads

In the original design report of Bédarieux's train shed, similar to Montauban's, the buckling risk was not verified for the lattice purlins. The resistance of the diagonals was checked by comparing the maximum stress in the net cross-section to the working stress $\sigma_{lim} = 11 \text{ daN/mm}^2$ (or kg/mm^2 using the old unit). Assuming the working stress to be the same for Montauban and using the maximum stress derived from Résal's approach $\sigma_w = 6.14 \text{ daN/mm}^2$ (see Tab. 3.1), the maximum working ratio in the diagonals made of single flats is $\rho = 0.56$. However, in practice, the most compressed diagonals were built

as double flats so the working ratio drops to $\rho = 0.28$ (see Fig. 7.3b).

Let us investigate the working ratios that would have been obtained if buckling had been verified using historical formulas. Montauban's train shed was built in 1903, that is right after the publication of the 1902 regulation concerning the design of train sheds, which contained no specifications regarding buckling (« Circulaire du ministre des travaux publics aux préfets du 25 janvier 1902 (Halles à voyageurs et à marchandises des chemins de fer) », 1904). However, the Rankine-type formula proposed by Résal for members in compression could have been applied (Résal, 1892, p. 510). According to Résal, using the notations of Eq. (7.4):

- a is the working stress defined for the project, corresponding to the allowable stress for elements in tension. Here, $a = 11 \text{ daN/mm}^2$.
- $b = 1/8000$ is the empirical parameter defined by Résal for mild-steel members.

Regarding the buckling length of the diagonals, let us consider that the compressed diagonals are restrained at mid-span by the crossing diagonal in tension. If the riveted joints between the diagonals and the chords are considered pinned, the resulting buckling length is L_w , with L_w the half-length of the diagonals. If the riveted joints are considered rigid, the resulting buckling length could be taken as $0.7L_w$ (Fig. 7.6).

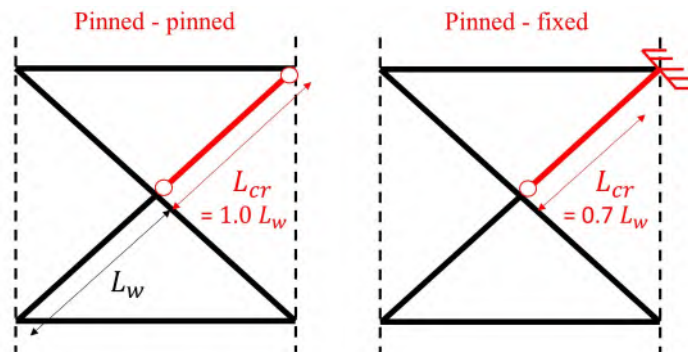


Figure 7.6 – Buckling length of the diagonals in the lattice purlin of Montauban depending on the assumptions regarding the riveted joints.

The allowable stress in a compressed member needs to be compared to the calculated stress in the gross section, instead of the net section. When assuming pinned connections, the working ratio is then 1.78, while when assuming rigid connections, it is 0.98. Considering double flats instead of single flats for the most compressed diagonals, the working ratios drop to 0.97 if connections are pinned and 0.54 if connections are rigid. The results are summarised in Tab. 7.1.

As mentioned earlier, several authors from the literature of the 19th century argued qualitatively that lattice web members did not need to be verified against buckling because their rigid riveted joints efficiently restrained them. It is interesting to note that those qualitative arguments agree with potential calculations: single diagonals can be assessed

Table 7.1 – Comparison of working ratios obtained from historical design checks.
 Stress check: verification of the stress in the net section.

Buckling check: verification of the member stability, when the end connections are considered pinned or rigid.

	Stress check	Buckling check	
		Pinned	Rigid
Single diagonal	0.56	1.78	0.98
Double diagonal	0.28	0.97	0.54

to be buckling-safe only if connections are assumed to be rigid. However, the comparison of working ratios for single and double diagonals shows that doubling the section of the most compressed diagonals was not an overly conservative measure.

7.3.3 Assessment according to Eurocode 3

Loads according to the Eurocodes

For the purpose of reassessing the structure, loads must be reevaluated following the prescriptions of the Eurocodes. In the 2012 renovation of Montauban’s train shed the transparent parts of the roof were restored with laminated glass, yielding a dead load of about 40 daN/m² on the metal structure (see Tab. 2.3). For wind and snow, the Eurocodes do not fit well the geometrical conditions of the train shed of Montauban. Therefore, they need to be interpreted.

Regarding snow, given the location of Montauban (Region A2, French National Annex of EN 1991-1-3, 2003), the characteristic value of the snow load is $s_k = 45$ daN/m². The roof can be likened to a cylindrical roof (EN 1991-1-3, 2003, §5.3.5). Considering the shape coefficients related to cylindrical roofs, the average vertical snow load around purlin n°4 is 43.8 daN/m² (Fig. 7.7). Thus, the purlin experiences a normal distributed load $s = 43.8 \times e \cos \beta = 119$ daN/m, where $e = 2.8$ m is the width of influence of the purlin along the roof slope and $\beta = 14^\circ$ is the inclination of the purlin compared to the vertical (for the geometry, see Section 3.3.1).

Regarding wind, given the location of Montauban (Region 1, French National Annex of EN 1991-1-4, 2005) and the proportions of the building, the peak velocity pressure is $q_p = 50$ daN/m². The roof can be regarded as a “canopy roof” (EN 1991-1-4, 2005, §7.3) because three sides of the shed are open (*ibid* §7.2.9(2)). The degree of blockage φ , which is the ratio of the area of obstructions divided by the cross-sectional area under the canopy, depends on the wind direction. In the longitudinal direction, $\varphi = 0$ and in the transversal direction, $\varphi = 1$. Both values yield the same downward wind loads. Considering an average roof slope of 30°, the maximum net pressure coefficient for downward wind is $c_{p,net} = 1.3$ (EN 1991-1-4, 2005, Tab. 7.7). Thus, the purlin experiences a downward

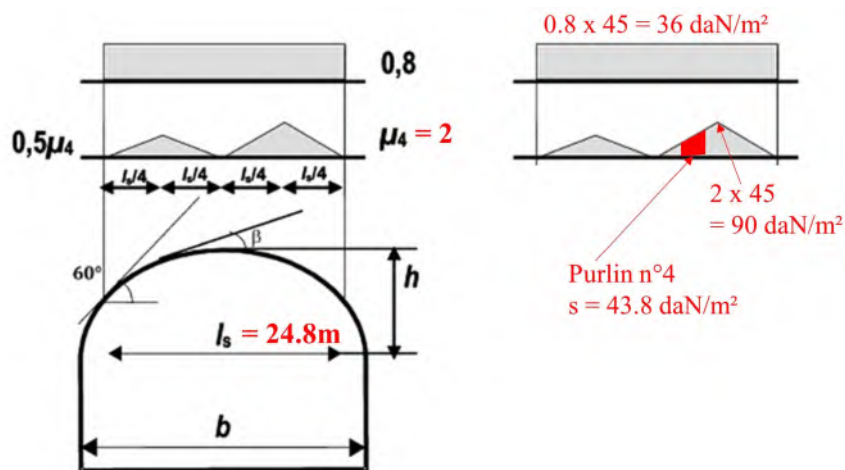


Figure 7.7 – Determination of snow loads on the roof of Montauban's train shed according to EN 1991-1-3, 2003, §5.3.5.

normal distributed load $w = 1.3 \times 50 \times 2.8 = 182 \text{ daN/m}$.

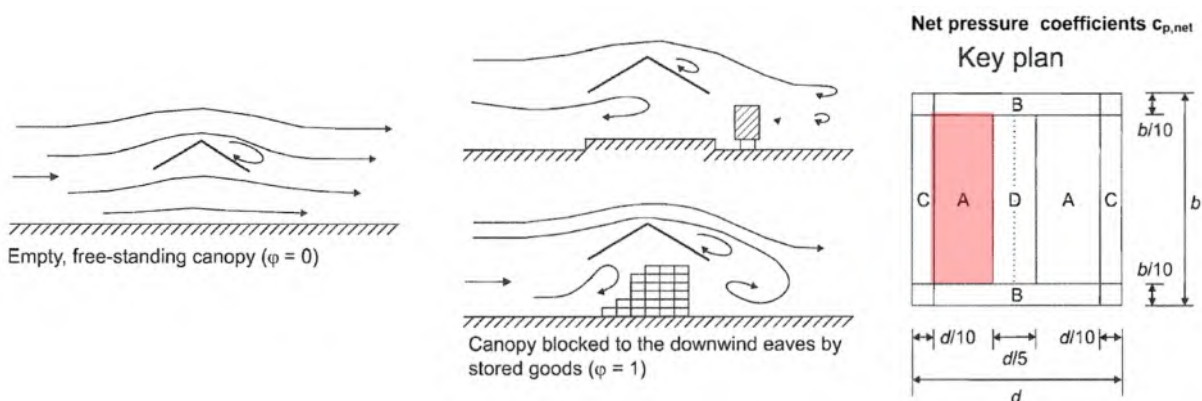


Figure 7.8 – Airflow on a canopy roof, depending on the degree of blockage φ (EN 1991-1-4, 2005, Fig. 7.15), and selection of the relevant roof area for the determination of net pressure coefficients $c_{p,net}$ (EN 1991-1-4, 2005, Tab. 7.7).

According to the Eurocodes, snow and wind must be considered simultaneously in load combinations. The extreme downward ULS load combination is $1.35g + 1.5w_1 + 0.75s$ yielding a uniform load of 555 daN/m.

Verification of the stress in the net section

Under the historical loads and using the working stress $\sigma_{lim} = 11 \text{ daN/mm}^2$, the stress check in the net section of the diagonals yielded a working ratio $\rho = 0.56$. Under the loads corresponding to ULS 1, the maximum axial force in the diagonals, calculated using Résal's analytical approach, becomes $D_{max} = 2497 \text{ daN}$. Assuming a yield strength $f_y = 230 \text{ MPa}$, the stress check in the net section of the diagonals yields $\rho = 0.53$. Even though the safety concepts and the load definitions are different, the historical and current approaches lead to similar working ratios. The high level of similarity here may be a

coincidence. However, it can be kept in mind that regardless of the design approach, the resistance of cross sections is rarely critical. In the current practice, the verification of stresses in the net section is seldom carried out, as it requires an extra manual input in finite element softwares. The automated stress verifications done by engineering softwares usually rely on the stresses calculated for the gross section attributed to the bars in the finite element model.

Verification of buckling based on the buckling curve approach

Let us consider the out-of-plane buckling of the diagonals. If secondary moments are neglected, diagonals can be checked with the rules applying to uniform members in compression (EN 1993-1-1, 2005, §6.3.1). Under the uniform load of 555 daN/m, the maximum axial force in the most compressed double diagonals becomes $D_{max} = 2709$ daN, using the finite element model FE3 (see Section 3.3.3).

Following the default recommendations of EN 1993-1-1, 2005, §BB.1.1(1), the buckling length L_{cr} for out-of-plane buckling of web members should be taken equal to the system length. Taking into account that each compressed diagonal is restrained in its midst by the crossing diagonal in tension, this corresponds to $L_{cr} = L_w$. Under this assumption, the working ratio in the most compressed double diagonals is determined from the buckling curve approach as follows:

- $N_{cr} = 877$ daN is the critical load of each flat, using Eq. (7.2).
- $N_{b,Rd} = 742$ daN is the design buckling resistance of each flat, using Eq. (7.8) and buckling curve c (rectangular cross-section - see EN 1993-1-1, 2005, Tab. 6.2).
- $N_{Ed} = D_{max}/2 = 1354$ daN is the design value of the axial force in each flat of the double diagonal.
- $\rho = N_{Ed}/N_{b,Rd} = 1.82$ is the working ratio. It means that the load capacity of the most compressed diagonals is exceeded by 82%.

It appears that when riveted joints are considered pinned, the working ratio for the most compressed diagonals is way above the acceptable limit of 1.0. Such an excessive working ratio requires strengthening measures. In the restoration of the train shed of Montauban in 2012, the double diagonals were reinforced by welding an additional 50 mm x 6 mm flat to one of the flats (see Fig. 2.17 and 2.15a). The welding stitches being closely spaced, the resulting cross-section of the double diagonals consisted of a 50 mm x 6 mm flat and a 50 mm x 12 mm flat. If the 50 mm x 6 mm flat buckles, all the load D_{max} flows into the reinforced 50 mm x 12 mm flat. This results in a working ratio $\rho = 0.56$ for this reinforced section, which proves the strengthening measure is efficient.

In model FE3 however, riveted joints are considered rigid out-of-plane, relying on the results from the experiments presented in Chapters 4 and 5. To estimate the buckling

length using LBA, the section of the double diagonals is reduced to one single plate in the model. This way, the model integrates the correct stiffness relevant for the buckling of each flat of the double diagonal. The shape of the first buckling mode of the most compressed diagonal obtained using LBA is presented in Fig. 7.9.

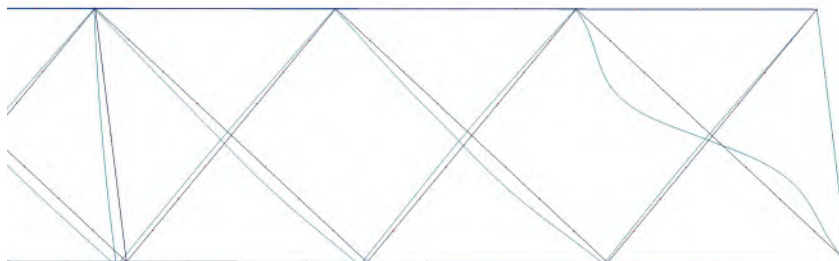


Figure 7.9 – Shape of the first buckling mode of the most compressed diagonal of the studied lattice purlin, determined by LBA on ROBOT.

The working ratio is obtained as follows:

- $N_{cr} = \alpha_{cr} D_{max} = 0.818 \times 2242 = 1998$ daN is the critical load of a single flat. $D_{max} = 2242$ daN is a bit lower than the previous value of 2709 daN because a single flat attracts less load than a double flat. Besides, $\alpha_{cr} < 1$ is not surprising as only one single flat was modelled instead of a double flat.
- $N_{Ed} = 1354$ daN is the design value of the axial force in each flat of the double diagonal.
- $\rho = 0.88$ is the working ratio.

The comparison of the various working ratios, summarised in Tab. 7.2, suggests that modelling the riveted joints as rigid could help avoid strengthening measures. Moreover, it must be pointed out that the buckling length derived from the calculated N_{cr} corresponds to an effective length factor $K = 0.66$. This is slightly inferior to the ideal value $K = 0.7$ for the pinned-fixed condition (see Fig. 7.6), because in the middle of the diagonal, there is a small clamping effect due to the continuity of the flat.

Table 7.2 – Comparison of working ratios obtained from Eurocode design checks.

Buckling check: verification of buckling, when riveted joints are considered pinned ($L_{cr} = L_w$) or rigid (L_{cr} derived from LBA).

	Buckling check	
	Pinned	Rigid
Double diagonal	1.82	0.88
Reinforced diagonal	0.56	

The presented working ratios are only an indication of the potential gain that can be brought by deriving buckling lengths from LBA while considering rigid riveted joints. The results regarding the necessity of strengthening measures need to be confirmed by

taking into account the secondary bending moments and using the interaction approach proposed by the Eurocode. Alternatively, GNIA could be used but the software ROBOT is inappropriate in this case, especially because it is difficult to accurately represent the behaviour of the double diagonals through a single bar member.

7.3.4 Conclusion of the case study

The case study showed that the constructive measures against buckling carried out on the lattice purlins of Montauban's train shed (double flats for the most compressed diagonals) were justified and sufficient when buckling was verified using a Rankine-type formula from the construction period. Conducting design checks using the historical approach showed that working ratios were acceptable only if the connections were considered rigid, which is what several authors argued qualitatively in the historical literature. It appears that in the 19th century, engineers could efficiently rely on shared experience and construction practice to design buckling-safe structures.

The buckling risk of the studied lattice purlin was then assessed using the buckling curve approach from Eurocode 3 and neglecting bending moments, as in the original design. Today, by lack of knowledge, engineers need to follow standards imposing conservative assumptions. When following the default recommendations of Eurocode 3 for the buckling of lattice structures, which correspond to assuming pinned connections, the obtained working ratio is such that strengthening measures are inevitable. When considering rigid joints instead and deriving the buckling length from linear buckling analysis, the working ratio becomes acceptable, even though much higher than the working ratio obtained under similar assumptions with historical formulas. This result suggests that experimentally proving that single-riveted joints are rigid can effectively reduce the predicted buckling risk. However, this conclusion needs to be sustained by more extensive and advanced numerical calculations, as well as the analysis of more case studies.

Overall, the case study of a lattice purlin in the train shed of Montauban conducted throughout the thesis highlighted the challenges and opportunities in assessing historic iron and steel structures. This study did not conclude whether the strengthening measures carried out in 2012 were necessary or which type of reinforcement should be preferred. However, it demonstrated the insights that can be gained from a specific line of inquiry that goes beyond structural assessment according to the Eurocodes. The study provided knowledge on the cultural significance of lattice girders and their construction details, as well as the pros and cons of replacing the transparent roofing with laminated glass and reinforcing lattice girders with welded flats and added brackets. This knowledge shall help in making decisions when defining restoration strategies and developing structural interventions. Discussions around modelling assumptions and design criteria improved

the understanding of how assessing historic structures can differ from designing new ones. The conservative assumptions regarding the rotational behaviour of riveted joints can be adapted by relying on historical design intentions and experimental and numerical investigations. The assessment of the buckling risk can then be refined by deriving the buckling lengths of chord and web members from linear buckling analysis.

7.4 Conclusion

Relying on a historical study, this chapter first discussed how buckling was understood and considered in the design of compressed members, especially made of iron or steel. Due to the theoretical struggle with the phenomenon of buckling, historical design criteria against buckling were even more diverse in the literature than recommendations on the working stress. In France, regulations on the design of iron and steel constructions withdrew from the debate and did not provide any specifications until 1915. Facing this disarray, designers verified buckling by calculations only for columns. The buckling safety of other compressed members was ensured with qualitative arguments and constructive measures, as has been shown using examples of train sheds. Moreover, not all buckling phenomena were known to designers. Constructive measures aimed to prevent the flexural buckling of compressed members. Lateral torsional buckling remained widely unknown in the period of interest. The same applies to shear buckling, which led engineers to underestimate the advantage of lattice over solid-web girders in terms of material utilisation. This enhances how important the aesthetic contribution of lattice girders was to French designers.

The various approaches for buckling design proposed by Eurocode 3 were then presented and discussed. Today, even though buckling is much better understood, the use of Eurocode 3 to predict the buckling risk of riveted lattice girders has theoretical and practical limitations. The buckling curve approach relies on an extensive experimental programme that did not comprise wrought-iron and mild-steel specimens. It is uncertain whether the buckling curves proposed by Eurocode 3 correctly cover the level of imperfections in flat and angle bars of riveted lattice girders. Moreover, the non-standard distributions of bending moments in the diagonals and chords of lattice girders make it difficult to obtain reliable results from the interaction approach proposed for beam-columns. The use of second-order analysis with imperfections seems to be an interesting alternative to assess lattice girders with intricate geometries. However, FEA softwares commonly used by structural engineers may be too limited to correctly represent the structural behaviour. So, in practice, using the buckling curve approach and deriving buckling lengths from linear buckling analysis seems the most suitable to obtain reliable results.

CONCLUSION

Given the growing scarcity of building resources and the environmental impact of new constructions, it is increasingly necessary to reuse existing structures. Restoring or transforming existing buildings also preserves or creates characterful places that contribute to cultural identity. Finally, it can prove economically more advantageous to restore than to demolish and reconstruct. To facilitate sustainable, heritage-friendly, and cost-effective renovation projects, this thesis proposed a novel assessment framework for existing structures. This framework brings together the assessment of their load-bearing capacity and their heritage value and anchors current practices in the history of engineering and construction. To demonstrate the potential synergies between the fields of structural engineering, history and heritage, the example of riveted lattice girders in historic French train sheds was used. This conclusion first summarises the main findings regarding this specific example and then highlights the methodological contributions of the thesis and the perspectives for future work.

Contributions to the assessment of riveted lattice girders

Chapter 1 enhanced the heritage value of structural components in historic metal train sheds. To efficiently and sensitively preserve an existing structure, it is essential to assess its value in more detail than by stating “this is a beautiful old structure and a testimony to blooming engineering and industry in the 19th century”. It is necessary to question the preservation of its attributes beyond its material substance or its architectural shape. In roof structures, the roof trusses are the primary structural components. In train sheds, roof truss typologies tell a story about national engineering trends, railway companies, and steel constructors. Even though, from a structural point of view, riveted lattice girders are secondary components, they reveal as much as roof trusses if not more. They are a blend of manufacturing know-how and theoretical developments. They play a major aesthetic role, and the layout of the lattice web, as well as construction details, can be traced back to the preferences of engineers or contractors.

Chapter 2 traced the history of restoration practices for train sheds and highlighted how industrial heritage was progressively acknowledged. Until the 1980s, train sheds were regularly restored with the only aim of preserving their functionality. In the 1970s and 1980s, original roofing materials, such as glass and zinc on timber boarding, were widely

replaced by plastic panels and steel decks, with no respect for the preservation of the original appearance. Structural interventions tended to be visually invasive and did not consider original design intentions. In contrast, train shed restorations carried out since 2005 demonstrate a clear commitment to preserving heritage, but still reveal some biases in the perception of cultural value. Our interpretation is that the priority is given to restoring the original architecture, for example by reproducing the original roofing, reconstructing skylights and favouring discrete repairs and strengthening measures. However, imitating the original roofing while fulfilling current safety requirements leads to an increase in the permanent loads supported by the structure, which, in turn, contributes to making structural reinforcements necessary. Furthermore, the strengthening measures carried out vary widely, both in their principle and their constructive implementation, even though their causes are similar. This indicates that the preservation of the structure itself could be better integrated as a criterion for successful heritage-friendly restorations. Together, **Chapters 1** and **2** thus identified restoration challenges and provided the background necessary for elaborating a context-based structural assessment.

For structural assessment, riveted lattice girders are usually analysed using finite element models and verified according to the Eurocodes. Historical research conducted in **Chapter 3** showed to what extent riveted lattice girders were considered truss-type structures. The layout of lattice girders was directly derived from truss bridges and their riveted joints were considered pinned for calculations. However, they were not designed as trusses but as beams, using Navier's bending theory. The internal loads transmitted by web members were even disregarded in calculations until the end of the 19th century, which is why web members can be critical when being assessed using finite element models. A review of recent literature highlights the range of uncertainties and current assumptions regarding the stiffness of riveted connections. This review suggests that we have not come much further in our knowledge of the rotational behaviour of riveted connections than our predecessors in the 19th century. The difference is that our computational tools make it easy to bypass uncertainties and pick the most conservative modelling assumptions. Riveted joints can be modelled as rigid connections in the plane of the lattice girder because this modelling assumption leads to additional bending moments. For out-of-plane rotations, they are rather modelled as pinned because it yields the highest buckling risk.

The experiments carried out on two reclaimed riveted lattice girders focused on assessing the out-of-plane rotational stiffness of the single-riveted joints. To start with, a modal testing methodology was developed. This methodology, presented in **Chapter 4**, confronted the results from the experimental modal analysis with modal properties obtained from finite element models. In these models, the chords and web members were modelled using beam elements and the web-member-to-chord connections were represented by kine-

matic conditions. In particular, the out-of-plane rotation of the joints was controlled by rotational springs with a stiffness k_r . The study evidenced two modal-based indicators suggesting that the single-riveted joints of the tested lattice girder are best represented using rigid connections ($k_r = \infty$). Another modal-based indicator was developed to detect stiffness variations between similar joints. Further investigations are desirable to verify to which family of single-riveted joints these results apply, in terms of geometry. Also, in order to use this non-destructive testing method for examining existing structures on-site, it should be adapted to operational conditions. In **Chapter 5**, the load test campaign carried out on another identical lattice girder showed that single-riveted joints exhibit the same rigid behaviour out-of-plane under dynamic and quasi-static loading. Additionally, the load tests showed that the rotational end-restraint provided to web members depends both on the joint stiffness as well as on the bending and the torsional stiffness of the chords. This result is important to understand why global modelling is necessary to derive meaningful buckling lengths of individual members. Overall, **Chapters 3, 4 and 5** helped refine modelling assumptions for structural analysis.

Chapter 6 discussed appropriate design values for material properties because their definition is a prerequisite for assessing the buckling resistance of lattice girders. It was shown that working stresses used for the original design can no longer be used for verification in accordance with the Eurocode because safety concepts have evolved too much. Test results derived from material sampling on the existing structure often lack statistical significance. Thus, the best practical approach seems to rely on recent literature to obtain characteristic values of yield strength, typically $f_y = 200$ MPa for wrought iron and $f_y = 230$ MPa for mild steel.

Regarding buckling design itself, historical research carried out in **Chapter 7** revealed that the buckling safety of compressed web members in lattice girders was originally not verified analytically. Still, the web members experiencing the highest compression loads were sometimes given a stiffer cross-section, demonstrating a constructive know-how that was certainly derived, once again, from bridge design. Today, even though buckling is much better understood, the use of Eurocode 3 to predict the buckling risk of riveted lattice girders has theoretical and practical limitations. It is, for example, uncertain whether the buckling curves proposed by Eurocode 3 correctly cover the level of imperfections in flat and angle bars of riveted lattice girders. However, relying on linear buckling analysis and using the assumption that riveted joints are rigid for out-of-plane rotations, the predicted buckling risk according to Eurocode 3's buckling curve approach is likely to remain within acceptable boundaries. Strengthening measures could then be avoided or reduced. In conclusion, **Chapters 6 and 7** gave insights on how to adapt current verification methods to riveted lattice girders to obtain a more meaningful assessment of the

load-bearing capacity.

Perspectives

The study of French train sheds restorations has shown that uncertainties regarding the structural behaviour of the metal structure have been responsible for strengthening measures that can be detrimental to authenticity. However, practices addressing old iron and steel structures vary enormously between and within European countries. Looking at other types of metal structures and other countries, further research could examine how uncertainties and the resulting adverse assessments guide adaptive reuse strategies and what retrofitting interventions are regarded as acceptable from a heritage point of view. The influence of national standards and guidelines in the practice of reuse and retrofitting in each country or, in their absence, what practitioners rely on to carry out successful renovation projects, is of particular interest.

This thesis has also pointed out some limitations of the current assessment practices which are related to the Eurocodes. The new generation of Eurocodes shall facilitate a less conservative assessment of existing structures. The new Eurocode 0 will encourage the use of data from existing structures to update the input parameters used for assessment and make it possible to adjust partial security factors or the target reliability level. However, the new design rules set out only general principles, so their potential beneficial effects on the verification of old iron and steel structures should be investigated. Besides, the new Eurocode 3 will provide clearer guidance regarding when and how to use more refined methods involving global critical buckling analysis and second-order effects. The buckling assessment of old iron and steel structures should be examined in more detail using these new guidelines. Further research based on case studies will be needed if the new regulatory framework is to be widely applied in practice.

From a methodological point of view, the thesis has illustrated how an existing structure benefits from being considered not as an isolated object but as belonging to a family of structures, or rather several, depending on the aspect studied. In the case of riveted lattice girders, the family of train sheds was relevant to enhancing the impact of strengthening measures, whereas the family of truss-type structures was useful for discussing structural analysis assumptions. The larger family of iron and steel structures built between 1850 and 1950 was interesting in determining design values of material properties. Working with surveys and databases is an effective way of obtaining relevant information for structural assessment. What's more, identifying significant structural features is key to demonstrating the heritage value of a structure and integrating its preservation into a renovation strategy. The proposed tagline is: "for the structure to serve the architecture,

restoration should serve the structure”.

Throughout the thesis, historical studies have been used as a tool to put current renovation and assessment practices into perspective. Knowledge of historical design practices helps identify the existing structure’s weaknesses and potentials and enhances the limitations of our current assessment methods and design criteria. We firmly believe that construction and engineering history should be systematically integrated into the civil engineering curricula, whenever they deal with assessing existing structures. However, uncertainties in current assessment practices are not only due to a lack of historical background but also to real knowledge gaps. For example, the out-of-plane rotational stiffness of single-riveted joints had never been investigated before. In that case, experimental and numerical investigations are of course necessary. Still, historical knowledge can help in scoping those investigations. It would be highly interesting to investigate other types of structures made of other materials, such as masonry or timber, to validate this approach.

Overall, this work has highlighted how interdisciplinarity can help to assess, preserve and reuse existing structures in a meaningful and effective way. The presented study draws on engineering and construction history, structural engineering and experimental mechanics, and heritage assessment. However, other disciplines are also essential to facilitate the restoration or transformation of buildings. For instance, insurance policies tailored to the specific needs and risks associated with existing structures are critical to the financial reliability of projects. Estimates of the carbon footprint of a renovation compared with a new build are essential indicators for balancing economic considerations. Therefore, research efforts should focus on developing interdisciplinary practices enabling decision-makers to make best-informed choices about restoration strategies and promote multi-faceted sustainability.

BIBLIOGRAPHY

Archival sources

- A. Moisant Constructeur. (1880, January 9). *Gare d'Hendaye, Comble de la halle des voyageurs, Calculs justificatifs. [Design report for the train shed of Hendaye].* Box 1331LM2420/007. Le Mans, Centre national des archives historiques de la SNCF.
- CNAH. (1981). *Note d'argumentation pour le financement de la rénovation des grands halls métalliques. [Note about the funding of train shed restorations].* Box 0823LM1024. Le Mans, Centre national des archives historiques de la SNCF.
- Daydé et Pillé. (1896, January 31). *Gare définitive de Bordeaux St Jean, Halle métallique, Calculs justificatifs des résistances. [Design report for the train shed of Bordeaux Saint-Jean].* Unreferenced SNCF archive.
- Daydé et Pillé. (1902, May). *Gare de Bédarieux, Halle métallique, Calculs justificatifs. [Design report for the train shed of Bédarieux].* Unreferenced SNCF archive.
- Etablissements Schmid, Bruneton, Morin. (1929, May 17). *Chemins de fer de l'Est, Gare de Paris, Hall de banlieue, Calculs justificatifs. [Design report for the train shed of Paris Est].* . Box 0760VP4932. Centre d'archives SNCF de Combs-la-Ville.
- Rigolet. (1868). *Halle métallique de Bayonne, exécutée de 1867 à 1868. [Design report for the train shed of Bayonne].* Unreferenced SNCF archive.
- Unknown. (1892). *Gare de Marseille, Evaluation des charges. [Design report for the train shed of Marseille St-Charles].* Unreferenced SNCF archive.
- Unknown. (1908, June 22). *Gare de St Germain-des-Fossés, Halle à voyageurs, Calcul des fermes. [Design report for the train shed of St-Germain des Fossés].* Unreferenced SNCF archive.

Historical sources (1800-1940)

- Ardant, P.-J. (1840). *Etudes théoriques et expérimentales sur l'établissement des charpentes à grande portée*. Metz, S. Lamort.
- Boca, E. (1886). Arrondissement de la Gare Saint-Lazare à Paris - Installation du service des messageries. *Le Génie civil*, 9(13), 194–195.
- Bresse, J. (1857). *Cours de mécanique appliquée*. Ecole impériale des Ponts et Chaussées.
- Brune, E. (1888). *Cours de construction professé à l'Ecole des Beaux-Arts*. Paris, Librairie des Imprimeries réunies.
- Buchetti, J. (1888). *Manuel des constructions métalliques et mécaniques*. Paris.
- Carret, E. (1909). Le verre armé. *Les travaux : Organe des travaux publics et particuliers en Algérie, en Tunisie et au Maroc*, 2(8), 67–69.
- Circulaire du ministre des travaux publics aux préfets du 25 janvier 1902 (Halles à voyageurs et à marchandises des chemins de fer). (1904). In *Recueil de lois, ordonnances, décrets, règlements et circulaires concernant les différents services du Ministère des travaux publics - 2^e série, tome XII* (pp. 47–52). Imprimerie administrative Jousset.
- Clark, E. (1850). *The Britannia and Conway Tubular Bridges* (Vol. 2). London, Dat & Son; John Weale.
- Collignon, E. (1864). Théorie des fermes à poutres droites et des fermes américaines. *Annales des Ponts et Chaussées, 4^e série, Tome VII*, 141–213.
- Collignon, E. (1869). *Cours de mécanique appliquée aux constructions - Résistance des matériaux*. Paris, Dunod.
- Considère, A. (1885). Mémoire sur l'emploi du fer et de l'acier dans les constructions. *Annales des Ponts et Chaussées, 6^e série, Tome IX*.
- Cordeau, A. L. (1901). Charpente en fer et serrurerie. In *Guide des constructeurs : traité complet des connaissances relatives aux constructions* (7th ed.). Paris, E. Lévy.
- Deharme, E. (1890). *Chemins de fer - Superstructure*. Paris, Librairie Polytechnique.
- Fairbairn, W. (1850). An experimental inquiry into the strength of wrought-iron plates and their riveted joints as applied to ship-building and vessels exposed to severe strains. *Philosophical Transactions of the Royal Society of London*, 140, 677–725.
- Flamand, A. (1886). *Stabilité des constructions. Résistance des matériaux* (1st ed.). Paris, Librairie Polytechnique.
- Flamand, A. (1909). *Stabilité des constructions. Résistance des matériaux* (3rd ed.). Paris, Librairie Polytechnique.
- Klasen, L. (1876). *Handbuch der Hochbau-Constructionen in Eisen und anderen Metallen: für Architekten, Ingenieure, Konstrukteure, Bauhandwerker und technische Lehranstalten*. Leipzig, W. Engelmann.

- Love, G.-H. (1851). Mémoire n°27 : résistance du fer et de la fonte, basée principalement sur les recherches expérimentales les plus récentes faites en Angleterre. *Mémoires de la Société des ingénieurs civils*, Vol. 4, 163–272.
- Mathieu, E. (1863). Etude générale sur les charpentes en fer (C. A. Oppermann, Ed.). *Nouvelles Annales de la Construction*, Vol. 1, 8–17.
- Meyer, A. G. (1907). *Eisenbauten, ihre Geschichte und Aesthetik*. Esslingen, Paul Neff Verlag.
- Moreau, A. (1898). *Traité des chemins de fer*. Paris, Fanchon et Artus.
- Morin, A. (1853). *Leçons de mécanique pratique*. Paris, Librairie de L. Hachette et Cie.
- Navier, C. L. M. H. (1833). *Résumé des leçons données à l'Ecole des Ponts et Chaussées sur l'application de la mécanique à l'établissement des constructions et des machines* (2nd ed.). Paris, Carilian-Goeury.
- Novat, J. (1900). *Cours pratique de résistance des matériaux professé à la Société d'enseignement professionnel du Rhône*. Paris, Librairie Polytechnique Ch. Béranger.
- Oslet, G. (1898). Traité de charpente en fer. In *Encyclopédie théorique & pratique des connaissances civiles & militaires*. Paris, Fanchon et Artus.
- Poncelet, J.-V. (1841). *Introduction à la mécanique industrielle, physique ou expérimentale* (2nd ed.). Metz & Paris.
- Regnauld, P. (1870). *Traité pratique de la construction des ponts et viaducs métalliques*. Paris, Dunod.
- Résal, J. (1892). *Constructions métalliques, élasticité et résistance des matériaux : fonte, fer & acier*. Paris, Baudry et cie.
- Résal, J. (1917). *Cours de ponts métalliques professé à l'école nationale des ponts et chaussées*. Paris & Liège, Librairie Polytechnique Ch. Béranger.
- Richou, G. (1888). Pl. I : Gare Saint-Lazare. Etablissement des nouvelles halles couvertes et allongement des halles actuelles. *Le Génie civil*, Tome XIII.
- Riegl, A. (1903). *Der moderne Denkmalkultus. Sein Wesen und seine Entstehung*. Vienna, Leipzig.
- Schwedler, J. W. (1851). Theorie der Brückenbalkensysteme. *Zeitschrift für Bauwesen*, 114–123, 162–173, 265–278.
- Secrétariat de la commission des Annales. (1855). Note n°121: Sur les combles du chemin de fer de l'Ouest (rive gauche), à Paris. *Annales des Ponts et Chaussées*, 3e série(2e semestre), 81–85.
- Sévène, L. (1871). Note n°1 : Sur la nouvelle gare des voyageurs du chemin de fer d'Orléans, à Paris. *Annales des Ponts et Chaussées*, 5e série(1er semestre), 1–8.
- Vierendeel, A. (1902). *La construction architecturale en fonte, fer et acier*. Louvain: Uyst-pruyst & Paris: Dunod.

Literature (1940-2023)

- Abdulameer, Z. A., & Abbas, S. S. (2020). Adaptive reuse as an approach to sustainability. *IOP Conference Series: Materials Science and Engineering*, 881(1), 012010. doi:10.1088/1757-899X/881/1/012010
- Åkesson, B. (2010). *Fatigue Life of Riveted Steel Bridges*. London, CRC Press. doi:10.1201/b10429
- Al-Emrani, M., & Kliger, R. (2003). FE analysis of stringer-to-floor-beam connections in riveted railway bridges. *Journal of Constructional Steel Research*, 59(7), 803–818. doi:10.1016/S0143-974X(02)00114-1
- Allemang, R. (2003). The modal assurance criterion—twenty years of use and abuse. *Sound and Vibration*, 37(8), 14–21.
- Antoni, J., & Schoukens, J. (2007). A comprehensive study of the bias and variance of frequency-response-function measurements: Optimal window selection and overlapping strategies. *Automatica*, 43(10), 1723–1736. doi:10.1016/j.automatica.2007.02.020
- Aristizabal-Ochoa, J. D. (1994). K-Factor for Columns in any Type of Construction: Nonparadoxical Approach. *Journal of Structural Engineering*, 120(4), 1272–1290. doi:10.1061/(ASCE)0733-9445(1994)120:4(1272)
- Autodesk - Robot Structural Analysis. (2024). <https://www.autodesk.fr/products/robot-structural-analysis/overview>
- Bates, W. (1984). *Historical structural steelwork handbook - Properties of U.K. and European cast iron, wrought iron and steel sections including design, load and stress data since the mid 19th century*. London, British Constructional Steelwork Assoc.
- Belhoste, J.-F. (1999). La gare Saint-Lazare, témoin exceptionnel des débuts de la construction métallique en France. *Revue d'histoire des chemins de fer*, (20-21), 161–173.
- Bowie, K. (2009). La quête des sources : les différents types de documents et de fonds disponibles. *Revue d'histoire des chemins de fer*, (40), 17–23. doi:10.4000/rhcf.708
- Braathen Granhaug, E., & Guust van de Pontseele, L. A. (2018). *Modal Analysis and Damage Identification of the Hell Bridge Test Arena* (Master's thesis). Norwegian University of Science and Technology.
- Brandes, K. (2008). Eigenschaften alter Eisen und Stähle und ihre adäquate Materialprüfung und Bewertung. *Bautechnik*, 85(6), 394–406. doi:10.1002/bate.200810031
- Buitrago, M., Bertolesi, E., Calderón, P. A., & Adam, J. M. (2021). Robustness of steel truss bridges: Laboratory testing of a full-scale 21-metre bridge span. *Structures*, 29, 691–700. doi:10.1016/j.istruc.2020.12.005

- Bussell, M. (2014). Wrought iron. In D. Doran & B. Cather (Eds.), *Construction Materials Reference Book* (2nd ed., pp. 65–82). London, Routledge.
- Carden, E. P., & Fanning, P. (2004). Vibration Based Condition Monitoring: A Review. *Structural Health Monitoring*, 3(4), 355–377. doi:10.1177/1475921704047500
- Casanelles, E., & Logunov, E. (2003). *The Nizhny Tagil Charter for the Industrial Heritage - The International Committee for the Conservation of the Industrial Heritage* (tech. rep.). TICCH. Nizhny Tagil.
- Celik, H. K., & Sakar, G. (2022). Semi-rigid connections in steel structures: State-of-the-art report on modelling, analysis and design. *Steel and Composite Structures*, 45(1), 1–21.
- Collette, Q. (2014). *Riveted Connections in Historical Metal Structures (1840-1940). Hot-driven Rivets: Technology, Design and Experiments* (Doctoral dissertation). Vrije Universiteit Brussel.
- D’Aniello, M., Portioli, F., Fiorino, L., & Landolfo, R. (2011). Experimental investigation on shear behaviour of riveted connections in steel structures. *Engineering Structures*, 33(2), 516–531. doi:10.1016/j.engstruct.2010.11.010
- de Bouw, M. (2010). *Brussels Model Schools (1860-1920) - Structural Analysis of the Metal Roof Trusses* (Doctoral dissertation). Vrije Universiteit Brussel.
- de Bouw, M., Wouters, I., Vereecken, J., & Lauriks, L. (2009). Iron and steel varieties in building industry between 1860 and 1914 – A complex and confusing situation resolved. *Construction and Building Materials*, 23(8), 2775–2787. doi:10.1016/j.conbuildmat.2009.03.009
- Dia, A. (2020). *Monitoring des câbles de structures du génie civil par combinaison de techniques vibratoires et émission acoustique* (Doctoral dissertation). Ecole centrale de Nantes.
- Eberhardt, S., & Pospisil, M. (2022). E-P Heritage Value Assessment Method Proposed Methodology for Assessing Heritage Value of Load-Bearing Structures. *International Journal of Architectural Heritage*, 16(11), 1621–1641. doi:10.1080/15583058.2021.1901160
- Emile, A., & Veston, V. (2020). Les "Grandes Halles Voyageurs" : une architecture durable. *Patrimoine industriel*, (77), 75–83.
- EN 1990. (2002). *Eurocode 0: Basis of structural design*. European committee for standardization (CEN).
- EN 1991-1-1. (2003). *Eurocode 1: Actions on structures - Part 1-1: General actions - Densities, self-weight, imposed loads for buildings*. European committee for standardization (CEN).
- EN 1991-1-3. (2003). *Eurocode 1: Actions on structures - Part 1-3: General actions - Snow loads*. European committee for standardization (CEN).

- EN 1991-1-4. (2005). *Eurocode 1: Actions on structures - Part 1-4: General actions - Wind actions*. European committee for standardization (CEN).
- EN 1993-1-1. (2005). *Eurocode 3: Design of steel structures - Part 1-1: General rules and rules for buildings*. European committee for standardization (CEN).
- EN 1993-1-8. (2005). *Eurocode 3: Design of steel structures - Part 1-8: Design of joints*. European committee for standardization (CEN).
- Espion, B., Provost, M., Wibaut, R., & Wouters, I. (Eds.). (2018). *Patrimoines de fonte, fer et acier: architectures et ouvrages d'art*. Bruxelles, Comité Patrimoine et Histoire de la FABI.
- Ewins, D. J. (2000). *Modal testing: theory, practice, and application* (2nd ed.). Baldock, Hertfordshire, England ; Philadelphia, PA, Research Studies Press.
- Feng, D., & Feng, M. Q. (2018). Computer vision for SHM of civil infrastructure: From dynamic response measurement to damage detection – A review. *Engineering Structures*, 156, 105–117. doi:10.1016/j.engstruct.2017.11.018
- Formichi, P. (2019). Towards the second generation of the Eurocodes. In *JRC Technical Report - The implementation of the Eurocodes in the National Regulatory Framework*. Luxembourg, Publications Office of the European Union.
- Gallegos Mayorga, L. (2016). *Contribution à la compréhension du comportement mécanique des assemblages rivetés anciens* (Doctoral dissertation). Université de Bretagne occidentale.
- Gallica - Bibliothèque nationale de France. (2023). <https://gallica.bnf.fr/>
- Gargiani, R. (2008). La résistance des colonnes : expériences sur la qualité des matériaux et calculs de la forme parfaite au cours du XVIIIe siècle. In R. Gargiani (Ed.), *La colonne: nouvelle histoire de la construction* (1st ed.). Lausanne, Presses Polytechniques et Universitaires Romandes.
- Gasnier, M. (2011). *Patrimoine industriel et technique: perspectives et retour sur 30 ans de politiques publiques au service des territoires*. Lyon, Lieux dits.
- Gasnier, M. (2019). Réflexion épistémologique sur le patrimoine industriel : De la pluridisciplinarité à l'interdisciplinarité. *Revue d'histoire des sciences*, 72(2), 309. doi: 10.3917/rhs.722.0309
- Gudina, M., & Prokofiev, E. (2021). Preservation of the structure of the building in the process of renovation of industrial architecture. *E3S Web of Conferences*, 274, 01006. doi:10.1051/e3sconf/202127401006
- HEXAGON - Marc. (2023). <https://hexagon.com/fr/products/marc>
- Hochreiner, G., & Styhler-Aydin, G. (2019). 19th century iron dome structures in the vienna hofburg. an insight into the simplified structural assessment of that period and its evaluation using modern engineering software. In R. Aguilar, D. Torrealva, S. Moreira, M. A. Pando, & L. F. Ramos (Eds.), *Structural Analysis of Historical*

- Constructions* (pp. 891–900). Cham, Springer International Publishing. doi:10.1007/978-3-319-99441-3_96
- Hollister, P. (1974). The Glazing of the Crystal Palace. *Journal of Glass Studies*, 16, 95–110.
- Holzer, S. (2006). Kleine Geschichte der Schnee- und Windlastannahmen im 19. Jahrhundert. *Bautechnik*, 83(11), 781–788. doi:10.1002/bate.200610069
- Holzer, S. (2010). The Polonceau Roof and its Analysis. *International Journal for the History of Engineering & Technology*, 80, 22–54. doi:10.1179/175812109X12547331530066
- Hondermarck, C. (2007). *Analyse vibratoire des câbles tendus - détermination des paramètres mécaniques de fonctionnement : tension, endommagement...* (Master's thesis). Laboratoire Central des Ponts et Chaussées.
- Hugues, A. F., Iles, D. C., & Malik, A. S. (2011). *Design of steel beams in torsion*. Askot, United Kingdom, SCI.
- Hunt, D. L. (1992). Application of an enhanced coordinate modal assurance criterion. *Proceedings of IMAC X*, 66–71.
- ICOMOS. (2003). *ICOMOS Charter - Principles for the analysis, conservation and structural restoration of architectural heritage* (tech. rep.). Victoria Falls, Zimbabwe.
- ICOMOS. (2011). *Joint ICOMOS–TICCIH Principles for the conservation of industrial heritage sites, structures, areas and landscapes. "The Dublin principles"* (tech. rep.). Paris.
- Imam, B. M., Righiniotis, T. D., & Chryssanthopoulos, M. K. (2007). Numerical modelling of riveted railway bridge connections for fatigue evaluation. *Engineering Structures*, 29(11), 3071–3081. doi:10.1016/j.engstruct.2007.02.011
- Jost, S. M. (2012). *Behavior of riveted connections in steel truss bridges* (Master's thesis). University of Washington.
- Kanai, A. (2005). *Les gares françaises et japonaises, halle et bâtiment principal - Une recherche comparative* (Doctoral dissertation). Ecole nationale des Ponts et Chaussées.
- Kefallinos, K. (2013). *Wire glass: history of technology & development* (Master's thesis). Columbia University.
- Krings, U. (1985). *Bahnhofsarchitektur. Deutsche Grossstadtbahnhöfe des Historismus*. Prestel.
- Kühn, B., Lukic, M., Nussbaumer, A., Günther, H.-P., Helmerich, R., Herion, S., Kolstein, M. H., Walbridge, S., Androic, B., Dijkstra, O., et al. (2008). *Assessment of existing steel structures: recommendations for estimation of remaining fatigue life* (tech. rep.). JRC European Commission.
- Kurrer, K.-E. (2018). *The history of the theory of structures: searching for equilibrium*. Berlin, John Wiley & Sons.

- Lauriks, L., Wouters, I., & Belis, J. (2018). Couvertures en fer et verre au XIXe siècle : matériaux, connexions, structures et rénovation. In B. Espion, M. Provost, R. Wibaut, & I. Wouters (Eds.), *Patrimoines de fonte, fer et acier: architectures et ouvrages d'art* (pp. 223–227). Bruxelles, Comité Patrimoine et Histoire de la FABI.
- Lee, S. (2013). *Effective length K-Factors for flexural buckling strengths of web members in open web steel joists* (Master's thesis). Bucknell University.
- Lemoine, B. (1986). *L'architecture du fer: France ; XIX. siècle*. Seyssel, Champ Vallon.
- Lemoine, B. (2022). *Une histoire des gares en France*. Paris, Archibooks.
- Leonetti, D., Maljaars, J., Pasquarelli, G., & Brando, G. (2020). Rivet clamping force of as-built hot-riveted connections in steel bridges. *Journal of Constructional Steel Research*, 167, 105955. doi:10.1016/j.jcsr.2020.105955
- Lepretre, E., Chataigner, S., Dieng, L., Gaillet, L., & Cannard, H. (2016). Numerical and experimental investigations of hot driven riveting process on old metal structures. *Engineering Structures*, 127, 583–593. doi:10.1016/j.engstruct.2016.08.056
- Link, M. (1999). Updating of analytical models - Basic procedures and extensions. In N. M. M. Silva & N. M. M. Maia (Eds.), *Modal Analysis and Testing* (pp. 281–304). Dordrecht, Springer Netherlands.
- Luechinger, P., & Fischer, J. (2015). *New European technical rules for the assessment and retrofitting of existing structures* (JRC Science and Policy Report). Publications Office of the European Union. Luxembourg.
- Luong, T. M. H. (2018). *Identification of the state of stress in iron and steel truss structures by vibration-based experimental investigations* (Doctoral dissertation). TU Cottbus-Senftenberg.
- Mager, T. (2016). *Schillernde Unschärfe: Der Begriff der Authentizität im architektonischen Erbe*. Berlin, De Gruyter.
- Maia, N., Silva, J., Almas, E., & Sampaio, R. (2003). Damage detection in structures: from mode shape to frequency response function methods. *Mechanical Systems and Signal Processing*, 17(3), 489–498. doi:10.1006/mssp.2002.1506
- Maquoi, R., & Chabrolin, B. (1998). *Frame design including joint behaviour*. Luxembourg, Office for official publications of the European communities.
- MARC 2018.1. (2018). *Volume B: Element library*. MSC Software.
- Martin-Lebredonchel, A., Erazmus, P., & Vignal, V. (2023). Analyse de l'influence de la corrosion sur les éléments de charpente métallique des GHV pour orienter les choix de rénovation. In M. Gasnier (Ed.), *Transitions, patrimoines et matériaux anciens : Patrimoine industriel et ferroviaire* (pp. 161–186). Belfort, Les Editions du Lion.
- Meeks, C. (1956). *The railroad station. An architectural history*. New Haven, Yale University Press.

- Memet, J.-B., Bayle, M., & de Viviès, P. (2021). Le diagnostic des charpentes métalliques et le cas de la Bourse du Commerce. In M. Porrino (Ed.), *Les matériaux métalliques: histoire d'une technique et sauvegarde du patrimoine du 19e siècle* (pp. 315–349). Paris, Infolio.
- Minor, O., & Ryjáček, P. (2019). Rotational Stiffness of Connections in a Historical Steel Railway Bridge. In *Structural Analysis of Historical Constructions* (pp. 1082–1089). Cham, Springer.
- Mottershead, J., & Friswell, M. (1993). Model updating in structural dynamics: a survey. *Journal of Sound and Vibration*, 167(2), 347–375. doi:10.1006/jsvi.1993.1340
- Moy, S., Clarke, H., & Bright, S. (2009). The engineering properties of victorian structural wrought iron. *Proceedings of the Institution of Civil Engineers-Construction Materials*, 162(1), 1–10.
- Newmark, N. M. (1949). A simple approximate formula for effective end-fixity of columns. *Journal of the Aeronautical Sciences*, 16(2), 116–116.
- Nowak, B. (1981). *Die historische Entwicklung des Knickstabproblems und dessen Behandlung in den Stahlbaunormen* (Vol. Heft 35). Veröffentlichung des Instituts für Statik und Stahlbau der Technischen Hochschule Darmstadt.
- O'Sullivan, M. (2013). *Assessment Procedures for Structural Wrought Iron* (Doctoral dissertation). University of Manchester.
- Palacio-Betancur, A., & Aristizabal-Ochoa, J. D. (2019). Statics, stability and vibration of non-prismatic linear beam-columns with semirigid connections on elastic foundation. *Engineering Structures*, 181, 89–94. doi:10.1016/j.engstruct.2018.12.002
- Patnaik, A., & Srivatsan, T. (2003). Effective lengths of members in parallel chord trusses made from hollow structural sections. *Current Trends in Civil & Structural Engineering*, 9(5). doi:10.33552/CTCSE.2023.09.000722
- prEN 1993-1-14. (2023). *Eurocode 3: Design of steel structures — Part 1-14: Design assisted by finite element analysis*. European committee for standardization (CEN).
- Real, E. (2015). Reconversions. L'architecture industrielle réinventée. *In Situ. Revue des patrimoines*, (26). doi:10.4000/insitu.11745
- Reynders, E. (2012). System Identification Methods for (Operational) Modal Analysis: Review and Comparison. *Archives of Computational Methods in Engineering*, 19, 51–124.
- Reynders, E., Magalhaes, F., De Roeck, G., & Cunha, A. (2009). Merging strategies for multi-setup operational modal analysis: application to the Luiz I steel arch bridge. *Proceedings of IMAC XXVII*. doi:10.1007/s11831-012-9069-x
- Ribeiro, D., Calçada, R., Delgado, R., Brehm, M., & Zabel, V. (2012). Finite element model updating of a bowstring-arch railway bridge based on experimental modal

- parameters. *Engineering Structures*, 40, 413–435. doi:10.1016/j.engstruct.2012.03.013
- Rinke, M., & Kotnik, T. (2010). The changing concept of truss design caused by the influence of science. In *First International Conference on Structures and Architecture, ICSA*. Boca Raton, Fla., CRC Press.
- Rinke, M., & Kotnik, T. (2013). From construct to type – the transformation of constituents in the development of trusses. In *Structures and Architecture: New concepts, applications and challenges* (pp. 1947–1954). CRC.
- Robert, J.-L. (1993). *Mesure de la tension des câbles par vibration - Méthode d'essai LPC n°35* (tech. rep.). LCPC. Paris.
- Rytter, A. (1993). *Vibration based inspection of civil engineering structures* (Doctoral dissertation). Aalborg University.
- Salter, J., Robinson, J., & Wiek, A. (2010). Participatory methods of integrated assessment — a review. *WIREs Climate Change*, 1(5), 697–717. doi:10.1002/wcc.73
- Sarou, L., Couchaux, M., Hjiiaj, M., Sire, S., Douroux, J.-F., & Desbordes, A. (2023). Compressive stiffness of L-stubs in contact with rigid and flexible foundations. *Journal of Constructional Steel Research*, 201, 107675. doi:10.1016/j.jcsr.2022.107675
- Schädlich, C. (2015). *Das Eisen in der Architektur des 19. Jahrhunderts* (1st ed.). Aachen, Geymüller Verlag für Architektur.
- Schueremans, L., Porcher, H., Rossi, B., Wouters, I., & Verstrynge, E. (2018). A Study on the Evolution in Design and Calculation of Iron and Steel Structures over the Mid 19th Century in Western and Central Europe. *International Journal of Architectural Heritage*, 12(3), 320–333. doi:10.1080/15583058.2017.1323244
- Schwartz, K. (2014). Polycarbonates in Construction. *The IAPD Magazine*. https://www.iapd.org/Documents/designing-with-plastics/PDF/PC_in_Construction.pdf
- Silva, J. M. M. (1999). An Overview of the Fundamentals of Modal Analysis. In N. M. M. Silva & N. M. M. Maia (Eds.), *Modal Analysis and Testing* (pp. 1–34). Dordrecht, Springer Netherlands.
- Smith, P. (1999). Le patrimoine ferroviaire en France : soixante-dix ans de protection juridique. *Revue d'histoire des chemins de fer*, (20-21), 329–347.
- Somma, G., & Vit, M. (2023). Experimental investigation of flaregroove weld stiffness in lattice girder beams by means of push-out tests. *Journal of Constructional Steel Research*, 202, 107780. doi:10.1016/j.jcsr.2023.107780
- Springer, J., Merwar, G., & Bosse, J. (2012). Sanierung der Bahnsteighalle des Wiesbadener Hauptbahnhofes. *Stahlbau*, 81(7), 519–529. doi:10.1002/stab.201201582

- Striffling-Marcu, A., & Veston, V. (2022). Patrimoine ferroviaire du XXe siècle : quelle reconnaissance et quelles adaptations pour sa conservation ? *In Situ. Revue des patrimoines*, (47). doi:10.4000/insitu.34395
- STRRES. (2014). *Réparation et rénovation des structures métalliques* [FAME - Version 2].
- Szopa, K., Iwaniec, M., & Iwaniec, J. (2020). Modelling and identification of bolted truss structure with the use of design of experiment approach. *Structures*, 27, 462–473. doi:10.1016/j.istruc.2020.05.047
- Tankova, T. S. (2018). *Stability design of steel columns, beams and beam-columns: behaviour, general formulation and reliability* (Doctoral dissertation). Universidade de Coimbra.
- Tanner, P. (2021). Standards for the Assessment of Existing Structures: Real Need or Caprice of Code Makers? *Hormigón y Acero*, 72(294-295), 77–84. doi:10.33586/hya.2021.3061
- Thomas, M., & Laville, F. (2007). *Simulation des vibrations mécaniques par Matlab, Simulink et Ansys*. Sainte-Foy, Presses de l'Université du Québec.
- Timoshenko, S. (1953). *History of strength of materials*. McGraw-Hill.
- Türker, T., Kartal, M. E., Bayraktar, A., & Muvafik, M. (2009). Assessment of semi-rigid connections in steel structures by modal testing. *Journal of Constructional Steel Research*, 65(7), 1538–1547. doi:10.1016/j.jcsr.2009.03.002
- van Es, S., Braendstrup, C., Slot, H., Seinen, J., & Dekker, R. (2023). Determination of actual material properties in existing structures using small specimens. *ce/papers*, 6(3-4), 339–345. doi:10.1002/cepa.2337
- Vitzthum, M., Volland, P., & Foster & Partners. (2006). Hauptbahnhof Dresden – Instandsetzung und Umbau der Bahnsteighallen. *Stahlbau*, 75(3), 211–218. doi:10.1002/stab.200610020
- Weller, B., & Tasche, M. (2006). Bahnhofshallen im Osten Deutschlands. *Stahlbau*, 75(3), 219–224.
- Wen, Q.-J., & Yue, Z.-X. (2020). Elastic buckling property of the upper chords in aluminum half-through truss bridges. *Structures*, 27, 1919–1929. doi:10.1016/j.istruc.2020.07.057
- Werner, F., & Seidel, J. (1992). *Der Eisenbau: vom Werdegang einer Bauweise*. Berlin / Munich, Verlag für Bauwesen.
- XP CEN/TS 17440. (2020). *Technical specification - Assessment and retrofitting of existing structures*. European committee for standardization (CEN).
- Yost, J., Robert, David, W. D., Gross, S. P., Pote, J. J., & Gargan, B. (2004). Strength and design of open web steel joists with crimped-end web members. *Journal of*

Structural Engineering, 130(5), 715–724. doi:10.1061/(ASCE)0733-9445(2004)130:5(715)

Zabel, V., & Brehm, M. (2009). Model updating methods – a comparative study. *Proceedings of IMAC XXVII*.

Zaharia, R., & Dubina, D. (2006). Stiffness of joints in bolted connected cold-formed steel trusses. *Journal of Constructional Steel Research*, 62(3), 240–249. doi:10.1016/j.jcsr.2005.07.002

Zuber, H. (2009). Archives de la SNCF et patrimoine ferroviaire. *Revue d'histoire des chemins de fer*, (40), 25–31. doi:10.4000/rhcf.711

Zureick, A.-H. (2023). The historical basis and critical appraisal of the shear buckling formulae for unstiffened orthotropic plates with recommended design equations for pultruded girder webs and plates. *Thin-Walled Structures*, 184, 110436. doi:10.1016/j.tws.2022.110436

PUBLICATIONS BY THE AUTHOR

Peer-reviewed journal papers

Franz, H., Rinke, M., Martin, J.-L., Chataigner, S., & Dieng, L. (2023a). French metallic train sheds of 1850 to 1930: structural specificities and the evolution of the restoration practices. *International Journal of Architectural Heritage*. doi:10.1080/15583058.2023.2272132

Franz, H., Lepretre, E., Chataigner, S., Rinke, M., & Dieng, L. (2024a). Assessment of the rotational stiffness of single-riveted joints in a steel lattice girder by modal analysis. *Engineering Structures*, 298, 117052. doi:10.1016/j.engstruct.2023.117052

Non-peer-reviewed journal papers

Franz, H., & Rinke, M. (2024b). Bewertung und Ertüchtigung von genieteten Gitterträgern in Dachkonstruktionen. *Bautechnik*, 101. doi:10.1002/bate.202400014

Book chapters

Franz, H., Martin, J.-L., Rinke, M., Chataigner, S., & Dieng, L. (2023c). Quelle résistance de calcul pour le fer puddlé et l'acier doux ? L'exemple des halles de gare du XIXème et début du XXème siècle. In M. Gasnier (Ed.), *Transitions, patrimoines et matériaux anciens : Patrimoine industriel et ferroviaire* (pp. 227–253). Belfort, Les Editions du Lion.

Conference papers

Franz, H., Rinke, M., Lepretre, E., & Dieng, L. (2022a). The gap between theory, practice and regulations in design criteria for iron and steel structures in 19th century France: the example of train sheds. In Campbell, WP, J. et al (Ed.), *Timber and Construction: Proceedings of the Ninth Conference of the Construction History Society* (pp. 287–300). Cambridge, Construction History Society.

Franz, H., Lepretre, E., Rinke, M., Chataigner, S., & Dieng, L. (2022b). Influence de la raideur des assemblages rivetés d'une poutre treillis sur son comportement vibratoire. *Congrès Français de Mécanique*.

- Franz, H., Chataigner, S., Dieng, L., & Rinke, M. (2023b). Modal analysis of a riveted lattice beam for improved retrofitting operations. *ce/papers*, 6(3-4), 333–338. doi: 10.1002/cepa.2279
- Franz, H. (2023). Une approche interdisciplinaire pour mieux évaluer la performance structurale de charpentes métalliques anciennes (1850-1930). *AJCE*, 41(1), 631–638.

APPENDIX

Extract of the original design report of Bédarieux's train shed

This appendix presents a short extract of the original design report drafted by Daydé et Pillé for the train shed of Bédarieux's railway station built in 1902. Fig. A.1 shows its front cover.

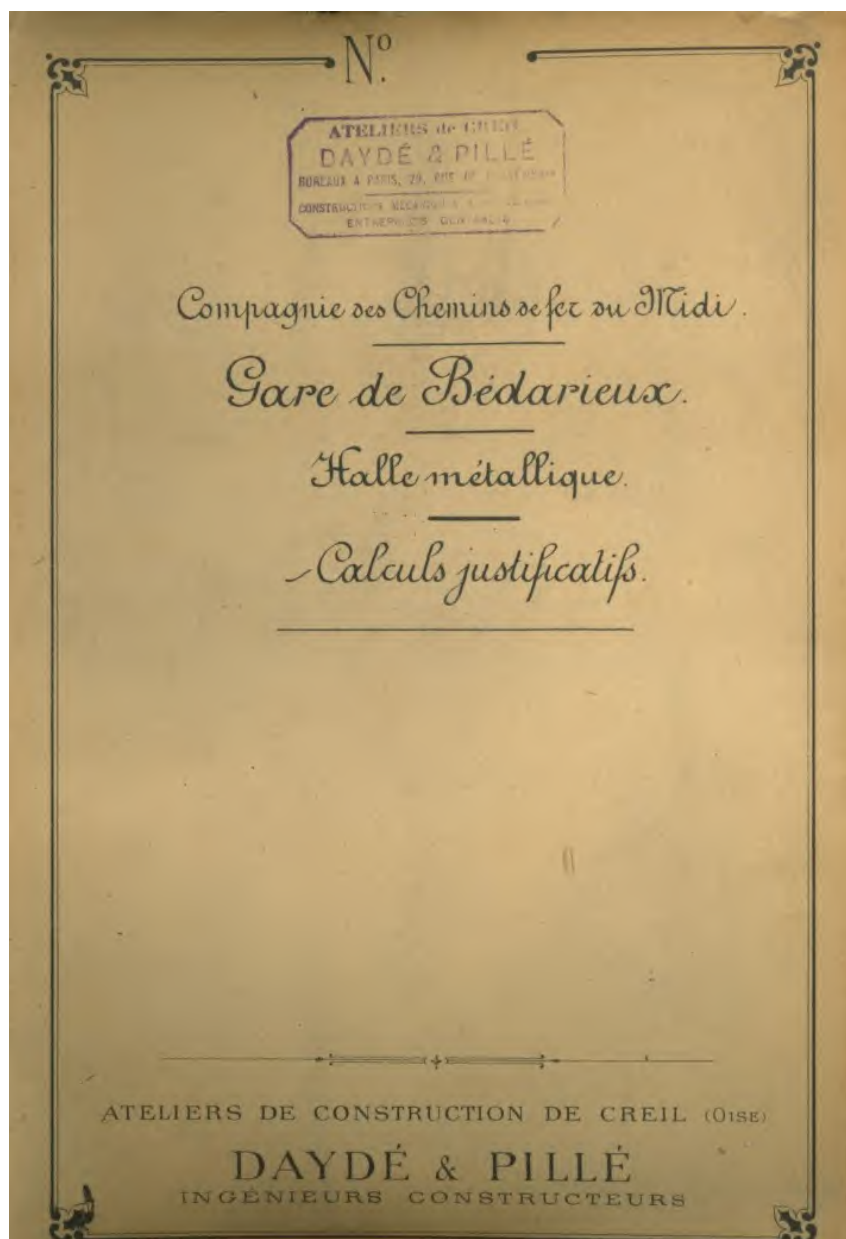


Figure A.1 – Front cover of the original design report of Bédarieux's train shed.

Fig. A.2 presents design calculations carried out for the ridge purlin, with typed annotations to help decipher them. In the first section, the loading is defined. Then, the chords are designed based on the estimated maximum bending moment. Finally, the diagonals are designed by deriving their axial stress from the shear load.

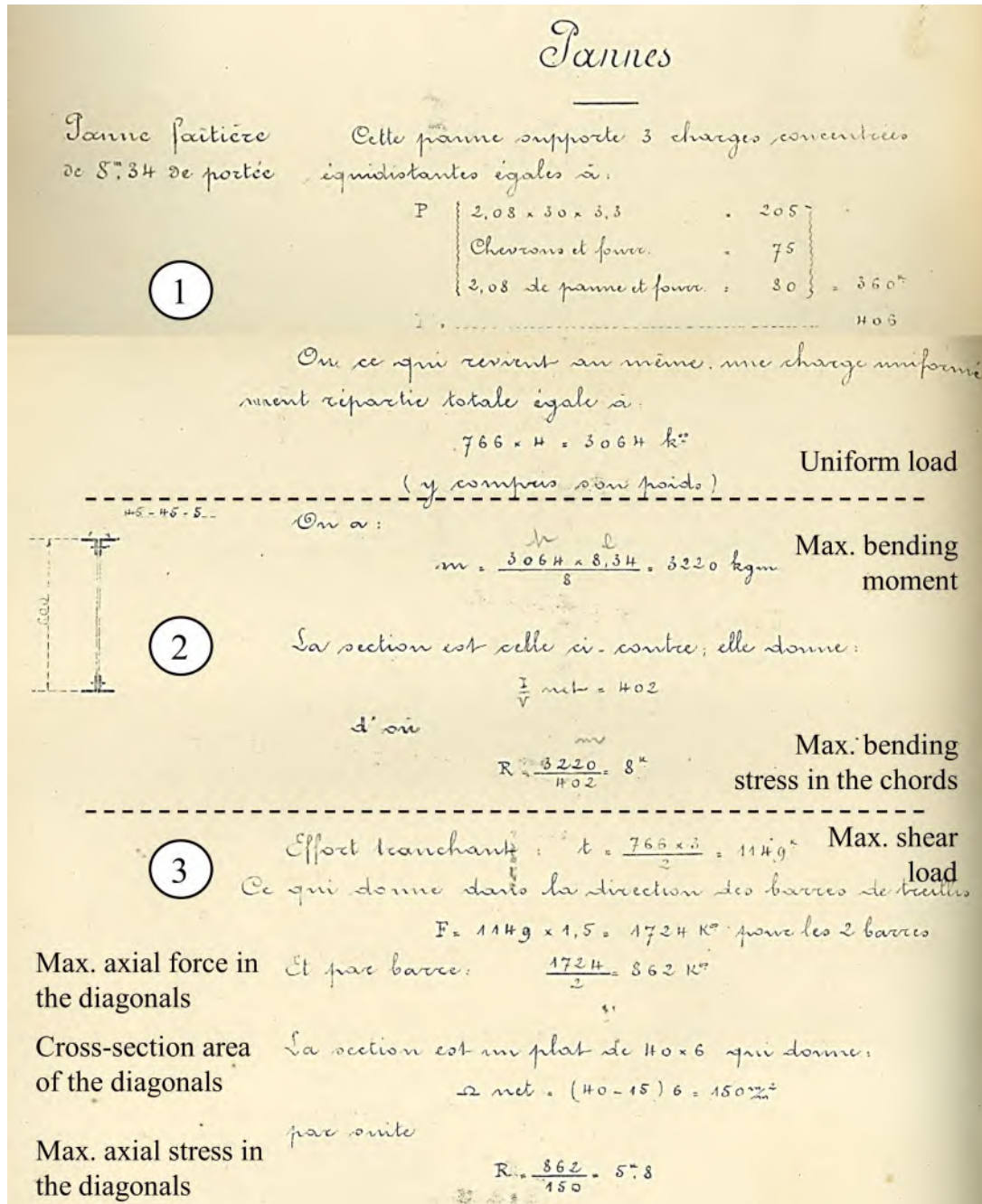


Figure A.2 – Design calculations for the ridge purlin of Bédarieux’s train shed.

Title: Towards an integrated assessment framework for existing structures:
Study of riveted lattice girders in French train sheds of 1850-1930

Keywords: iron and steel structures, heritage, history of engineering, modal testing, buckling

Abstract: Wrought-iron and mild-steel riveted lattice girders are essential constituents of the French metallic construction heritage of 1850 to 1930. In recent restorations of historic train sheds conducted by the French national railway company SNCF, riveted lattice girders have often been reinforced because of numerically identified stability problems. In reality, however, excessive deformations due to buckling are rarely witnessed. In order to limit invasive structural interventions, this thesis, therefore, proposes a novel integrated assessment methodology. The methodology, applied to riveted lattice girders in French metallic train sheds, is decomposed into three steps. Firstly, structural features conveying heritage value are identified relying on the history of engineering,

and the impact of renovation strategies on the structure is discussed using an inventory of previous renovations. Secondly, modelling assumptions for structural analysis are debated based on a review of historical and recent literature. The rotational stiffness of riveted joints, a key parameter for buckling, is assessed using experimental and numerical investigations carried out on a reclaimed riveted lattice girder. Thirdly, current design criteria used for assessment are discussed by comparing them with historical verification methods. The proposed methodology sets the basis of an assessment framework that could be extended to heritage structures of all materials, and broadly to most types of existing structures.

Titre : Vers une évaluation intégrée des structures existantes :
Etude des poutres treillis rivetées dans les halles de gare françaises de 1850-1930

Mots clés : structures métalliques, patrimoine, histoire de l'ingénierie, analyse modale, flambement

Résumé : Les poutres treillis rivetées en fer puddlé et en acier doux sont des éléments essentiels du patrimoine de la construction métallique française des années 1850 à 1930. Lors des récentes restaurations de halles de gare historiques à charpente métallique menées par la SNCF, les poutres treillis rivetées ont souvent été renforcées en raison de problèmes de stabilité identifiés numériquement. En réalité, des déformations excessives dues au flambement sont rarement observées. Afin de limiter des interventions structurales invasives, cette thèse propose une méthodologie novatrice d'évaluation. La méthodologie, appliquée aux poutres treillis rivetées dans les halles de gare françaises est décomposée en trois étapes. Tout d'abord, les caractéristiques structurelles ayant une valeur patrimoniale sont identifiées en

s'appuyant sur l'histoire de l'ingénierie, et l'impact des stratégies de rénovation sur la structure est discuté à l'aide d'un inventaire des rénovations précédentes. Ensuite, les hypothèses de modélisation pour l'analyse structurale sont débattues à partir de la littérature historique et récente. La raideur rotationnelle des assemblages rivetés, paramètre clé pour le flambement, est évaluée grâce à des investigations expérimentales et numériques sur une poutre treillis rivetée historique. Enfin, les critères de dimensionnement actuels sont discutés en les comparant aux méthodes de vérification historiques. La méthodologie développée à travers cette thèse peut être appliquée aux structures patrimoniales de tous matériaux, et plus largement aux structures existantes.